Title : The loss of PI3K C2□is associated with a heightened immune response

Name : Emma K. Buick

UNIVERSITY OF BEDFORDSHIRE

The loss of PI3K C2β is associated with a heightened immune response

E.K. Buick

A thesis submitted to the University of Bedfordshire in partial fulfilment of the requirements for the degree of Doctor of Philosophy

December 2016

ABSTRACT

The phosphoinositide 3-kinase (PI3K) enzymes are well known for their regulation of pro-survival signalling cascades that result in increased cell survival and proliferation. However, most of what we understand is based on Class I PI3K enzymes and much less is understood about the Class II enzymes.

Loss of PI3K C2α in mice results in embryonic lethality, or severe glomerular injury with increased morbidity. In contrast, PI3K C2β deficient mice display no apparent phenotype and are healthy and viable. Previous work in our laboratory revealed that administration of a sub-nephritogenic dose of nephrotoxic serum led to an augmented immune response resulting in glomerular damage and impaired renal function, which was associated with T-cell infiltration. Elucidating the immunological basis of this sensitivity was the basis of my project.

In response to a subcutaneous injection of sheep IgG in complete Freund's adjuvant, the spleens of PI3K C2β–/– mice showed prominent germinal centre associated cell proliferation that was absent in the controls. Analysis of splenocyte populations revealed that PI3K C2β–/– mice had an increased population of CD4+ T-cells and when cultured in vitro within a total splenocyte population, the increased CD4+ T-cell population was maintained. However, this effect was lost when T-cells were purified and maintained *ex vivo.* These data suggest that the increased PI3K C2β–/– CD4+ proliferation may be due to additional factors within the total splenocyte population.

B-cell populations from the spleens of PI3K C2β–/– mice had higher CD19 expression compared to B-cells from control mice. Elevated levels of CD19 are associated with a reduced activation threshold. In response to stimulation with a sub-optimal dose of LPS and IL-4 PI3K C2β–/– B-cells underwent increased class switch recombination, displayed increased metabolic activity and remained viable for longer than B-cells from control mice. B-cell lysates from PI3K C2β–/– mice also revealed increased levels of phosphorylated MEK1/2. These data indicate that PI3K C2β may serve as a negative regulator of B-cell function and that loss of this PI3K enzyme isoform activity produces a heightened immune response which may lead to a predisposition to associated pathologies.

AUTHOR'S DECLARATION

I declare that this thesis is my own unaided work. It is being submitted for the degree of Doctor of Philosophy at the University of Bedfordshire.

It has not been submitted before for any degree or examination in any other University.

Name of candidate: Emma Buick Signature 

Date: 18th December 2016

ACKNOWLEDGEMENTS

Firstly, I would like to thank my supervisor Professor Jan Domin, for his wealth of knowledge, his insight, patience and analogies. I always left our meetings feeling inspired. Thank you for this opportunity.

Dr Barbara Guinn, whose support and enthusiasm have been overwhelming. Thank you for your kindness and for letting me use your multi-channel pipettor.

Dr Maria Simon, I don't know where to start. Thank you for your guidance, for pushing me. You have taught me so much.

Professor Charles Pusey, thank you for your kind support.

Dr M, thank you for introducing science into my life, even though it can be a bit of a mixed bag at times.

To the Staff in the Department of Life Sciences, we have an amazing department and I have loved being part of it.

To my lab buddies, especially Viki, Kay and Khadar.

I would also like to say a special thank you to Emma Rowley, who is just amazing.

To Andrew, there are no words to describe how much your support has meant. Thank you.

This is for my mum, who believes I can do anything.

Contents

List of tables

List of figures

List of abbreviations

ANOVA	Analysis of variance
AnV	Annexin V
APC	Antigen presenting cell
BCA	Bicinchoninic acid
BMMC	Bone marrow derived mast cells
BCR	B-cell receptor
BSA	Bovine serum albumin
CCL19	Chemokine, C-C motif, Ligand 19
CCL21	Chemokine, C-C Motif, Ligand 21
CD	Cluster of differentiation
cDNA	Complementary deoxyribonucleic acid
CFA	Complete Freund's adjuvant
CSR	Class switch recombination
CXCL12	Chemokine, CXC Motif, Ligand 12
CXCL13	Chemokine, CXC Motif, Ligand 13
CXCR4	Chemokine, C-X-C Motif, Receptor 4
CXCR5	Chemokine, C-X-C Motif, Receptor 5
DAMP	Damage associated molecular pattern
DC	Dendritic cell
dsRNA	Double stranded ribonucleic acid
DZ	Dark zone
EAE	Experimental autoimmune
ECL	Enhanced chemiluminescence
EDTA	Ethylenediaminetetraacetic acid
EMH	Extra medullary haematopoiesis
FCS	Foetal bovine serum
FDC	Follicular dendritic cell
Fo	Follicular
GAPDH	Glyceraldehyde 3-phosphate dehydrogenase
GC	Germinal centre
gDNA	Genomic deoxyribonucleic acid
HEK293	Human embryonic kidney 293 cell line
HL60	Human promyelocytic leukemia cell line
hr	Hour
IFN-γ	Interferon gamma
Ig	Immunoglobulin
IL	Interleukin

IMS	Industrial methylated spirits
LPA	Lysophosphatidic acid
LPS	Lipopolysaccharide
LZ	Light zone
MHC	Major histocompatability complex
mTOR	Mammalian target of rapamycin
MTT	3-(4,5-dimethylthiazol-2-yl)-2,5 diphenyltetrazolium bromide
NTS	Nephrotoxic serum
PAGE	Polyacrylamide gel electrophoresis
PALS	Periarteriolar Lymphoid Sheath
PAMP	Pathogen associated molecular pattern
PBS	Phosphate buffered
PCNA	Proliferating cell nuclear antigen
PCR	Polymerase chain reaction
PE	Phycoerythrin
PI	Phosphoinositide
PI	Propidium iodide
$PI3,4P_2$	Phospsoinositide-3,4-phosphate
PI3K	Phosphoinositide 3-kinase
PI3P	Phospsoinositide-3, -phosphate
PMSF	Phenylmethylsulphonyl fluoride
PRR	Pattern recognition receptor
PTEN	Phosphatase and tensin homolog
PVDF	Polyvinyledine difluoride
PX	Phox homology domain
RAG	Recombination activating gene
RBD	Ras binding domain
RNA	Ribonucleic acid
RP	Red pulp
RPMI	Roswell Park Memorial Institute 1640 medium
SDS	Sodium dodecyl sulphate
S1P	Sphingosine-1-phosphate
SHIP1	SH2-containing inositol phosphatase 1
SHM	Somatic hyper-mutation
TAE	Tris acetate EDTA buffer
TBS-T	Tris buffered saline-Tween 20
TAE	Tris acetate EDTA buffer
TCR	T-cell receptor
TD	T-cell dependent
TBS-T	Tris buffered saline-Tween 20

TI	T-cell independent
TNF-α	Tumour necrosis factor alpha
TRIM27	Tripartite motif containing protein 27

1 Introduction

1.1 Overview of the innate and adaptive immune systems

There are two arms of the immune system, innate and adaptive, although there is an interdependent relationship between the two (Hancock et al., 2012; Iwasaki and Medzhitov, 2015). The innate immune system is present from birth and is the first line of defence against invading pathogens, it consists of immune cells that are specialized in recognising molecular patterns, such as lipopolysaccharides and dsRNA, which are expressed by many bacteria, viruses and fungi. These pathogen associated molecular patterns (PAMPs) are recognised by pattern recognition receptors (PRRs) on host immune cells, and importantly are able to distinguish self from non-self (Janeway and Medzhitov, 2002). The response to infectious agents is carefully coordinated and is dependent on the location and the nature of the pathogen, and maybe initiated by non-immune cells such as PRR expressing epithelial cells. For example, a breach in the epithelium causes epithelial cells to release chemokines that recruit leukocytes to the area. Following stimulation of PRRs, dendritic cells release chemokines, cytokines and antimicrobial peptides, if this is insufficient and the pathogen is detected in the circulation a systemic response may be triggered. This includes recruitment of monocytes and neutrophils which release cytotoxic chemicals and phagocytose the pathogen (Iwasaki and Medzhitov, 2015).

In addition to eliminating infection, the innate immune system initiates the inflammatory response. While apoptosis is a normal physiological event

that occurs in a highly controlled manner, necrosis is typically the result of cell trauma and is associated with tissue damage, resulting in the loss of membrane integrity. As a result of necrosis, the contents of the cell escape into the local environment, releasing molecules that contain damage associated molecular patterns (DAMPs), which are thought to be recognised by PRRs on innate immune cells. These cells induce an inflammatory response and also engage the adaptive immune system (Kono and Rock, 2008).

The adaptive (also referred to as acquired) immune system is not present at birth and is developed over time in response to antigen exposure. Lymphocytes provide incredible antigen specificity via unique receptors that are produced by gene rearrangement during cell development. The adaptive response also provides immunological memory, which allows the immune system to recognise pathogens that it has previously encountered, facilitating a rapid response and mediating damage (Janeway and Medzhitov, 2002). Initiation of the adaptive response is largely dependent on signals from the innate immune system, such as chemokines and cytokines as well as the presentation of antigen by dendritic cells and macrophages (Hancock et al., 2012). However, the relationship between innate and adaptive immune systems is interdependent, including the recruitment of basophils, neutrophils and eosinophils by CD4+ T-cells, to sites of inflammation and infection. T-cells also induce microbicidal activity

by macrophages in response to infection (Zhu and Paul, 2015). Lymphocytes will be discussed later in the chapter.

1.2 Cell Signalling

Cell fate is controlled by a multitude of signalling pathways, which ultimately allow the cell to respond appropriately to the intracellular and extracellular environment. Under physiological conditions the downstream result is either of direct benefit to the cell (growth, proliferation, repair), or to the surrounding environment (secretion of cytokines). Alternatively, to protect the organism as a whole the cell can receive instruction to undergo programmed cell death (apoptosis). Signal transduction can be initiated when a receptor binds with a ligand, generating second messenger molecules such as Ca2+, cAMP or phosphoinositides. The role of second messengers is to amplify the original signal to produce a response.

1.2.1 Phosphoinositides

Phosphoinositides (PtdIns) are a phosphorylated form of phosphatidylinositol, which is derived from phospholipid within the plasma membrane. The third, fourth and fifth positions of the hydroxyl ring can be phosphorylated by different kinases to produce a combination of phosphoinositides (**Figure 1.1**); phospsoinositide-3-phosphate (PI3P), phospsoinositide-3,4-phosphate ($PI3,4P_2$), phospsoinositide-3,4,5-phosphate ($PI3,4,5P_3$) and phosphoinositide-3,5-phosphate ($PI3,5P_2$) (Vanhaesebroeck and Waterfield, 1999), phospsoinositide-4-phosphate (PI4P), (Hammond et al., 2012) and phospsoinositide-5- phosphate (PI5P)

(Nunès and Guittard, 2013). Phosphatases also have an important role in the regulation of phosphoinositide signalling by dephosphorylating the inositol ring. Signalling pathways mediated by PI3P and PI3,4,5P_3 are regulated by the lipid phosphatases; phosphatase and tensin homologue (PTEN), myotubulin (MTM) and Src homology 2 (SH2) containing tyrosine phosphatase-1 (SHP-1) (Majerus and York, 2009). The importance of phosphoinositides as second messengers is highlighted by the many human diseases that have been linked to their dysregulation, either through increased production or lack of phosphatase activity. Such diseases include cancer, autoimmune disorders including multiple sclerosis MS, systemic lupus erythematosus (SLE), asthma, chronic obstructive pulmonary disorder (COPD), rheumatoid arthritis and myopathies such as Charcot-Marie Tooth disease (Foster et al., 2012; Nicot and Laporte, 2008).

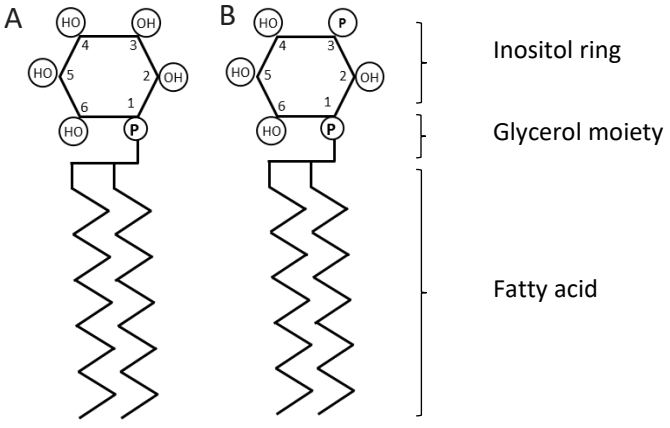

Figure 1.1 Schematic of A; phosphatidylinositol (PtdIns) and B; phosphoinositide-3-phosphate (PI3P)

1.2.2 The phosphoinositide 3-kinases (PI3K)

There are eight members of the PI3K family, separated into three classes, which are responsible for phosphorylating phosphoinositide at the 3'

position of the inositol ring (**Figure 1.1**). Classification is based on structural properties and substrate specificity (Domin and Waterfield, 1997).

The class I enzymes are heterodimers consisting of a catalytic unit and an adaptor unit, and have been further divided into class IA and IB (**Figure 1.2**). In vivo, the class I enzymes phosphorylate PI3,4P_2 to generate PI3,4,5P_3, although in vitro they can also phosphorylate PI4P to produce PI3,4P_2 . PI3,4,5P_3 and PI3,4P_2 bind to downstream effector proteins via the pleckstrin homology (PH) domain (Vanhaesebroeck and Waterfield, 1999). Both p110α and p110β have ubiquitous expression, while p110δ and p110γ are expressed predominantly in haematopoietic cells. As regulators of cell proliferation, differentiation and survival their dysregulation plays a role in diseases such as cancer and autoimmunity (Domin, 2006).

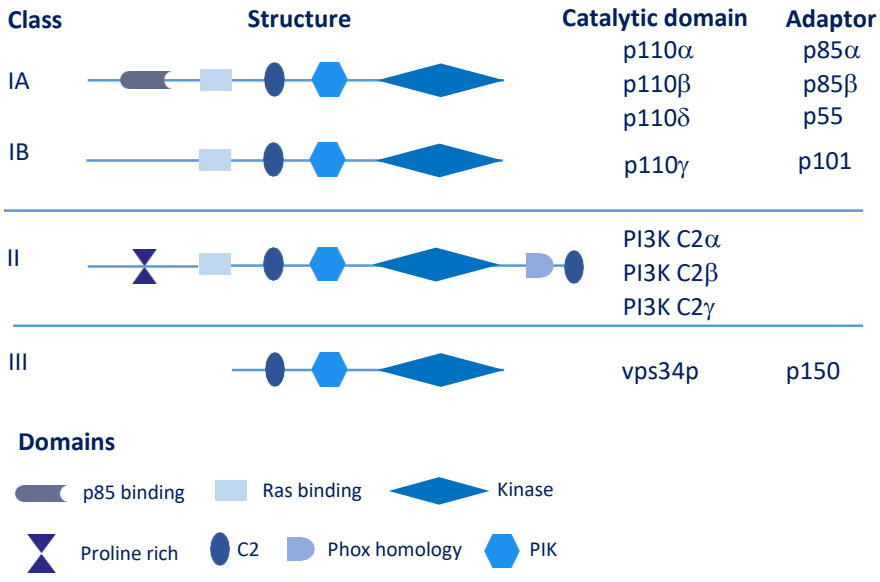

Figure 1.2 Classification of PI3K enzymes. There are eight isoforms of PI3K which have been separated into three classes depending on their structure and substrate specificity. Adapted from Domin and Waterfield (1997).

The class III PI3Ks consist of a single enzyme which is the homologue of Vps34p found in yeast, and like the class I enzymes it is a heterodimer. It is widely expressed and plays a role in maintaining cellular levels of PI3P required for vesicle trafficking (Cockcroft, 2000). It is also attributed as the source of PI3P within the endoplasmic reticulum, which is required for the regulation of autophagy. Although recently it has been demonstrated that class II PI3Ks may also play a role in this process (Devereaux et al., 2013).

1.2.3 Class II PI3K

Class II PI3Ks contain three members; PI3K C2α, PI3K C2β and PI3K C2γ, all of which are large monomeric proteins (>170kD). PI3K C2α and PI3K C2β show a wide distribution (El Sheikh et al., 2003), whereas PI3K C2γ expression is restricted to the liver (Ono et al., 1998). Recently, a requirement for PI3K C2γ has been described in the regulation of glycogen synthase production, and mice deficient in PI3K C2γ were unable to store glycogen which led to obesity and insulin resistance (Braccini et al., 2015).

Historically wortmannin and LY2094002 are thought of as pan-inhibitors of PI3K activity. However, the discovery of PI3K C2α led to the re-evaluation of both wortmannin and LY2094002, as their effect on PI3K C2α is greatly reduced (Domin et al., 1997). Similarly, PI3K C2β shows limited inhibition following treatment with LY2094002 (Ciraolo et al., 2014).

Both PI3K C2α and PI3K C2β appear to share a substrate specificity for PtdIns (Falasca and Maffucci, 2007) and they are structurally similar with

the exception of their N-terminus, however, it has been demonstrated that they can mediate different functions. PI3K C2α appears to play a critical role in cell survival, whereas this does not appear to be the case for PI3K C2β. For example, in over twenty cancer cell lines, knock down of PI3K C2α using siRNA was found to cause a six-fold increase in apoptosis compared to the controls, while the knockdown of PI3K C2β had no effect (Elis et al., 2008). Different roles have also been observed in HUVECs (human umbilical vein endothelial cells), knockdown of PI3K C2α using siRNA induced apoptosis suggesting a role in cell survival, whereas knock down of PI3K C2β had no effect on cell survival but did inhibit sphingosine-1-phosphate (S1P) dependent migration (Tibolla et al., 2013). In vivo experiments have highlighted the differences between the two isoforms. In mice, loss of PI3K C2α was found to be embryonically lethal due to severe vascular defects. The study went on to show that an endothelial cell specific knockdown led to impaired endosomal trafficking, signalling and defective receptor internalization (Yoshioka et al., 2012), indicating the importance of PI3K C2α in cell survival. PI3k C2β deficient mice have previously been described as viable, fertile with no pathological phenotype (Harada et al., 2005).

1.2.4 PI3K C2β

Like the other class II isoforms, PI3K C2β is a monomeric protein with extensions at both the amino and carboxyl termini. Differences within the N-terminus differentiate it from the other class II members.

Despite the lack of obvious phenotype in PI3K C2β deficient mice, PI3K C2β is involved in the regulation of a diverse range of cellular functions (**Table 1.1**). It has also been suggested that PI3K C2β may be required to optimize activation of downstream pathways in association with class I PI3Ks. For example, in small cell lung cancer cancer (SCLC) cells stimulated with polypeptide growth factors, Akt activation by p110α was enhanced by the addition of PI3K C2β (Arcaro et al., 2002).

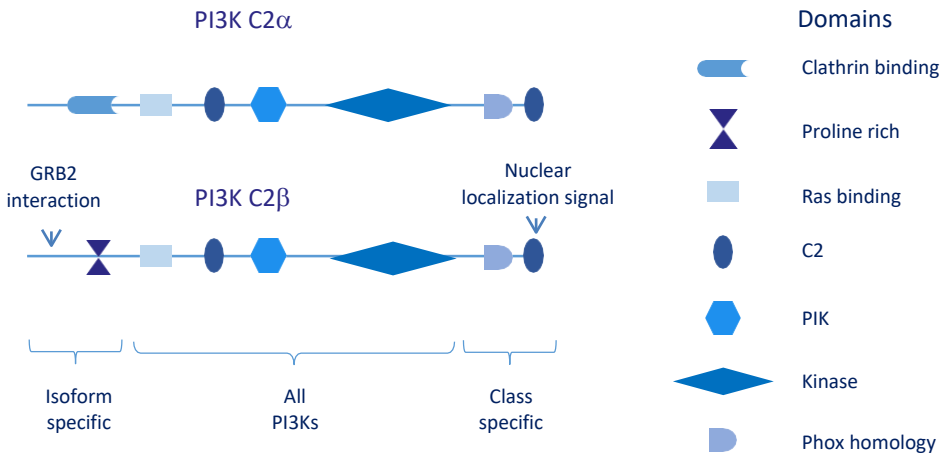

Figure 1.3 Schematic of PI3K C2α and PI3K C2β. Although structurally similar they differ at the N-terminus. The class II members have a PX and an additional C2 domain at the C-terminus.

In addition, a potentially cooperative role has been described for PI3K C2β in S1P dependent migration in HUVECs. While knockdown of P110γ reduced S1P induced migration, simultaneous knockdown led to a greater reduction in S1P dependent migration (Tibolla et al., 2013). More recently, studies have revealed a role for ceramide in suppressing metastasis in ovarian cancer via its effect on PI3K C2β function (Kitatani et al., 2015). Ceramide is a bio-active lipid that contains sphingosine which can be metabolised to

produce S1P, and while S1P is associated with cell survival, ceramide has been shown to induce apoptosis (Ponnusamy et al., 2010). The efficacy of ceramide was due to interaction with the PIK domain (**Figure 1.3**), which appears to effect the localization of PI3K C2β. By drawing PI3K C2β away from lamellipodia cell motility is inhibited. P110γ was also shown to be redirected away from lamellipodia in the presence of ceramide, which also affected motility, which may indicate either a functional overlap or possibly a cooperative role (Kitatani et al., 2015).

Of particular interest was the discovery of a possible role for PI3K C2β in the negative regulation of the GTPase Ras. Although previous in vitro studies indicated that Ras and PI3K C2β do not interact (Arcaro et al., 1998), a more recent study has revealed that PI3K C2β can interact with nucleotide free Ras via the Ras binding domain (RBD). The nucleotide free Ras/PI3K C2β complex appears to stabilize Ras and also inhibit PI3K C2β catalytic activity. Intersectin 1 (ITSN1) was also shown to interact with PI3K C2β via proline rich residues and this binding of ITSN1 was thought to release nucleotide free Ras, allowing activation by GTP loading and re-establishing PI3K C2β catalytic activity (Wong et al., 2012b).

Table 1.1 Signalling events involving PI3K C2β

Cell Line	**Function**	**Reference**
HEK293	The C-terminus C2 domain was shown to negatively regulate catalytic activity by competitively binding substrate. PI3K C2β was found not to bind with either the class I p85α regulatory subunit or GTP-bound Ras.	(Arcaro et al., 1998)
LNCaP, HEK293, A431	PI3K C2β was shown to bind to Grb2 and Shc. Binding of Grb2 was via the proline rich domain and increased PI3K C2β catalytic activity.	(Wheeler and Domin, 2001)
A431	PI3K C2β and C2α were found to be activated by EGF, and were shown to co-IP with the EGFR and ErbB-2.	(Arcaro et al., 2000)
Hela , SKOV-3, COS7	LPA was shown to activate PI3K C2β and knockdown inhibited LPA dependent migration.	(Maffucci, 2005)
A431 cells, HEK293, NIH-3T3	PI3K C2β was shown to interact with clathrin at the N-terminus and catalytic activity was increased.	(Wheeler and Domin, 2006)
A431 cells	Following EGF activation PI3K C2β was shown to form a complex with Abi1, Eps8 and SOS, regulating Rac activity. This resulted in increased motility and cytoskeleton reorganisation	(Katso et al., 2006)
Neuroblastoma cells, primary cortical neurons	ITSN1 was found to interact with PI3K C2β via the proline rich domain, increasing kinase activity and Akt signalling. Loss of ITSN1 increased apoptosis, independently of its role in vesicle trafficking.	(Das et al., 2007)
HEK293 cells	PI3K C2β translocates to the nuclear matrix following EGF activation, by way of a nuclear localization signal within the C-terminus C2 domain.	(Banfic et al., 2009)
EC9706 , EC-1, Eca109 and Eca109	Knockdown of PI3K C2β increased sensitivity to cisplatin mediated apoptosis. Possibly by interrupting the Akt pathway. Examination of patient samples appeared to show a correlation between PI3K C2β and metastasis.	(Liu et al., 2011a)
NIH3T3 cells	PI3K C2β was shown to form a complex with Grb2 and Dbl and was also shown to co-IP with Grb2 and Src.	(Błajecka et al., 2012)
COS7 cells	PI3K C2β is shown to bind to Ras in its nucleotide free form, preventing GTP loading and activation. This reveals a potential role in negative regulation.	(Wong et al., 2012)
HUVEC	PI3K C2β involvement in S1P dependent migration was demonstrated.	(Tibolla et al., 2013)

LNCaP prostate cancer cell line; **HEK293** human embryonic kidney cells; **A431** epithelial carcinoma cells; **Hela** cervical epithelial cancer cells; **SKOV-3** ovarian epithelial cancer cells, **COS7** kidney fibroblasts from African green monkey; **NIH-3T3** murine embryonic kidney cells; **EC9706 , EC-1, Eca109 , Eca109** oesophageal squamous cell carcinoma cell lines; **Co-IP** co-immunoprecipitation; **LPA** Lysophosphatidic acid; **EGF** epidermal growth factor; **EGFR** epidermal growth factor receptor; **S1P** sphingosine-1-phophsphate; **ITSN** intersectin.

1.2.5 PI3K C2β in the immune system

Class I PI3Ks are known to play an important role in the immune system, in particular PI3Kδ and PI3Kγ are both highly expressed in leukocytes, and the involvement of p110β has also been recognised (Blunt and Ward, 2012). Their dysregulation has been observed in many immune related disorders and as such the function and regulation of the class I PI3Ks have been extensively studied, which has recently led to the first FDA approved inhibitor targeting p110δ (Okkenhaug et al., 2014).

Until recently the role of PI3K C2β has received little attention. However, studies have identified several signalling pathways in which PI3K C2β plays a regulatory role, including a potential function within the immune system (**Figure 1.4**). A role for PI3K C2β has been described in human T lymphocytes (T-cells) involving regulation of calcium influx by regulating the calcium (Ca^{2+}) activated potassium (K^{+}) channel KCa3.1. PI3K C2β is recruited to the T-cell receptor (TCR), following activation, which leads to PI3P synthesis and stimulation of KCa.3.1 via nucleoside diphosphate kinase B (NDPK-B), the efflux of K+ ensures a negative membrane potential which allows extracellular Ca^{2+} to enter the cell (Srivastava et al., 2009). Increased intracellular Ca2+ is required for effective T-cell activation. KCa3.1 mediated Ca^{2+} entry is negatively regulated by tripartite motif containing protein 27 (TRIM27). TRIM27 ubiquinates PI3K C2β which inhibits the production of PI3P. In the absence of PI3P, NDPK-B is unable to activate KCa3.1 (Cai et al., 2011). Due to differences in KCa3.1 expression between T-cell subsets, this

method of TCR activation affects type 1 helper T-cells (Th1) and type 2 helper T-cells (Th2), whereas type 17 helper T-cells (Th17) and regulatory T-cells (Tregs) are unaffected (Ohya and Imaizumi, 2014).

In addition, Ca^{2+} regulation by PI3K C2β and TRIM27 has also been observed in primary murine bone marrow derived mast cells (BMMCs) via the activation of the high affinity IgE receptor FcεRI. In mast cells activation of the FcεR1 leads to the release of cytokines, proteases and histamine, it also induces the synthesis of additional cytokines. Knockdown of PI3K C2β in BMMCs using siRNA resulted in a reduction in mRNA for interleukin 6 (IL-6), IL-13 and tumour necrosis factor 6 (TNFα). Conversely, mRNA from these cytokines were upregulated in BMMCs from TRIM27$^{-/-}$ mice (Srivastava et al., 2012). While blocking KCa3.1 in T-cells and mast cells appears to negatively regulate activation, in human natural killer (NK) cells inhibition of KCa3.1 increases their cytotoxicity and proliferation which has been shown to increase their ability to kill tumour cells (Koshy et al., 2013). As dysregulation of Ca^{2+} signalling through KCa3.1 is implicated in various pathologies including multiple sclerosis, rheumatoid arthritis, atherosclerosis, asthma and transplant rejection, identifying mechanisms of activation would be of interest (Ohya and Imaizumi, 2014).

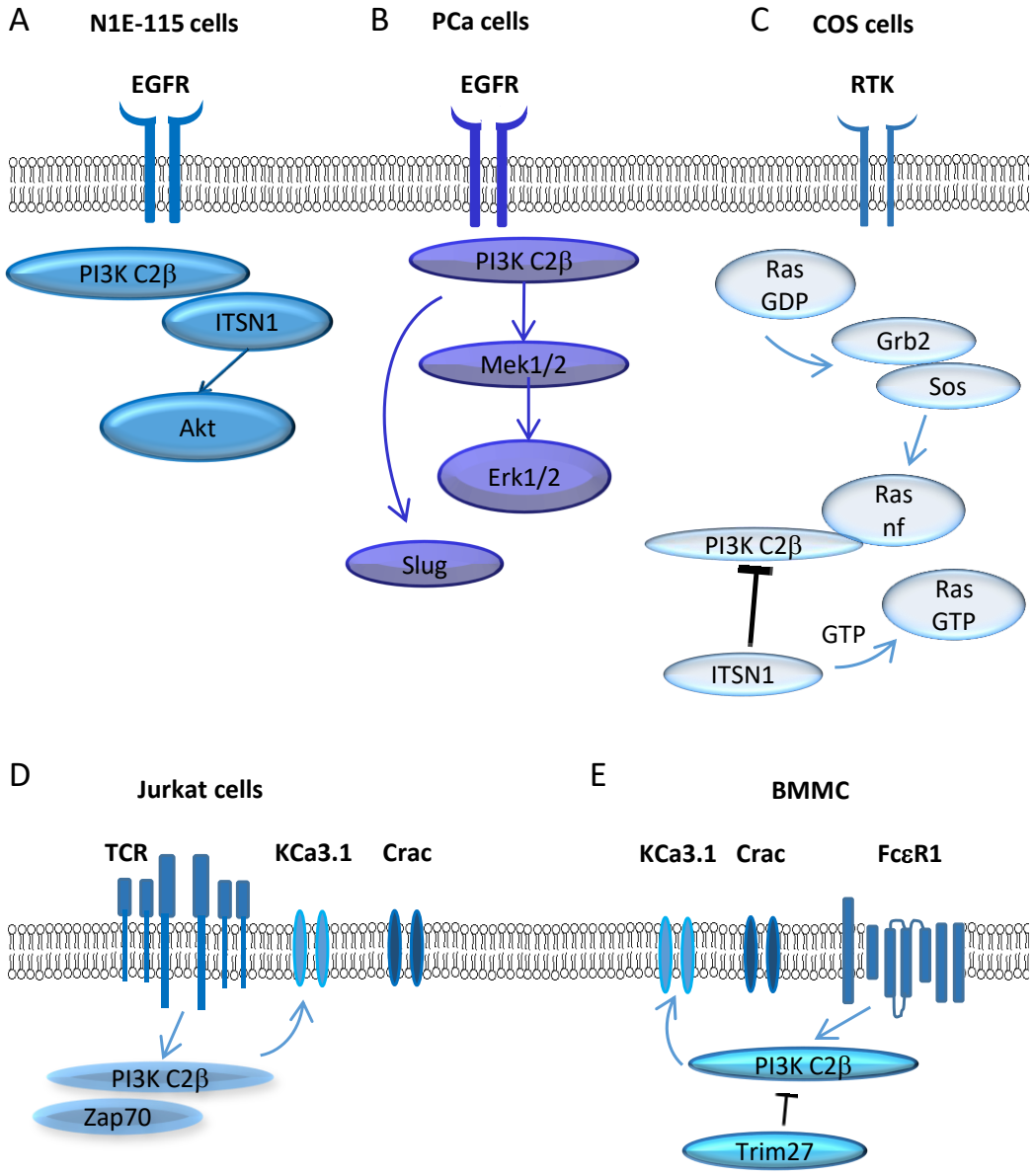

Figure 1.4 Schematic of potential ways in which PI3K C2β influences cell function. **A**; following activation via the EGFR, PI3K C2β was shown to interact with ITSN1. The binding of ITSN1 was shown to increase the lipid kinase activity of PI3K C2β, resulting in increased AKT activation. This pathway was shown to regulate survival of N1E-115 (neuronal) cells (Das et al., 2007). **B**; Activation of PI3K C2β via the EGFR was shown to activate MEK1/2 and ERK1/2, which contributed to cell migration in a prostate cancer cell line. Following inhibition of PI3K C2β, downregulation of the transcription factor Slug was observed which was independent of MEK / ERK activation. The reduction of Slug was found to inhibit cell invasion (Mavrommati et al., 2016). **C**; the Grb2/Sos complex causes GDP to disassociate from Ras, PI3K C2β was shown to bind to nucleotide free (nf) Ras competitively, preventing nf Ras binding GTP. This is believed to stabilize nf Ras, preventing GTP binding and activating Ras. Binding of ITSN1 with the PI3K C2β/nf Ras complex, releases nf Ras allowing GTP to bind with Ras. Activated Ras is then able to recruit effector molecules, activating downstream signalling pathways (Wong et al., 2012a). **D**; In T-cells, activation via the T-cell receptor (TCR) leads to up regulation of KCa3.1 and increased channel activity. Knockdown of PI3K C2β resulted in a reduction of KCa3.1 mediated Ca2+ influx. PI3K C2β was shown to co-localise with Zap70 and the TCR at the immunological synapse. It is suggested that PI3K C2β is required for full activation of KCa3.1 channels and activation of NFAT signalling pathways (Srivastava et al., 2009). **E**; Activation of FceR1 results in Ca2+ influx followed by degranulation in mast cells. PI3K C2β was found to be necessary for activation of KCa3.1. Trim27 was shown to negatively regulate this process (Srivastava et al., 2012).

1.3 The Spleen

The spleen is a secondary lymphoid organ and is located within the abdominal cavity, underneath the diaphragm in mice and humans. It has an unusual structure and complex vasculature, consisting of both open and closed circulation, which are essential for its primary functions; blood filtration and immunity. In addition to red blood cells, it contains immune cells from both the innate and adaptive immune systems (Mebius and Kraal, 2005).

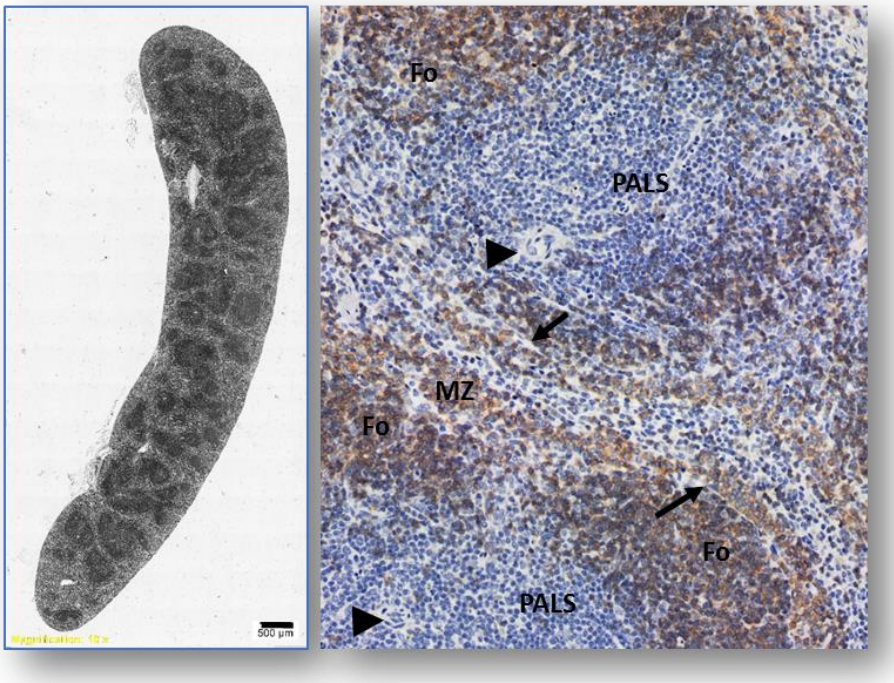

Figure 1.5 Mouse spleen. A; section from a mouse spleen showing areas of white pulp (WP) and red pulp (RP). Original magnification 10x. Length bar represents 500µm. B; section of mouse spleen stained with anti-B220 (brown), to identify the B-cell rich follicles (Fo), the periarterial lymphoid sheaths (PALS) contain predominantly T-cells. The marginal zone (MZ) separates the white pulp from the red pulp. Arrowheads show the central arteries. Arrows highlight the marginal sinus that separates the white pulp from the marginal zone. Original magnification 10x, section counter stained with haematoxylin.

Blood enters the spleen via the splenic artery, which branches off ending up as central arterioles. Lymphoid tissue surrounds the central arterioles, referred to as the white pulp (WP). Some of these arterioles branch off

further, supplying nutrients to the WP, others terminate within the marginal sinus. Arterioles that do not terminate within the WP continue into the red pulp (RP) becoming penicillar arteries and finally arterial capillaries which terminate in the RP. The RP has a largely open circulation and blood from the arterial capillaries empties into a sponge-like mesh, which is made up of reticular fibres, reticular cells and splenic cords (sometimes referred to as the cords of Billroth). Red blood cells (RBCs) and other circulating cells filter through this network and eventually re-enter the circulation via the sinusoids, which lead to the trabecular vein before leaving the spleen (Cesta, 2006).

1.3.1 Marginal Zone (MZ)

In mice, the MZ forms a ring around areas of WP and is separated from the lymphoid tissue by the marginal sinus. Blood from the circulation empties into the marginal sinus, before migrating towards the RP, making cells within the MZ the first line of defence against blood borne pathogens. The MZ provides an important link between innate and adaptive immunity. The MZ is populated predominantly by non-circulatory B-cells, macrophages (metalophillic and MZ) and dendritic cells (Cesta, 2006; den Haan and Kraal, 2012). MZ B-cells are specialized in T-cell independent responses, in part, by recognising particular molecular patterns (PAMPs) that are often associated with bacteria and viruses. Interaction with such antigens causes the B-cell to become activated resulting in proliferation, cytokine production and the excretion of antibodies (typically IgM) (Tsolaki, 2011). In addition to phagocytosing bacteria and viruses, macrophages gathered at the marginal

sinus play an important role in clearing apoptotic cells, as they arrive from the circulation. Disruption of this function has led to the development of autoimmune disorders in both mice and humans. High concentrations of cellular antigen can lead to a loss of self-tolerance and the production of autoantibodies (den Haan and Kraal, 2012). Dendritic cells specialize in antigen presentation and a population of MZ dendritic cells have been shown to be efficient at presenting to B-cells in addition their usual target, naïve T-cells (Chappell et al., 2012).

1.3.2 Periarteriolar Lymphoid Sheaths (PALS)

The PALS form around the central artery, the inner PALS are predominantly made up of CD4+ T-cells, CD8+ T-cells (also referred to as cytotoxic T-cells or CTLs) are also present but in fewer numbers and interdigitating dendritic cells which present antigen to naïve T-cells (Cesta, 2006). The outer PALS contain a mixture of T-cells and migrating B-Cells passing through from the MZ to the follicles (Steiniger et al., 2005). The outer PALS also contain populations of dendritic cells that have migrated from the MZ to present antigen to T-cells. It is also thought that some macrophage populations may also activate T-cells via antigen presentation (den Haan and Kraal, 2012).

1.3.3 Follicles

The predominant population of cells within the follicles are re-circulating B cells. B-cells leaving the circulation pass through the MZ and PALS and into the follicles, during this migration they interact with antigen presenting dendritic cells. If they are exposed to antigen that is specific to their B-cell

receptor (BCR), they are retained within the follicle where they proliferate and initiate a germinal centre reaction, which is the major source of long lived antibody secreting plasma cells and memory B-cells. Follicles that contain a germinal centre are known as secondary follicles. Germinal centres are only generated in response to a B-cell interacting with its cognate antigen, they are transient structures and disappear once the immunological challenge has been eliminated (Steiniger, 2005). In addition to B-cells and dendritic cells, there are populations of CD4+ T-cells and specialized tingible body macrophages whose function is to clear apoptotic B-cells. This is particularly important during the germinal centre reaction, when there are high numbers of proliferating B-cells. Many of these B-cells undergo apoptosis if they fail to produce a high affinity antigen receptor. Clearance of these cells prevents the release of potential self-antigen and autoreactive B-cells into the periphery (den Haan and Kraal, 2012).

1.3.4 Red Pulp

Within the open circulation of the red pulp (RP), dead and dying red blood cells (RBCs) get caught in the splenic cords, where they are phagocytosed by strategically placed RP macrophages (Cesta, 2006). In addition to maintaining the RBC population, RP macrophages are essential for iron metabolism and recycling (den Haan and Kraal, 2012). There is also a large reservoir of monocytes in the RP, where they reside until recruitment in response to acute inflammation. Although more typical in young animals, extra medullary haematopoiesis (EMH) is not uncommon in the rodent spleen (Suttie, 2006), as such the RP may also contain a variety of erythroid,

myeloid, and megakaryocytic cells (Cesta, 2006). Plasmablasts dependent on dendritic cells for survival are also located in the RP, as are differentiated long lived plasma cells, it is thought that this positioning in the spleen allows easy access to the circulation (den Haan and Kraal, 2012; Mebius and Kraal, 2005).

1.3.5 Micro-environment of the spleen

In addition to the physical structure of the spleen, cellular compartmentalization and function of the splenic environment is largely governed by the milieu of cytokines and their complex interactions. These chemical messengers ensure correct localization to allow function, they regulate cell differentiation and can modulate the expression of the receptors required to mediate an appropriate cellular response (Lund, 2008; Stein and Nombela-Arrieta, 2005; Steiniger and Barth, 1999). Chemotaxis is mediated by chemokines and select bio-active molecules such as sphingosine-1-phosphate (S1P). Within the germinal centres of the spleen (**Section 1.8**), for example, by modulating the expression of the chemokine receptors CXCR4 and CXCR5 B-cells shuttle between the dark zone, in response to CXCL12, and the light zone, in response to CXCL13 (Allen et al., 2004). This allows germinal centre B-cells to interact with follicular helper T-cells (Tfh) and receive the appropriate signals to maintain the germinal centre reaction (Gitlin et al., 2014). The lymphocyte response to S1P within the spleen is primarily regulated by the expression of the S1P receptors S1P1, S1P2 and S1P3. T-cells in the spleen predominantly express S1P1 (M Graeler and E J Goetzl, 2002), while, depending on their function

and location B-cells can express any of the S1P receptors (Cinamon et al., 2004; Green et al., 2011).

The concentration gradient of S1P differs between splenic compartments and also between the spleen and the periphery (Sic et al., 2014). As such, S1P1 expression allows lymphocytes to leave lymphoid organs where S1P concentrations are low, and enter the circulation (Maceyka et al., 2012; Stein and Nombela-Arrieta, 2005). Within the spleen, expression of S1P2 retains GC B-cells within the germinal centre, by inhibiting the response to chemoattractants produced in follicles (Green et al., 2011). The expression of S1P1 and S1P3 are required for the correct localization of MZ B-cells (Steiniger, 2015).

In addition to directing cells to the correct location, a myriad of cytokines modulate the cellular responses. For the purpose of this thesis, cytokines affecting the lymphocyte populations within the spleen GCs and follicles will be discussed. Cellular function is closely linked to the cytokines they produce, and as such lymphocyte subsets are often distinguished by their cytokine expression profile. Frequently cytokines are characterized as either pro-inflammatory or anti-inflammatory, although this would appear to be a broad generalization as many cytokines mediate various responses (Raphael et al., 2014). The combination of cytokines produced, and the relative level of expression also determines the effect on the cellular environment. **Table 1.2** provides a non-exhaustive list of cytokines within the spleen, the cells that produce them and the associated physiological effect.

Table 1.2 Selection of cytokines within the spleen

Cytokine	Sources	Known functions	References
TGF-β	Breg, Tregs	Suppression of the immune response	(Lund, 2008)
IFNα	pDC	Induces S1P1 activity, induction of GCs, induces BAFF production	(Mountz et al., 2011) (Vincent et al., 2013)
IFNγ	Be-1, Fo B-cells, Th1, Th17	Increases expression of TLRs, , B-cell CSR to IgG, upregulation of MHCI and MHCII on APCs, suppression of Th17 differentiation	(Raphael et al., 2014)
TNFα	Be-1, Be-2, memory B-cells, Th1	Formation of B-cell follicles, TD antibody responses	(Lund, 2008) (Raphael et al., 2014)
BLys (BAFF)	Tfh, monocytes	Selection of high affinity GC B-cells, promotes B-cell survival	(Goenka et al., 2014) (Vincent et al., 2013)
APRIL	Moncocytes/ macrophages, DCs	Lymphocyte proliferation, promotes TI response	(Medema et al., 2003)
LTα	Memory B-cells, ILCs	Formation of B-cell follicles, DC development	(Lund, 2008) (Magri et al., 2014)
IL2	Be-2, Th1	Induces Th2 differentiation	(Lund, 2008) (Raphael et al., 2014)
IL-4	Be2, Th2, Tfh	GC response, B-cell CSR to IgG/IgE, B and T-cell survival, Induces PC and Th2 differentiation	(Mountz et al., 2011) (Raphael et al., 2014)
IL-5	Th2	TD antibody responses	(Raphael et al., 2014)
IL-6	Be2, DC, monocytes, MZ B-cells	Induces Th17, Tfh and B-cell differentiation	(Lund, 2008) (Mountz et al., 2011) (Eto et al., 2011)
IL-10	B-reg, MZ B-cells, T2 B-cells, Fo B-cells, Th17, Tregs	Suppression of immune response	(Lund, 2008) (Raphael et al. 2014)
IL-12	Be2, memory B-cells, Th2	Induces Th1 differentiation	(Lund, 2008) (Raphael et al., 2014)
IL-13	Be2, Th2, DC, Tregs	Humoral immune response	(Lund, 2008) (Raphael et al., 2014)
IL-17	Th17, Tfh	Increased ICAM-1	(Raphael et al., 2014)
IL-21	Tfh, Th17	GC response, induces Tfh and PC differentiation	(Mountz et al., 2011) (Raphael et al., 2014) (Eto et al., 2011)
IL-23	ILCs, DCs, macrophages,	Induces Th17 differentiation	(Raphael et al., 2014) (Magri et al., 2014)

DC dendtric cells; **pDC** plasmacytoid dendritc cell; **GC** germinal centre**; Breg** regulatory B-cells; **Be-1** type 1 effector B-cells; **Be2** type 2 effector B-cells; **MZ** marginal zone; **T2** transitional type 2 B-cells; **LT** lymphotoxin; **Fo B-cell** Follicular B-cells; **ICAM** intracellular adhesion molecule; **TLR** toll-like receptors; **MHC** major histocompatibility complex; **CSR** class switch recombination; **TD** T-cell dependent, **Th** helper T-cells, **Treg** regulatory T-cell, **ILC** innate lymphoid cell; **APC** antigen presenting cell; **BLys** B lymphocyte stimulator; **BAFF** B cell activation factor; **APRIL** a proliferation inducing ligand; **TI** T-cell independent.

T-cells to develop over the course of approximately three weeks (**Figure 1.6**). There are two T-cell lineages that develop from these precursors; a small population of γδ T-cells and the major population which are αβ T-cells. These distinctions are based on the development of different types of T-cell receptor (TCR). Interaction with stromal cells within the thymus stimulates development and commitment to the T-cell lineage. Initially, T-cells do not express a TCR or either of the co-receptors associated with mature T-cells (CD4 and CD8), they express CD44, and are referred to as double negative, stage 1 (DN1). As cells move to stage 2 (DN2), they also express CD25 and begin gene rearrangement of the diverse β (Dβ) and joining β (Jβ) loci. Rearrangement of variable β (Vβ) and diverse-joining β (DJβ) indicates that the T-cell has progressed to DN3. CD44 is downregulated and cells that have failed to produce a successfully rearranged β-chain are arrested in DN3 and eventually undergo apoptosis. CD25 and CD44 expression is lost and the successfully rearranged β-chain is expressed in addition to a surrogate α-chain, which with CD3 makes up the pre-T-cell receptor. The expression of the pre-TCR marks the transition to DN4 and further rearrangement of the β-chain is stopped. Gene rearrangement and expression of CD4 and CD8 is followed by proliferation, which produces the double positive (DP) population (CD4+ and CD8+). DP cells undergo positive and negative selection at this point, and approximately 98% fail to transition to single positive CD4 or CD8 T-cells. T-cells that survive the selection process rearrange the α-chain, after which a functioning TCR is expressed and T-cells lose expression of either the CD4 or CD8 co-receptor. Commitment to either

CD4 or CD8 expression is determined as part of the selection process, depending on whether T-cells interact with major histocompatibility complex class one (MHC I), or MHC II (Janeway et al, 2001).

Following expression of a functional TCR and single co-receptor, T-cells upregulate expression of S1P1 (Section 1.3.5) and migrate to secondary lymphoid organs, such as the spleen (Chen, 2004; Weinreich and Hogquist, 2008)

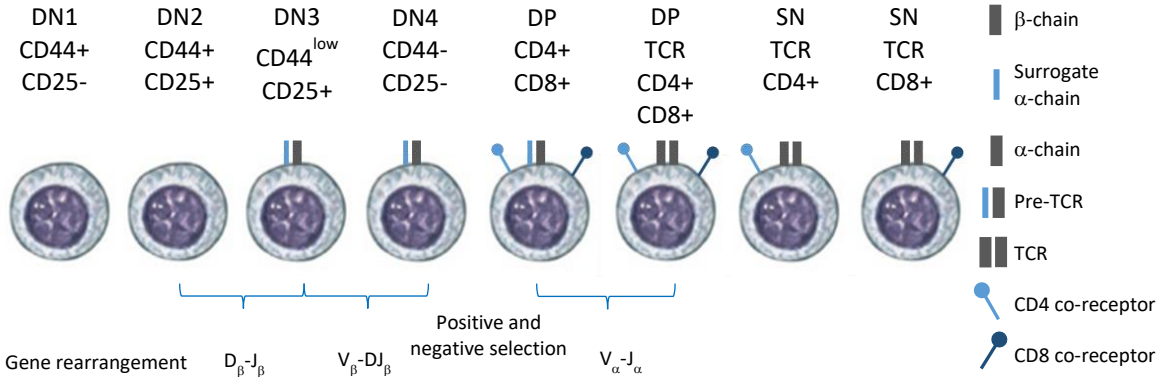

Figure 1.6 T-cell development in the thymus. T-cell precursors arrive in the thymus from the bone marrow and develop into functioning T-cells over approximately three weeks. The developmental stages are shown with gene rearrangements to produce a functioning T-cell receptor (TCR) and a single co-receptor. **DN** double negative; **DP** double positive; **SN** single negative. Adapted from Parham (2014).

The predominant population of naïve T-cells entering the spleen are CD4+ and upon arrival they home to the PALS (**Section 1.3.2**), in response to chemokines CCL19 and CCL21 produced by stromal cells and also dendritic cells. Subsequent interactions with accessory cells and the local cytokines produced leads to differentiation into specific subsets, thereby governing their function (Mebius and Kraal, 2005). Naïve T-cells survive in the periphery in response to low affinity TCR interactions, until they are

activated. For T-cell activation, antigen presenting cells (APCs) expressing the co-stimulatory molecules CD80 and CD86 (B7.1 and B7.2) are required to present antigen displayed on MHC I (CD8+ T-cells) or MHC II (CD4+ T-cells). Activation results in proliferation and differentiation into an effector subset (Broere et al., 2011). Development of these subsets is carefully regulated by cytokines and cell to cell interactions within the local environment to maintain a balance, loss of homeostasis is associated with immune pathologies such as chronic inflammation and autoimmunity (Zhu and Paul, 2015).

1.4.1 T-cell subsets

Although there are additional subsets, the principle CD4+ subsets in the spleen are helper T-cell type 1 (Th1), helper T-cell type 2 (Th2), helper T-cell type 17 (Th17), follicular T-cell helper (Tfh) and regulatory T-cells (Tregs) (**Table 1.3**).

1.4.2 Type 1 and type 2 helper T-cells

Differentiation from a naïve T-cell into a Th1 or Th2 cell is dependent on whether they are required for a type 1 or type 2 immune response. Type one responses are associated with infection that require pathogens to be cleared from the system, while a type two response occurs in response to infection by large pathogens that cannot be cleared by phagocytosis. Although a type one response will result in antibody production, the type two function is to generate a robust humoral response. Factors that determine which subset is produced are predominantly governed by the

cytokines in the local environment (**Table 1.2**). High levels of IL-12 produced by innate immune cells in response to bacteria, in addition to IFN-γ and IL-2 will induce Th1 differentiation. Th1 cells, in turn, secrete IFN-γ which stimulates phagocytosis, intracellular killing by innate immune cells. They also induce upregulation of MHC I and MHC II on other cell types, which are required for antigen presentation to T-cells thereby maintaining the response. Both naïve and Th1 can differentiate into Th2 cells in response to IL-4, IL-25 and IL-33. Secretion of IL-4, IL-12, and IL-13 by Th2 cells induces B-cell proliferation and antibody production. In particular Th2 cells are associated with inducing IgG and IgE production in B-cells (Spellberg and Edwards, 2001).

1.4.3 Type 17 helper T-cells

The Th17 subset is a more recent discovery and are so named due to their production of IL-17. IL-17 is a family of six cytokines, two of which are known to be produced by Th17 cells; IL-17A and IL-17F. Although they play an important role in protection from bacterial and fungal pathogens, they are implicated in a range of immune pathologies (Raphael et al., 2014). Cytokines known to induce Th17 differentiation include IL-23, transforming growth factor-β (TGF-β), IL-21 and IL-6 and in response, Th17 cells produce IL-17A, IL-17F, IL-21, IL-22, TNF-α, IL-9, IL-10, IFN-γ (Singh et al., 2014). Although Th17 cells are largely associated with pathogenic outcomes, production of the anti-inflammatory cytokine IL-10 indicates that they may also have the ability to reduce inflammation. The pathogenic role of the Th17 subset is partly attributed to a positive feed-back loop in which innate

immune cells are recruited to the area in response to cytokines released by Th17 cells, they then release cytokines that induce increased cytokine production by Th17 cells. This scenario leads to tissue damage and further exacerbates the inflammatory response (Raphael et al., 2014).

1.4.4 Regulatory T-cells

At least two types of Treg have been identified, natural Tregs (nTreg), which develop in the thymus as a distinct lineage and upon entering the periphery their role is to suppress auto-reactive T-cells. Inducible Tregs (iTreg), leave the thymus as naïve T-cells and differentiate into iTregs in response to TGF-β. Their role is to suppress the immune response and regulate inflammation by producing cytokines such as TGF-β and IL-10 (Noack and Miossec, 2014). IL-10 has been shown to act on antigen presenting cells (APCs) by causing them to down regulate MHC II and the co-stimulatory molecules CD80 and CD86, which reduces their ability to activate CD4+ T-cells via antigen presentation. IL-17 production, associated with Th17 cells is suppressed by TGF-β (Raphael et al., 2014). As such, iTregs are believed to have a function in counteracting Th17 mediated diseases (Noack and Miossec, 2014).

1.4.5 Follicular helper T-cells (Tfh)

Follicular helper T-cells are involved in initiating and regulating the B-cell germinal centre reaction. The induction of Tfh differentiation is still subject to investigation, but it is thought to be dependent on interactions with dendritic cells. Cytokines produced by dendritic cells vary depending the nature of antigen encountered and the subset, which is also thought to be

important. For example IL-6 leads to expression of the cytokine receptor CXCR5, which allows homing to the germinal centre (Ballesteros-Tato and Randall, 2014; Yu and Vinuesa, 2010).

Table 1.3 T-cell subsets

Subset + markers	Factors promoting differentiation	Cytokine production	Effects
Th1	IFN-y, IL-2, IL-12, strong TCR signals	IFN-y, TNF	Pro-inflammatory Increased TLR expression, B-cell CSR to IgG, increased MHCI and MHCII antigen presentation
Th2	IL-4, IL-25, IL-33	IL-4, IL-12, IL-13	Anti-inflammatory Defence against parasites, B-cell CSR to IgG1 and IgE, suppression of Th1 differentiation
Th17	IL-23, TGF-b, IL-21, IL-6	IL-17, IL-10, IFN-y	Pro-inflammatory and anti-inflammatory GC induction, enhances PC differentiation, reduces B-cell apoptosis
T-regs	TGF-β	TGF-b, IL-10	Anti-inflammatory Down regulates MHCII and co-stimulatory molecules on APCs, activates B-cells, inhibit IL-17 production, may suppress allergic responses mediated by Th2, enhances PC differentiation.
Tfh	IL-21, IL-6 possibly IL-12	IL-21, IL-4	Initiating and regulating the GC reaction. Positive selection of proliferating B-cells.

(Raphael et al. 2014; Yu & Vinuesa 2010; Ballesteros-Tato & Randall 2014)

1.5 B-cells

B-cells have a diverse range of functions within the immune system, although they are most well-known for providing immunological memory as memory B-cells, and also the production of highly specific antibodies, as differentiated plasma cells. Following development in the bone marrow and migration into secondary lymphoid organs such as the spleen, they continue

to differentiate in response to their environment. Differentiation into one of the B-cell subsets, is associated with changes in cytokine profile, expression of surface markers and specific effector or regulatory functions (Allman and Pillai, 2008; Lund, 2008).

1.5.1 B-cell development and the B-cell receptor

The pro-B-cell is the earliest cell of the B-lineage within the bone marrow (**Figure 1.7**) and is defined by gene rearrangement of the immunoglobulin heavy chain (IgH). Gene rearrangement occurs following the induction of the variable (V), diversity (D), joining (J) recombinases known as RAG-1 and RAG-2 (recombination activating gene).

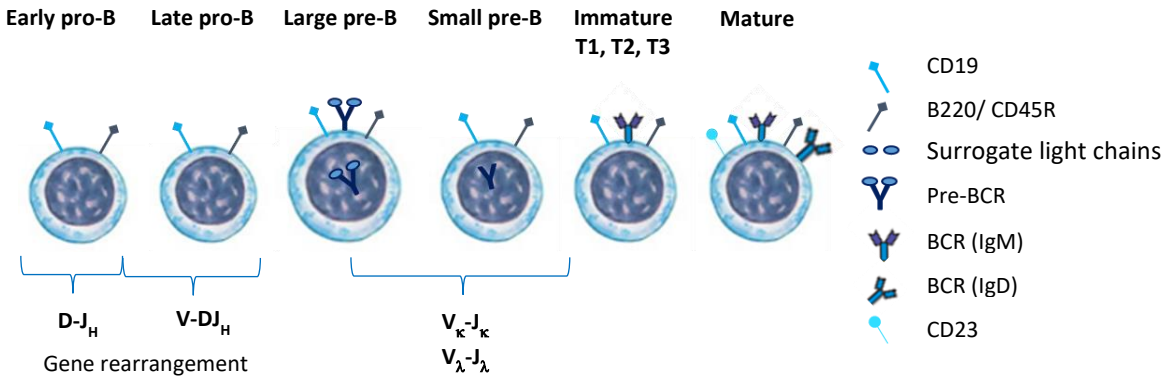

Figure 1.7 B-cell development. B-cells are produced in the bone marrow and undergo a series of developmental stages, including gene rearrangement of the B-cell receptor (BCR) to produce an antigen receptor with unique specificity. Upon expression of a functional BCR, immature B-cells enter the periphery and migrate to secondary lymphoid organs such as the spleen as immature transitional (T) B-cells. There are three stages of transition; T1, T2 and T3. Adapted from Parham (2014).

Successful V (D) J recombination results in the expression of the μ heavy chain which signals the B-cell to produce a pre-B-cell receptor (pre-BCR), if IgHμ is not produced the pro-B-cell undergoes apoptosis (negative selection).

In addition to the IgH-μ, assembly of the pre-BCR involves production of surrogate light chains (λ5 and VpreB) and Igα (CD79α) and Igβ (CD79β). Expression of the pre-BCR signifies the B-cells' transition into a large pro-B-cell, and it undergoes proliferation before transitioning into a small pre B-cell. Rearrangement of the light chain occurs following re-expression of the RAG proteins, which results in each of the clones having a different antigen specificity due the variation in light chain rearrangement. The rearranged light chains, Igα and Igβ assemble with IgHμ to form the BCR, which is a membrane bound IgM. The expression of membrane bound IgM signifies the transition from late pre-B-cell to immature B-cell. (Janeway et al., 2001).

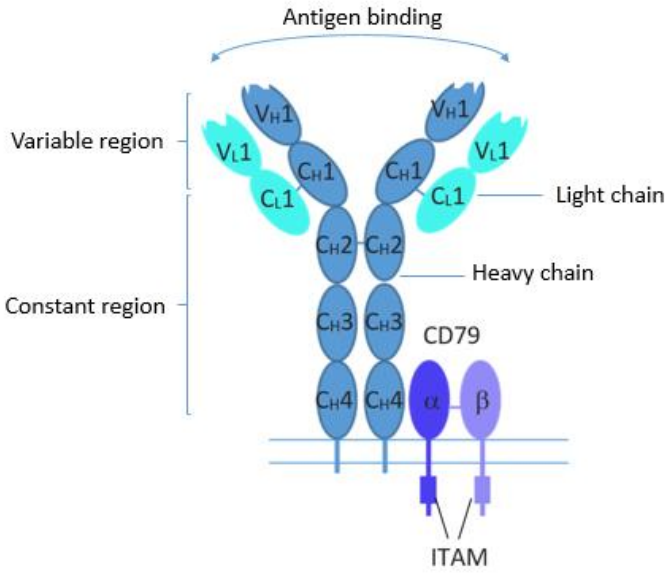

Figure 1.8 Schematic of the mature BCR. Following V (D) J rearrangement of heavy chain, rearrangement of the light chain and production of Igα and Igβ, the mature B-cell antigen assembled and expressed of the cell surface. Adapted from Berry et al (2011).

1.5.2 Selection of immature B-cells

The diversity of the BCR created by random gene arrangements during BCR development increases the number of pathogenic antigens recognised with

extreme specificity, allowing an effective immune response to occur. However, it also has the potential to create a BCR that recognises self-antigens, thereby triggering an inappropriate response as seen in autoimmune diseases (Ireland et al., 2012; Montes et al., 2007; Vossenkämper et al., 2012). Therefore, before being released into the periphery, immature B-cells are subject to rigorous positive and negative selection processes. To maintain self-tolerance, immature B-cells that recognise self-antigens can be directed to undergo apoptosis, known as clonal deletion (Chung et al., 2003). If self-antigen binding to the BCR is weak the B-cell can be rescued by a process known as receptor editing, which involves additional rearrangement of the light chain, providing an opportunity to produce a BCR that no longer recognises self-antigen (Edry and Melamed, 2004). Evidence of receptor editing, by identifying secondary rearrangements in the light chain locus, have been observed in more than half of immature B-cells within the bone marrow (Melchers, 2006). B-cells can also be rendered anergic following recognition of self-antigen, which renders the cell unable to respond to activation via antigen binding (Sandel and Monroe, 1999). Anergic B-cells have a reduced lifespan, and altered signalling that results in arrested development, therefore minimising the risk of releasing autoreactive cells into the periphery (Merrell et al., 2006).

Immature B-cells also undergo positive selection to allow them to continue differentiating. This involves the BCR providing low level, antigen independent survival signals. However, in order to generate these 'tonic'

survival signals, the BCR must be expressed at sufficient levels. Failure to express a sufficient number of BCRs to provide 'tonic' signalling results in arrested differentiation and apoptosis (Pelanda and Torres, 2012).

1.5.3 Immature transitional B-cells

Following the expression of functional BCR and survival of initial selection processes in the bone marrow, immature B-cells migrate towards the spleen to continue the maturation process (Carsetti et al., 1995; Loder et al., 1999) B-cell maturation in the periphery is typically described as a sequential process. Immature B-cells arrive in the spleen from the bone marrow as Transitional 1 (T1) where they reside in the red pulp before developing into Transitional 2 (T2) B-cells and from T2 to mature B-cells. Transitional B-cells undergo additional negative and positive selection before maturation. In response to BCR engagement T1 B-cells are subject to negative selection, as transitional B-cells cells do not engage in receptor editing, this leads to apoptosis (Luning Prak et al., 2011; Wang et al., 2007). It is thought that T2 cells are no longer sensitive to negative selection in response to BCR engagement. However, they undergo positive selection which is thought to be regulated by B-cell activating factor (BAFF). In response to BCR engagement, T2 cells upregulate expression of the BAFF receptor (BAFF-R), in order to compete for BAFF in the local environment. Failure to upregulate BAFF-R in response to BCR engagement also leads to apoptosis (Tussiwand et al., 2012; Wang et al., 2007).

A third immature transitional stage has also been described (T3) (Allman et al., 2001). It is thought that T3 B-cells arrive in the spleen having been rendered anergic as a method of silencing autoreactivity, which suggests that T3 are not actually transitional, as they are not undergoing maturation. T3 cells have been identified in unimmunized wild type mice, which might indicate that they are a normal physiological occurrence (Cambier et al., 2007; Merrell et al., 2006), and although anergy is a method to silence autoreactivity, it has been shown to be reversible (Cambier et al., 2007). The hyporesponsive phenotype is maintained by chronic BCR engagement and can be reversed if the BCR is no longer bound to autoantigen, which under specific conditions may provide a source of self-reactive antibodies (Yarkoni et al., 2010). Studies in mice have shown that disruption of Src homology-2 (SH2)-containing inositol 5-phosphatase (SHIP-1) signalling, which is involved in maintaining anergy, leads to the production of self-reactive antibodies and development of a lupus-like autoimmune disease (O'Neill et al., 2011). In a comparative study of four different strains of lupus prone mice and four different strains of wild type mice, there was a significant reduction of T3 B-cells in the lupus prone strains (Teague et al., 2007).

1.6 B-cell markers: Cluster of differentiation (CD)

The development of monoclonal antibodies (mAb) recognising different epitopes of the same surface antigen gave rise to various names being attributed to the same molecule. The cluster of differentiation (CD) nomenclature was designed to provide clarity by grouping together mAbs

based on the antigen rather than the specific epitope (Chan et al., 1988). Although originally designed for human antigens, the CD nomenclature is also applied to mouse antigens. When a mouse antigen is identified as a human homologue it is assigned the same CD identification (Lai et al., 1998). Identification of CD markers is useful in many aspects of cell biology, but plays a particularly important role for immunophenotyping.

1.6.1 B220 (CD45R)

Alternatively spliced isoforms of the tyrosine phosphatase CD45 are expressed on cells of myeloid lineage (Loder et al., 1999). B220, also known as CD45R is the isoform expressed on the surface of B-cells, from the pre-B-cell developmental stage through to B-cell maturity (Hardy and Hayakawa, 2001). Although minor subsets of Natural Killer (NK) cells and T-cells can be B220+, it is generally considered as a pan B-cell marker.

In B-cells, B220 is primarily associated with positive regulation during BCR activation. Experiments using splenic B-cells from CD45 knock out mice revealed hyper-phosphorylation of Lyn following BCR activation. Lyn's role in negative regulation via activation of CD22 (**Sections 1.6.3 and 1.6.4**), indicates that B220 serves as a positive regulator in B-cell activation, which is further supported by the observation that overexpression of CD45 leads to inactivation of Lyn (Shrivastava et al., 2004; Zikherman et al., 2012). A potential role in B-cell development in the bone marrow was uncovered by showing that upregulation of CD45 could increase BCR signal strength leading to increased populations of immature B-cells with secondary

rearrangements of the BCR light chain (**Section 1.5.1**), suggesting that CD45 might be involved in receptor editing (Zikherman et al., 2012).

1.6.2 The CD19 complex

CD19 is a transmembrane receptor protein that controls the threshold required to induce B-cell activation (Inaoki et al., 1997; Tedder et al., 1997). CD19 expression is present on follicular DCs, however, it is predominantly found on the surface of B-cells from the pro-B stage of development until differentiation into a plasma cell (Tedder et al., 1997) and as such it is considered a pan B-cell marker (Wang et al., 2012).

CD19 has been shown to bind, internalize and present antigen to CD4+ T-cells in vivo, in doing so the co-stimulatory proteins CD80 and CD86 (also known as B7.1 and B7.2, respectively) are upregulated ensuring effective CD4+ T-cell activation (Yan et al., 2005). Although CD19 has been shown to elicit other independent functions (Chung et al., 2012; Hampel et al., 2011), its role is typically associated as part of a larger complex that can associate with the BCR.

The CD19/CD21 complex, as it is frequently known, includes CD21, (complement receptor 2), CD225 known as Leu-13 or IFITM (Interferon-induced transmembrane protein) and CD81, which is also referred to as TAPA1 (target of the anti-proliferative antibody 1). As CD81 and CD225 are found in a complex in several cell types, it is thought that the presence of additional signalling proteins, such as CD19 produce lineage specific signalling effects (Tedder et al., 1997).

CD19 activity is regulated by phosphorylation of tyrosine residues within the cytoplasmic tail. Of the nine tyrosine residues (Y), differential phosphorylation of three particular residues (CD19-Y513, CD19-Y482 and CD19-Y391) have been shown to be important for regulating CD19 function. The location of CD19, either within or outside of lipid rafts has also been shown to impact on the phosphorylation profile (Ishiura et al., 2010; Wang et al., 2002). Following activation, the BCR clusters within lipid rafts and CD19 has been shown to maintain the BCRs localisation and prolong the BCR signal by preventing BCR internalisation (Cherukuri et al., 2001).

CD19 regulates the response to LPS stimulation via toll-like receptor 4 (TLR4) and is attributed with production of IL-6, IL-10 and TGF-β (Iwata et al., 2009), which suggests a role in the innate immune response. Phosphorylation of CD19 following LPS stimulation, leads to the formation of a complex with the tyrosine kinase; Lyn, and Vav (Yazawa et al., 2003). It has also been suggested that this complex is constitutively expressed, and is important for regulating tonic signalling (Fujimoto et al., 1999).

The role of CD19 is typically linked to positive regulation including proliferation and increased survival (Hasegawa et al., 2001b). As such, over expression of CD19 has been shown to lead to a break in tolerance and predispose B-cells to autoantibody production (Hasegawa et al., 2001a; Inaoki et al., 1997). In addition to the production of antibodies, B-cells play an important role in T-cell activation (Yan et al., 2005), and cytokine secretion via CD19 (Fujimoto and Sato, 2007).

1.6.3 Lyn

Src family protein tyrosine kinases (SFKs) have six functional domains and share a strong structural and functional homology (Gauld and Cambier, 2004). In B-cells Lyn is constitutively associated with lipid rafts (Gupta and DeFranco, 2007) and has been shown to mediate several cell fates, including negative selection of immature transitional B-cells that exhibit a strong BCR signal, by phosphorylating Syk which activates apoptotic pathways. Independently of Syk, Lyn is also thought to induce B-cell anergy following a weak interaction with self-antigen. Lyn exerts control on positive and negative signalling following BCR activation by phosphorylating both CD19 and CD22 and a hyper-responsive phenotype has been observed in Lyn deficient B-cells (Gauld and Cambier, 2004). Negative signalling attributed to Lyn includes the phosphorylation of immunoreceptor tyrosine-based inhibition motifs (ITIMs) in negative regulatory co-receptors such as CD22 and FcyRIIB (Tsubata, 2012). In addition Lyn mediates negative regulation by phosphorylating an immunoreceptor tyrosine-based activation motif (ITAM) on CD79a (**Figure 1.8**), which although is normally associated with positive regulation, also activates the phosphatase SHIP-1. Dysregulation of this regulatory pathway has been linked to a loss of anergy, resulting in autoimmunity (O'Neill et al., 2011).

1.6.4 CD22

CD22 is a negative regulatory co-receptor of the BCR. Binding with its ligand α2, 6-linked sialic acid (2,6sia) results in the formation of homo-oligomers which are distinct from the BCR until activation. Recruitment of CD22 to the

BCR follows BCR activation at which point CD22's two cytoplasmic immunoreceptor tyrosine-based inhibition motifs (ITIMs), are phosphorylated by Lyn (Nitschke, 2014). ITIM phosphorylation leads to the recruitment of phosphatases such as Src homology 2 domain containing protein tyrosine phosphatase-1/2 (SHP-1), SHP-2 and SH-2-containing inositol phosphatase (SHIP). The resulting dephosphorylation of downstream effectors inhibits signalling pathways triggered by BCR activation (Tsubata, 2012). Targets for dephosphorylation include CD19 and Vav-1 (Walker and Smith, 2008).

Using primary splenic B-cells from wild-type mice, CD22 has been shown to co-immunoprecipitate with Grb2, in addition to SHIP and Shc. It has been proposed that CD22 acts as a scaffold to mediate docking and that the complex negatively regulates calcium influx (Poe et al., 2000). CD22 may also play a role in regulating the strength of tonic signalling by moderating the strength of the signal generated by the BCR. Although the majority of mature peripheral B-cells express CD22, expression is downregulated in germinal centre B-cells, which are proliferating and in an activated state. This is thought to be a result of stimulation via CD40 which is necessary for the T-cell dependent (TD) activation required for the induction and maintenance of the germinal centre reaction (**Section 1.8**) (Poe et al., 2012).

1.6.5 CD23

CD23 is the low affinity receptor for IgE, also known as Fc ε RII. Surface expression is absent from immature, and T1 B-cells, and with the exception

of MZ B-cells which are CD23 negative, it is expressed on mature naïve B-cells (Best et al., 1995). The differential expression of CD23 makes it useful for identifying the maturational state of B-cells. Following BCR activation, CD23 expression is briefly increased before being down-regulated until expression is lost on B-cells following class switch recombination (Rabin et al., 1992). The microenvironment has been shown to influence CD23 expression and IL-4 has been shown to upregulate CD23, whereas the presence of IFN-γ inhibits expression (Sukumar et al., 2006).

Surface CD23 is thought to negatively regulate IgE synthesis, which is supported by the observation that loss of CD23 in mice is associated with increased IgE production (Gould and Sutton, 2008). It has also been proposed that antigen/IgE complexes can be presented to naïve T-cells via surface CD23, leading to T-cell proliferation (Carlsson et al., 2007). However, more recent findings suggest that CD23+ B-cells transport the IgE/antigen complex to dendritic cells, which activate CD4+ T-cells (Henningsson et al., 2011).

While binding of surface CD23 inhibits production of IgE, soluble CD23 has been shown to both negatively and positively regulate IgE production. This appears to be due to differences in oligomerization that occur depending on how CD23 is cleaved from the cell surface (Acharya et al., 2010). Cleavage by the dust mite related protease der p1 produces a monomeric soluble CD23 which inhibits IgE synthesis (Hibbert et al., 2005) When cleaved by the metalloproteinase ADAM10 (Lemieux et al., 2007), soluble CD23 forms a

trimer, which has been found to increase IgE production (Acharya et al., 2010).

Given its potential regulation of IgE, CD23 has become a target for research into allergy and asthma (Gould and Sutton, 2008). In particular the stabilization of surface CD23, which would reduce soluble CD23 (Bowles et al., 2011).

1.6.6 Toll like receptors (TLRs)

While the highly antigen specific BCR is the key to an adaptive humoral immune response, TLRs link B-cells to the innate immune system. TLRs are a type of pattern recognition receptor (PRR) that recognise a unique molecular pattern that is typically found in a bacteria but not in the host, and individual TLRs are specific for a particular pathogen-associated molecular pattern (PAMP) (Pone et al., 2010). The range of PAMPs recognised by TLRs include polysaccharides, lipoproteins, lipids, and proteins from bacteria, viruses and parasites. In mice, lipopolysaccharide (LPS) is recognised by TLR4, and upon activation a complex is formed with the adapter protein MD2. This triggers a MyD88 dependent pathway, the complex is then internalized which triggers a second signalling pathway. Both pathways are required to activate NF-κB which results in the production of inflammatory cytokines (Kawai and Akira, 2010).

1.7 B-cell subsets in the spleen

B-cell subsets in mice are typically separated into B1 and B2. In the spleen the predominant population is B2 B-cells, which can be further separated

into transitional B-cells (**Section 1.5.3**), follicular (Fo), marginal zone (MZ) and regulatory B-cells (Bregs) (Baumgarth, 2011).

1.7.1 Follicular B-cells

Follicular B-cells (Fo) (**Section 1.3.3**) are the major population in the spleen, accounting for approximately 70% of total B-cells (Baumgarth, 2011). B-cells enter the spleen from the circulation and migrate towards the follicles in response to the chemokine CXCL13 (Shen and Fillatreau, 2015). The Fo population predominantly consists of recirculating naïve B-cells (Fillatreau et al., 2008), and are the primary population to take part in the germinal centre reaction following T-cell dependent (TD) activation. T-cell dependent activation is necessary for Fo B-cells to differentiate into either short lived plasma or long lived antibody secreting plasma cells (Lund, 2008). Fo B-cells have an interdependent relationship with follicular dendritic cells (FDCs) via production of LTα1β2, which induces FDCs to produce CXCL13 and the presence of CXCL13 results in further production of LTα1β2. Fo B-cell derived LTα1β2 is also required to support stromal cells in the T-cell rich PALS (**Section 1.3.2**), as such they play an important role in maintaining the local environment (Shen and Fillatreau, 2015).

1.7.2 Marginal zone B-cells

Due to their location, marginal zone (MZ) B-cells provide a link between innate and adaptive immunity (**Section 1.3.1**). Mouse MZ B-cells are typically non-circulating and account for between 5-10% of the splenic B-cell population (Loder et al., 1999). Although this population is non-

circulating, MZ B-cells have been shown to be highly motile and migrate between the MZ and the follicles to present antigen to FDCs (Arnon et al., 2013). Unlike Fo B-cells, MZ B-cells can be activated in a TD or a T-cell independent (TI) manner via interaction with innate antigen presenting cells, and in response are able to rapidly differentiate into antibody secreting plasmablasts (Cerutti et al., 2013). Production of IL-10 indicates that MZ B-cells have regulatory properties and recently it has been proposed that Bregs may be derived from Transitional 2 MZ precursors (T2MZP) (Lund, 2008; Mauri and Bosma, 2012).

1.7.3 Regulatory B-cells

Regulatory B-cells (Bregs) account for 1-2% of the splenic B-cell population. There may be more than one subset of regulatory B-cell, as some studies suggest that the only regulatory cytokine produced is IL-10 (Matsushita et al., 2010), while others have described the production of both IL-10 and TGF-β (Lund, 2008). Bregs have been shown to indirectly suppress T-cell activation by inhibiting antigen presentation of monocytes and dendritic cells. They have also been studied during the induction of experimental autoimmune encephalomyelitis (EAE), which is a mouse model of multiple sclerosis (MS). By suppressing the production of IFNγ and TNFα by CD4+ T-cells, disease severity was moderated (Matsushita et al., 2010). Bregs are thought to be derived from T2 marginal zone pre B-cells (T2-MZP) (Mauri and Bosma, 2012).

1.8 Germinal centre reaction

Germinal centres (GCs) are the source of long lived plasma cells that produce high affinity antibodies following class switch recombination (CSR) and somatic hypermutation (SHM) (**Section 1.8.1**), memory B-cells are also a product of the GC reaction. Within the follicles B-cells interact with a network of antigen presenting dendritic cells and upon interaction with their cognate antigen, naïve B-cells migrate to the edge of the periarterial lymphoid sheath (PALS). This area is rich in helper T-cells (Th), and interaction with Th via costimulatory molecules CD40, expressed by B-cells and CD154 (also known as CD40L) which is expressed by T-cells results in B-cell activation. At this point the B-cell can either differentiate into a short lived plasma cell outside of the follicle, or re-enter the follicle and initiate the GC reaction (Klein and Dalla-favera, 2008). It is thought that class switch recombination (CSR) is initiated at this point, following the initial B-cell-Tfh interaction (Vinuesa et al., 2009). Re- entry to the follicle is dependent on the expression of the chemokine receptor CXCR5, which is upregulated in response to Th interaction (Allen et al., 2007). In the follicle, activated B-cells undergoes rapid proliferation, cell cycle can occur in as little as 6-12 hour (Klein and Dalla-favera, 2008), and a preliminary GC can be identified approximately four days post initiation.

Following initial proliferation, B-cells migrate to the light zone (LZ) in response to the chemokine CXCL12 by upregulating the receptor CXCR4 (Klein and Dalla-favera, 2008). As they enter the LZ, interaction with FDCs

expressing integrin vascular adhesion molecule 1 (VCAM1) helps to increase contact, providing the best chance for B-cells to bind antigen (Gatto and Brink, 2010). Antigen is then presented to Tfh via MHC II. Germinal centre B-cells are highly susceptible to apoptosis following down-regulation of factors such as BCL-2, and they rely on survival signals provided by Tfh and FDCs. B-cells that fail to present antigen to Tfh undergo apoptosis in the absence of these signals (Vinuesa et al., 2009). B-cells that are most successful at binding antigen with high affinity receive survival signals and are directed back to the dark zone (DZ) to undergo SHM to produce a BCR with even higher antigen affinity, and CSR which defines antibody isotype (De Silva and Klein, 2015). This cycle of shuttling back and forth between the DZ and LZ is thought to happen repeatedly, producing B-cells with increasingly high affinity antigen receptors. It also allows successive rounds of CSR. It is currently unknown what causes cessation of the GC reaction and the release of newly differentiated plasma cells and memory cells into the circulation (De Silva and Klein, 2015; Oropallo and Cerutti, 2014). Although it is thought that modulation of the sphingosine 1-phosphate receptors may play a role (Green et al., 2011).

1.8.1 Class switch recombination (CSR) and somatic hypermutation (SHM)

CSR, also known as isotype switching involves rearrangement of the genes that encode the heavy chain constant region (CH) of the immunoglobulin, and is influenced by cytokines in the environment, such as IL-4 which produces a switch to IgG1 and IgE (Deenick et al., 2005). Murine B-cells can

switch heavy chain from Cμ to Cγ1, Cγ2a, Cγ2b, Cγ3, Cα and Cε, producing IgG1, IgG2a, IgG2b, IgA and IgE (**Figure 1.9**). Antigen specificity is unchanged, but differences in isotype allows for a broader range of effector functions to a single antigen. The process of SHM modifies the antigen binding site which requires rearrangement of the variable regions of both the immunoglobulin heavy chain (IgH) and the immunoglobulin light chain (IgL). Although these processes can occur at the same time and require activation-induced cytidine deaminase (AID), they are independent events (Chaudhuri and Alt, 2004).

Germinal centre CSR occurs in a TD manner by way of antigen engagement and CD40, which is expressed on B-cells and CD40 ligand (CD40L), expressed by Tfh (Durandy et al., 2013). However, CSR can also occur following TI activation, , which is also independent of CD40/CD40L (Castigli et al., 2005; Cerutti et al., 2013; Kim et al., 2011). This is associated with the induction of AID by the transmembrane activator and calcium-modulator and cytophilin ligand interactor (TACI) and also B-cell activation factor (BAFF) (Castigli et al., 2005; Kim et al., 2011).

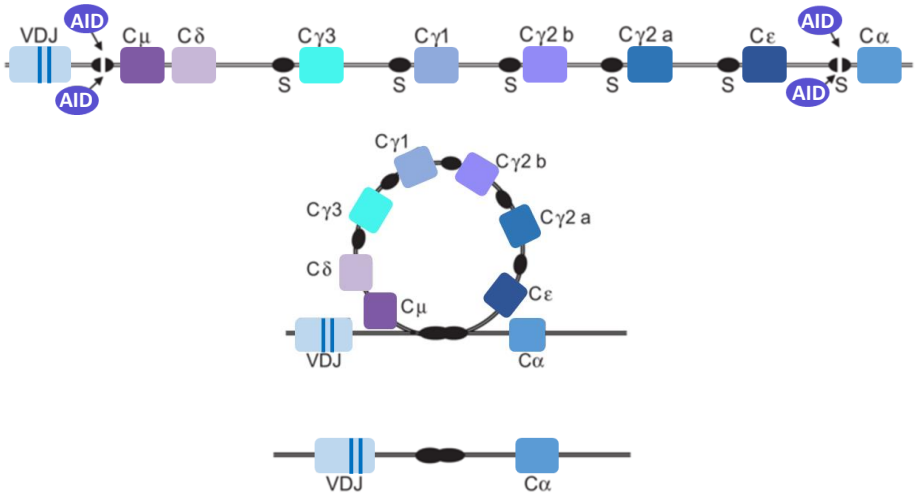

Figure 1.9 Schematic of class switch recombination (CSR). Activation-induced cytidine deaminase (AID) targets switch regions on the on the constant heavy (CH) chain. Following a double stranded break in the DNA, a non-homologous end joining (NHEJ) event recombines the DNA excluding the excised sequence. Depicted above is CSR from IgM to IgA. Adapted from Stavnezer et al. (2008).

CSR requires the generation of double stranded breaks in the switch region of the transcript which is initiated by AID. The double stranded breaks are repaired by a process known as non-homologous end joining (NHEJ) during G1 of the cell cycle. The excision of the region between the two switch regions results in the production of an alternative isotype (Chaudhuri and Alt, 2004). B-cells have been shown to undergo both direct CSR, as shown in **Figure 1.9** and sequential class switching, in which regions are removed separately, which, for example, could produce IgG1 and then IgE following additional CSR. It has been shown that sequential switching to IgE can result in high affinity antibodies that have been associated with anaphylaxis in mice (Xiong et al., 2012).

1.9 Hypothesis

The Class II Phosphoinositide 3-kinase enzyme PI3K C2β has been linked to a variety of cellular processes. Recently a role for PI3K C2β was described in T-cells, where it mediates Ca^{2+} signalling via the potassium channel KCa3.1. The increased intracellular Ca^{2+} associated with the efflux of K^{+} following KC3.1 activation is required for full T-cell activation (Srivastava et al., 2009). Inhibition of KCa3.1 has been shown to ameliorate colitis in a mouse model of the disease, which was due to defective CD4+T-cell receptor signalling, resulting in a reduction in T-cell activation (Di et al., 2010). A recent study revealed that the bioactive lipid ceramide was effective at inhibiting PI3K C2β mediated metastasis in ovarian cancer cells (Kitatani et al., 2015), while in oesophageal squamous cell carcinoma, loss of PI3K C2β was shown to increase the efficacy of cisplatin mediated apoptosis (Liu et al., 2011). However, mice deficient in PI3K C2β do not appear to be negatively affected by its loss. The mice are viable and fertile, with no obvious health defects (Harada et al., 2005). In our laboratory, PI3K C2β$^{-/-}$ mice were rederived and also found to be viable and fertile. However, when provided with an immune challenge PI3K C2β$^{-/-}$ mice displayed a heightened immune response that was not observed in the control mice (Balakrishnan, 2012).

My hypothesis was that mice deficient in PI3K C2β are predisposed to a heightened immune response.

1.10 Aim

The aim of my project was to identify whether splenocytes from PI3K C2β–/– mice could predispose the mice to an altered immune response.

1.11 Objectives

Chapter 3

Question: Does the loss of PI3K C2β–/– result in a specific phenotype? Following an immunological challenge, can a change be identified between the spleens of PI3K C2β–/– and control mice?

Data were collected over an eighteen month period to determine whether PI3K C2$\beta^{-/-}$ mice displayed an altered phenotype compared to the control mice, this included breeding data, animal weight and spleen weight. To study the effect of an immunological challenge, the spleens from control and PI3K C2β–/– mice were examined using either mice kept under basal conditions or following immunization with sheep IgG and complete Freund's adjuvant (CFA). Immunohistochemistry was performed to compare germinal centre reactions, between PI3K C2β–/– and control mice under both conditions. Differences in spleen weight as a percentage of animal weight were also recorded.

Chapter 4

Question: Under basal conditions, are there any differences in lymphocyte populations from PI3K C2β–/– mice that might predispose them to a heightened immune response?

Lymphocyte populations from PI3K C2β–/– and control mice were quantified. T-cell populations were examined at 0 hr and within splenocyte cultures following stimulation. B-cells were also examined at 0 hr and as part of a total splenocyte culture following stimulation. Splenocyte viability was examined, as differences may provide insight into the previously observed heightened immune response seen in PI3K C2β–/– mice.

Chapter 5

Question: Could the differences between the control and PI3K C2β–/– splenic B-cells identified in chapter 4 provide a mechanism for an altered immune response?

B-cell population analysis was performed using isolated B-cells at 0 hr post isolation and following stimulation. To identify whether PI3K C2β–/– B-cells exhibited an altered activation threshold in comparison to control B-cells, isolated B-cell cultures were stimulated with optimal and sub-optimal concentrations of lipopolysaccharide (LPS) and IL-4. Viability, activation state and class switch recombination were assessed.

2 Materials and methods

Table 2.1 Details of the reagents used during the project.

Product	Product number	Company
10% neutral buffered formalin	#HT501320	Sigma
Agarose	#A9539	Sigma
Ammonia	#A/3240/PB15	Fisher Scientific
Ammonium acetate	#09691	Sigma
Ammonium persulphate	#248614	Sigma
Annexin V-FITC Apoptosis Detection Kit	#ab14085	Abcam
Antibiotic-antimycotic	#152-062	Gibco
Anti-CD19 (Rabbit)	#3574	CST
Anti-CD45R (Rat)	#Ab64100	Abcam
Anti-CD45R (Rat) isotype control	#Ab18450	Abcam
Anti-PCNA (Rabbit)	#Ab2426	Abcam
Anti-PCNA IgG (Rabbit) isotype control	#Ab27472	Abcam
Anti-phospho-MEK1/2	#9121	CST
Anti-PI3K C2β (rabbit)	#sc-134766	Santa Cruz
Anti-rabbit secondary antibody (HRP)	#P0448	Dako
Anti-mouse secondary antibody (HRP)	#P0447	Dako
β mercaptoethanol	#11508916	Fisher Scientific (Gibco)
BCA protein assay kit	#23225	Pierce
Blue Juice	#10816-015	Fisher Scientific
Bromophenol blue	#403140100	Sigma
BSA	#A7030	Sigma
Chloroform	#C/4920/15	Fisher Scientific
Complete Freund's adjuvant	#F5881	Sigma
Dako Envision+ System-HRP/DAB	#K4010	Dako
DPX mounting media	#06522	Sigma
EDTA	# 03690	Sigma
Ethanol (absolute)	#E/0650DF/17	Fisher Scientific
Ethanol (IMS)	#M/4450/17	Fisher Scientific
FBS	#EU-000F (150201)	Sera Labs
Glycine	#G/0800/600	Fisher Scientific
Harris haematoxylin	#HHS80	Sigma
LPS	#L4392	Sigma
Lympholyte M	#CL5030	Cedarlane
Lyophilised sheep IgG	#I5131	Sigma
Methanol	#10284580	Fisher Scientific
MTT	#15224654	Fisher Scientific (Acros)
NaCl	#10112640	Fisher Scientific
Non-essential amino acids	#12084947	Gibco

Product	Product number	Company
Pan B-cell isolation kit	#130-095-813	Miltenyi Biotec
Pan T-cell isolation kit	#130-095-130	Miltenyi Biotec
Propidium Iodide	#ABIN412371	eBioscience
Proteinase-K	#P2308	Sigma
Protoscript First Strand cDNA Synthesis Kit	#E6300S	NEB
QIAquick Gel Extraction Kit	#28104	Qiagen
ReadyMix	#P4600	Sigma
Recombinant IL-2	#402-ML-020	R&D Systems
Recombinant IL-4	#404-ML-010	R&D Systems
RNAse A	#R6513	Sigma
RPMI 1640 media	#11879020	Fisher Scientific (Gibco)
SDS	#10607443	Fisher Scientific
Seroblock	#BUF041B	AbD Serotec
Sodium azide	#12695107	Fisher Scientific (Acros)
Sodium citrate	#10787024	Fisher Scientific
Sterile PBS	#10388739	Fisher Scientific
T-cell activation/expansion kit	#130-093-627	Miltenyi Biotec
TEMED	#T9281	Sigma
Tris base	#10724344	Fisher Scientific
Tris HCl	#10001223	Fisher Scientific
Triton-X-100	#X100	Sigma
Tween-20	#P9416	Sigma
Xylene	#534056	Sigma

2.1 PI3K C2β–/– and control mice

Previously generated PI3K C2β–/– mice (Harada et al., 2005) were rederived in our lab (Balakrishnan, 2012), and maintained at Burlington Danes unit, Central Biomedical Services (CBS) facility, Hammersmith Campus, Imperial College, London. All procedures were carried out within British Home Office regulations and ethical guidelines (Animals (Scientific Procedures) Act 1886) under Home Office project licence PPL70 7104 (Professor Charles Pusey) and my personal licence PIL 70/25001.

2.1.1 Housing conditions of experimental animals

Control and PI3K C2β–/– mice were caged separately and kept in a pathogen free environment with air filtering technology, which is designed to prevent pollutants and particles from entering the facility. In addition, animals were kept in individually ventilated cages (IVCs), which results in air being ventilated twice. The mice had free access to the standard autoclaved chow, and autoclaved water and were re-caged weekly into clean IVCs. Stocking density within the facility is seven mice, up to a weight of 30g. However, post weaning, mice were typically housed at a maximum of five animals per IVC. The cages were stacked, with the roofs of the top row being covered so that all mice experienced the same level of lighting. Rooms in which the mice are housed are programmed with ambient lighting, to reflect dusk and dawn. Individual experiments used groups of three mice, which were typically housed together. Repeat experiments would therefore use mice from different cages **(Table 2.2)**.

Table 2.2. Details of the experimental animals used in this project.

Corresponding figure	Experiment details	Number of controls*	Number of PI3K C2β−/−*	Group number	Experiment 1	Experiment 2	Experiment 3	Experiment 4
3.1	Genotyping	20	26					
3.2	Breeding data (see Appendix 1)							
3.3	Animal weight	29	36					
3.4	Spleen weight as a percentage of bodyweight (IgG/CFA and basal)	27	31		F_18-35 wk	F_18-35 wk		
3.5	PCNA and B220 immunostaining of spleen from control and PI3K C2β−/− mice kept under basal conditions.	4	6		F_18-35 wk			
3.6	PCNA and B220 immunostaining of spleen from control and PI3K C2β−/− mice treated with IgG/CFA.	4	5		F_18-35 wk	F_18-35 wk		
3.7	Quantification of germinal centre associated proliferation.	8	11		F_18-35 wk	F_18-35 wk		
4.1	Splenocyte population breakdown at 0 hr (B220, CD19)	9	9	1,4,6	m_33-35 wk	m_31-33 wk	m_31-33 wk	
4.1	Splenocyte population breakdown at 0 hr (CD4, CD8)	12	12	1,4,6,7	m_33-35 wk	m_31-33 wk	m_31-33 wk	m_15-17 wk
4.2	Confirmation of T-cell populations within total splenocytes (CD3, CD4 dual staining)	6	6	5,6	m_8-9 wk	m_31-33 wk		
4.3	CD19 and B220 expression levels	9	9	2,4,3	f_32-35 wk	m_31-33 wk	f_22-24 wk	
4.4	Isolation of T-cells							
4.5	CD8+ cells within isolated T-cell population at 72 hr	3	3	8	m_16-18 wk			
4.6	T-cell viability at 72 hr	4	4	5,8	m_8-9 wk	m_16-18 wk		
4.7	T-cell populations (CD3, CD4, CD8) within total splenocyte cultures at 86 hr	6	6	7,8	m_15-17 wk	m_16-18 wk		

4.8	CD19+ populations within total splenocyte cultures at 86 hr	6	6	8,5	m_16-18 wk	m_8-9 wk		
4.9	Propidium iodide staining of splenocytes after 80 hr stimulation with LPS (20 µg/ml) and IL-4 (50 ng/ml)	6	6	4,6	m_31-33 wk	m_31-33 wk		
5.1	Isolation of B-cells							
5.2	Presence of PI3K C2β−/− in control mice	3	3					
5.3	CD19 expression on isolated B-cells at 0 hr	9	9	13,10,12	f_25-30 wk	f_28-31 wk	f_16-20 wk	
5.4	B-cell viability at 24 hr (Annexin V and propidium iodide)	6	6	11,10	f_24-26 wk	f_28-31 wk		
5.5	B-cell viability at 72 hr (Annexin V and propidium iodide)	9	9	11,10	f_24-26 wk	f_28-31 wk		
5.6	B-cell metabolic activity (MTT assay)	6	6	9,14	m_20-24 wk	m_16-18 wk		
5.7	Cell cycle analysis at 0 hr, 24 hr and 72 hr	6	6	10,11	f_28-31 wk	f_24-26 wk		
5.8	Analysis of the sub G0/G1, and G0/G1 populations	6	6	10,11	f_28-31 wk	f_24-26 wk		
5.9	IgM expression at 0 hr	12	12	10,11,7, 13	f_28-31 wk	f_24-26 wk	m_15-17 wk	f,25-30 wk
5.1	IgM expression profile at 0 hr	12	12	10,11,7, 13	f_28-31 wk	f_24-26 wk	m_15-17 wk	
5.11	IgG expression at 0 hr	9	9	2,11,7	f_32-35 wk	f_24-26 wk	m_15-17 wk	
5.12	IgE expression at 0 hr	6	6	2,5	f_32-35 wk	m_8-9 wk		
5.13	CD23 expression at 0 hr	9	9	10,11,13	f_28-31 wk	f_24-26 wk		
5.14	CD23 expression profile at 0 hr	9	9	10,11,13	f_28-31 wk	f_24-26 wk		
5.15	CD19hi, CD23hi population at 0 hr	6	6	11,13	f_24-26 wk	f_25-30 wk		
5.16	CD19, CD23 expression profile at 0 hr	6	6	11,13	f_24-26 wk	f_25-30 wk		
5.17	CD23low and IgMlow expression profile 0 hr	3	3	10	f_28-31 wk			
5.18	CD23- and IgMhi population at 0 hr	3	3	10	f_28-31 wk			

5.19	IgG expression at 86 hr following optimal stimulation	7	7	4,7	m_31-33 wk	m_15-17 wk		
5.19	IgE expression at 86 hr following optimal stimulation	6	6	4,7	m_31-33 wk	m_15-17 wk		
5.2**0**	IgG expression at 86 hr following sub-optimal stimulation	9	9	2,11,7	f_32-35 wk	f_24-26 wk	m_15-17 wk	
5.21	IgE expression at 86 hr following sub-optimal stimulation	12	12	2,11,7	f_32-35 wk	f_24-26 wk	m_15-17 wk	
5.22	IgM expression at 86 hr following sub-optimal stimulation	9	9	2,11,7,10	f_32-35 wk	f_24-26 wk	m_15-17 wk	f_28-31 wk
5.23	CD23 expression at 86 hr following sub-optimal stimulation	9	9	10,11,13	f_28-31 wk	f_24-26 wk	f_25-30 wk	
5.24	MEK 1/2	2	2					

Details of the animals used during this project, including sex (m or f) and age in weeks (wk) with the corresponding experiment and figure number. Group numbers have been provided to indicate when mice were used for multiple experiments. * total number of animals used.

2.2 Extracting genomic DNA from ear punches.

Ear punches were digested in lysis buffer (50 mM Tris-HCl (pH 8.0), 0.1 M NaCl, 1% SDS (sodium dodecyl sulphate), 20 mM EDTA (ethylene diamine tetra acetic acid) autoclaved) and 10 mg/ml proteinase-K (Sigma #P2308) overnight at 50˚C. 1.8 M ammonium acetate (Sigma #09691) was added to the tissue, it was then vortexed and incubated on ice for at least 10 minutes. Chloroform was added, before being centrifuged at 14000 rpm for 10 minutes at 4˚C. Supernatant transferred to a tube containing 100% ethanol. After centrifugation at 14000 rpm for 5 minutes at room temperature, DNA was re-suspended in molecular grade water.

2.3 Polymerase chain reaction (PCR)

PCR was used to amplify gDNA from control and PI3K C2$\beta$$^{-/-}$ mice for genotyping: PCR reactions contained 25 μl of ReadyMix (Sigma #P4600), 10 pm of each of the forward and reverse primers (control: 74/75 or PI3K C2$\beta$$^{-/-}$ 76/77), 50 ng of gDNA, and the volume was brought to 50 μl using molecular grade water. The thermo cycler was set to: Denature 95^{0}C for 2min, melt 95^{0}C for 40sec, anneal 60^{0}C for 40sec, extension 72^{0}C for 40sec and final extension 720C for 4min followed by an indefinite hold at 4^{0}C for 35 cycles (melt, anneal and extension). Reverse transcription was used to confirm the presence of PI3K C2β mRNA in B-cells from control mice with an expected product size of 858bp. Primers were designed to cross exons so that gDNA contamination could be excluded. PCR parameters were the same as before.

Control primers (74/75)

Designation: 74/75 (expected product 300bp)

Forward: 5'-GGCACACACTAACCACAGCACC-3'

Reverse: 5'-TCGATGCACGT CTCTCCGC-3'

PI3K-C2β−/− primers (76/76)

Designation: 76/77 (expected product 404bp)

Forward: 5'-TGTTAGAACCTGCCGCCTTTAC-3'

Reverse: 5'-CCGAATCAGCCTCATTTCCTCTC-3'

Primers 235/235 (expected product size 858bp)

Forward: 5'-TGTTAGAACCTGCCGCCTTTAC-3'

Reverse: 5'-CCGAATCAGCCTCATTTCCTCTC-3'

2.3.1 Agarose gel electrophoresis

1.5% agarose gels were used to resolve PCR products (1.5% agarose (Sigma #A9539), in 1X TAE buffer), agarose powder was melted in 1x TAE buffer and allowed to cool to approximately 55^0C before adding ethidium bromide at 0.5 μg/ml. A DNA ladder and each of the samples in 10x loading buffer (Blue Juice ThermoFisher #10816-015) were loaded on to the gel once set, and samples electrophoresed at 100V in TAE buffer for approximately 1hr before being visualized using UV light.

2.3.2 DNA sequencing

Following gel extraction (QIAquick Gel Extraction Kit; Qiagen #28104) of each PCR band, 100 ng of PCR product was resuspended 10 ml of molecular grade water and sent to Cambridge University for sequencing.

2.4 Sheep IgG and complete Freund's adjuvant activation of mice

Lyophilised sheep IgG (Sigma #I5131) was dissolved in saline (150 mM sodium chloride) to make a 10 mg/ml stock. For use, 20μl of stock was diluted in 180 μl saline (per animal) and mixed with complete Freund's adjuvant (CFA) in a 50:50 ratio (Sigma #F5881). Reagents were placed in a glass universal and mixed thoroughly using a hypodermic syringe until thick and opaque. Mice were given subcutaneous injections of 0.2 mg sheep IgG/CFA (400 μl total volume) which were administered by technicians in Central Biomedical Services, Imperial College London. Mice were sacrificed after seven days by cervical dislocation.

2.5 Measurement of spleen and body weight

Body weight was measured at culling and spleens were excised and weighed immediately. To take into account the variability in animal weight, spleen weight was then calculated as a percentage of animal weight.

2.6 Processing of spleens for histology and immunohistochemistry

Freshly excised spleens were fixed overnight in 10% neutral buffered formalin (Sigma # HT501320), spleens were then transferred to 70% ethanol and taken to the Histology Department, South Kensington Campus, Imperial College London for paraffin embedding and sectioning (4μm).

2.6.1 De-waxing and rehydration

Formalin fixed, paraffin embedded sections were de-waxed by immersion in xylene twice for 8min each, after which they were rehydrated by successive

immersing in 100%, 95% and 70% ethanol for 5min each. Sections were kept in distilled water for a minimum of 10min before antigen retrieval.

2.6.2 Antigen retrieval

Formalin fixation can result in the cross linking of proteins, resulting in the masking of antigenic epitopes and loss of immunoreactivity. Heat induced epitope retrieval (HIER) was performed by placing de-waxed, rehydrated sections in 400ml of pre-heated sodium citrate buffer (0.1 M Sodium citrate, 0.05% Tween 20, pH 6.0, in distilled water) and microwaving for 15 minutes at 400W. Slides were then placed in distilled water until processing.

2.6.3 Immunohistochemistry

IHC was performed using Dako Envision+ System-HRP/DAB (# K4010) to examine germinal centres within the spleen. Anti-CD45R (Rat) at 1:250 (Abcam #64100) and anti-PCNA (Rabbit) at 1:100 (Abcam #Ab2426) and their isotype controls (Dako #P0450) and (Abcam #27478), were used. Following antigen retrieval, sections were treated with serum-free block (Dako) for 1 h in a humidified chamber, followed by a gentle wash in TBS-T (tris buffered saline; sodium chloride and tris-HCl at pH 7.6 + 0.1% TWEEN-20). Primary antibody was applied to one tissue section and isotype control was applied to the second section (two sections per slide). Slides were incubated in a humidified chamber for 1hr, followed by 2X5 min washes in TBS-T (0.25%). Peroxidase block (Dako) was added for 15 min before 2x5min washes in TBS-T (0.025%). Secondary antibody was applied (HRP labelled polymer) and slides were incubated in a humidified chamber for

45min, followed by 2x5min washes. DAB + buffer (1:50) (approximately 40µl per section) was added for approximately 2min. Slides were then placed in distilled water before counterstaining.

2.6.4 Counterstaining with haematoxylin

Slides were dipped in Harris haematoxylin 3x5 seconds followed by washing under gently running tap water for 5min. Slides were briefly dipped in 1% acid alcohol before washing under gently running tap water for 5min. Slides were then immersed in 0.37 M ammonia for 1min followed by 5min wash under gently running tap water. Slides were allowed to dry before being rehydrated by sequential immersion in increasing concentrations of ethanol for 5min each; 70%, 95% and 100% followed by immersion in xylene twice for 8min each. Slides were then mounted using DPX mounting media (Sigma #06522).

2.7 Microscopy

The BX63 (Olympus) was used for imaging. Measurements for spleen area and germinal centre areas were made using CellSens software.

2.8 Splenocyte isolation

Mice were culled by cervical dislocation, weighed, and sprayed with 70% ethanol before spleen excision. Connective tissue was carefully removed and spleens were weighed. Spleens were then briefly immersed in 96% absolute ethanol before immersing in RPMI X2. Spleens were then transferred to individual 15 ml falcon tubes containing 'travel' media (RPMI

1640, 3% heat inactivated FBS, 2 mM Glutamine, 20 mM HEPES (pH 7), 50 μM β-ME, antibiotic-antimycotic (Gibco #152-062), non-essential amino acids (Gibco #12084947), filter sterilized), before being placed on ice and transported to the University of Bedfordshire.

Splenocyte isolation was carried out under aseptic conditions. Spleens were transferred through two additional RPMI washes before disaggregation. Using a plunger from a sterile 5 ml syringe, tissue was pressed through a 70 μm pre-wetted cell strainer into a 6 cm tissue culture dish containing 2 ml of B-cell media (RPMI 1640, 10% heat inactivated FBS, 2 mM glutamine, 20 mM HEPES (pH 7), 50 μM β-ME, antibiotic-antimycotic (Gibco #152-062), non-essential amino acids (Gibco #12084947), filter sterilized), the strainer was rinsed with 2 ml of media and splenocytes were collected.

2.9 Removal of red blood cells

Red blood cells were removed from splenocyte suspensions using Lympholyte M cell separation media (Cedarlane #CL5030) as per manufacturer's instructions. Briefly, collected splenocytes were carefully layered on top of 5 ml of Lympholyte M in a 15 ml falcon tube and centrifuges at 1200g for 20 min at room temperature. Lymphocytes were then collected and transferred to a fresh falcon tube, the cell suspension was made up to 10 ml using B-cell media. The cells were centrifuged at 300g, the supernatant was discarded and the splenocytes were resuspended in 10 ml of B-cell media before being counted using a haemocytometer.

2.10 B-cell isolation

B-cell isolation was carried out using a pan B-cell isolation kit from Miltenyi Biotec (#130-095-813), as per the manufacturer's instructions. Cells were pelleted, supernatant discarded and resuspended at 10^7 cells per 40 µl of Macs buffer (PBS, (pH 7.2), 0.5% bovine serum albumin (BSA), and 2 mM EDTA; all filter sterilized). 10 µl of Pan B Cell Biotin-Antibody Cocktail was added to each 10^6 total cells and cells were incubated for 5min on ice. 30 µL of cold buffer was added per 10^6 total cells, followed by 20 µl of anti-Biotin MicroBeads per 10^6 cells, for 10 min on ice. The cell suspension was then made up to a minimum volume of 500 µl. B-cells were then separated by negative selection using Macs columns (Miltenyi #LD130-042-901) and magnetic separators. Separation columns were prepared by adding 2 ml of Macs buffer and letting it flow through by gravity. The cells were then added to the column and cells were collected. 2 ml of Macs buffer was then passed through the column and collected. The enriched B-cell population was pelleted at 300 g and initially resuspended in 5 ml of B-cell media and counted.

2.11 T-cell isolation

T-cell isolation was carried out using a pan B-cell isolation kit from Miltenyi Biotec (#130-095-130). The process is the same as for B-cell separation with the exception of the antibody, which was 10 µL of Pan T Cell Biotin-Antibody Cocktail per 10^7 total cells.

2.12 Cell culture and stimulation

Following negative selection, splenocytes, B-cells and T-cells were plated in complete B-cell media at 1-2 x 10^6 per ml and allowed to 'rest' for one hour at 37°C, 5% $C0_2$ before stimulation. Stimulation for splenocytes and B-cells was provided by lipopolysaccharide (LPS) (Sigma #L4391) and recombinant IL-4 (R&D Systems #404-ML-010). LPS was dissolved in RPMI media at 1 mg/ml, aliquoted and stored at -20^0C. Splenocytes and B-cells were stimulated with either 20 μg/ml or 2 μg/ml. IL-4 was dissolved in RPMI media at 0.01 mg/ml, aliquoted and stored at -20^0C. Splenocytes and B-cells were stimulated with either 50 ng/ml or 20 ng/ml. T-cells were stimulated using recombinant IL-2 (R&S Systems #402-ML-020) and a T-cell activation/expansion kit (Milteni #130-093-627), as per manufacturer's instructions. Anti-biotin MACSiBead particles and biotinylated antibodies against mouse CD3ε and CD28 were prepared in advance; 100 μL of CD3ε-Biotin and 100 μL CD28-Biotin were mixed well in a sterile 2 ml centrifuge tube, 300 μl of PBS (pH 7.2) containing 2 mM EDTA was added, followed by 500 μL anti-biotin MACSiBeads (10^8 beads). The suspension was incubated for 2 hr at 4^0C, while being rotated. 40 μl of resuspended beads were added to 1 ml of B-cell media and centrifuged at 300g for five minutes at 4^0C. Supernatant was aspirated and beads were resuspended in 1 ml B-cell media (approximately 4x10^6 beads) containing IL-2. Beads were used at a bead to cell ratio of 2:1. Following stimulation, cell cultures were maintained in a humidified 5% CO_2 incubator at 37^0C.

2.13 Flow cytometry

All flow cytometric analysis was carried out using the C6 cytometer (BD Accuri). Calibration was performed at the beginning of each session. Although the C6 is designed with predictable fluorescence overspill values, compensation was checked and adjusted as necessary when co-staining.

2.13.1 Labelling cells for cytometric analysis

The same procedure was used to prepare cells for flow cytometric analysis. However, some of the antibodies were used in different concentrations and were incubated for different periods of time as detailed in **Table 2.3.**

Table 2.3. Fluorophore conjugated antibodies used for flow cytometry

Marker	Volume per 10^6 (to a final volume of 50µl in FACS buffer)	Incubation time (on ice in the dark)	Isotype control
B220 (CD45R) AbD Serotec MCA1258A488T	5µl	40min	rat anti-mouse IgG2a AbD Serotec #MCAA488
CD19 BD Pharmingen CD19 #557684	5µl	40min	rat anti-mouse IgG2a BD Pharmingen #557690
CD3 BD Pharmingen 555274	5µl	40min	Rat IgG2b BD Pharmingen #553988
CD4 AbD Serotec #MCA1767A647T	10µl	40min	rat anti-mouse IgG2b AbD Serotec #MCA1125A647
CD8 AbD Serotec #MCA609A647T	10µl	40min	rat anti-mouse IgG2a AbD Serotec #MCA1212A647
CD23 Miltenyi Biotech #130-102611	5µl	15min	Rat IgG2a Miltenyi Biotec #130-102-654
IgM Southern Biotech #1140-09	1µl	40min	Rat IgMλ SouthernBiotech #0120-09
IgG1 AbD Serotec #STAR132PE	10µl	40min	Rat IgG1κ SouthernBiotech #0116-19
IgE Southern Biotec #1130-09	10µl	40min	Rat IgG1κ SouthernBiotech #0116-19

Cells were counted prior to being washed twice in FACS buffer (PBS, 2% FBS, 1 mM EDTA, 0.1% sodium azide) by centrifugation at 300g for 5 min at 4^0C. The supernatant was carefully removed and cell pellets were gently resuspended in FACS buffer containing Seroblock (AbD Serotec #BUF041B) and incubated for 10 min on ice, in the dark. Antibody dilutions were prepared to a final volume of 50 μl/ $1x10^6$ cells in FACS buffer and were aliquoted into individual round bottomed 2ml centrifuge tubes on ice at 50 μl/ 10^6 cells. After blocking cells were mixed gently and were added to the appropriate antibody (final concentration: $1x10^6$ cells/ 100μl). Cells were incubated on ice in the dark. Following incubation 1 ml of FACS buffer was added to each tube before centrifuging at 300g for 5 min at 4^0C. The supernatants were removed and cells were washed a further two times in FACS buffer. After the final wash cells were resuspended in 200 μl of FACS buffer per 10^6 cells and were analysed on the flow cytometer.

2.13.2 Median fluorescent intensity

Fluorescent intensity was used as an indication of relative protein expression between fluorophore labelled cell populations from control mice and PI3K C2β−/− mice. Fluorescent intensity data is sometimes presented using the mean fluorescent intensity. However, this may not be an accurate representation if fluorescence is recorded using a logarithmic scale, as the arithmetic mean does not take into account the skewed distribution of log-amplified data. As such, to assess relative protein expression between samples, median fluorescent intensity (MFI) has been used. As the central

value is not as sensitive to the distribution of logarithmic data, the median is considered to be a more robust measure of relative fluorescent intensity (Demishtein et al., 2015; Givan, 2001).

2.13.3 Cell cycle analysis

Following isolation, the splenic B-cells were allowed to rest for 1 hr. 10^6 B-cells were removed prior to stimulation for the 0 hr analysis. Cells being used for 24 hr and 72 hr analysis were then stimulated with 2 ug/ ml LPS and 20 ng/ ml IL-4. Cells were centrifuged at 300g for 5 min at 4^0C, the supernatant was aspirated and the pellet was resuspended in 1 ml of cold PBS and centrifuged for 5 min at 300g at 4^0c. The supernatant was removed and the pellet was resuspended, dropwise in ice-cold 70% ethanol (stored at -20^0C) while being vortexed to minimize cell clumping. Cells were then stored at 4^0C until cells for 24 hr and 72 hr had been collected. Following the final collection, cells were kept at 4^0C overnight to ensure sufficient fixation of the 72hr sample. Staining and analysis of all three timepoints was conducted at the same time. Cells were centrifuged at 850 g for 5 min at 4^0C, supernatant was discarded and cells were washed twice in cold PBS. Following the final wash, pellets were treated with 50 μl of RNase A (100 μg/ ml) to remove contaminating RNA. 400 μl of propidium iodide (PI) was then added (50 μg/ ml in FACs buffer) and cells were carefully resuspended and incubated at room temperature for 10 min before analysis using a C6 cytometer (BD Accuri). An initial plot of FSC (area) vs FSC (height) was used

to exclude doublets, which could lead to false positive readings in the G2/ M gate. PI was read in the FL-2 channel.

2.13.4 Annexin V and propidium iodide staining (cell viability)

Annexin V-FITC Apoptosis Detection Kit (Abcam #ab14085) was used to examine cell viability as per manufacturer's instruction. 0.5 x 10^6 cells were collected and centrifuged at 300g for 5 min at room temperature. The pellet was resuspended in 500 μl of binding buffer and 5 μl of Annexin V-FITC and 5 μl of PI were added. Cells were then incubated in the dark for 5 min at room temperature before analysis by flow cytometry. Annexin V was analysed using the FL-1 channel and PI was read in FL-2. Compensation was set to eliminate fluorescence overspill between FL-1 and FL-2. A minimum of 20,000 events were collected per sample.

2.14 MTT assay

Freshly isolated B-cells were plated in triplicate at 0.1 x 10^6 per well in a 96 well plate, in 200 μl of media and allowed to rest for two hr before being stimulated with LPS (2 μg/ ml) and IL-4 (20 ng/ ml). 20 μl of MTT (5 mg/ ml) was added to the wells being analysed at 0 hrs, and cells were returned to 5% CO_2 incubator at 37^{o}C for four hr before adding the MTT solvent (20% SDS in 0.2 M HCl) (Young et al., 2005). Cells were returned to the incubator for a further two hr before reading the absorbance at 570 nm. This was repeated at 72 hr.

2.15 Cell lysis

Total cell lysate was prepared by adding 2X sample buffer (500 mM tris base, 25% v/v glycerol, 15% v/v SDS, 10% v/v β-mercaptoethanol, 0.5 M EDTA and 0.05% w/v bromophenol blue), directly to prewashed cell pellets at a 1:1 ratio. Total cell lysate was boiled and stored at -20^{0}C.

Cell extract lysates were prepared using lysis buffer (1% Triton X-100, 10 mM Tris-HCL, 5 mM EDTA, 50 mM sodium chloride, 30 mM sodium pyrophosphate, 1 mM phenylmethylsulfonyl (PMSF), 1:100 v/v aprotinin, 1 μg/ ml pepstatin and 5 μg/ ml leupeptin. Cells were washed in ice-cold PBS before being incubated for 20 mins on ice with complete lysis buffer. Lysates were harvested, centrifuged at 14000rpm, at 4^{o}C for 15 mins before storage at -80^{o}C.

2.16 BCA assay

Protein concentration of lysates was determined using a BCA protein assay kit (Pierce #23225) as per manufacturer's instructions.

2.17 SDS PAGE

Proteins from cell lysates were separated using SDS-PAGE prior to western blotting. For detection of PI3K C2β–/–, lysates were separated using a 7% resolving gel, for CD19 and pMEK1/2 a 10% resolving gel was used topped by a 4% stacking gel. Resolving gel; (31.75% v/v dH_2O, 1.5 M Tris-base at pH 8.8, 30% v/v acrylamide, 2% Bis, 0.5% v/v of 20% SDS, 0.33% v/v of 10% ammonium persulphate (APS) and 0.05% v/v TEMED) and 4% stacking gel

(46.5% v/v dH2O, 34% 1.5 M tris-HCl (pH 6.8), 13.5% v/v acrylamide, 3.5% v/v Bis, 0.7% v/v of 20% SDS, 0.35% v/v of 10% APS, 0.14% v/v TEMED). Proteins were denatured in sample buffer (Section 2.15) and gels were run at 65V overnight or for 1 hr at 190 V using Mini-PROTEAN system (BioRad) in running buffer (25 mM tris-base, 200 mM glycine and 0.1% SDS).

2.18 Western blotting

Following protein separation by SDS-PAGE, proteins were transferred to a polyvinyledine difluoride (PVDF) membrane. Gels were equilibrated in transfer buffer (25 mM tris-base, 192 mM glycine, 0.1% SDS and 10% v/v methanol) for 15mins prior to transfer, which was carried out at 24V for 5 hrs at room temperature. Following transfer, the PVDF membrane was blocked in 5% non-fat dairy milk (NFDM) in TBS-T. Primary antibodies were diluted in TBS-T, 5% bovine serum albumin (BSA) and 0.005% sodium azide as per manufacturer's instructions: anti-PI3K C2β (rabbit) at a 1:600 dilution (Santa Cruz #sc-134766), anti-CD19 (Rabbit) at a 1:1000 dilution (CST #3574) and anti-phospho-MEK 1/2 (Rabbit) at a 1:1000 dilution (CST #9121). Membranes were incubated in primary antibody overnight at 4^0C after which they were washed 2 X 5mins in TBS-T. Secondary antibody (anti-rabbit) (DAKO), labelled with horseradish peroxidase was diluted as per manufacturer's instructions in TBS-T and 5% NFDM. Incubation was carried out for 1 hour at room temperature. The membrane was then washed 3 x 5 mins in TBS-T before exposure using the Medical Film Processor SRX-101A, Konica) and chemiluminescence (ECL, GE Life Sciences).

2.19 Statistical analysis

Analysis was performed using GraphPad Prism version 6.01 for Windows, GraphPad Software, San Diego California USA. Where possible, normality of data was assessed using a Kolmogorov-Smirnov normality test. Data identified as having normal distribution were analysed using an unpaired, two-tailed Student t-test, with differences in variance being corrected for using Welch's test (**Figure 5.15**). Results were considered statistically significant at p=0.05. This method of analysis has been previously used in the literature (Adachi et al., 2015; Allen et al., 2012; Hampel et al., 2011). When multiple t-tests were used, multiple comparisons were corrected for using the Sidak-Bonferroni method and results were considered significant at p=0.005 (**Figure 4.1**). For analysis of two or more experiments that were not combined (such as median fluorescent intensity) a two-way ANOVA was performed, corrected for multiple comparisons using Sidak's multiple comparisons test (**Figure 5.3**). Preliminary experiments using very small sample sizes (n = 3), were analysed to detect whether they were powered to detect changes using an unpaired, two-tailed t-test (**Figure 5.17**), using; Java Applets for Power and Sample Size [Computer software], available at: http://www.stat.uiowa.edu/~rlenth/Power.

3 PI3K C2β–/– mice

The Class I PI3Ks are well established as mediators of signalling cascades within immune cells following activation via G protein coupled receptors (GPRCs), or antigen receptors such as the B-cells receptor (BCR) and the T-cell receptor (TCR) (Werner et al., 2010). Augmented signalling has been linked to many human diseases and their inhibition is associated with reduced disease severity (Hawkins and Stephens, 2015). As such there is much interest in developing PI3K inhibitors for therapeutic purposes and several are being used in clinical trials (Westin, 2014). The use of genetically modified mice with distinctive phenotypes has played an important role in what has been learned so far (Hawkins and Stephens, 2015). However the role of the Class II PI3Ks is still to be elucidated.

A mouse model deficient in PI3K C2β was previously established to study the role of PI3K C2β in epidermal differentiation. These mice did not display a specific phenotype under the conditions in which they were studied and were both viable and fertile (Harada et al., 2005). Our laboratory has been working with PI3K C2β–/– mice which were rederived to examine the role of PI3K C2β in the kidney, during which time a potentially dysregulated immune response was observed (Balakrishnan, 2012).

The purpose of my project was to identify a potential role for PI3K C2β in the immune system, with a particular emphasis on the spleen. This chapter focuses on genotyping the mice and identifying any phenotypic differences in health, weight or breeding patterns. It will also show a basic examination

of spleens from control and PI3K C2β–/– mice kept under basal conditions and also following stimulation with sheep IgG and complete Freund's adjuvant (CFA).

3.1 Genotyping

All mice were genotyped prior to analysis of the spleen. Ear punches were collected and genomic DNA was extracted. The primers used to determine the genetic background of the mice had been previously designed (Harada et al., 2005). For the floxed control animals (B6.129.PIK3C2btm pkh/J) the primers, designated 74/75, had been designed to amplify a region of intron between exons two and three, encompassing the first LoxP site, with an expected product size of 300bp **(Figure 3.1)**. The primers (designated 76/77) were used to confirm successful knock out of PI3K C2β (B6.129.PIK3C.KO), and generated a product of 404bp, if the region between the LoxP sites has successfully been excised. If this region was not excised it would span 2673bp, resulting in no product under the conditions used.

Following amplification by PCR, products were separated by agarose gel electrophoresis and imaged under UV light **(Figure 3.1)**. Both strains generated a product of the expected size (300bp from control gDNA and 404bp from PI3K C2β–/– gDNA). Bands from three controls and three knockouts were extracted from the agarose gels, and following purification were sent for sequencing. Analysis of sequences, using Bio-Edit (Hall, 1999) confirmed that the intended sequences had been amplified. Comparison of the cDNA sequences generated by primers 74/75 (control) and 76/77 (PI3K

C2β–/–) allowed identification of the LoxP sites. As previously described (Harada et al., 2005), these were located within intron three and intron six. Identification of the LoxP sites also confirmed that the sequence remained in frame, and therefore the generation of PI3K C2β protein in the control mice should remain unaffected.

A

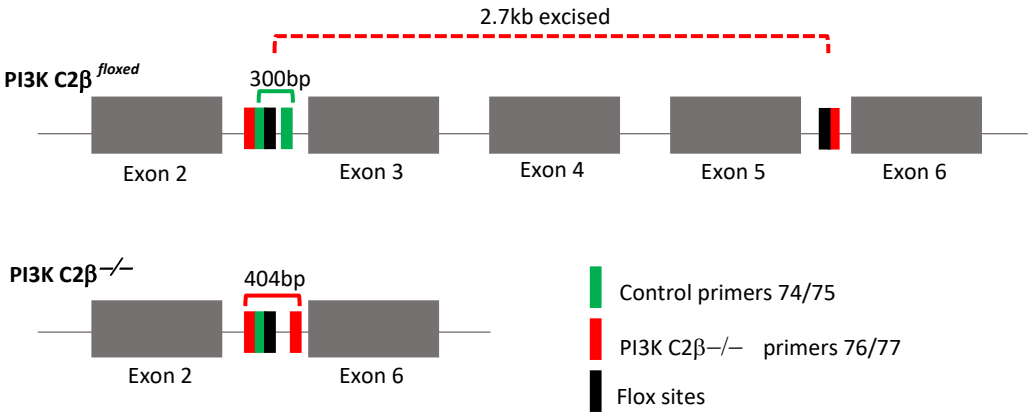

B

Control primers
Designation: 74/75 (expected product 300bp)
Forward: 5'-GGCACACACTAACCACAGCACC-3'
Reverse: 5'-TCGATGCACGTCTCTCCGC-3' (GCGCAGAGACGTGCATCGA)
PI3K-C2β−/− primers
Designation: 76/77 (expected product 404bp)
Forward: 5'-TGTTAGAACCTGCCGCCTTTAC-3'
Reverse: 5'-CCGAATCAGCCTCATTTCCTCTC-3′ (GAGAGGAAATGAGGCAGATTCGG)

C

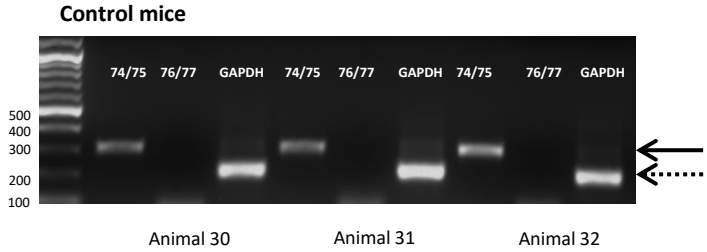

D

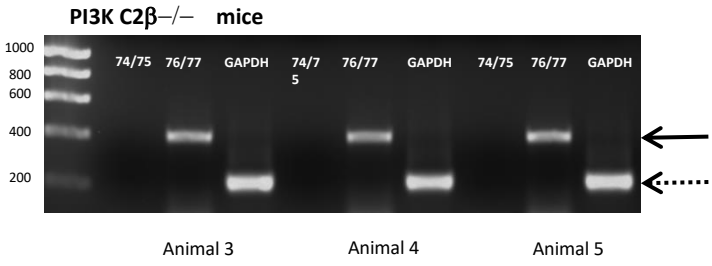

Figure 3.1 Genotyping PI3K C2β knockout mice (B6.129.PIK3C.KO) and control mice (B6.129.PIK3C2btm pkh/J). Genomic DNA was extracted from ear punches and PCR was used to genotype the animals. **A**; schematic of knockout strategy. **B**; primers 74/75 generated a product of approximately 300bp in the PI3K-C2β^{floxed} control mice. Primers 76/77 generated a product of 404bp, PI3K-C2β−/− mice. **C** and **D**; representative agarose gels showing PCR products following amplification using primers 74/75 (control) and 76/77 (KO). Solid arrows; expected product, dashed arrows; positive control GAPDH (200bp).

3.2 Phenotypic differences displayed by PI3K C2β–/– mice

Consistent with earlier reports, under basal conditions PI3K C2β–/– mice appear healthy and do not exhibit any obvious health issues. During the course of the project I noted that PI3K C2β–/– to any increase in the G2/M phase mice appeared to be better breeders producing more female offspring than control animals. Also, PI3K C2β–/– mice were slightly smaller than the controls.

3.3 Breeding data

While setting up breeding cages designed to produce age matched litters it was noted that the PI3K C2β–/– mice produce more offspring than the control mice. To test this hypothesis, births were monitored over an eighteen month period. Data was collected from four breeding cages from each strain, which were matched for age, the date that they were established and the breeding period (**Appendix 1**). Data shown in **Figure 3.2** demonstrates that PI3K C2β–/– mice successfully weaned 36% more offspring (158) than control mice (101). Of these pups the control mice produced 48 males and 53 females, which represents 9% more females compared to males. PI3K C2β–/– mice produced 66 males compared to 92 females, which represents 29% more females. These data indicate that PI3K C2β–/– mice analysed not only weaned more pups, but that the sex ratio was skewed towards female offspring.

The increased number of offspring produced by PI3K C2β–/– mice was not due to larger litters, as the average litter size was five pups, compared to

the control animals, which was six pups. However, the number of litters produced over the same period of time was higher in the PI3K C2β–/– mice (41 litters), compared to the controls (31 litters).

Data for pre-weaned mice is more limited, as disturbing female mice and their pups can cause undue stress and is therefore avoided. However, it was noted that there were more litters 'found dead' in the control breeding cages (9 litters), compared to the PI3K C2β–/– breeding cages (6 litters). Excluding the litters that were found dead, PI3K C2β–/– mice produced 167 offspring compared to 128 from control mice. This suggests that fewer PI3K C2β–/– pups died between birth and weaning (5%), compared to the controls (21%).

A

	Control	PI3K C2β$^{-/-}$	Difference	Percentage difference
Male pups weaned	48	66	18	27%
Female pups weaned	53	92	39	42%
Percentage difference	9%	29%		

B

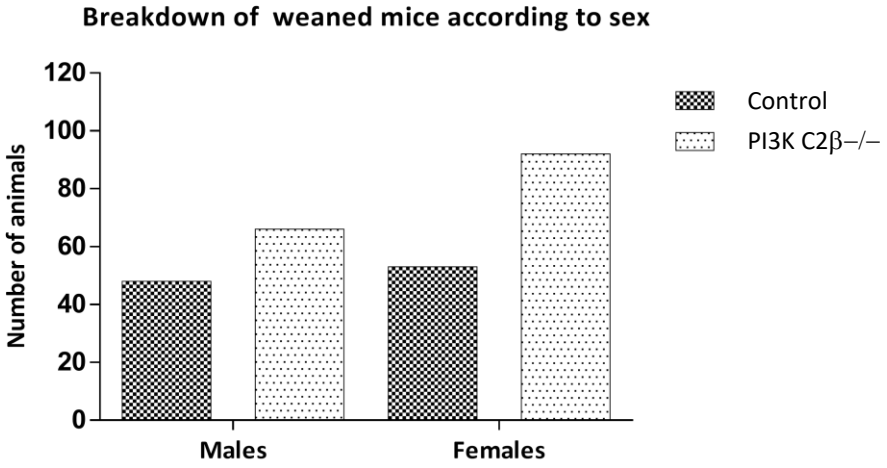

Figure 3.2 Breeding data from control and knockout mice, collected over an eighteen month period. Data was collected from four matched breeding cages from each strain, over the same time period. **A**; PI3K C2β$^{-/-}$ mice successfully weaned 158 pups compared to 101 pups successfully weaned by the controls. **B**; control mice had a male to female ratio of 1:1.1 (48 and 53 pups respectively). The male to female ratio for PI3K C2β$^{-/-}$ mice was 1:1.4 (66 male and 92 female pups). See also **Appendix 1**.

3.4 PI3K C2β–/– mice weigh less than control counterparts over time

Mice used during the project were weighed at culling and data were collected over the course of eighteen months. The range of age was chosen to represent young mice, prime breeding age (10-18 weeks), mature mice that were still within breeding age (19-35 weeks) and post-breeding age (36-52 weeks) **(Table 3.1 and Figure 3.3).**

Male PI3K C2β–/– mice were of a comparable weight to the control mice at 10-18 weeks (26.7g vs 27.0g respectively) and at 19-35 weeks (29.2g vs 29.6g). PI3K C2β–/– males were 11.8% smaller than the controls at 36-52 weeks (30.2g vs 34.2g). The overall difference in male animal weight was considered significant when calculated using a two-way ANOVA (p=0.02). The female PI3K C2β–/– mice showed a more pronounced difference in weight (p=0.001), compared to control mice. At 10-18 weeks female PI3K C2β–/– mice were 8.7% lighter and 10.1% lighter at 36-52 weeks.

Gene knockout in mice can lead to a reduction in bodyweight in approximately one third of viable strains (Reed et al., 2008), and therefore the modest reduction in weight observed in the PI3K C2β–/– mice was not considered any further at this point. However, it was taken into account when assessing spleen weight **(Figure 3.4)**, and as such spleen weight was calculated as a percentage of bodyweight (Sellers et al., 2007).

Table 3.1 Analysis of mouse weight

	Mouse age		
	10-18 weeks	**19-35-weeks**	**36-52 weeks**
Control males	27.1 (n=21)	29.6 (n=6)	34.2 (n=7)
PI3K C2β–/– males	26.7 (n=17)	29.17 (n=9)	30.2 (n=7)
Difference between means	0.03	0.5	4.0
Percentage difference	1.2%	1.5%	11.8%
Control females	22.7(n=14)	23.5 (n=7)	25.8(n=8)
PI3K C2β–/– females	20.7 (n=21)	24.4 (n=4)	23.2 (n=11)
Difference between means	2	0.9	2.6
Percentage difference	8.7%	3.7%	10.1%

Weights are presented in grams and were collected over an eighteen month period.

A

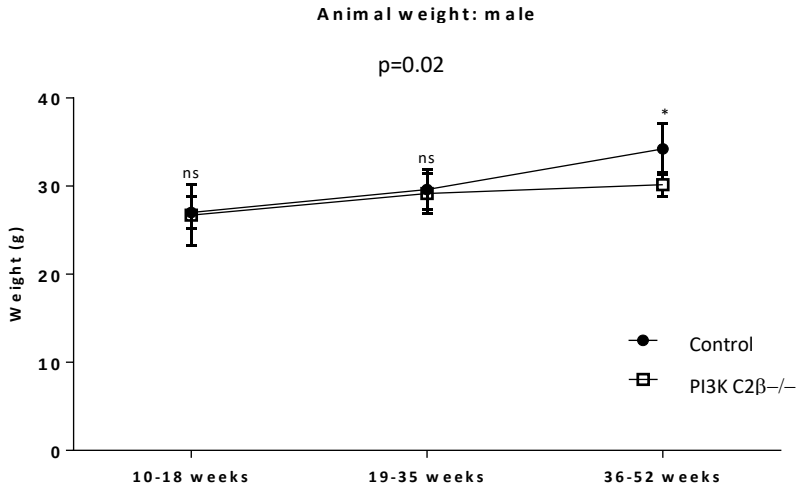

B

Males	10-18 weeks	19-35 weeks	36-52 weeks
Control	21	6	7
PI3K C2β$^{/-}$	17	9	7

C

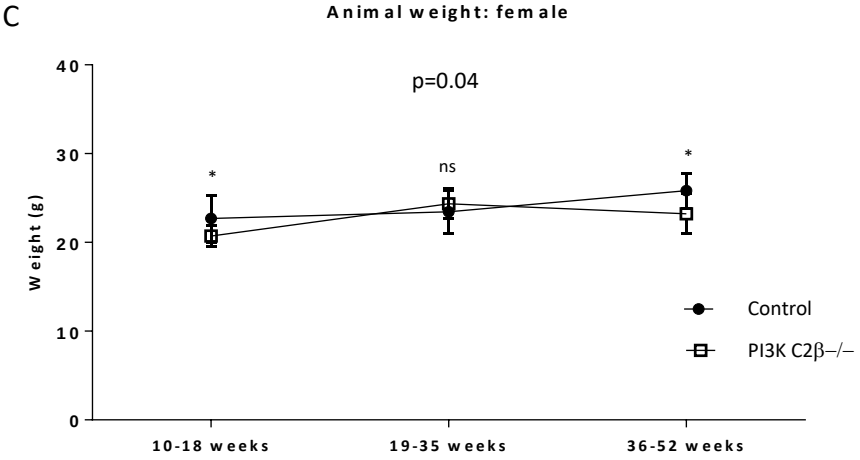

D

Females	10-18 weeks	19-35 weeks	36-52 weeks
Control	14	7	8
PI3K C2β$^{/-}$	21	4	11

Figure 3.3 Comparison of total bodyweight. Mice were weighed immediately after being culled over an eighteen month period. **A**; the weight of control mice and PI3K C2β–/– male mice was comparable at 10-18 weeks and 19-35 weeks. Between the age of 36-52 weeks PI3K C2β–/– males were on average 4.04g lighter. Overall the difference in weight was considered statistically significant (p=0.02). **B**; shows the number of male mice analysed within each age range. **C**; female mice also showed a difference in weight (p=0.04), with PI3K C2β–/– mice being lighter at 10-18 weeks and 36-52 weeks, between 19-35 weeks the weights were comparable. **D**; shows the numbers of female mice weighed within each age range. Statistical analysis was calculated using a two-way ANOVA, * = p<0.05. Data represent mean values ± SEM.

3.5 Spleen overview

Previous work from our laboratory had suggested that PI3K C2β−/− mice exhibit an altered immune response following administration of a sub-nephritogenic dose of nephrotoxic serum (NTS), and as a result PI3K C2β−/− mice developed enlarged spleens (Balakrishnan, 2012). The spleen plays an important role in both the adaptive and innate immune response and is the largest lymphoid organ. Consequently, its analysis has been a longstanding focus for those researchers involved in studying the response of organisms to immunological challenge (Mebius and Kraal, 2005).

3.6 Spleen weight as a percentage of animal weight (Basal and IgG/CFA)

To examine the effect of an immune challenge on spleen morphology, female mice aged between 18-35 weeks were given a subcutaneous injection of a sheep IgG (0.2mg) in PBS with complete Freund's adjuvant (CFA) in a 50:50 ratio. After seven days the mice were culled and the spleens were excised, weighed and fixed in 10% buffered formalin before being processed for immunohistochemistry (IHC).

Spleens from mice treated with IgG/CFA and mice kept under basal conditions were examined (**Table 3.2, Table 3.3 and Figure3.4**). To take into account any variation in animal weight which might influence spleen weight, data for spleen weight are expressed as a percentage of animal weight. Statistical analysis was performed using unpaired multiple t-tests, corrected for multiple comparisons using the Sidak-Bonferroni method.

As a percentage of animal weight, spleens in PI3K C2β–/– mice were slightly smaller than those of control mice that were untreated (basal). The difference between female PI3K C2β–/– and control mice (0.3% ± 0.01 and 0.4% ± 0.01, respectively) which equates to a 13.2% difference in spleen weight as a percentage of animal weight (p= 0.007).

Following IgG/CFA treatment, spleen weight as a percentage of animal weight was greater in the PI3K C2β–/– mice, compared to the controls (0.6% ± 0.04 vs 0.4% ± 0.02, respectively), representing an increase of 29.5% (p=0.01). Although treatment with IgG/CFA increased spleen weight in both PI3K C2β–/– mice and controls, it produced a greater effect in PI3K C2β–/– mice. In control mice the difference in spleen weight between IgG/CFA treated and untreated mice was 0.1% ± 0.02 (p=0.005), representing a 15.8% difference. In comparison, spleens from PI3K C2β–/– mice treated with IgG/CFA were 72.7 % greater than spleens from untreated PI3K C2β–/– mice (p=<0.0001).

Table 3.2 Analysis of spleen weight as a percentage of animal weight.

	Basal	**IgG/CFA**	**Difference**	**Significance**
Control	0.4% ± 0.01 (n=14)	0.4% ± 0.02 (n=13)	0.1 ± 0.02	p=0.005
PI3K C2β–/–	0.3% ± 0.01 (n=16)	0.6% ± 0.04 (n=15)	0.2 ± 0.04	p=< 0.0001
Difference	0.05 ± 0.02	0.1 ± 0.04		
Significance	p=0.007	p= 0.01		

Female mice aged between 18-35 weeks were examined either under basal conditions or following treatment with sheep IgG and CFA. Spleen weight as a percentage of bodyweight was examined. Statistical analysis was performed using unpaired multiple t-tests, corrected for multiple comparisons using the Sidak-Bonferroni method. Data represent mean values ± SEM.

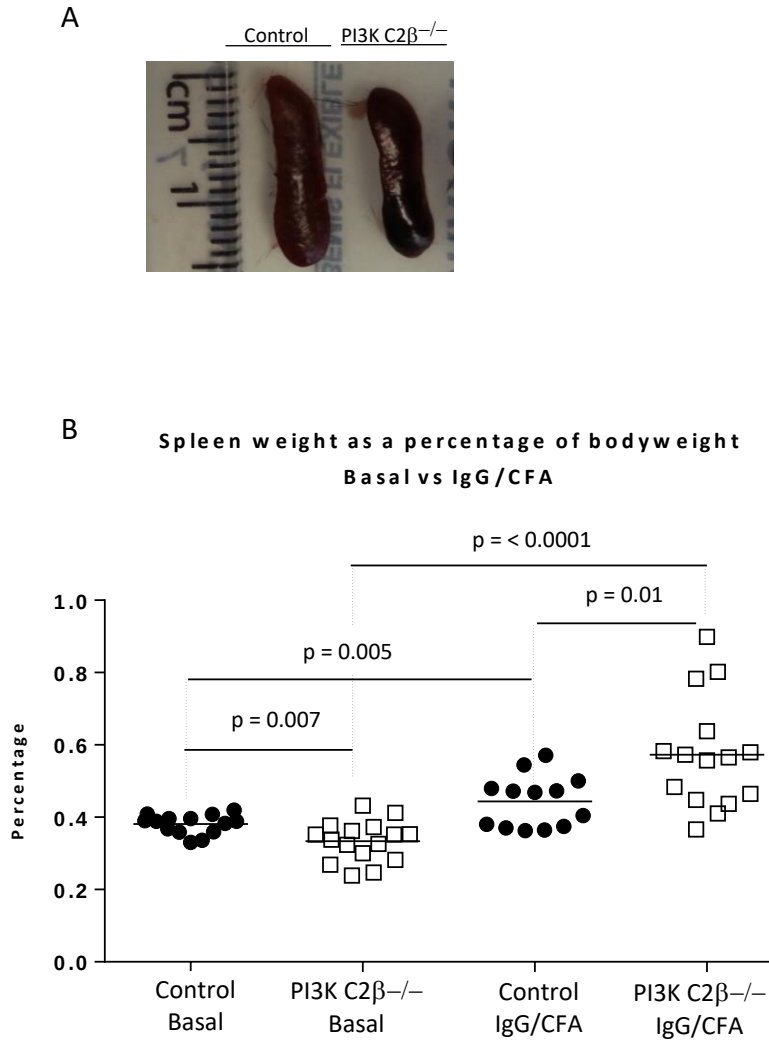

Figure 3.4 Spleen weight as a percentage of animal weight from mice kept under basal conditions or mice treated with IgG/CFA. Female mice between 18-35 weeks of age were used in this experiment, and were culled after seven days, post subcutaneous injection with IgG and CFA. **A**; images of freshly isolated spleens from control and PI3K C2β−/− mice kept under basal conditions. **B**; Spleen weight expressed as a percentage of animal weight in animals treated with (IgG/CFA) or without (Basal) sheep IgG and CFA. Under basal conditions the spleens of PI3K C2β−/− mice were 0.3% ± 0.01 of the total body weight (n=15), compared to 0.4% ± 0.01 in the controls (n=14). When treated with IgG/CFA this trend was reversed and PI3K C2β−/− spleens were 0.6% ± 0.04 of the total body weight (n=15), while the spleens of control mice were 0.4% ± 0.02 (n=13). Statistical analysis was performed using unpaired multiple t-tests, corrected for multiple comparisons using the Sidak-Bonferroni method, with p=<0.005 being considered statistically significant. Data represent mean values ± SEM

3.7 Immunohistochemistry (Basal vs IgG/CFA)

Following stimulation with sheep IgG/CFA, PI3K C2β−/− mice had shown a greater increase in spleen weight compared to control mice. As a reservoir for B-cells and T-cells and an important mediator of both innate and adaptive immune responses, I wanted to investigate whether the increase in spleen weight reflected an altered immune response in the PI3K C2β−/− mice. Following excision, spleens were fixed in 10% neutral buffered formalin for approximately 16 hrs, transferred to 70% ethanol before processing at the Histology Department, Imperial College, London.

3.8 Germinal centre associated proliferation in unimmunized and IgG/CFA treated mice

As the PI3K C2β−/− mice had shown a greater increase in spleen weight as a percentage of animal weight in response to IgG/CFA treatment, I initially examined whether there were any differences in the rates of splenocyte proliferation. Formalin fixed paraffin embedded sections were de-waxed, rehydrated and subjected to HIER before treatment with anti-PCNA (proliferating cell nuclear antigen), which is a marker of cell proliferation, and visualised with DAKO EnVision+ System-HRP. Following the addition of DAB substrate chromogen, sections were counterstained with haematoxylin, dehydrated and mounted prior to analysis. Greater numbers of PCNA positive cells were detected in the follicles of spleens from PI3K C2β−/− mice compared to controls, both under basal conditions and following an immunological challenge with IgG/CFA (**Figure 3.5 and Figure 3.6**). These areas appeared to be germinal centres, which are areas of B-cell

proliferation that occur in response to antigen activation. Immunostaining with the pan B-cell marker B220 confirmed that the germinal centres had been correctly identified. Measurements were performed using CellSens software (Olympus), on stitched images of whole spleens. Spleens from four control mice and five PI3K C2β−/− mice were analysed from each group (Basal and IgG/CFA treated).

The areas of PCNA positive germinal centres were compared to the area defined by B220 staining. Under basal conditions, the mean germinal centre area, as defined by B220 staining in PI3K C2β−/− mice was 1.4 mm^2 ± 0.1. In the control mice this value was 1 mm^2 ± 0.02 (p=0.03). Following treatment with IgG/CFA the mean area of germinal centre associated proliferation was 1.8 mm^2 ± 0.1 in PI3K C2β−/− mice and 0.8 mm^2 ± 0.2 in controls (p=0.0001). Given the earlier concern that differences in animal weight might influence spleen size, the area of the germinal centres was expressed as a percentage of spleen area. The percentage of GC associated proliferation was increased in comparison to the controls, under basal conditions and following treatment with sheep IgG/CFA (**Figure 3.7**). Measurement of spleen area showed that under basal conditions PI3K C2β−/− spleen area was reduced in mice compared to the controls (17.2 mm^2 vs 29.6 mm^2) p=0.0002. Spleen area was comparable between control and PI3K C2β−/− mice following IgG/CFA treatment (26.3 mm^2 vs 26.3 mm^2) p=0.4.

Table 3.3 Analysis of germinal associated cell proliferation.

Area of Germinal Centre associated cell proliferation (mm^2)

	Basal	IgG/CFA
Control	1 ± 0.02	0.8 ± 0.2
	n=4	n=4
PI3K C2β$^{-/-}$	1.4 ± 0.1	1.8 ± 0.1
	n=5	n=5
Difference	0.4 ± 0.1	1.1 ± 0.2
Significance	p= 0.03	p= 0.001

Germinal Centre area expressed as a percentage of spleen area

	Basal	IgG/CFA
Control	0.1 ± 0.02	0.04 ± 0.01
	n=4	n=4
PI3K C2β$^{-/-}$	0.3 ± 0.04	0.3 ± 0.1
	n=5	n=5
Difference	0.2 ± 0.04	0.2 ± 0.1
Significance	p= 0.01	p= 0.03

Total spleen area (mm^2)

	Basal	IgG/CFA
Control	29.6 ± 2.4	26.3 ± 2.02
	n=4	n=4
PI3K C2β$^{-/-}$	17.2 ± 0.2	24 ± 1.6
	n=6	n=5
Difference	12.4 ± 2.42	2.3 ± 2.6
Significance	p=0.0002	p=0.4

Cell proliferation in spleen germinal centres was determined after IHC analysis using anti-PCNA and anti-B220 antibodies. Statistical analysis was performed using unpaired multiple t-tests, corrected for multiple comparisons using the Sidak-Bonferroni method. Data represent mean values ± SEM.

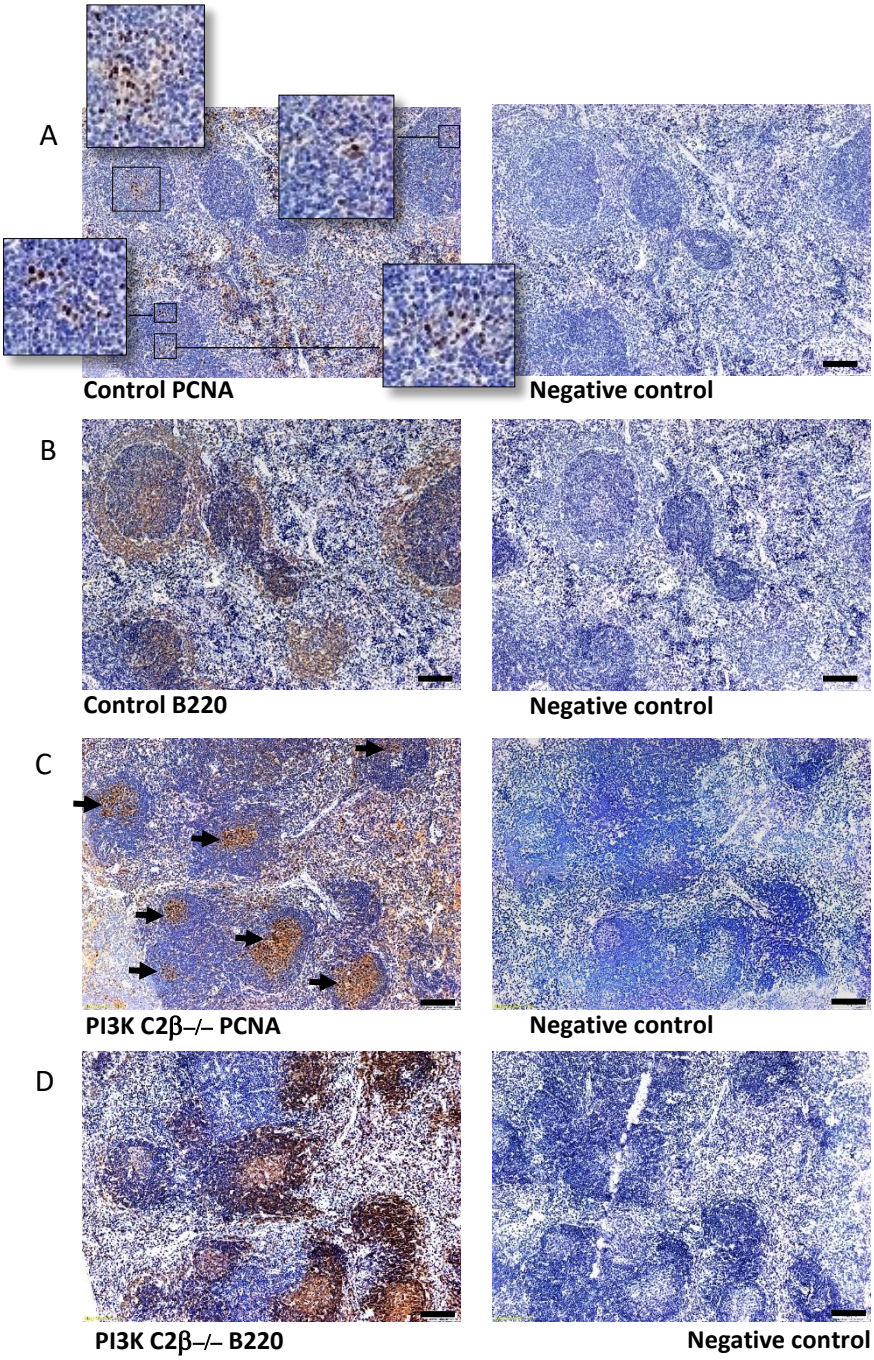

Figure 3.5 PCNA and B220 immunostaining of spleen from control and PI3K C2β–/– mice kept under basal conditions. Formalin fixed paraffin embedded serial spleen sections from control and PI3K C2β–/– mice kept under basal conditions, were immunostained with anti-PCNA or an isotype control (**A** and **C**). **B** and **D** matched sections were stained with anti-B220 or an isotype control to confirm that proliferation was associated with germinal centres. Increased areas of PCNA staining in PI3K C2β–/– spleens, are highlighted (black arrows). Original magnification was at 10X. Size bar represents 100µm.

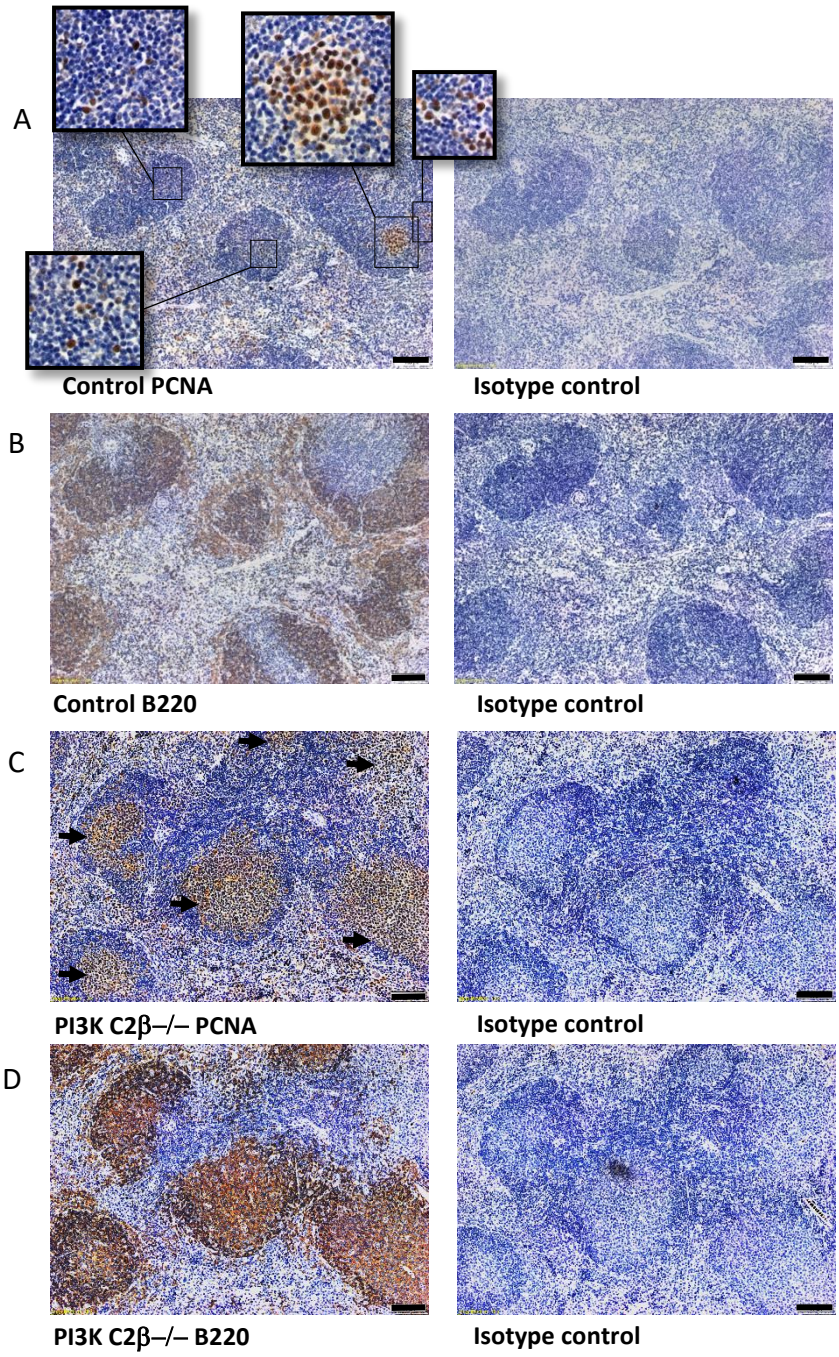

Figure 3.6 PCNA and B220 immunostaining of spleen from control and PI3K C2β–/– mice treated with IgG/CFA. Formalin fixed paraffin embedded serial spleen sections from control and PI3K C2β–/– mice treated with IgG/CFA, were immunostained with anti-PCNA or an isotype control (**A** and **C**). **B** and **D** matched sections were stained with anti-B220 or an isotype control to confirm that proliferation was associated with germinal centres. Increased areas of PCNA staining in PI3K C2β–/– spleens, are highlighted (black arrows).Original magnification was at 10X. Size bar represents 100µm.

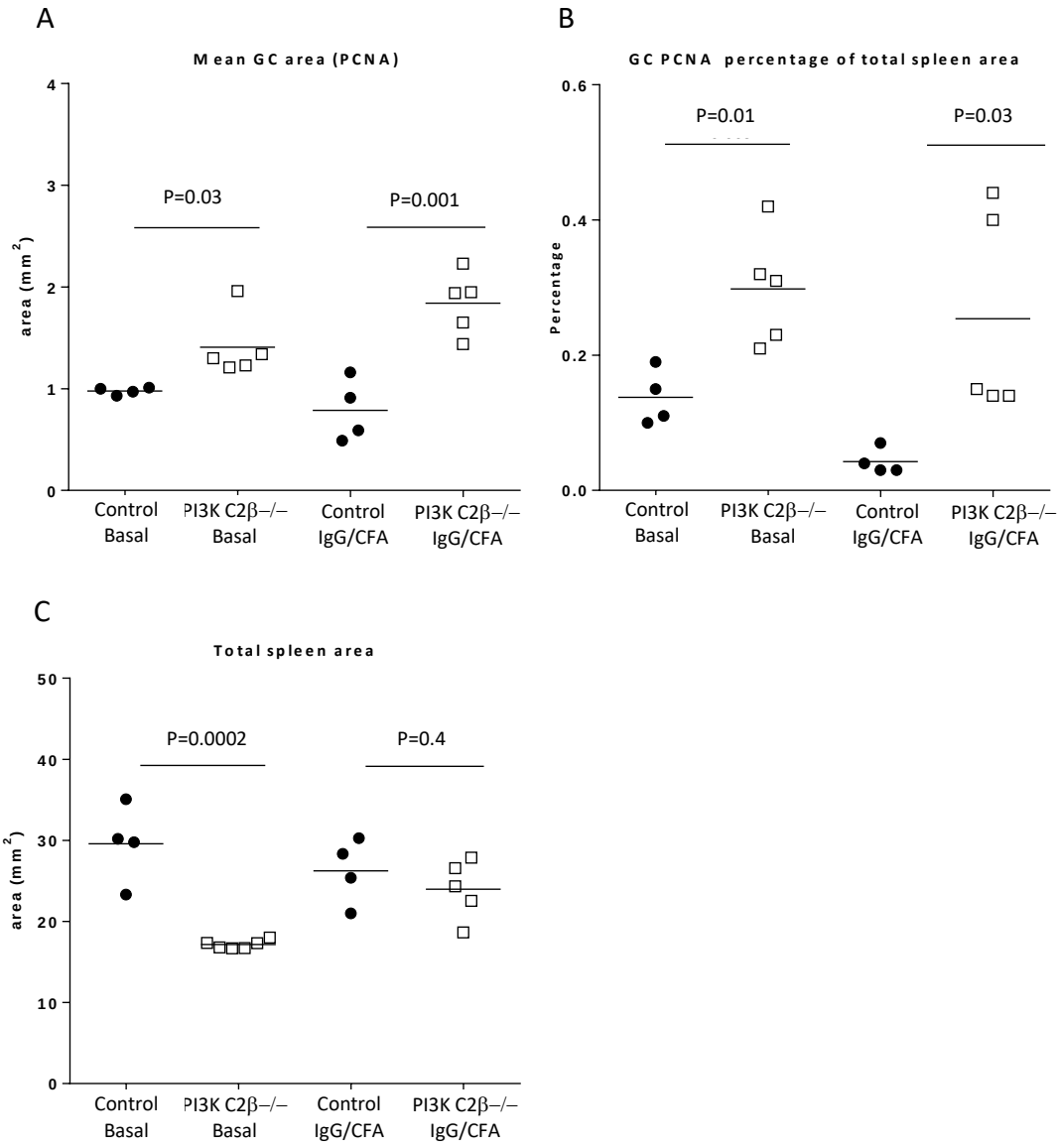

Figure 3.7 Quantification of germinal centre associated proliferation using anti-PCNA. Spleens from control and PI3K C2β−/−mice kept either under basal conditions or treated with sheep IgG/CFA, were excised and stained with anti-PCNA or an isotype control. To confirm that the areas of proliferation were germinal centres, matched sections were also stained with anti-B220 or an isotype control. Germinal centre proliferation was then measured using the Olympus BX63 CellSens software. **A**; the mean area of germinal centre associated proliferation (PCNA positive) from the spleens of PI3K C2β−/− mice was greater than the controls, both under basal conditions ($1.4mm^2$ vs $1mm^2$) p=0.03, and when treated with IgG/CFA, although the greatest increase was seen following IgG/CFA treatment ($1.8mm^2$ vs $0.8mm^2$) p=0.001. **B**; as a percentage of the total spleen area, the area of GC related proliferation was also greater in PI3K C2β−/− mice under both conditions, the greatest difference was observed under basal conditions (0.3% vs 0.1%) p=0.01 **C**; measuring total spleen area showed that PI3K C2β−/− mice had a smaller surface area than age matched, sex matched control mice under basal conditions ($17.2mm^2$ vs $29.6mm^2$) p=0.0002. However, following treatment with IgG/CFA the difference in total spleen area was comparable ($24mm^2$ vs $26.2mm^2$) p=0.4. Statistical analysis was performed using unpaired multiple t-tests, corrected for multiple comparisons using the Sidak-Bonferroni method. Data represent mean values ± SEM.

3.9 Discussion

These results show that the mean area of GC associated proliferation was greater in the spleens of unimmunized PI3K C2β−/− mice, and the difference was increased following treatment with IgG/CFA, compared to controls. However, analysis of total GC related proliferation, calculated as a percentage of spleen area, indicates that unimmunized PI3K C2β−/− mice have an increased background level of GC associated proliferation compared to control mice. Germinal centres are dynamic structures that occur in response to T-cell dependent (TD) activation with a cognate antigen and contain two distinct compartments referred to as the dark zone (DZ) and the light zone (LZ). The DZ is where rapid proliferation occurs (Vinuesa et al., 2009), which has been supported by gene array analysis showing the upregulation of genes involved in cell division and an increased population within the G2/M phase of the cell cycle, which was absent within the LZ. Cells within the LZ showed upregulation of genes associated with signalling and apoptosis (De Silva and Klein, 2015; Victora et al., 2010; Vinuesa et al., 2009).

The difference between GC associated proliferation in unimmunized PI3K C2β−/− and control mice was intriguing because both strains were kept under the same conditions within a pathogen free environment. The interaction between the DZ and LZ is thought to be coordinated by CD4+ follicular helper T-cells (Tfh), residing mainly within the LZ. Following activation, B-cells migrate to the LZ where they present antigen to the Tfh

cells as part of an MHC II complex. B-cells with the highest affinity for their antigen, determined by the concentration of antigen presented, are signalled to return to the DZ and proliferate. B-cells with a low affinity for antigen remain in the LZ, and presumably undergo apoptosis (Victora et al., 2010).

The controlled environment in which the mice are kept make it unlikely that PI3K C2β−/− B-cells encounter their cognate antigen more frequently, resulting in Tfh cells driving the GC reaction forward. It is possible that PI3K C2β−/− mice mount a GC reaction in response to self-antigen, as spontaneous GC formation is associated with autoimmunity in mouse models (Luzina et al., 2001). However, although neither strain of mice have undergone examination by a professional pathologist, there have been no reports of health issues or reduced lifespan that might be expected if PI3K C2β−/− mice were predisposed to spontaneous autoimmunity (Jolly et al., 2001; Singh et al., 2007).

The increased area of individual GCs may indicate that PI3K C2β−/− B-cells are unable to exit the GC/DZ as efficiently as the controls. B-cells are highly motile within the GC, shuttling between the DZ and the LZ (De Silva and Klein, 2015; Oropallo and Cerutti, 2014). Fo B-cells have been observed entering and leaving the GC (Meyer-Hermann et al., 2012) and MZ B-cells regularly deliver antigen to follicles (Arnon et al., 2013). This movement is regulated by chemokines produced by accessory cells within the local environment, and changes in receptor expression, such as CXCR5 and

CXCR4. Dendritic cells within the LZ produce CXCL13, facilitating the migration of B-cells expressing CXCR5 from the DZ into the LZ. Upregulation of CXCR4 in response to CXCL12 allows B-cells to migrate from the LZ to the DZ (Allen et al., 2004). Research into GC maintenance and homeostasis has revealed a role for the extracellular signalling molecule Sphingosine-1-phosphate (S1P), which mediates the exiting of B-cells from the GC via five specific G protein coupled receptors (GPCRs). These receptors referred to as S1P1-5, allow cells to respond to the S1P gradient, which is higher in the blood than in the spleen (Blaho and Hla, 2014; Maceyka et al., 2012). GC B-cells express high levels of S1P2 which was shown to be important in mediating the egress of GC B-cells. S1P2 deficient mice develop chronically enlarged GCs over time, as GC B-cells are unable to respond to S1P and exit the GC (Green et al., 2011). In a previous experiment, loss of S1P2 led to a high incidence of age related diffuse large B-cell lymphoma (DLBCL) in mice (Cattoretti et al., 2009). PI3K C2β has recently been shown to have a contributory role in S1P dependent cell migration following gene knock down in human umbilical vein endothelial cells (HUVEC). siRNA gene targeting against PI3K C2α, PI3K C2β and Class I P110γ revealed that loss of PI3K C2α had little effect on migration, whereas loss of either P110γ or PI3K C2β resulted in significant inhibition of S1P dependent migration. Knock down of both of these genes led to the most significant effect on migration suggesting that the role of PI3K C2β is not redundant (Tibolla et al., 2013).

A loss of S1P mediated migration from the GC provides a potential connection to the increased GCs in the PI3K C2β$^{-/-}$ spleens. However, the

study by Tibolla (2013) did not investigate whether the specific S1P receptor influences the contribution of PI3K C2β to S1P mediated migration. The influence of S1P to B-cell function is dependent on the S1P receptor signalling pathway and could be a contributing factor in primary immunodeficiencies, such as chronic lymphocytic leukaemia (CLL) and multiple sclerosis (MS) (Sic et al., 2014). An additional complication is that S1P receptors appear to operate in a coordinated manner (Kono et al., 2004), and appear to modulate the expression and function of other S1P receptors (Sic et al., 2014).

4 Splenocyte populations in control and PI3K C2β–/– mice.

Immunohistochemistry data presented in the previous chapter demonstrated increased cell proliferation in the germinal centres of PI3K C2β–/– spleens, both in unimmunized mice and following treatment with sheep IgG/CFA. Consequently, I focused on B-cells and T-cells as the major leukocyte populations resident in the spleen. These were characterised using flow cytometry and fluorophore conjugated antibodies. T-cells were of particular interest given their role in the formation of germinal centres.

4.1 Splenic T-cell population under basal conditions (0hr)

The spleen is a major reservoir for T-cells, which are predominantly located in the periarteriolar lymphoid sheath (PALS) of the splenic white pulp (WP) and are associated with the adaptive immunity. Initial T-cell populations were quantified using anti-CD4 and anti-CD8 antibodies. CD4 is a T-cell co-receptor associated with interactions involving major histocompatibility complex II (MHC II) molecules and are often referred to as regulatory T-cells or helper T-cells (Th). T-cells that are CD8+, referred to cytotoxic T-cells associate with major histocompatibility complex I (MHC I) molecules, differentiating them from CD4+ T-cells.

Splenocytes were isolated from freshly harvested spleens and allowed to rest for between one and two hr, prior to labelling with fluorophore conjugated antibodies and analysis by flow cytometry.

My data (**Figure 4.1**) showed a significant increase in the PI3K C2β–/– CD4+ splenocyte number compared to the controls (20.6% ± 1 vs 14.9% ± 0.4, respectively) (p=<0.0001). No difference was seen in the CD8+ populations (control 10.1% ± 0.4 vs PI3K C2β–/– 10.6% ± 0.4). These data were from four independent experiments, using a total of twelve control and twelve PI3K C2β–/– mice.

Having observed a consistently elevated CD4+ population in the PI3K C2β–/– splenocytes, I next wanted to confirm that this increase was the result of increased T-cell numbers rather than increased numbers of dendritic cell or NK cells, as these cell types can also express CD4. Freshly isolated splenocytes were co-stained with the pan T-cell marker CD3 and CD4 (**Figure 4.2**). These results closely reflected my initial data. Spleens from PI3K C2$\beta^{-/-}$ mice showed 5.2% more CD3+/CD4+ positive splenocytes than did spleens from control mice (18.8% ± 1.2 vs 13.6% ± 0.4). This increase was significant when analysed by student t-test (p=0.002). Data are from two independent experiments using six control and six PI3K C2β–/– mice.

Table 4.1 Lymphocyte populations at 0 hr.

	B220	CD19	CD4	CD8	CD3+/CD4+
Control	62.7 % ± 2.7	65 % ± 1.7	14.9 % ± 0.4	10.1 % ± 0.4	13.6 % ± 0.4
PI3K C2β$^{-/-}$	63.4 % ± 3	56.6 % ± 2.7	20.6 % ± 1	10.6 % ± 0.4	18.8 % ± 1.2
Difference	0.7 ± 4.0	8.3 ± 3.2	5.7 ± 1.1	0.5 ± 0.6	5.2 ± 1.2
Significance	p=0.9	p=0.02	p=< 0.0001	p=0.4	p=0.002

A student t-test was used to determine whether the difference between populations was statistically significant. Results are from three independent experiments, using nine control and nine PI3K C2β$^{-/-}$ mice (B220 and CD19), or four experiments using twelve control and twelve PI3K C2β$^{-/-}$ mice (CD4 and CD8). Statistical analysis was performed using unpaired multiple t-tests, corrected for multiple comparisons using the Sidak-Bonferroni method, results were considered significant at p=< 0.005. Data represent mean values ± SEM.

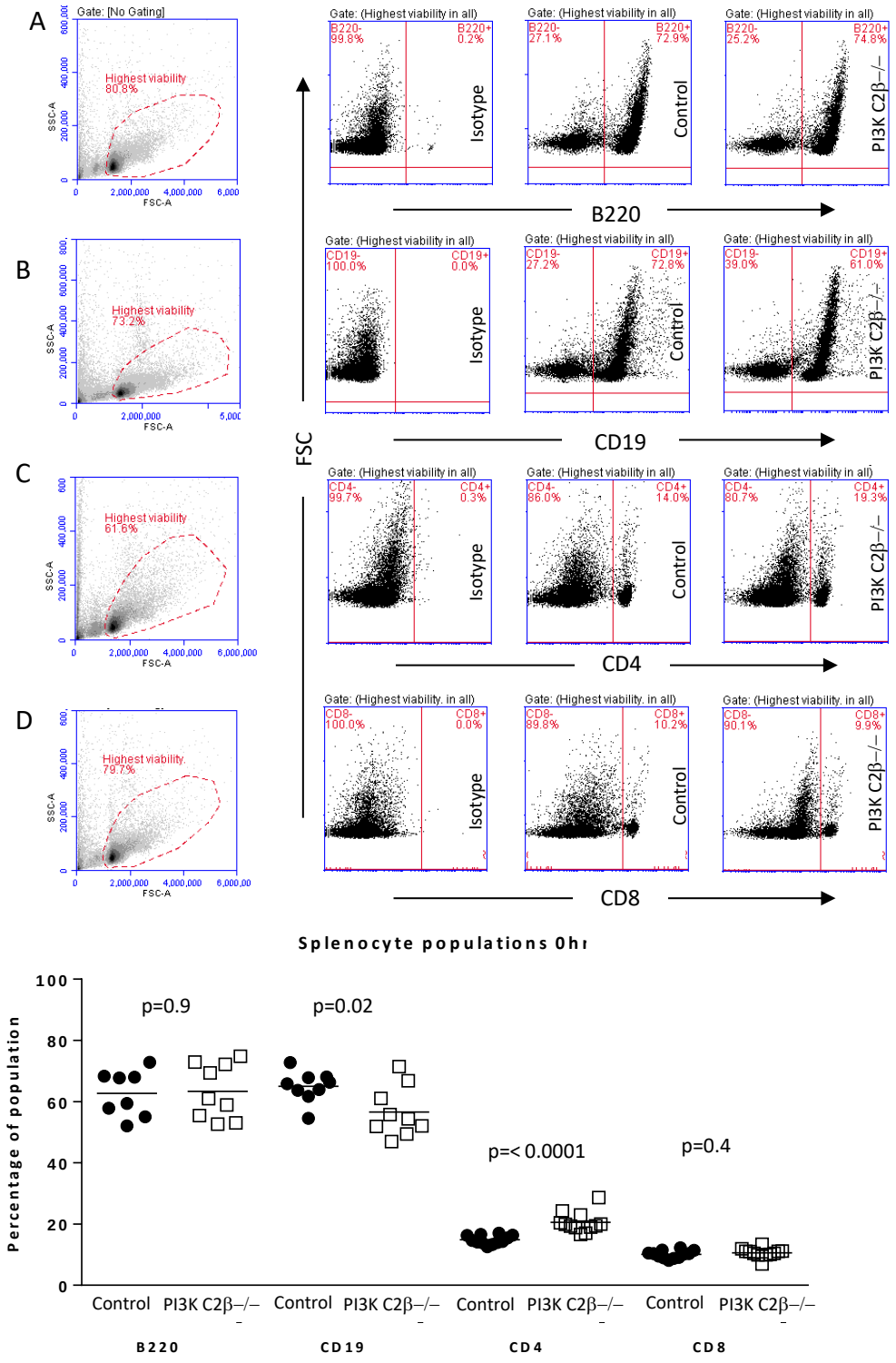

Figure 4.1 Splenocyte population breakdown at 0 hr. Freshly isolated, unstimulated splenocytes were allowed to rest for 1-2 hr before each sample was labelled with fluorophore conjugated antibodies to anti CD19, anti B220, anti CD4, anti CD8 and the relevant isotype controls. **A** to **D**; representative plots for B220, CD19, CD4 and CD8 populations. Left to right; initial gating for highest viability cells, negative isotype control and labelled populations for control and PI3K C2β–/– splenocytes. A minimum of 30,000 events were recorded for each plot. **E**; analysis of results showed that PI3K C2β–/– and control splenocytes had comparable populations of B220+ (63.4% ± 3 and 62.7% ± 2.7 respectively) p=0.9, and CD8+ cells (10.6% ± 0.4 and 10.1% ± 0.4 respectively) p=0.4, there was a reduced CD19+ population in the PI3K C2β–/– samples (56.6% ± 2.7 compared to 65% ± 1.7 in controls) p=0.02. There was a small but significant increase in the PI3K C2β–/– CD4+ population, compared to controls (20.6% ± 1 and 14.9% ± 0.4) p=< 0.0001. Results are from three independent experiments (B220 and CD19) and four independent experiments (CD4 and CD8). Statistical analysis was performed using unpaired multiple t-tests, corrected for multiple comparisons using the Sidak-Bonferroni method. Results were considered significant at p=< 0.005 Data represent mean values ± SEM.

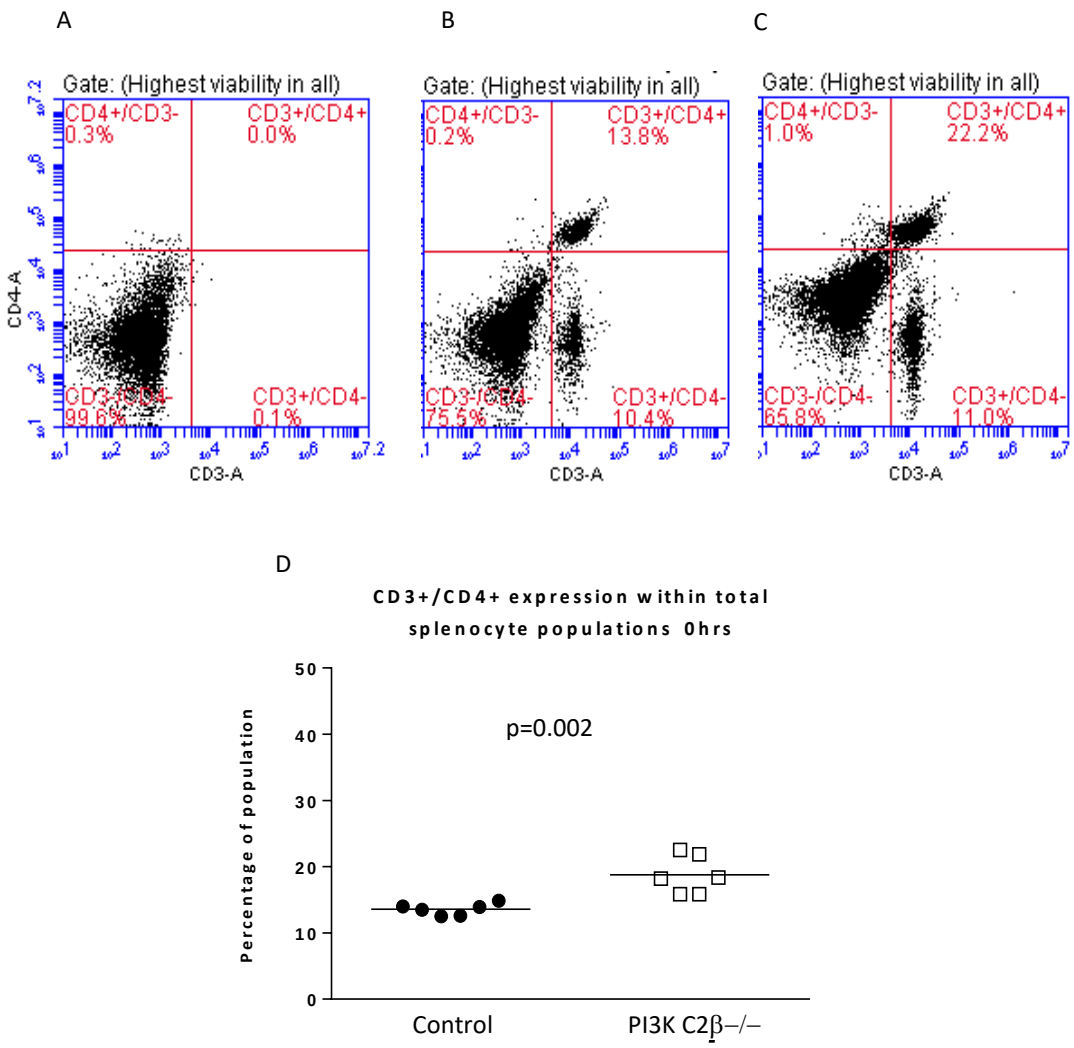

Figure 4.2 Confirmation of T-cell populations. Analysis of CD4+ splenocytes had shown a small but significant increase in the PI3K C2β$^{-/-}$ population. To confirm that the increase was as a result of an expanded T-cell population freshly isolated splenocytes were labelled with fluorophore conjugated antibodies to the pan T-cell marker CD3, in conjunction with CD4. A minimum of 30,000 events were recorded for each plot. **A**; representative plot showing staining for the isotype control, used for gating. **B** and **C**; co-staining results from control and PI3K C2β$^{-/-}$ splenocytes, respectively. **D**; the significant increase in the PI3K C2β$^{-/-}$ CD4+/CD3+ population correlated well with the previously seen increase in CD4+ T-cells (18.8% ± 1.2 compared to 13.6% ± 0.4) p=0.002. An unpaired, two tailed Student t-test was used to determine statistical significance. Data represent mean values ± SEM.

4.2 Splenic B-cell population 0 hr

Identification of B-cell populations was performed using the pan B-cell markers B220 (CD45R) and CD19. Splenocytes were isolated from freshly harvested spleens and allowed to rest for one to two hr before being labelled with fluorophore conjugated antibodies and analysed by flow cytometry. To examine the relative level of antigen expression, median fluorescent intensity (MFI) was measured.

Data from three independent experiments using the B-cell marker B220 showed that both PI3K C2β−/− and control splenocytes had comparable populations (62.7 % ± 2.7 vs 63.4% ± 3, respectively) (**Figure 4.1**). Use of the B-cell marker CD19 provided similar results for the control splenocytes, with 65 % ± 1.7 splenocytes being positive for CD19. The mean CD19 positive cell population was 56.6 % ± 2.7 in PI3K C2β−/− mice, a difference of 8.4% compared to the controls (p=0.02). However, as statistical analysis was performed using unpaired multiple t-tests, corrected for multiple comparisons using the Sidak-Bonferroni method, this result was not considered statistically significant. MFI for CD19 was also measured and revealed a significant increase (p=0.0001) in the population within the PI3K C2β$^{-/-}$splenocytes (**Figure 4.3)**. Together, these data indicate that PI3K C2β$^{-/-}$ mice had fewer CD19 positive splenocytes than control animals, but the level of CD19 expression within this CD19 positive cell population was increased. These data were obtained from three independent experiments using nine control and nine PI3K C2β−/− mice.

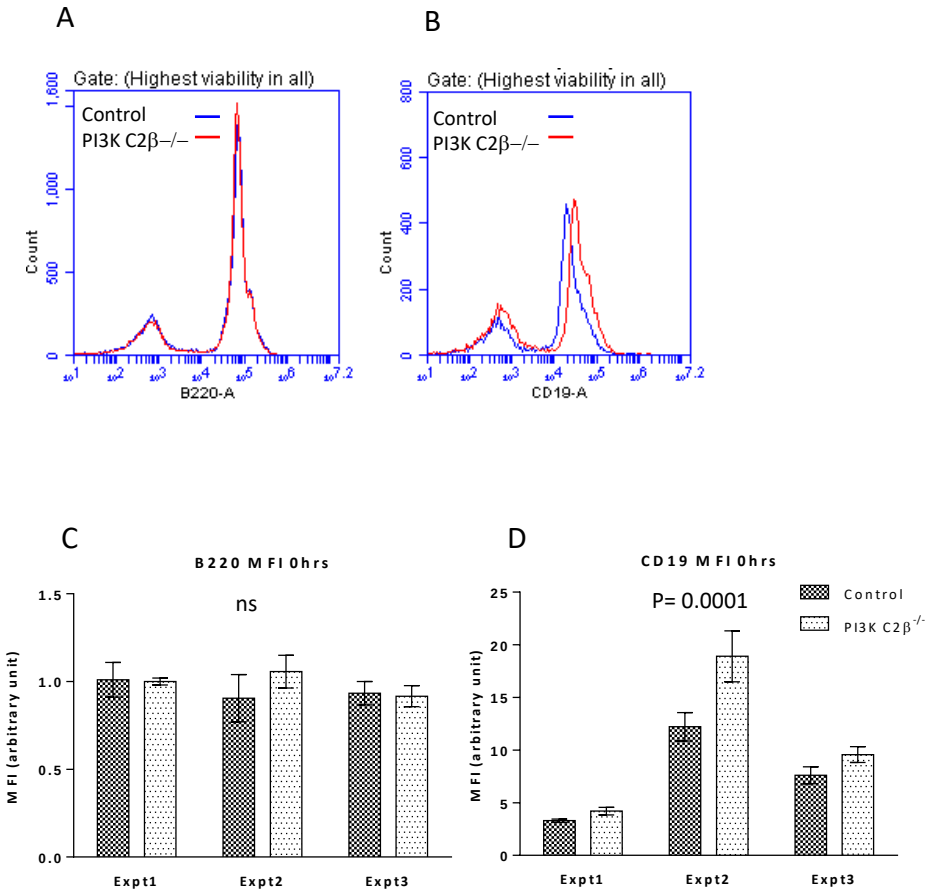

Figure 4.3 Median fluorescence intensity (MFI) for B220 and CD19. Median fluorescent intensity was analysed following initial lymphocyte population analysis, using the BD Accuri C6 software. 30,000 events were recorded per plot. Representative overlaid histograms showing **A**; median fluorescent intensity for B220 and **B**; CD19 populations found in spleens of control (blue line) and PI3K C2β–/– (red line) mice **C**; MFI is shown for B220 staining of control and PI3K C2β–/– splenocytes. **D**; MFI is shown for CD19 staining for control and PI3K C2β–/– splenocytes. Data for B220 are from two independent experiments, using a total of six control and six PI3K C2β–/– mice. CD19 data were generated from three independent experiments, using a total of nine control and nine PI3K C2β–/– mice. Statistical analysis was calculated using a two-way ANOVA.

4.3 Isolated splenic CD4 positive T-cells

To examine whether differences exist upon stimulation between CD4 positive T-cells obtained from the spleens of control and PI3K C2β–/– mice, isolated T-cells were stimulated with CD3ε/CD28 coated beads. This approach would exclude the possible influence of accessory cells found in the intact spleen or total splenocyte populations.

T-cells were isolated from the spleens of age-matched and sex-matched control and PI3K C2β–/– mice by negative selection. T-cell purity was assessed using a FITC-conjugated antibody to the pan T-cell marker CD3, resulting in an enriched T-cell population which was shown to exceed 98% (**Figure 4.4**).

4.4 The CD4/CD8 ratio appears to be unaffected in isolated T-cells

Analysis of T-cell populations at 0 hr, within isolated splenocytes had shown that compared to the controls, PI3K C2β–/– mice had an increased CD4+ T-cell population (**Figure 4.2**). To assess whether CD4/CD8 populations would be affected differently when cultured in isolation, a preliminary experiment using isolated T-cells, stimulated with anti-CD3ε and anti-CD28 coated beads was conducted. T-cells were cultured as recommended by the manufacturer of the 'activation beads' (Miltenyi Biotec), for 80 hr before analysis using flow cytometry. Results revealed no difference in the number of CD8 positive T-cells. The means were 50.3% ± 2.8 for the controls and 49.9% ± 0.6 for PI3K C2β–/– (**Figure 4.5**). These data indicate that when cultured under the same conditions the CD4+ and CD8+ populations

respond comparably. Three control and three PI3K C2β−/− mice were used, these data are from a single experiment. Statistical analysis has not been applied as this experiment was not powered to detect a difference between the samples.

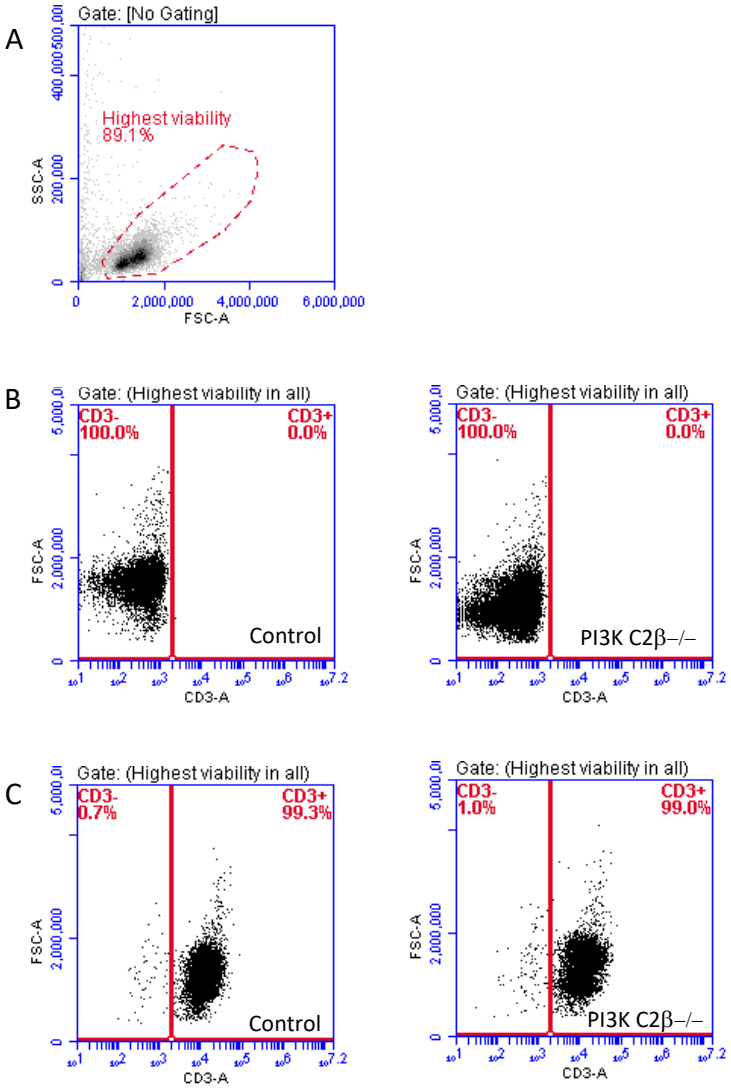

Figure 4.4 T-cell isolation. T-cells were harvested from the spleens of freshly culled control or PI3K C2β−/− mice, using negative isolation. Flow cytometry using the pan T-cell marker CD3 was used to determine the purity of T-cell populations. A minimum of 10,000 events were recorded per plot. **A**; a representative plot showing gating strategy. Cells within the highest viability gate were analysed. **B**; representative plots showing results for the isotype control to exclude any non-specific binding. **C**; cells were labelled with anti-CD3 (FITC) and were found to be >98% positive for both control (left) and PI3K C2β−/− cultures.

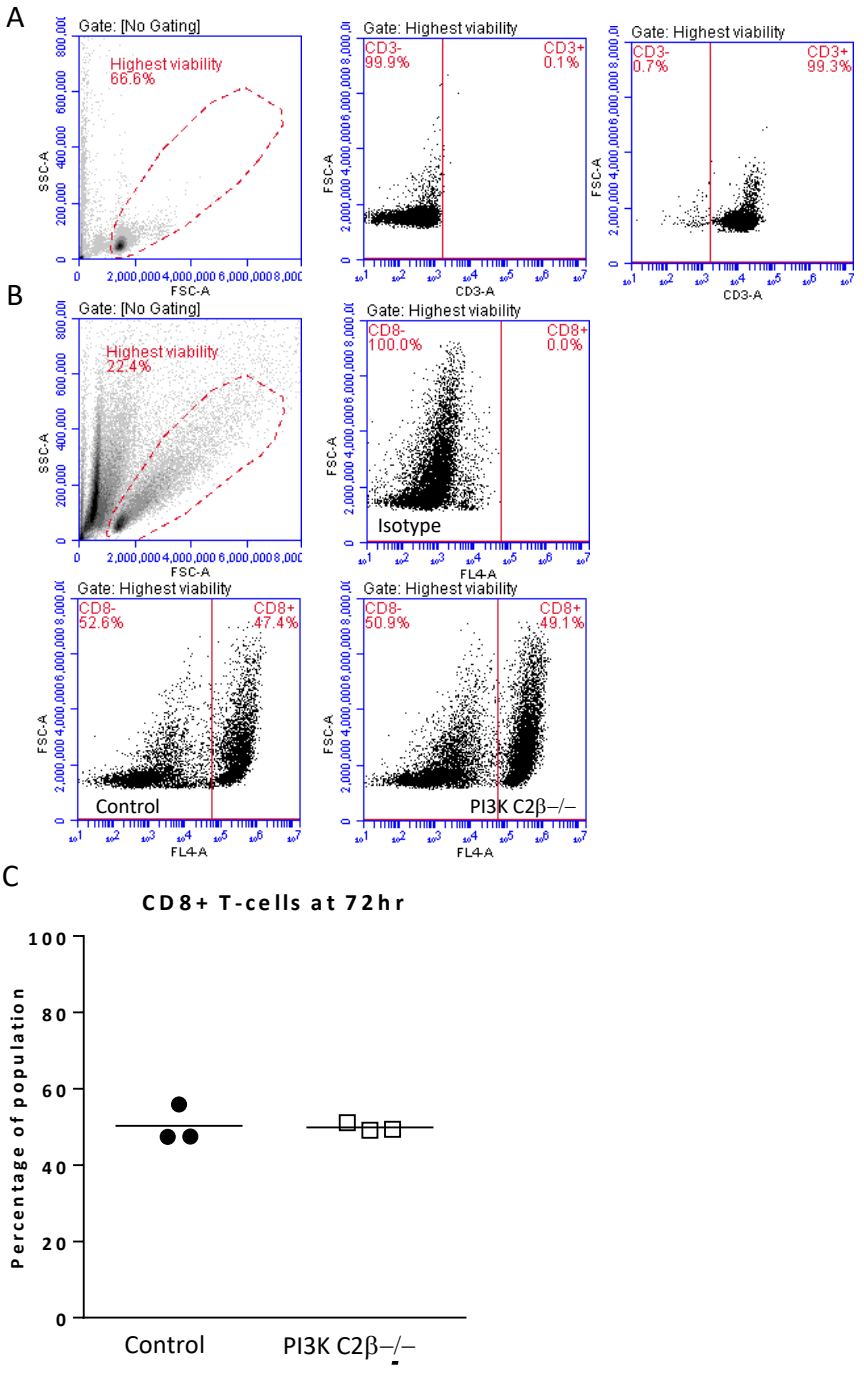

Figure 4.5 CD8+ T-cell populations at 72 hr. Following isolation, T-cell purity was examined. Cells were plated at 2x10^6/ml and stimulated with anti-CD3ε and anti-CD28 coated beads. A minimum of 10,000 events were recorded per plot. **A**; representative plots showing T-cell purity following isolation which were >98% CD3+. **B**; plots showing T-cells at 72 hr, cells were assessed from the highest viability population (upper left), cells were labelled with an isotype control (upper right), or anti CD8 (lower panels). **C**; analysis of results showed no difference between the percentage of CD8+ T-cell isolated from control and PI3K C2β−/− animals (50.3% ± 2.83 and 49.9% ± 0.6, respectively). Results are from a single experiment using three control and three PI3K C2β−/− mice.

4.5 Control and PI3K C2β–/– T-cell viability is comparable

Within isolated splenocytes, analysis of the T-cell populations had shown that while the CD8+ populations were comparable, PI3K C2β–/– mice had an increased CD4+ population, compared to the control animals. However, following T-cell isolation and activation with anti-CD3ε and anti-CD28 coated beads, there was no difference in the T-cell populations (**Figure 4.5**).

To analyse viability of control and PI3K C2β–/– T-cells an Annexin V, propidium iodide assay was used. The AnnexinV/ Propidium iodide (AnV/PI) assay is a widely used approach to analyse cell viability. AnV binds to the negatively charged phospholipid phosphatidylserine (PS), which under physiological conditions are present on the inner plasma membrane. During the early stages of apoptosis, loss of phospholipid asymmetry results in PS being externalized to the outer plasma membrane, which makes it useful for flow cytometric analysis (Koopman et al., 1994). Late stages of apoptosis are identified by the uptake of PI, which binds to nucleic acids. PI can only enter the cell in the late stages of apoptosis once membrane integrity has been lost (Darzynkiewicz et al., 1992). Therefore, cells can be separated into viable (AnV/PI negative), early apoptotic (AnV positive, PI negative), or late apoptotic/ necrotic (AnV positive/ PI positive). Finally, to avoid false positive readings, staining debris is gated out.

Isolated T-cells were assessed by flow cytometry at 72 hr post stimulation with CD3ε/CD28 beads (**Figure 4.6**). When plots were gated to exclude debris, no statistical difference was found between the percentage of control and PI3K C2β–/– T-cells that were viable (AnV-/PI-), early apoptotic (AnV+/PI-) or late apoptotic (AnV+/PI+). However, when gated on the highest viability population, 5.4 % ± 1.8 fewer PI3K C2β–/– T-cells were in the latest stage of apoptosis compared to controls (10.7% vs 16.1%) (**Table 4.2**). These results are from two independent experiments, using four control and four PI3K C2β–/– mice in total.

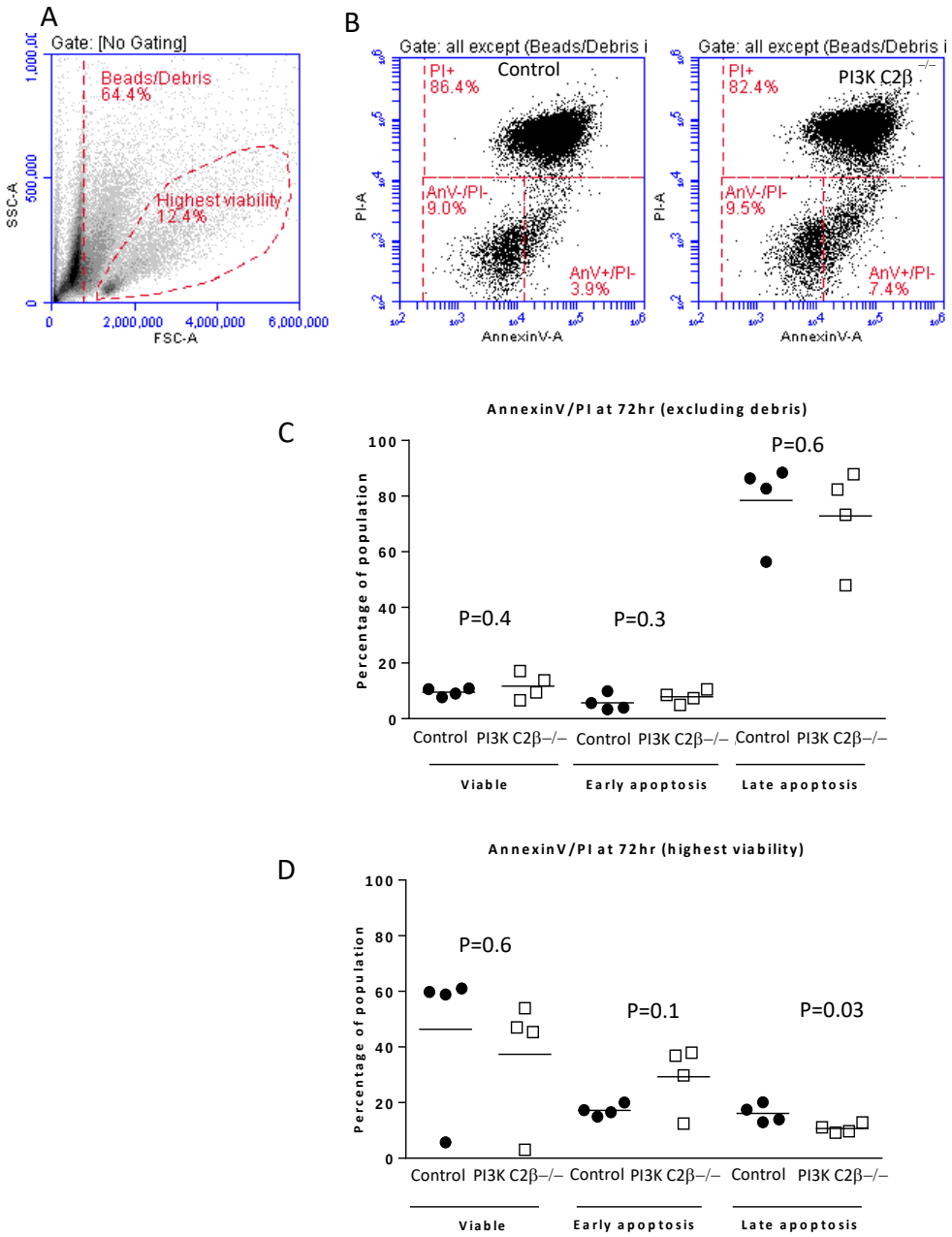

Figure 4.6 T-cell viability at 72 hr following stimulation with anti-CD3ε and anti-CD28 beads. T-cell viability was examined using AnnexinV/PI staining and analysis by flow cytometry, with a minimum of 30,000 events being recorded. **A**; plot showing FSC versus SSC following flow cytometry. **B**; typical plots showing AnnexinV/PI staining for control (left) and PI3K C2β–/– (right) T-cells. Beads and debris were excluded from analysis to avoid false negative readings. **C**; analysis of results showed that there were no significant differences in viability between control and PI3K C2β–/– T-cells at 72 hr post stimulation. **D**; gating on the highest viability population, showed that the percentage of late apoptotic (PI negative) PI3K C2β–/– T-cells was slightly decreased compared to the control T-cells (10.7% vs 16.1%). Results are from two independent experiments using four control and four PI3K C2β–/– mice in total. Statistical analysis was performed using unpaired multiple t-tests, corrected for multiple comparisons using the Sidak-Bonferroni method. Results were considered significant at p=< 0.005 Data represent mean values ± SEM.

Table 4.2 T-cell viability at 72 hr following stimulation with anti-CD3ε and anti-CD28

Gating	Excluding debris			Highest viability		
	Viable (AnV/PI)	Early apoptosis (AnV+/PI-)	Late apoptosis (PI+/AnV+)	Viable (AnV-/PI-)	Early apoptosis (AnV+/PI-)	Late apoptosis (PI+/AnV+)
Control	9.6 % ± 0.8	5.7 % ± 1.5	78.5 % ± 7.5	46.4 % ± 13.6	17.2 % ± 1.1	16.1 % ± 1.7
PI3K C2β$^{-/-}$	11.7 % ± 2.3	7.9 % ± 1.2	72.9 % ± 8.8	37.4 % ± 11.6	29.3 % ± 5.9	10.7 % ± 0.8
	p=0.4	p=0.3	p=0.6	p=0.6	p=0.1	p=0.03

Results are from two independent experiments using four control and four PI3K C2β$^{-/-}$ mice. Statistical analysis was performed using unpaired multiple t-tests, corrected for multiple comparisons using the Sidak-Bonferroni method. Results were considered significant at p=< 0.005. Data represent mean values ± SEM.in total

4.6 Splenic T-cell populations at 80 hrs

Characterisation of isolated T-cells revealed comparable CD4/CD8 ratios and viability, between control and PI3K C2β$^{-/-}$ mice. However, having observed a difference in the PI3K C2β$^{-/-}$ T-cell ratios in splenocytes at 0hr, their response within a splenocyte culture was examined. Within the total splenocyte populations, the presence of additional cell types has the potential to influence the population dynamics, both through cell-to-cell contact and through the production of cytokines. Although this mechanism is likely to be complex, an assessment of the CD4+ population within total splenocyte cultures might provide a useful insight into the effect of additional cell types on the CD4+ population.

Lipopolysaccharide (LPS) and interleukin-4 (IL-4) are commonly used as B-cell stimuli in vitro, T-cells also respond to both factors. IL-4 is required for the differentiation of naïve T-cells into CD4+ Th2 T-cells, which in turn

secrete IL-4 (Swain et al., 1990). LPS has been linked to CD4+ inhibition (González-Navajas et al., 2010; Srinivasan and McSorley, 2007). However, in the presence of additional accessory cells, which could be the case in the splenocyte cultures, LPS was shown to induce proliferation and cytokine production (Mattern et al., 1998).

To assess the T-cell populations within the splenocyte cultures, splenocytes were cultured in LPS (20µg/ml) and IL-4 (50ng/ml) for approximately 80 hr before being stained with anti-CD4, anti-CD8 or anti-CD3 antibody and analysed by flow cytometry (**Figure 4.7**). Labelling with CD3 revealed that under these conditions a greater reduction in the overall T-cell population was observed in splenocytes from PI3K C2β–/– mice compared to splenocytes prepared from control mice (50.4% ± 3.9 vs. 61.2% ± 4.4, respectively). However, the difference of 10.8 % was not statistically significant (p=0.04), as the statistical analysis was performed using unpaired multiple t-tests, corrected for multiple comparisons using the Sidak-Bonferroni method. As such, the significance threshold was set at p=< 0.005, rather than p=0.05. Further analysis of the T-cell population showed that the number of CD8+ cells was reduced in the splenocyte population isolated from PI3K C2β–/– mice compared to controls by 16.4% (25 % ± 3.8 vs 41.3 % ± 2.5) (p=0.005). The CD4+ population also differed but the number of CD4+ cells increased in the cultures of PI3K C2β–/– splenocytes (27 % ± 2) compared to cultures from control animals (16.9 % ± 0.8) (p=0.0007). Data

were derived from two independent experiments using six control and six PI3K C2β−/− mice.

These results suggest that the conditions within the splenocyte cultures preferentially supported CD4+ T-cells over CD8+ T-cells in cultures from PI3K C2β−/− mice and that the overall reduction in T-cell number was a reflection of CD8+ cell loss, which was not observed in the control cultures.

The increased CD4+ population in PI3K C2β−/− splenocyte cultures and the link between CD4 T-cells and B-cell activation suggested a potential explanation for the increase in germinal centre associated proliferation observed in these knockout animals **(Figure 3.5**).

4.7 Splenic B-cell population at 80hrs

Under basal conditions splenic B220 positive cell populations were comparable within splenocyte populations isolated from control and PI3K C2β−/- mice, with no difference observed in median fluorescent intensity (MFI). Analysis of CD19+ cells within the splenocyte populations revealed that PI3K C2β−/− mice had a slight reduction in the CD19+ splenic population (**Figure 4.1**). Further analysis of the CD19+ population showed that the MFI was consistently increased on the CD19+ PI3K C2β−/− cells, indicating that the level of expression may be upregulated (**Figure 4.3**). Murine B-cells express CD19 from the pro-B stage until differentiation into plasma cells (Inaoki et al., 1997). The association with B-cell development, activation and survival is well established (Depoil et al., 2008; Engel et al., 1995; Tedder et al., 1994) making the CD19 receptor an interesting target.

4.8 CD19 expression at 80hrs following treatment with LPS and IL-4

Splenocyte cultures were stimulated with 20µg/ml lipopolysaccharide (LPS) and 50ng/ml IL-4. After 80 hr stimulation they were labelled with anti-CD19 antibody (AlexaFluor-647) and analysed by flow cytometry. Results are from two independent experiments using a total of six control and six PI3K C2β−/− mice (**Figure 4.8**).

At 80 hr the mean CD19+ population within the control cells was 24.5 % ± 2.1 and 38 % ± 1 in cells derived from PI3K C2β−/− mice (p=0.0002). In addition to having an increased CD19+ cell number, the MFI was also slightly higher in CD19+ cells from PI3K C2β−/− animals (p=0.03) indicating an increase in its expression on the cells.

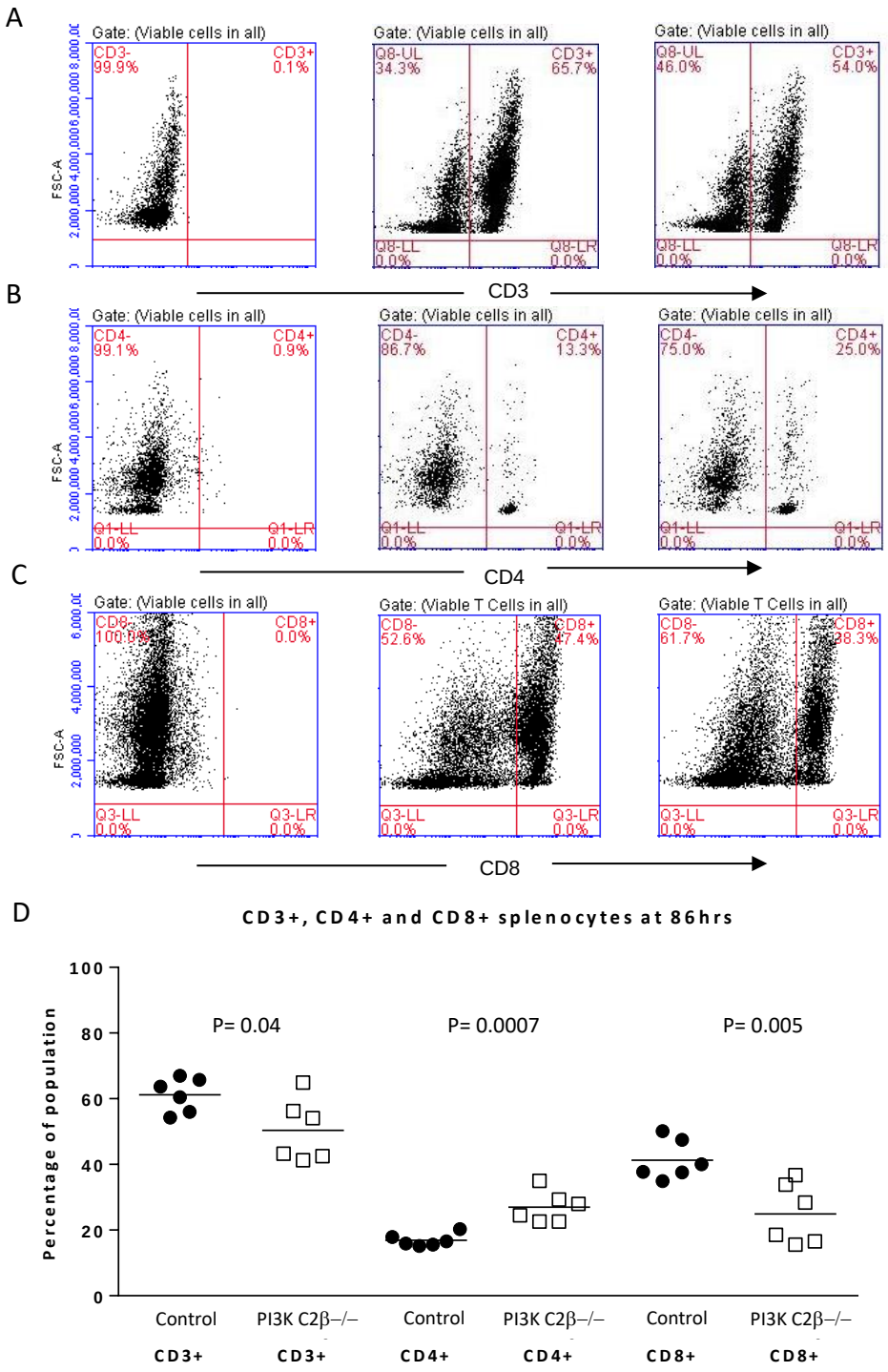

Figure 4.7 T-cell populations within splenocyte cultures at 86 hr. Total splenocyte populations were stimulated with 20µg/ml LPS and 50ng/ml IL-4 for 80 hr. Cells were labelled with anti-CD3, anti-CD4, anti CD8 or the relevant isotype control. Representative plots following analysis by flow cytometry are shown (Panels **A-C**). A minimum of 10,000 events were recorded per plot. In each case the left panel shows the staining pattern of the isotype controls, the middle column and right hand columns show positive staining for control and PI3K C2β–/– splenocytes respectively. **D**; At 86 hr post-harvest (80 hr stimulation) the PI3K C2β–/– there were 10.8% fewer CD3+ cells than in the control cultures (p=0.03). The percentage of CD4+ cells was 10.1% higher in PI3K C2β–/– cultures compared to the controls (p=0.0007) while the population of CD8+ cells was 16.3% lower in the PI3KC2β–/– cultures (p=0.005). Data are from two independent experiments using six control and six PI3K C2β–/– mice. Statistical analysis was performed using unpaired multiple t-tests, corrected for multiple comparisons using the Sidak-Bonferroni method. Results were considered significant at p=< 0.005. Data represent mean values ± SEM.

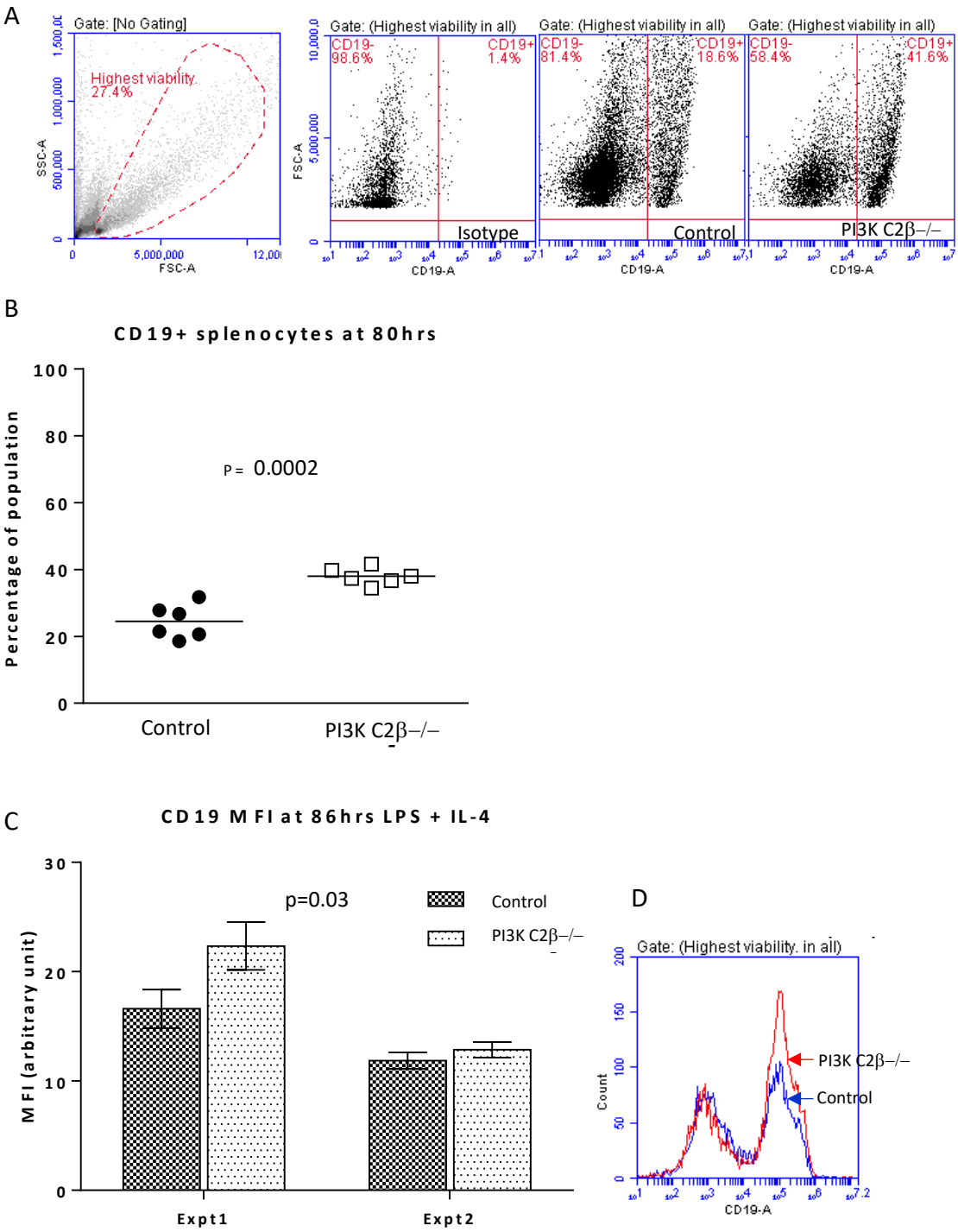

Figure 4.8 Response of CD19+ populations to LPS / IL-4. A; from left to right, representative plots showing the highest viability gate from which cells were analysed, the isotype control and representative plots from control and PI3K C2β–/– splenocytes stimulated with LPS (2µg/ml) and IL-4 (20ng/ml). 30,000 events were counted, per sample. **B**; analysis of data showed that stimulated splenocytes from PI3K C2β–/– mice had a significantly higher number of CD19+ cells compared to splenocytes from control animals (p=0.0002). **C**; analysis of MFI showed a slight increase in PI3K C2β–/– CD19+ populations. **D**; A representative histogram shows the difference in MFI. Data are from two independent experiments, using a total of six control and six PI3K C2β–/– mice. A Student's t-test was used for statistical analysis (B), or a two-way ANOVA (C).

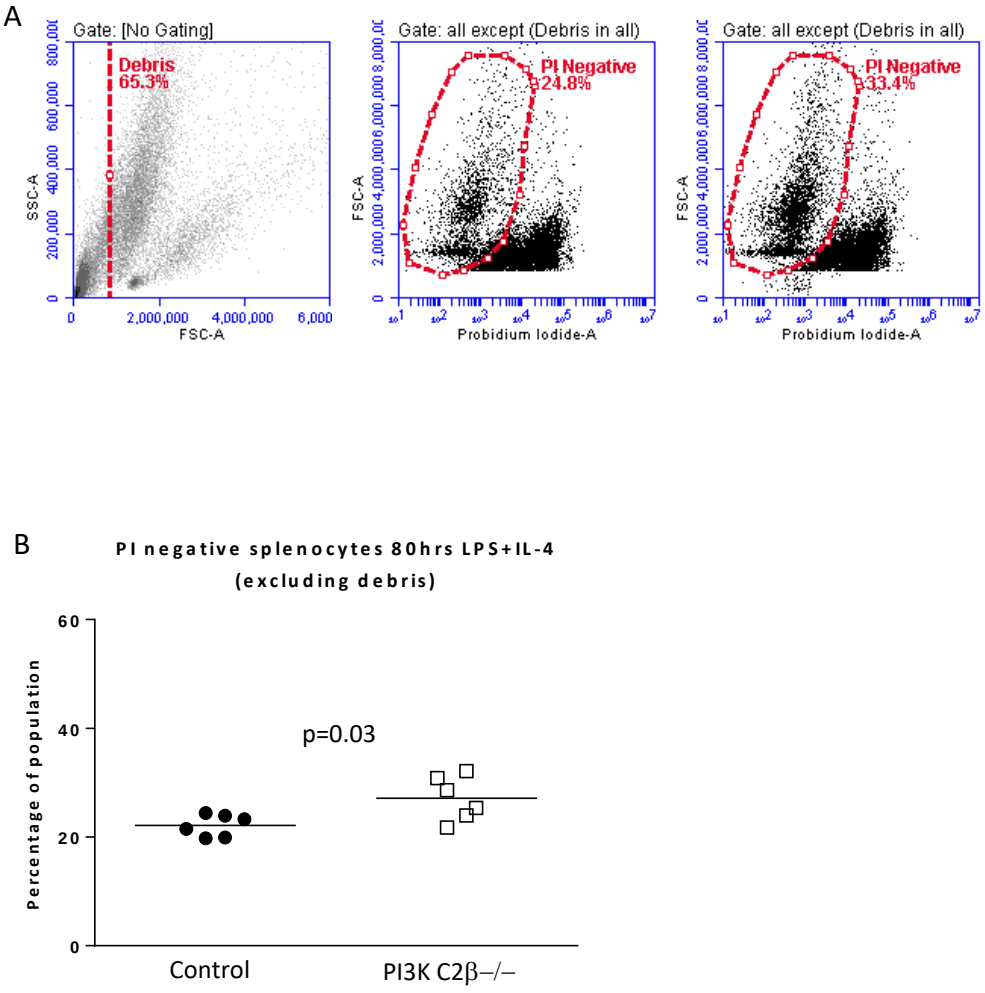

Figure 4.9 Propidium iodide (PI) staining of splenocytes after 80 h stimulation with LPS (20 μg/ml) and IL-4 (50 ng/ml). A; from left to right, representative plots show the total splenocyte population, centre and right-hand plots show PI staining for control and PI3K C2β–/– splenocytes respectively. 30,000 events were analysed from each culture and plots were gated to exclude debris. **B**; following stimulation with LPS and IL-4 splenocyte cultures from PI3K C2β–/– mice had a higher population of live cells (PI negative) than splenocytes isolated from control animals (27.1 % ± 1.7, compared to 22.1 % ± 0.8, respectively) (p=0.02). Data are from two experiments using six control and six PI3K C2β–/– mice. Analysis was performed using an unpaired, two-tailed Student's t-test. Data represent mean values ± SEM.

4.9 Splenocyte viability following stimulation with LPS/IL-4

As a mechanism to maintain immunological homeostasis both B-cells and T-cells are highly susceptible to apoptosis, and as such dysregulation of apoptotic pathways is linked to a pathological outcome. Following stimulation with LPS (20μg/ml) and IL-4 (50ng/ml) for 80 hr, splenocytes were stained with PI and analysed by flow cytometry. Excluding debris ensured that non-staining artefacts were not included in the analysis, which may otherwise have led to an increased false negative reading **(Figure 4.9)**. Results showed that splenocytes from PI3K C2β−/− mice had a live population (PI negative) of 27.1 % ± 1.7, compared to 22.1 % ± 0.8 from controls (p=0.02). These data are from two independent experiments each using six control and six PI3K C2β−/−mice. Statistical analysis was performed using a Student's t-test.

4.10 Discussion

Analysis of total splenocyte populations revealed consistently higher numbers of CD4 positive T-cells in PI3K C2β−/− mice spleens compared to spleens from control mice. However, when T-cells were isolated from splenocyte preparations and stimulated for 80 hr with anti-CD3ε and anti-CD28 antibody, CD4/ CD8 T-cell ratios were equivalent and there was no difference in cell viability between the control and PI3K C2β−/− populations. These data indicated that a different cell type within the total splenocyte population may be responsible for the increased number of T-cells observed in PI3KC2β−/− mouse spleens.

Splenocyte populations were then stimulated with LPS and IL-4, factors often used to stimulate B-cells in vitro. Under these conditions the numbers of CD4+ cells increased and the numbers of CD8+ cells decreased. However, LPS and IL-4 can stimulate other cell types present within splenocyte cultures, both directly and indirectly. In a study examining isolated CD4+ T-cells from murine model of experimental colitis, LPS activation via toll-like receptor 4 (TLR4) led to CD4+ T-cell inhibition (González-Navajas et al., 2010). Conversely, T-cell proliferation and cytokine production was observed when T-cells were cultured with monocytes displaying bound LPS (Mattern et al., 1998), and although the study did not discriminate between CD4+ and CD8+ T-cell populations, monocytes would be present within the total splenocyte cultures (Drutman et al., 2012; Strauss-Ayali et al., 2007; Swirski et al., 2009). In the presence of accessory antigen presenting cells (APCs), increased CD4+ T-cell survival was reported following LPS treatment

(McAleer and Vella, 2008), while Xu (2008) describes how LPS treated B-cells mediate T-cell differentiation into a Th2 phenotype. The effect of IL-4 on T-cells appears less controversial and has been shown to direct CD4+ T-cells towards a Th2 phenotype in an autocrine manner (Le Gros et al., 1990; Swain et al., 1990).

An additional consideration regarding the differences between control and PI3K C2β$^{-/-}$ cultures is the role PI3K C2β has in calcium signalling. For example, in human T-cells PI3K C2β activates the K+ channel, KCa3.1, following stimulation of the T-cell receptor (TCR) (Srivastava et al., 2009). Functional studies in KCa3.1$^{-/-}$ mice have shown that while CD4+ T-cell differentiation was not affected by loss of KCa3.1, cytokine production and proliferation following TCR stimulation was impaired in Th1 and Th2 subsets while Th17 and Tregs remained unaffected (Di et al., 2010).

In a mouse model of autoimmunity, Th17 cells, which are CD4+, were found to promote the generation of spontaneous autoreactive germinal centres through the production of IL-17. Increased IL-17 was found to initiate germinal centre (GC) formation and size by increasing cell numbers, and reducing B-cell migration (Hsu et al., 2008). Furthermore, expression of the IL-17 receptor (IL-17RA) by follicular helper T (Tfh) cells appears to be necessary for retention of Tfh cells within the light zones (LZ) of the GC and loss of IL17RA led to loss of Tfh from the LZ (Ding et al., 2013).

Within total splenocyte cultures, the presence of different subsets belonging to several cell types is likely to result in variations between cultures, both as a result of cell interactions and the production of cytokines.

However, the consistent increase in CD4+ population and increased viability of splenocyte cultures, indicated that loss of PI3K C2β−/− was not necessarily inhibitory when in a mixed cell culture. Results obtained from the isolated T-cell cultures suggest that when provided with the same stimuli, PI3K C2β−/− and control T-cells react in a comparable manner. However, the slightly increased CD4+ population at 0 hr and results from total splenocyte cultures may indicate that conditions within the total splenocyte cultures preferentially maintain the PI3K C2β−/− CD4+ population both ex vivo and in vitro. Maintenance of the CD4+ population could be due to the increased CD19+ population within the PI3K C2β−/− cultures. B-cells are efficient APCs and in addition to mediating immune responses via the B-cell receptor (BCR), they can stimulate T-cells by binding, processing and presenting antigen via CD19, and in doing so upregulate the co-stimulatory molecules CD80 and CD86 (also known as B7.1 and B7.2) (Yan et al., 2005).

Examination of B-cells within the splenocyte populations had shown that CD19 expression at 0 hr was elevated in the PI3K C2β−/− cultures, compared to control cultures. Analysis at 80 hr following stimulation with LPS and IL-4 had shown that not only was CD19 MFI increased in PI3K C2β−/− splenocyte cultures, but also the percentage of CD19+ cells was higher, compared to control cultures. This was of particular interest because increased CD19 expression has been linked to a hyper-responsive phenotype in B-cells and increased cell survival (Hasegawa et al., 2001a; Sato et al., 1996). Splenocytes from PI3K C2β−/− spleens had shown a small increase in the

percentage of live cells at 80 hr, which would be consistent with an increased CD19+ population and increased expression. As such, a more detailed examination of the B-cell population was conducted (Chapter 5).

5 B-cells

Histological examination revealed that PI3K C2β−/− mice had larger germinal centres (GC), as a percentage of total spleen area compared to control mice and that their number was also greater (Chapter 3). This difference was exaggerated in mice treated with sheep IgG/CFA to induce an immunological response. PI3K C2β−/− splenocytes had shown increased viability following LPS/IL-4 stimulation. Examination of isolated T-cells, suggested that T-cell viability was comparable between PI3K C2β−/− and control T-cells, suggesting that increased viability may not be due to the T-cell population. Increased CD19 MFI on PI3K C2β−/− CD19+ cells, indicated that CD19 was upregulated. As such, isolated B-cells were examined in more detail. Initially, I wanted to establish the presence of PI3K C2β in murine B-cells and to confirm that CD19 upregulation was B-cell related.

5.1 Isolation of splenic B-cells

B-cells were isolated via negative selection from the spleens of control mice and PI3K C2β−/− mice. Following a resting period of 1-2 hr splenocytes were labelled with either anti-B220 (Alexa-Fluor 648), or an isotype control before B-cell purity was analysed by flow cytometry. Negative selection resulted in >96% B220+ population (**Figure 5.1**).

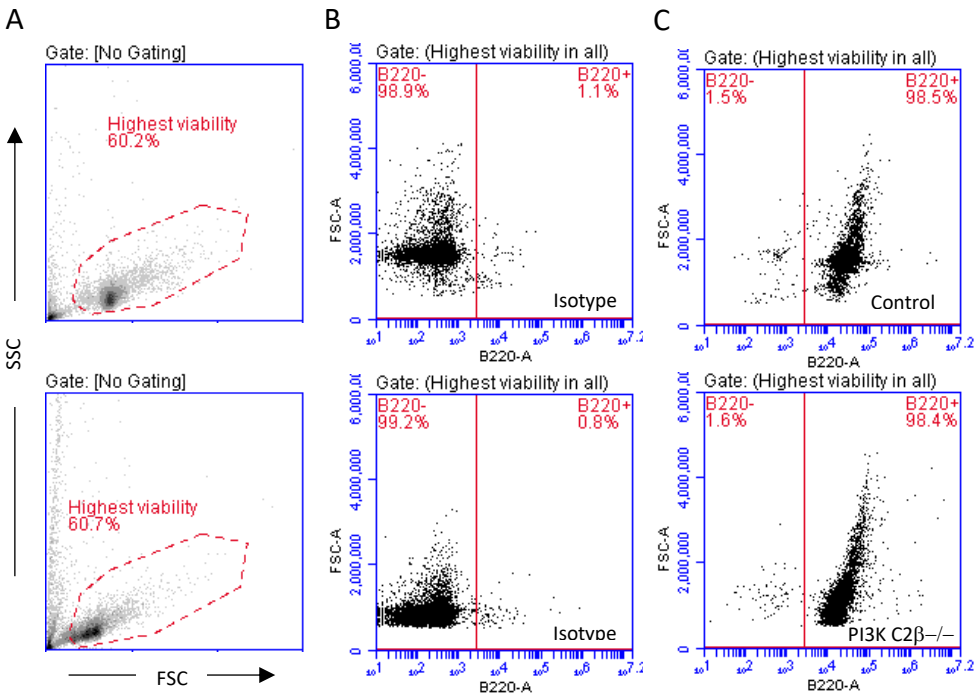

Figure 5.1 Isolation of B-cells from spleens of control and PI3KC2β−/− mice. B-cells were isolated from freshly harvested splenocytes by negative selection. A minimum of 10,000 event were recorded per plot. Cells were then labelled with either anti-B220 (Alexa-Fluor 648), or an isotype control before B-cell purity was analysed by flow cytometry. **A**; plots show typical FSC vs SSC of B-cells isolated from spleens of control (upper) and PI3KC2β−/− mice (lower). **B**; a negative isotype control was used to exclude non-specific staining control (upper) and PI3KC2β−/− mice (lower). **C**; cells labelled with anti-B220 used to determine B-cell purity control (upper) and PI3KC2β−/− mice (lower). Over the course of the project the percentage of B220+ cells isolated in this way was >96%.

5.2 PI3K C2β expression in murine B-cells

The expression of PI3K C2β in T-cells has been previously reported (Balzarotti et al., 2015; Ohya and Imaizumi, 2014; Srivastava et al., 2009). PI3K C2β is reported to be expressed in human B-cells based on gene expression analysis (Jelinek et al., 2003; McCarthy et al., 2015), but its expression in murine B-cells has not been described. Cells of the immune system are greatly affected by the micro environment, including cell to cell contact as well as their exposure to various cytokines and chemokines. As such, a cell may be indirectly affected by the loss of PI3K C2β without expressing the enzyme itself. However, determining whether PI3K C2β is expressed in murine B-cells would allow a better understanding of its role and provide insight into its effect on B-cell biology.

Expression of PI3K C2β in B-cells from control mice was confirmed using reverse transcription PCR (RT PCR) and Western blot analysis (**Figure 5.2**). The forward primer (235) was designed to anneal to the end of exon 26 and the start of exon 27, and the reverse primer should anneal within exon 33. Successful PCR amplification produced a cDNA product of 858bp from control B-cells, which was absent in cells isolated from PI3K C2β–/– mice. The presence of the protein was then confirmed using Western blot analysis on B-cell lysates.

A

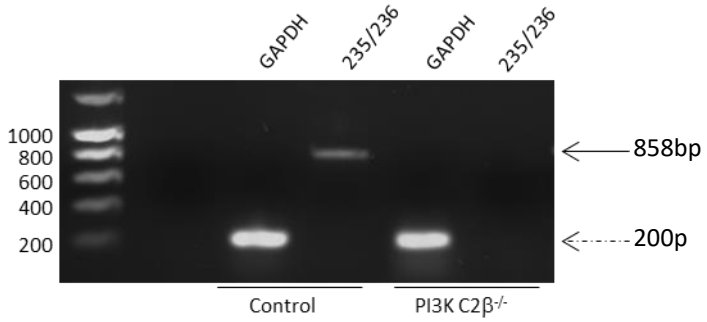

Expected product size:
GAPDH ~ 200bps
235/236 858bps (235 crosses exons 26-27 and 236 anneals within exon 33)

B

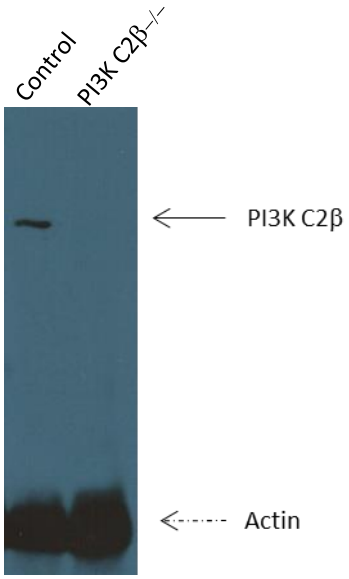

Figure 5.2 Expression of PI3K C2β in murine B-cells. Reverse transcription PCR and Western blot. **A**; cDNA was isolated and PCR was used to identify the presence of PI3K C2β mRNA in B-cells from control mice (expected product size of 858bp), and its absence from PI3K C2β–/– mice. Primers were designed to straddle exons 26 and 27 so that gDNA contamination could be excluded. **B**; following the fractionation of B-cell lysates by SDS PAGE, proteins were immunoblotted with anti-PI3K C2β antibody and visualised using ECL. A band was seen at approximately 170kD, in B-cells from control mice which was absent from PI3K C2β–/– mice. Actin was used to determine loading.

5.3 B-cells isolated from PI3K C2β−/− mice have an increased level of CD19 expression compared to controls

Differences in CD19 expression had been observed within total splenocyte populations both basally and following their stimulation with LPS/ IL-4. A strong association between CD19 expression and B-cell activation thresholds has been previously reported making increased CD19 expression of particular interest (Fujimoto et al., 2000; Inaoki et al., 1997).

Following B-cell isolation, cells were labelled with anti-CD19 (Alexa-Fluor 647) and analysed by flow cytometry. The cell populations assessed were within the highest viability gate as determined by PI staining. In each experiment CD19+ MFI was increased by >25% on B-cells isolated from PI3K C2β−/− mice, compared to the controls (p=<0.0001). Results are from three independent experiments using nine control and nine PI3K C2β−/− mice, statistical analysis was calculated using a two way ANOVA.

To further validate the increased levels of CD19 expression on PI3K C2β−/− B-cells, lysates from freshly isolated B-cells were fractionated by SDS-PAGE, immunoblotted and probed with anti-CD19 antibody. Anti- β-actin antibody was used to confirm loading. Chemiluminescent detection confirmed that PI3K C2β−/− B-cell lysates, expressed higher levels of CD19 protein compared to the control lysates (**Figure 5.3**).

Table 5.1 CD19 expression on isolated B-cells at 0 hr.

	Expt 1	Expt 2	Expt 3	Mean ± SEM
Control	2.3 ± 0.1	2.6 ± 0.04	3.3 ± 0.2	2.7 ± 0.2
PI3KC2β –/–	3.3 ± 0.2	3.4 ± 0.1	4.67 ± 0.2	3.8 ± 0.4
Difference	1	0.9	1.4	1.1

Data shown is shown as arbitrary units and was collected over three independent experiments, using nine control and nine PI3K C2β–/– mice. The increased MFI on PI3K C2β–/– B-cells was considered statistically significant (p=<0.0001). Statistical analysis was calculated using a two-way ANOVA. Data are presented ± SEM.

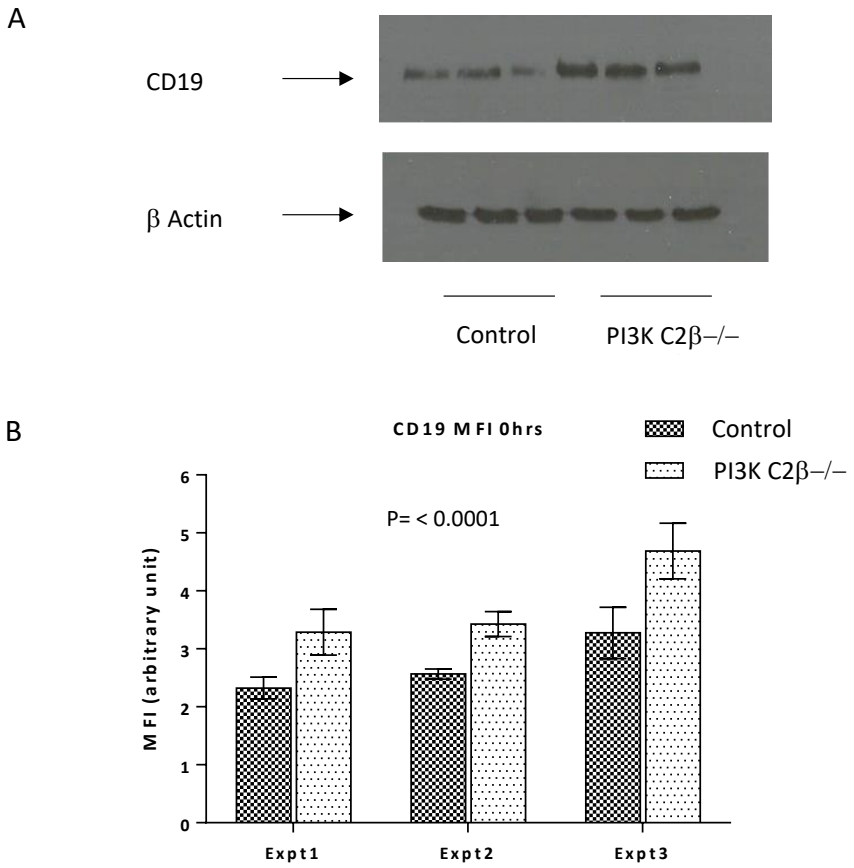

Figure 5.3 CD19 expression is increased in PI3K C2β–/– B-cells. **A**; following the fractionation of B-cell lysates by SDS PAGE, proteins were immunoblotted with anti-CD19 antibody and visualised by ECL. 40µg of total protein was loaded and β-actin was used as a loading control **B**; B-cells isolated from spleen of either control or PI3K C2β–/– mice were labelled with anti-CD19 antibody conjugated to alexa-fluor 647 and median fluorescent intensity (MFI) was analysed. In each experiment MFI was higher on PI3K C2β–/– B-cells compared to control B-cells (see **Table 5.1**). A minimum of 10,000 events were recorded per experiment. A two-way ANOVA was used to determine statistical significance (p=< 0.0001). The results are from three independent experiments using a total of nine control mice and nine PI3K C2β–/– mice.

5.4 B-cell viability

Previously, PI staining of total splenocyte populations demonstrated that cells isolated from the spleens of PI3K C2β−/− mice survived longer ex vivo than splenocytes from control mice (**Figure 4.9**), and that CD19 expression was elevated in the PI3KC2β−/− splenocytes (**Figure 4.3**). Previous unpublished work from our laboratory showed that a marked immune response was generated in PI3K C2β−/− mice following a sub-nephritogenic dose of NTS. Analysis of splenocyte populations had indicated that PI3K C2β−/− mice had a slightly expanded CD4+ population upon isolation which was still apparent after 80hr in culture (**Table 4.2 and Figure 4.7**). However, a preliminary examination of isolated T-cells had shown that viability was comparable between control and PI3K C2β−/− cultures. Since these data suggested that the increased splenocyte survival may not be T-cell mediated B-cell viability was examined.

B-cells have a tightly regulated lifecycle and undergo apoptosis if they do not receive the appropriate stimuli. These stimuli can be provided by cytokines in the local environment and interactions with other cell types including T-cells, and professional antigen presenting cells (APCs), such as dendritic cells. In turn, B-cells can activate T-cells through antigen presentation in addition to producing cytokines that support and regulate the T-cell immune response (Baumjohann et al., 2013; Wollenberg et al., 2011). If the B-cell population is not kept under strict control, B-cell related pathologies result and dysregulation of the T-cell response may occur

(González-Navajas et al., 2010; Singh et al., 2014; Zhu and Paul, 2015). My earlier analysis of splenocyte viability had used stimulation with LPS at 20μg/ml and IL-4 at 50ng/ml, which are concentrations that had previously been optimised in our lab and that are often utilised for B-cell culture (Heise et al., 2014; Lin and Calame, 2004; Omori et al., 2006). As LPS has been shown to induce B-cell activation and proliferation in a dose-dependent manner (Xu et al., 2008), and having identified increased CD19 expression (**Figure 5.3**) which is associated with a reduced activation threshold (Carter and Fearon, 1992; Inaoki et al., 1997), isolated B-cell cultures were stimulated with reduced doses of LPS and IL-4. A preliminary experiment was conducted in which B-cells from control and PI3K C2β−/− mice were stimulated with 10μg/ml LPS and 5μg/ml (**Appendix 2**). The results indicated that the B-cells remained alive at the lower concentrations and that the PI3K C2β−/− B-cells were more responsive to the reduced stimuli, they appeared to form more foci and had an increased population of live cells at 72 hr. A final concentration of 2μg/ml LPS and 20ng/ml was tested and used.

5.5 Analysis of B-cell viability using AnnexinV and propidium iodide (AnV/PI)

Initial analysis following stimulation with 2μg/ml LPS and 20ng/ml, using PI only showed that PI3K C2β−/− cultures had an increased percentage of live cells compared to controls at 24 hr, which was greater at 72 hr. Two distinct populations were identified as highest viability and mixed viability, and were analysed individually. PI3K C2β−/− B-cells appeared to remain within the

high viability gate for longer than B-cells from control mice, which underwent a shift into the mixed viability gate more quickly (**Appendix 3** and **Appendix 4**). This analysis was performed using propidium iodide (PI), which is useful for identifying cells in late apoptosis, however PI cannot identify cells at the early stages of apoptosis when the cell membrane is still intact. To identify cells in the early stages of apoptosis AnnexinV was used, as it binds to the cell membrane via phosphatidylserine which is exposed on the surface of apoptotic cells (Koopman et al., 1994).

Cells were analysed after 24 hr and 72 hr stimulation with LPS (2μg/ml) and IL-4 (20ng/ml) **(Table 5.2, Figure 5.4 and Figure 5.5)**. After 24 hr stimulation both control and PI3K C2β−/− B-cells had comparable percentages of cells that were PI negative/AnV negative (54 % ± 2.6 and 55.1 % ± 1.80), they also had comparable populations of AnV positive/PI negative (early apoptotic) B-cells (11.1 % ± 0.9 and 13 % ± 0.7). However there was a smaller population of PI3K C2β−/− B-cells that were PI positive/AnV positive (late apoptosis), compared to the controls (14 % ± 1 compared to 21.7 % ± 2.04, respectively). The difference of 5.7 % ± 1.2 was significant (p=0.001).

After 72 hr stimulation the percentage of AnV negative /PI negative B-cells from control and PI3K C2β−/− mice were again comparable (7.2 % ± 1.2 and 6.9 % ± 1.4). The percentage of B-cells that were AnV positive/PI negative was significantly higher (p=0.003) in the PI3K C2β−/− population compared to the controls (36.4 % ± 2.4 and 25.2 % ± 2.2, respectively). However, the percentage of B-cells that were PI positive/AnV positive was now higher in

the control samples (64.5 % ± 3.5) compared to B-cells from PI3K C2β−/− mice (51.9 % ± 1.7), (p=0.005).

The AnV negative/PI negative results showing comparable populations at both time points suggest that the earliest stage of apoptosis occurs at a similar time in both control and PI3K C2β−/− B-cells. However, the build-up of PI3K C2β−/− B-cells in the AnV positive/PI negative (early apoptosis) gate, in conjunction with the reduction in the AnV positive/ PI positive (late apoptosis) at 72 hr might indicate that PI3K C2β−/− B-cells remain in a state of early apoptosis for longer than the control B-cells before entering late apoptosis.

Table 5.2 AnnexinV/PI staining of B cells from control and PI3KC2β$^{-/-}$ mice

	24 hr		72 hr	
	Early apoptosis (AnV+/PI-)	**Late apoptosis (PI+/AnV+)**	**Early apoptosis (AnV+/PI-)**	**Late apoptosis (PI+/AnV+)**
Control	11.1 % ± 0.9 n=6	21.7 % ± 2.04 n=6	25.2 % ± 2.2 n=9	64.5 % ± 3.5 n=9
PI3K C2β$^{-/-}$	13 % ± 0.7 n=6	14.02 % ± 1 n=6	36.4 % ± 2.4 n=9	51.9 % ± 1.7 n=9
Difference ± SEM	+1.9 ± 1.2	-5.7 ± 1.2	+11.2 ± 3.2	-12.7 ± 3.9
Significance	p=0.14	p= 0.001	p= 0.003	p= 0.005

B-cells were stimulated with LPS (2μg/ml) and IL-4 (20ng/ml) for 24 hr and 72 hr. Data are from two (24 hr) or three (72 hr) independent experiments. Statistical analysis was performed using unpaired multiple t-tests, corrected for multiple comparisons using the Sidak-Bonferroni method. Data represent mean values ± SEM.

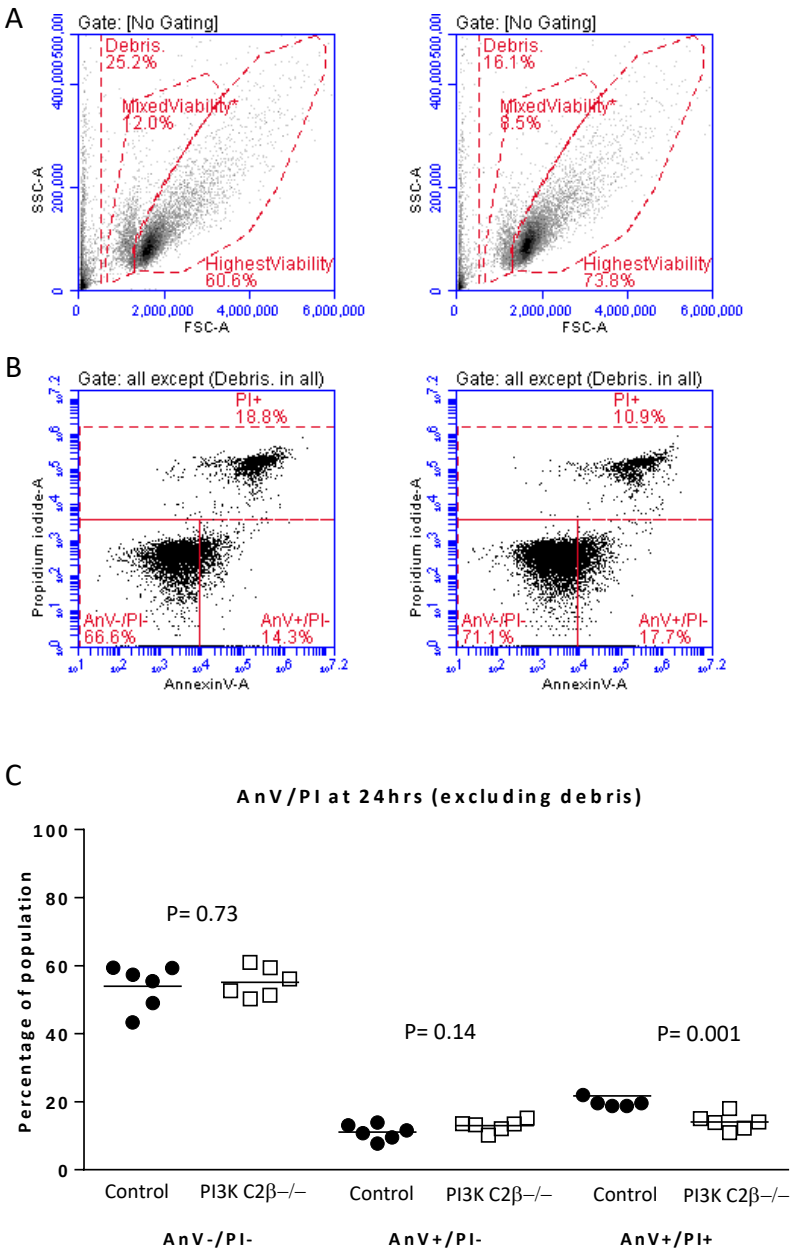

Figure 5.4 AnnexinV/PI staining of B cells from control and PI3KC2β−/− mice stimulated with LPS (2μg/ml) and IL-4 (20ng/ml) for 24 hr. B-cells were stained with Annexin V (AnV) and propidium iodide (PI) and analysed using flow cytometry, 30,000 events were recorded per plot. **A**; representative plots of FSC vs SSC at 24 hr for control (left) and PI3K C2β−/− (right) B-cells**. B**; AnnexinV/PI staining at 24 hr showing gating. **C**; Analysis the data showed comparable populations of AnV-/PI- (viable) B-cells (p=0.7). AnV+/PI- (early apoptotic) populations were also comparable (p=0.14). However the difference between control and PI3K C2β−/− PI+/AnV+ (late apoptotic) populations (19.7 % ± 1.2 and 14 % ± 1, respectively) was significant (p=0.001). Results are from two independent experiments using six control and six PI3K C2β−/− mice. Statistical analysis was performed using unpaired multiple t-tests, corrected for multiple comparisons using the Sidak-Bonferroni method. Data represent mean values ± SEM.

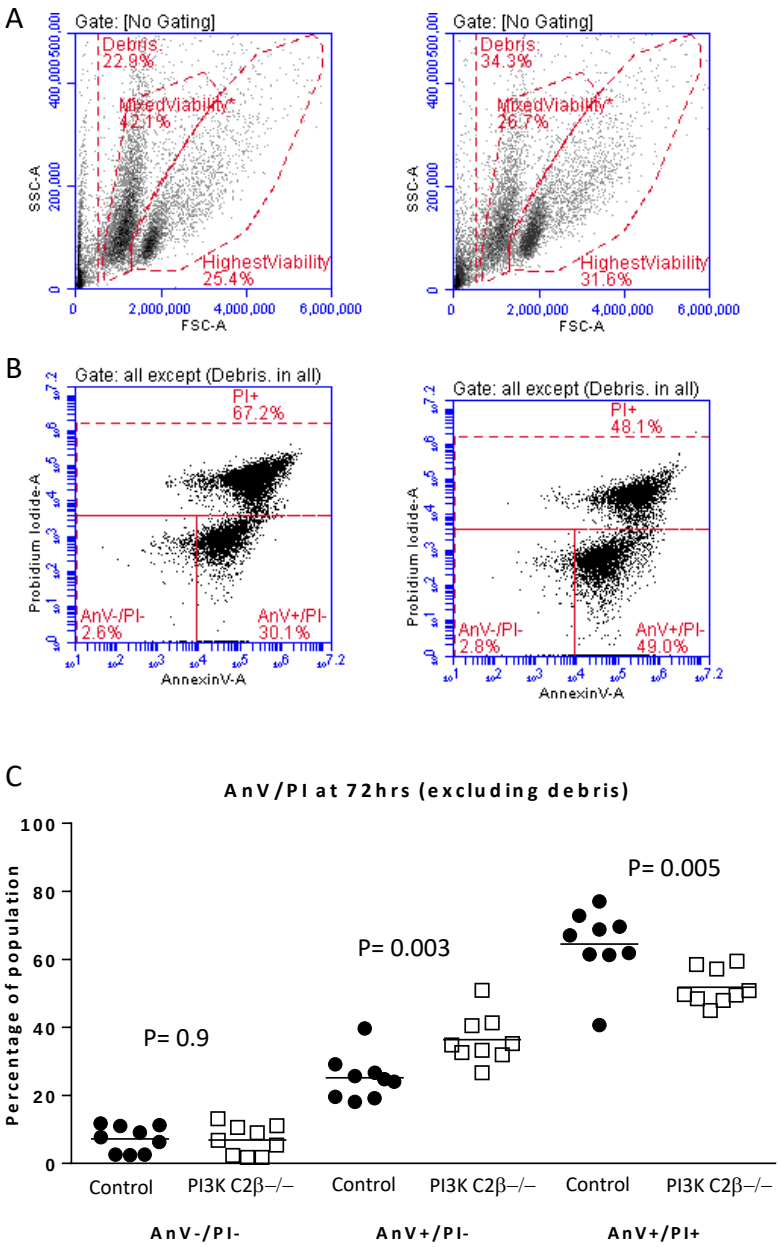

Figure 5.5 AnnexinV/PI staining of B cells from control and PI3KC2β−/− mice stimulated with LPS (2μg/ml) and IL-4 (20ng/ml) for 72 hr. B-cells were stained with Annexin V (AnV) and propidium iodide (PI) and analysed using flow cytometry, 30,000 events were recorded per plot. **A**; representative plots of FSC vs SSC at 72 hr for control (left) and PI3K C2β−/− (right) B-cells. **B**; AnnexinV/PI staining at 72 hr showing gating. **C**; Analysis of data showed that populations of AnV-/PI- (viable) B-cells were comparable (p=0.9). AnV-/PI+ (early apoptotic) populations were higher in the PI3K C2β−/− B-cells (36.4% ± 2.4) compared to the control B-cells (25.2% ± 2.2) (p=0.003). PI+/AnV+ (late apoptotic) populations in PI3K C2β−/− B-cells were smaller (51.9% ± 1.7) compared to the controls (64.5% ± 3.5) (p=0.005). Results are from three independent experiments using nine control and nine PI3K C2β−/− mice. Statistical analysis was performed using unpaired multiple t-tests, corrected for multiple comparisons using the Sidak-Bonferroni method. Data represent mean values ± SEM.

In culture, despite showing signs of being in early apoptosis by AnV/PI staining, B-cells from PI3K C2β−/− mice appeared to maintain an increased level of activity compared to control B-cells. For example; when B-cells were stimulated with LPS (2μg/ml) and IL-4 (20ng/ml) and cultured at the same density, the media from PI3K C2β−/− flasks became acidic more quickly indicating increased metabolic activity (**Figure 5.6**) and examination by light microscopy showed PI3K C2β−/− B-cells generated foci more quickly than the controls. These observations coupled with the discovery that PI3K C2β−/− B-cells survived for longer than the control B-cells and that the shift from early to late apoptosis appeared to be delayed, could provide an insight into the altered response that was previously demonstrated by the PI3K C2β−/− mice. To examine whether a delay in the progression from early to late apoptosis correlated with increased metabolic activity, a 3-(4,5-dimethylthiazol-2-yl)-2,5-diphenyltetrazolium bromide (MTT) assay was used.

5.6 MTT assay

The MTT reagent is converted to purple formazan crystals, by metabolically active cells. The formazan crystals are then dissolved before being read by spectrophotometer at 570nm. The rate at which formazan crystals are produced correlates to the metabolic activity of the cells and decreases as cells become less viable, which makes the MTT assay a useful tool for evaluating metabolic activity and cell viability.

Freshly isolated B-cells were examined following a brief rest period, or were stimulated with LPS (2μg/ml) and IL-4 (20ng/ml) to be examined at 72 hr. Results are from two independent experiments using six control and six PI3K C2β−/− mice. Statistical significance was calculated using a Student's t-test (**Figure 5.6**.)

Following dissolution of the formazan crystals absorbance was read (570nm), the results for isolated B-cells at 0 hr was comparable for the control (0.06 ± 0.001) and PI3K C2β−/− cells (0.06 ± 0.001). At 72 hr post stimulation PI3K C2β−/− wells had an increased absorbance reading of 0.8 ± 0.04 compared to the controls which was 0.6 ± 0.02. The difference of 0.2 ± 0.05, represented a 14.4 ± 0.7 fold increase in the PI3K C2β−/− samples, compared to an 11.9 ± 0.5 fold increase in the control samples. Fold increase was calculated by dividing the absorbance at 72 hr for each sample (the mean of three replicates) by the absorbance of the corresponding sample at 0 hr (the mean of three replicates).

The increase in absorbance in PI3K C2β−/− B-cells was considered significant ($p=0.006$). This result correlated well with the previous AnV/PI data which had shown that PI3K C2β−/− B-cells appeared to have a delayed shift from early to late apoptosis. This suggests that despite being in the early stages of apoptosis, as shown by the AnV/PI results, PI3K C2β−/− B-cells remained metabolically active and displayed increased metabolic activity compared to the controls.

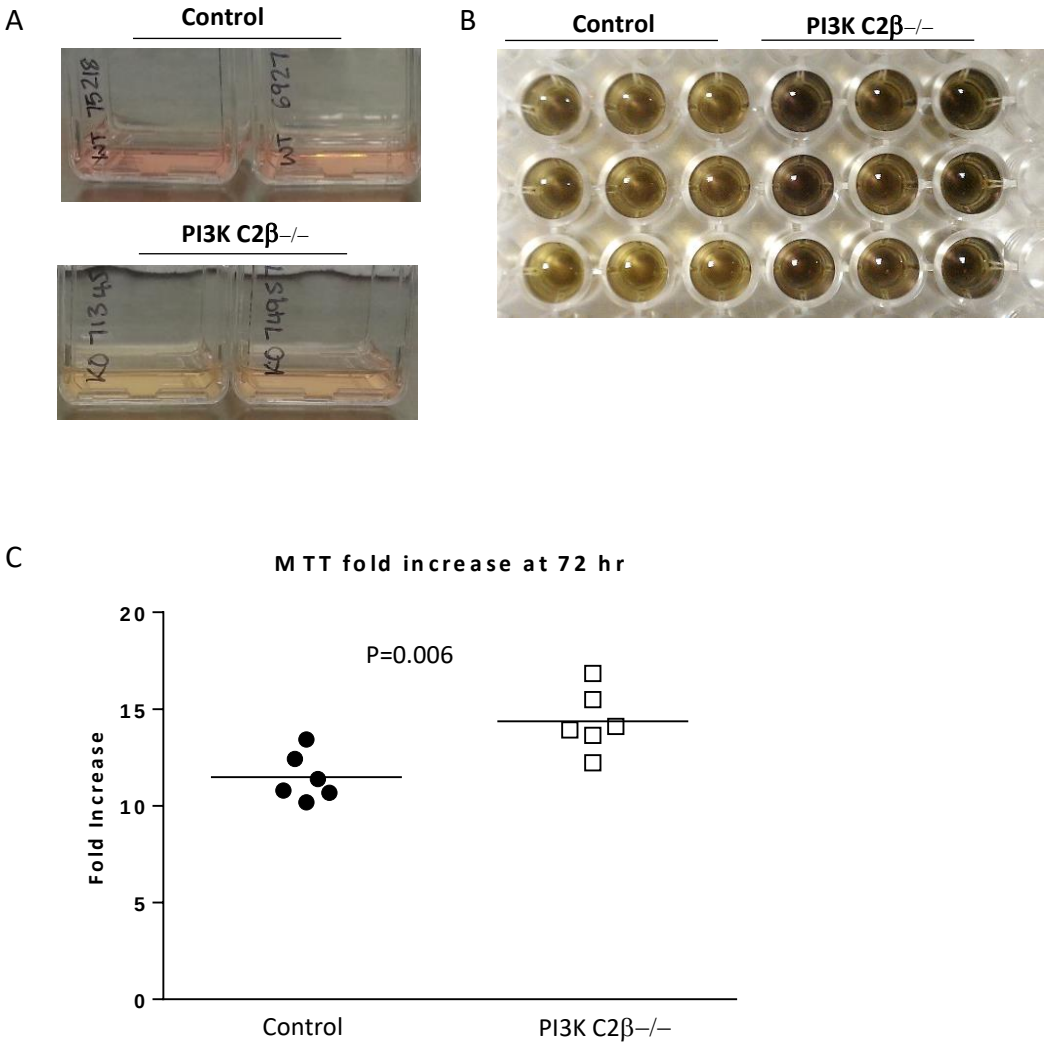

Figure 5.6 Assessment of B-cell metabolic activity using an MTT assay at 0 hr and 72 hr post stimulation with LPS (2μg/ml) and IL-4 (20ng/ml). A; flasks showing control and PI3K C2β−/− B-cells seeded at $1X10^6$ cells/ml and cultured under the same conditions. The change of colour seen in the PI3K C2β−/− flasks indicates that the pH indicator (phenol red), has become more acidic, suggesting increased metabolic activity. **B**; representative MTT assay following solubilisation of the formazan crystals at 72 hr. Samples were assessed in triplicate using B-cells from three control and three PI3K C2β−/− mice. **C**; analysis of the absorbance readings at 570 nm showed a 20% increase in PI3K C2β−/− samples compared the control samples (14.4 ± 0.7 and 11.5 ± 0.5, respectively). The difference was statistically significant (p=0.006). The experiment was conducted in triplicate and repeated twice, using a total of six control and six PI3K C2β−/− mice. Statistical analysis was performed using an unpaired, two tailed t-test. Data represent mean values ± SEM.

5.7 Cell cycle analysis

Data had shown that PI3K C2β–/– B-cells appeared to have a delay in transitioning from early apoptosis to late apoptosis and showed higher metabolic activity than their control counterparts. However, cell proliferation had not been addressed; analysis of AnV/PI staining by flow cytometry involves the analysis of a pre-determined number of cells and results are assessed as a percentage. The MTT assay, is often referred to as a proliferation assay, as cells are seeded at equal predetermined densities and therefore increased metabolic activity could be as a result of increased cell numbers. Additionally, IHC of spleen sections from unimmunized mice and mice treated with sheep IgG and CFA had shown increased areas of PCNA staining, which is a marker of cell proliferation. To assess whether PI3K C2β–/– B-cells showed any differences in proliferation, cell cycle analysis was performed on two separate occasions, using six control and six PI3K C2β–/– mice.

Analysis was conducted at 0, 24 and 72 hr following stimulation with LPS (2µg/ml) and IL-4 (20ng/ml). Cells were harvested and washed with PBS, cell pellets were then fixed in 70% ethanol and stored at 4^{o}C until use (at least overnight). Following treatment with RNase and the addition of PI, cell cycle was assessed by flow cytometry (**Figure 5.7**). Following the exclusion of debris and doublets, gates were set to show the percentage of cells within the sub-G0/G1, G0-G1, synthesis (S) and G2/mitosis (M) phases of the cell cycle. Examination of the sub G0/G1 gate allowed further gating to the

highest viability population. Results from both the total population (excluding doublets and debris) and the highest viability population were assessed.

At 0 there was minimal difference between control and PI3K C2β–/– B-cells in any phases of the cell cycle, in either the total population or the highest viability population (**Appendix 5**). At 24 hr, there was a smaller percentage of PI3K C2β–/– cells in sub-G0/G1 within the highest viability populations (p=0.003). By 72 hr, control and PI3K C2β–/– B-cells had very similar percentages of the population within the S and G2/M phases, however differences could be seen in the sub G0/G1 and G0/G1 phases. Within the total B-cell populations, there was 9.2% more control B-cells within the sub G0/G1 gate compared to PI3K C2β–/– B-cells. This difference rose to 12.2% within the highest viability population (p=<0.001). Differences were also observed within the G0/G1 gate, with 10.1% more PI3K C2β–/– cells from the total population, although this was not considered statistically significant when analysed using multiple t-tests, with multiple comparisons corrected for using the Sidak-Bonferroni method. Within the highest viability population there was 14.9% PI3K C2β–/– cell, compared to the controls (57.8% and 43.8%, respectively), which was statistically significant (p=<0.0001). Analysis of the phases of the cell cycle as a time series (**Table 5.3** and **Figure 5.8**), using a two-way ANOVA indicated that over the 72 hr period a lower percentage of the PI3K C2β–/– cells fell within the sub-G0/G1 gate in both the total population (excluding debris) and the highest viability

population (p=0.003 and p=0.007, respectively). This pattern was reversed when observing the G0/G1 populations, with the PI3K C2β−/− B-cells having an increased percentage over time within the total population (excluding debris) and the highest viability populations (p=0.006 and p=0.005, respectively). Within the total population (excluding debris), there was also a very slight increase in the percentage of PI3K C2β−/− cells within the G2/M gate over the time course (p=0.047).

Table 5.3 Summary of cell cycle analysis of B-cells from control and PI3K C2β–/– mice after 0, 24 and 72 h incubation with LPS (2 μg/ml) and IL-4 (20 ng/ml).

Total population (excluding debris/ doublets)

Sub G0/G1	**Control**	**PI3K C2β–/–**	**Difference**	
0 hr	8% ± 0.66	6.6% ± 0.56	1.4± 0.9	
24 hr	20.2% ± 2.7	14.4% ± 2.01	5.1 ± 3.4	
72 hr	67.8% ± 3.44	58.6% ± 1.4	9.2 ± 3.7	
				p= 0.003
G0/G1				
0 hr	88.3% ± 0.6	89.8% ± 0.6	1.5 ± 0.9	
24 hr	75.3% ± 2.8	79.6% ± 2.8	4.3 ± 4	
72 hr	23.5% ± 3.1	29.8% ± 1.2	6.2 ± 3.3	
				p= 0.006
Synthesis				
0 hr	1.1% ± 0.1	1.1% ± 0.2	0 ± 0.2	
24 hr	6.2% ± 0.9	7.8% ± 0.5	1.1 ± 1.1	
72 hr	4.8% ± 0.4	3.9% ± 0.3	0.9 ± 0.5	
				p= 0.86
G2/M				
0 hr	2.1% ± 0.2	2.2% ± 0.2	0.2 ± 0.3	
24 hr	1.2% ± 0.1	2.1% ± 0.4	0.9 ± 0.4	
72 hr	0.5% ± 0.1	0.5% ± 0.1	0 ± 0.1	
				p= 0.047

Highest viability population

Sub G0/G1	**Control**	**PI3K C2β–/–**	**Difference**	
0 hr	2.7% ± 0.5	2.7% ± 0.3	0 ± 0.6	
24 hr	15.9% ± 3.2	8.2% ± 1.8	7.7 ± 3.7	
72 hr	43.5% ± 5.3	31.4% ± 2	12.2 ± 5.6	
				p= 0.007
G0/G1				
0 hr	94.4% ± 0.5	94.3% ± 0.4	0.1 ± 0.6	
24 hr	84.4% ± 2.5	75.8% ± 4.2	8.6 ± 4.9	
72 hr	43% ± 4.6	57.8% ± 2.5	14.9 ± 5.3	
				p= 0.005
Synthesis				
0 hr	2.5% ± 0.7	1.6% ± 0.4	1.6% ± 0.4	
24 hr	2.5% ± 0.3	2.7% ± 0.5	0.2 ± 0.6	
72 hr	7.8% ± 1	6.1 ± 0.5	1.7 ± 1.1	
				p= 0.12
G2/M				
0 hr	2.4% ± 0.2	2.5% ± 0.2	0.4 ± 0.3	
24 hr	1.4% ± 0.1	2.5% ± 0.6	1.1 ± 0.6	
72 hr	0.8% ± 0.2	0.8% ± 0.1	0 ± 0.2	
				p= 0.68

B-cells were gated on the total population (excluding debris/doublets) and on the highest viability populations. Results are from two independent experiments using six control and six PI3K C2β–/– mice. Statistical analysis was performed using a two-way ANOVA. Data represent mean values ± SEM.

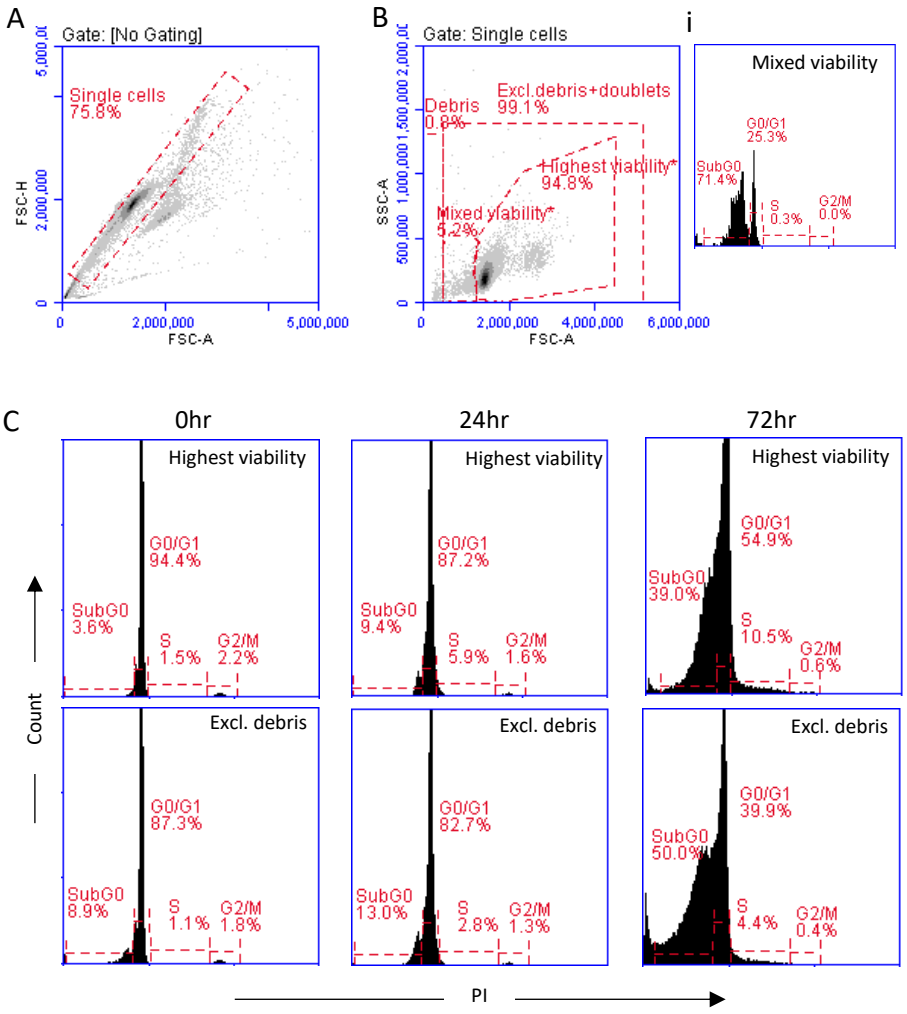

Figure 5.7 Cell cycle analysis of isolated B-cells from the spleens of control and PI3K C2β−/− mice Cells were fixed in ethanol, permeabilized and treated with RNAse before being stained with PI and assessed using flow cytometry, 10,000 events were recorded per sample. **A**; an initial plot of FSC (area) vs FSC (height) was used to exclude doublets which could lead to false positive readings in the G2/M gate. **B**; FSC vs SSC gated to include single cells only. Gates were set to exclude debris (false negatives) and the highest viability and mixed viability gates were determined based on the percentage of the population that fell within the sub G0/G1 gate (mixed viability (i)) or the G0/G1, synthesis (S) or G2/M gates (highest viability). **C**; representative histograms at 0 hr, 24 hr and 72 hr, gated on highest viability (top) or gated to exclude debris (bottom).

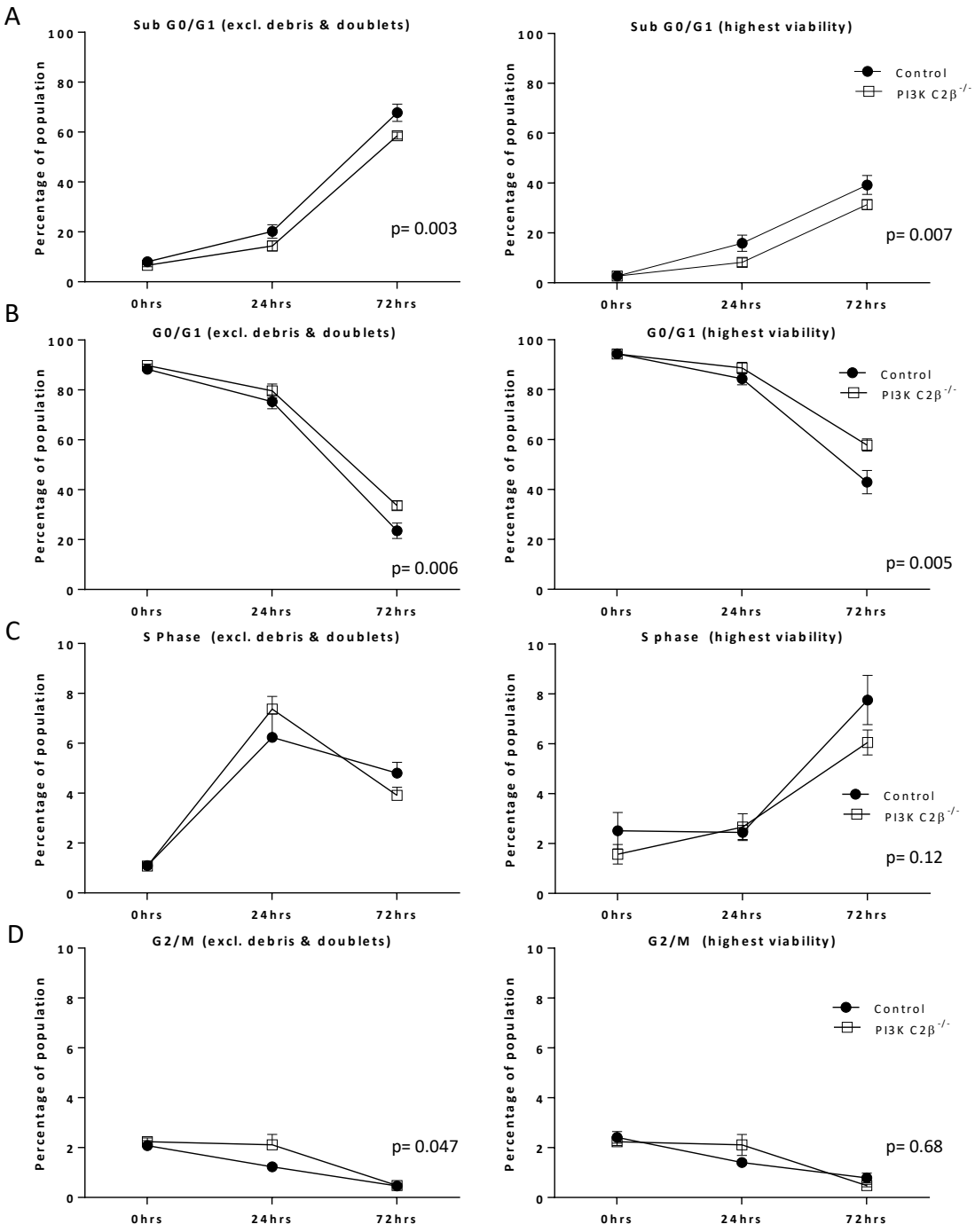

Figure 5.8 Phases of the cell cycle analysis presented as a time series. Analysis of the cell cycle data collected at 0, 24 and 72 hr **(Figure 5.7)** revealed that the differences between control and PI3K C2β−/− B-cells were not significant when assessed at each time point individually. However, when analysed by gate, there were consistent differences within the sub G0/G1 and G0/G1 gates over time. **A**; the PI3K C2β−/− sub G0/G1 population was reduced at each time point, within the 'excl. debris and doublets' gate (left) and the highest viability gate (right) (p=0.003 and p=0.007, respectively). **B**; within the G0/G1 gate the PI3K C2β−/− population was higher in both instances (p=0.006 and p=0.005). **C**; the results from PI3K C2β−/− and control cells were comparable for S-phase. **D;** there was a small but statistically significant increase in the percentage of PI3K C2β−/− B-cells in G2/M-phase of the cell cycle when analysed to exclude debris (p=0.047), however, no difference between the groups was observed when analysing the highest viability population. The results are from two independent experiments, using six control and six PI3K C2β−/− mice. Statistical significance was calculated using a two-way ANOVA.

5.8 BCR isotype expression

Surface IgM (sIgM) is the first immunoglobulin isotype to form the BCR on pro-B-cells (Loder et al., 1999) and it continues to be expressed on mature naïve B-cells until activation and subsequent isotype switching (Chaudhuri and Alt, 2004; Jung et al., 1994; Stavnezer et al., 2008). The expression of sIgM may remain following activation, but this is dependent on the method of activation. For example, T-cell dependent activation results in isotype class switching of sIgM to sIgG, sIgE or sIgA. However, following T-cell independent activation sIgM remains present (Charles A Janeway et al., 2001b). Levels of sIgM expression also vary depending on the location or type of B-cell, follicular B-cells (Fo) typically express lower levels of IgM, while sIgM is highly expressed on marginal zone (MZ) B-cells (Loder et al., 1999). As such, surface immunoglobulin expression can help identify the stage of B-cell differentiation.

5.9 PI3K C2β−/− mice have fewer splenic IgM+ B-cells and reduced IgM expression.

Analysis of surface IgM (sIgM) expression was assessed by labelling freshly isolated splenic B-cells with anti-IgM (PE) and analysing cells by flow cytometry. Results are shown from four independent experiments using a total of twelve control and twelve PI3K C2β−/− mice. Statistical analysis was calculated using a Student's t-test (total population) and two-way ANOVA (MFI).

The sIgM population was reduced in PI3K C2β−/− B-cells (**Figure 5.9**). Control B-cells had a mean sIgM+ population of 89.6% ± 1, compared to 81.1% ± 1.5 on PI3K C2β−/− B-cells (p=0.0001). In addition to a reduced sIgM+ population, a consistent reduction in MFI suggested that the level of sIgM expression was also reduced on the PI3K C2β−/− B-cells (p=<0.0001).

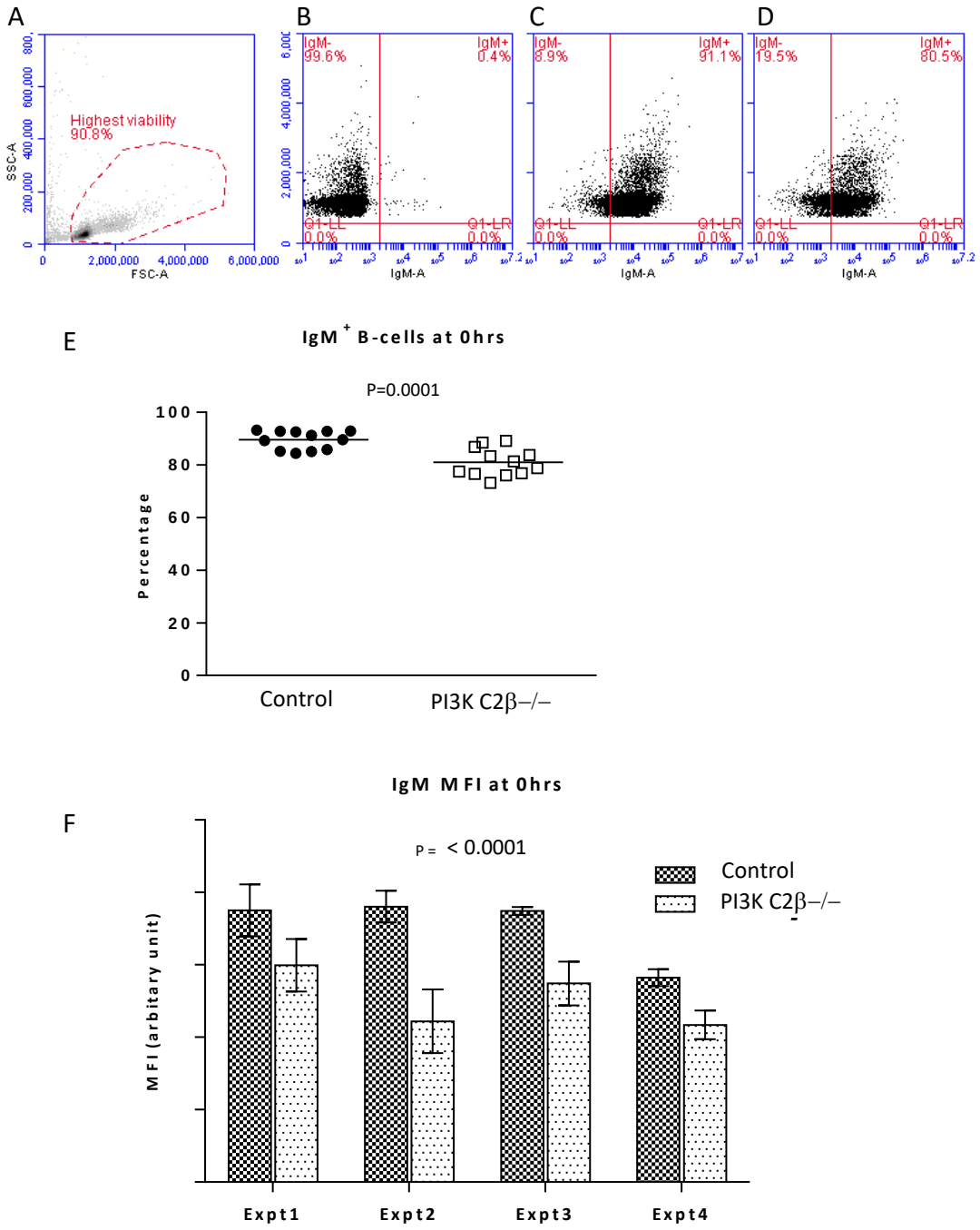

Figure 5.9 sIgM expression on isolated B-cells at 0 hr. Freshly isolated B-cells were allowed to rest for 1-2 hr before being labelled with a fluorophore conjugated antibody to sIgM, or an isotype control. Samples were analysed by flow cytometry with a minimum of 10,000 events recorded per plot. **A**; shows the B-cell population being analysed. **B**; representative dot plot for the isotype control. **C** and **D**; typical sIgM+ plots for control and PI3K C2β–/–, respectively. **E**; analysis of the results revealed that PI3K C2β–/– B-cells contained a lower percentage of sIgM+ cells compared to the control B-cells (81% ± 1.5 and 89.6% ± 1, respectively) this was statistically significant at p= 0.0001. **F**; sIgM+ B-cells from PI3K C2β–/– mice also had a consistent reduction in median fluorescent intensity (p=<0.0001). The results are from four independent experiments, using twelve control and twelve PI3K C2β–/– mice. An unpaired, two tailed Student t-test was used to calculate statistical significance for the sIgM+ populations (E) and a two-way ANOVA was used to assess MFI (F). Data represent mean values ± SEM.

5.10 Differential surface IgM+ expression between control and PI3K C2β–/– B-cells

Basic analysis of surface IgM (sIgM) on freshly isolated B-cells at 0hr showed that PI3K C2β–/– B-cells had a reduced sIgM+ population and that the level of expression within the population was reduced (**Figure 5.9**). Further assessment of the sIgM+ populations against forward scatter revealed a distinct expression pattern when compared to the control IgM+ B-cells (**Figure 5.10**). B-cells were gated according to the level of sIgM expression (high, mid or low). From the total population of sIgM+ B-cells, 18.2% of control B-cells were IgM^{hi}, compared to 9.5% of the PI3K C2β–/– sIgM+ B-cells. This represents a 48% reduction (p=<0.0001). There were also fewer PI3K C2β–/– IgM+ B-cells within the IgM^{mid} gate compared to the controls (35.6% and 40.7% respectively) (p=0.008). The trend was reversed for IgM^{low} B-cells, with 36.7% of PI3K C2β–/– B-cells being IgM^{low}, compared to 29.2% of the controls, which represents a 20.5% increase (p=0.0006). These data suggest that in addition to PI3K C2β–/– splenic B-cells containing fewer sIgM+ B-cells under basal conditions, there is also a difference in the expression profile. The reduction in the total population appears to be as a result of fewer IgM^{hi} and IgM^{mid} expressing B-cells. The increased IgM^{low} population in the PI3K C2β–/– B-cells suggests that the difference was not simply due to an overall reduction in the sIgM+ population.

Table 5.4 Summary of sIgM expression at 0hr

	IgM+ population	IgM^{hi}	IgM^{mid}	IgM^{lo}
Control B-cells	89.6 % ± 1	18.2 % ± 1.2	40.7 % ± 0.6	29.2 % ± 1.2
PI3K C2β$^{-/-}$ B-cells	81.01 % ± 1.5	9.5 % ± 1.1	35.6 % ± 1.6	36.7 % ± 1.5
Difference	8.6 % ± 1.8	8.7 % ± 1.6	5.02 % ± 1.7	7.5 % ± 1.9

$IgM^{hi,mid}$ and ^{low} refers to the gating strategy (**Figure 5.10**). Results are from four independent experiments using twelve control and twelve PI3K C2β−/− mice. Data represent the mean ± SEM.

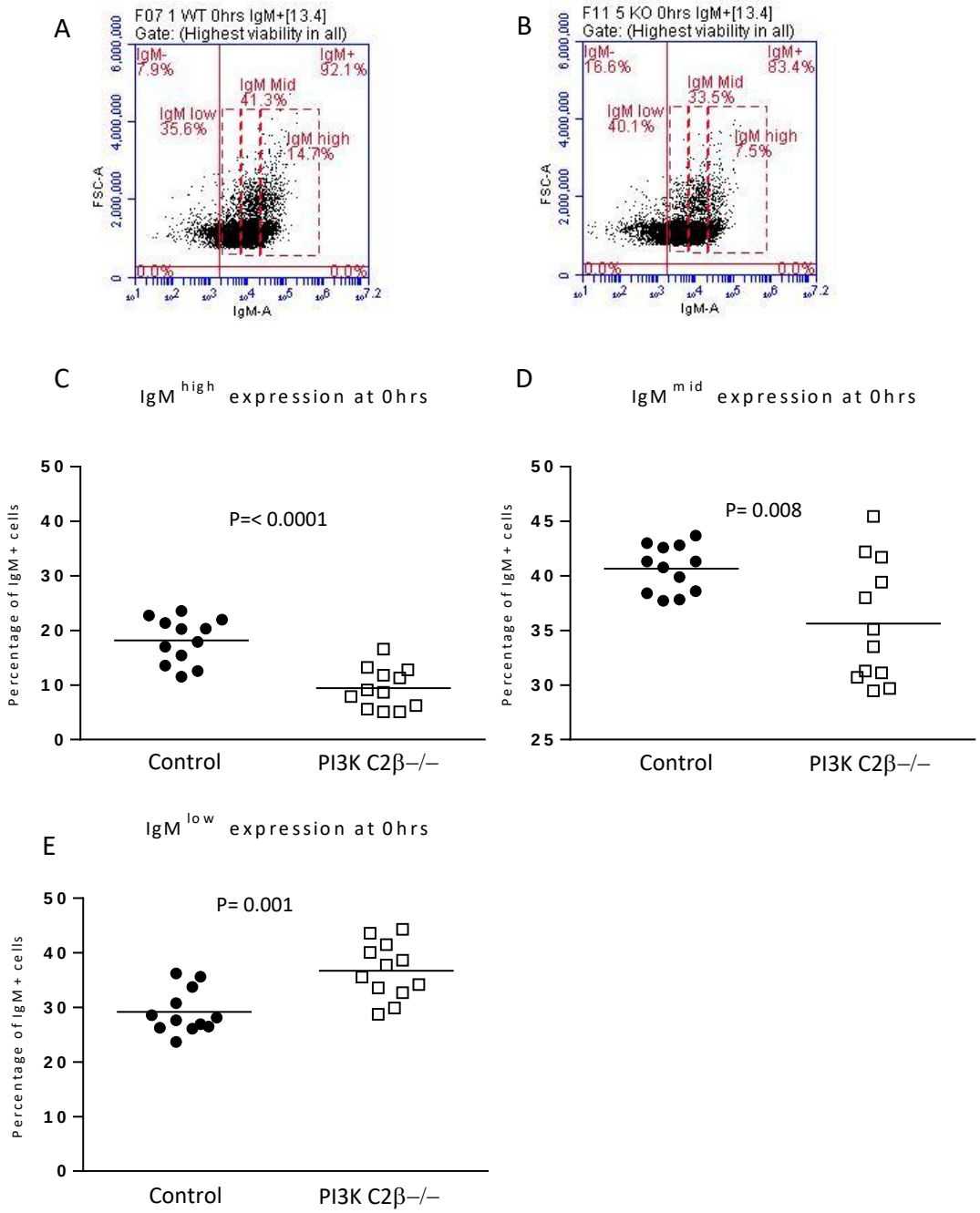

Figure 5.10 Differences in sIgM expression in unstimulated, freshly isolated B-cells. Results had shown that the sIgM+ population was consistently smaller in B-cells from PI3K C2β–/– mice, compared to the controls (**Figure 5.9**). The difference in MFI suggested that this was not simply due to PI3K C2β–/– mice having fewer sIgM+ B-cells. To examine the expression profile, cells were gated as high, medium or low expression based on the expression levels in the control B-cells. A minimum of 10,000 events were recorded per experiment. **A** and **B**; show representative plots with gating for IgM^{hi}, IgM^{mid} and IgM^{lo} populations, for control and PI3K C2β–/– B-cells, respectively. **C**; the mean IgM^{hi} populations were consistently reduced in the PI3K C2β–/– B-cells (9.5 % ± 1.1) compared to the controls (18.2 % ± 1.2). This difference was considered very significant (p<=0.0001). **D**; within the IgM^{mid} gate, the PI3K C2β–/– population (35.6 % ± 1.6) were also significantly reduced compared to the controls (40.7 % ± 0.6) (p=0.008). **E**; the trend was reversed for the IgM^{low} population, which had a consistently higher mean population of PI3K C2β–/– B-cells (36.7 % ± 1.5) compared to the controls (29.2 % ± 1.2) (p=0.001). The results are from four separate experiments using a total of twelve control and twelve PI3K C2β–/– mice, a student t-test was used for statistical analysis. Data represent mean values ± SEM.

5.11 sIgG1 and sIgE expression at 0hr

Freshly isolated, unstimulated PI3K C2β−/− B-cells had reduced sIgM+ populations and reduced MFI compared to B cells from control animals indicating that the level of expression was also reduced (**Figure 5.9**). Following isotype switching, which occurs within the germinal centre in response to activation, B-cells exchange surface IgM for IgG, IgE or IgA.

The increased size of germinal centre cross sectional areas previously observed in PI3K C2β−/− spleens (**Figure 3.5 and Figure 3.6**), in addition to a reduction in the sIgM+ populations on freshly isolated B-cells, may indicate that spleens in these knockout mice contain a higher background level of isotype switched B-cells. To explore this hypothesis, anti-IgG (PE), anti-IgE (PE) or an isotype control were used to label freshly isolated B-cells, following a two hour rest period. Flow cytometric analysis revealed that B-cells from PI3K C2β−/− mice had small but statistically significant increases in both sIgG1 and sIgE populations at 0 hr (**Figure 5.11** and **Figure 5.12**). sIgG1 was detected on 6% ± 0.5 of PI3K C2β−/− B-cells, compared to 3.8% ± 0.2 of control cells (p=0.002), while sIgE was detected on 2.9% ± 0.1 of PI3K C2β−/− B-cells and 2.04% ± 0.1 of control B-cells (p=0.0005). Although small, these increases could suggest that PI3K C2β−/− mice kept under basal conditions have a slightly higher background of class switched splenic B-cells. Analysis of MFI revealed no difference in the expression of sIgE on B cells from control and PI3KC2β−/− mice (data not shown). Examination of the sIgG1 positive samples, demonstrated an increased population of PI3K

C2β−/− B-cells, falling within the sIgG1 'switching gate' (**Figure 5.11**). This population lay between the IgG1- and IgG1+ populations, and had an increased MFI compared to the controls, which might indicate that they were in the process of up-regulating sIgG1 as a result of class switching ($p=0.02$).

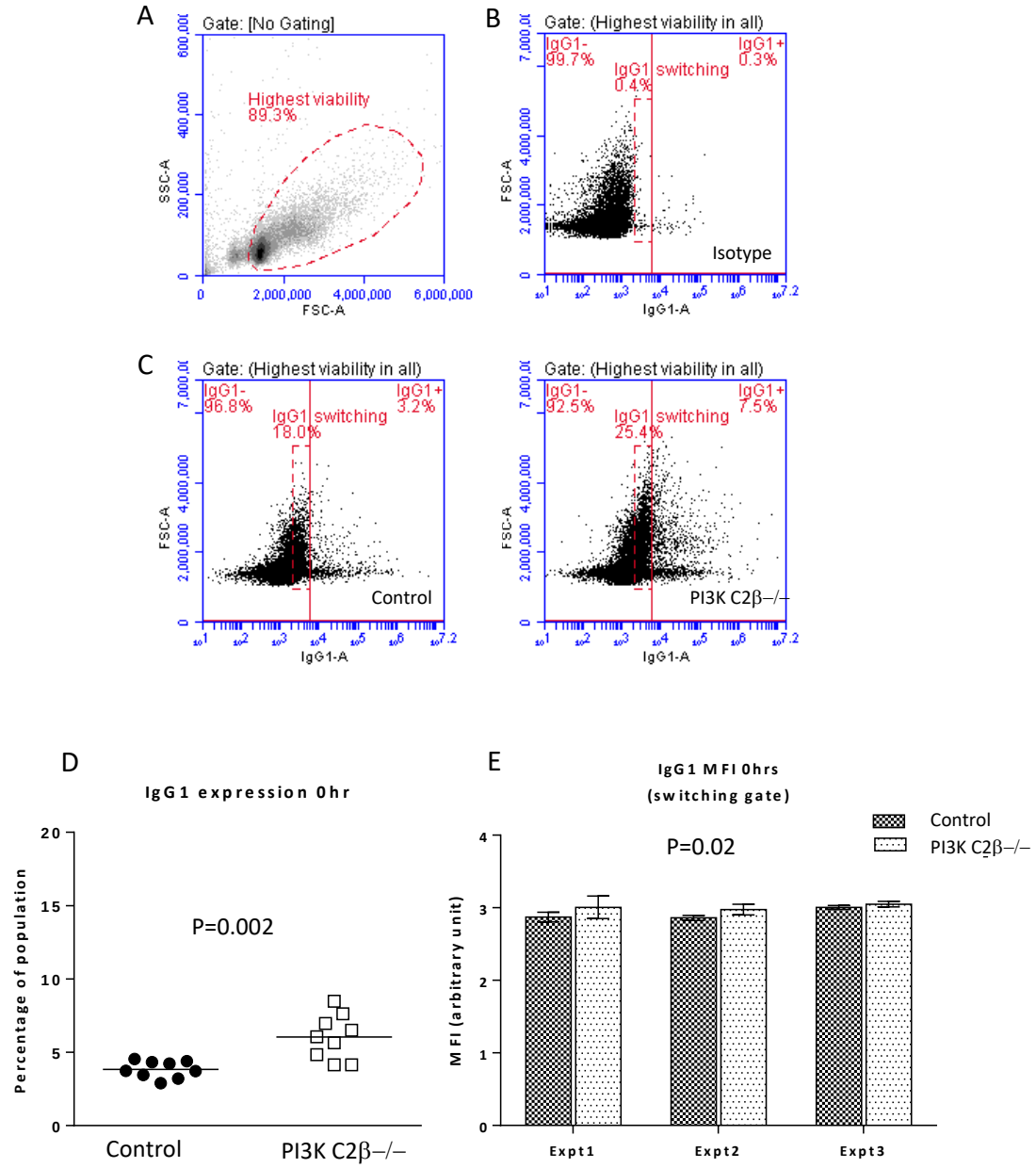

Figure 5.11 Analysis of IgG1 expression on freshly isolated B-cells (0 hr). Following isolation, B-cells were allowed to rest for 1-2 hr before being labelled with fluorophore conjugated antibodies to IgG or an isotype control. 10,000 events were recorded per plot. **A**; all cells were gated to include the highest viability population. **B**; a typical plot showing the isotype control used for gating. **C**; representative plots of IgG1+ B-cells from control (left) and PI3K C2β–/– (right) mice **D**; results showed a small but significant increase in IgG1+ B-cells from the PI3K C2β–/– mouse spleens, compared to the control mice. **E**; cells were gated to examine IgG1 MFI, of B-cells that were on the borderline between negative and positive (B and C), PI3K C2β–/– B-cells consistently had a slight increase in MFI (p=0.02). The increase in MFI might suggest that the PI3K C2β–/– B-cells have small population that are in the process of class switching. Results are from three independent experiments, using nine control and nine PI3K C2β–/– mice. Statistical analysis was performed by Student's t-test (**D**) and two-way ANOVA (**E**). Data represent mean values ± SEM.

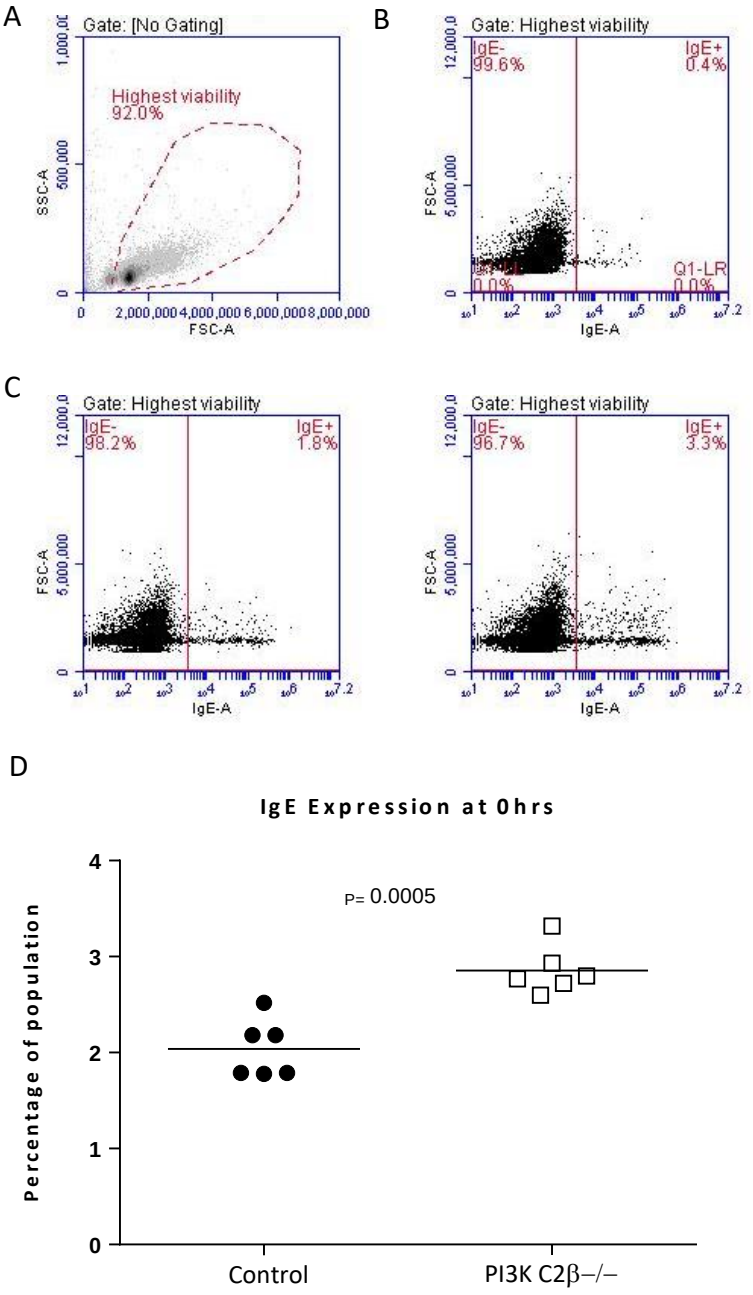

Figure 5.12 Analysis of IgE expression on freshly isolated B-cells (0 hr). Following isolation, B-cells were allowed to rest for 1-2 hr before being labelled with fluorophore conjugated antibodies to IgE or an isotype control and analysed by flow cytometry. 10,000 events were recorded per plot. **A**; cells were gated to include the highest viability population. **B**; a typical plot showing the isotype control used to exclude non-specific binding. **C**; representative plots of IgE+ B-cells from control (left) and PI3K C2β–/– (right) samples. **D**; results showed a small but significant increase in IgE+ B-cells from the PI3K C2β–/– samples (2.9% ± 0.1), compared to the controls (2% ± 0.1) (p=0.0005). Results are from two independent experiments, using six control and six PI3K C2β–/– mice. Statistical analysis was performed using an unpaired, two tailed Student's t-test. Data represent mean values ± SEM.

5.12 Differential surface CD23 expression between control PI3K C2β–/– B-cells

In the splenic B-cell population, the low affinity IgE receptor, FcεRII (CD23) is expressed on the surface of mature follicular (Fo) B-cells, but is absent from immature transitional stage 1 (T1), and MZ B-cells (Best et al., 1995). Newly activated B-cells initially upregulate surface CD23 (sCD23), however expression is reduced post activation (Rabin et al., 1992) and is lost following class switch recombination (CSR) (Kehry and Hudak, 1989). These differential expression patterns make sCD23 useful for identifying the stage of B-cell maturation, activation state and specific populations when used in conjunction with other markers. Freshly isolated B-cells were stained with anti-CD23 (FITC) and analysed by flow cytometry. To determine the CD23+ populations, cells were gated on the highest viability cells and a negative isotype control was used to exclude any non-specific antibody binding (**Figure 5.13**). Analysis was performed over three individual experiments using a total of nine control and nine PI3K C2β–/– mice. PI3K C2β–/– mice had a reduction of 30.2% ± 1.5 of their overall sCD23+ B-cell population compared to control B-cells which were consistently >80% sCD23 positive (mean = 87.8% ± 0.7), as opposed to the PI3K C2β–/– B-cells, for which the mean sCD23+ population was 57.6% ± 1.4 of total B-cells (p= < 0.0001).

Breakdown of the sCD23+ populations showed that PI3K C2β–/– B-cells had an increased population of $CD23^{low}$ B-cells compared to the controls (**Figure 5.14**). The association between sCD23 expression and the stage of B-cell maturation and activation state made this population of potential interest.

B-cell populations were gated to show the sCD23^{low} populations, revealing a significant increase in the PI3K C2β–/– samples (p=<0.0001).

25.2% ± 1.4 of all control B-cells within the highest viability gate were CD23^{low}, compared to 48.1% ± 1.2 of the PI3K C2β–/–B-cells (**Figure 5.14**), which represents 28.0% ± 1.5 of the sCD23+ population (control) compared to 82.2% ± 0.8 (PI3K C2β–/–). Examination of FSC revealed a small but consistent increase in the PI3K C2β–/– sCD23^{low} B-cells of 9% (mean of three experiments), indicating that cell size was increased, relative to the control B-cells. Measurement of MFI was also reduced in the PI3K C2β–/– samples, in each of the three experiments (by 61%, 62% and 55%). This indicated that in addition to having fewer sCD23+ B-cells, the sCD23 expression was lower in the PI3K C2β–/– B-cells compared to the control B-cells.

Table 5.5 sCD23+ breakdown

	CD23^{low} population (of all viable B-cells)	**CD23^{low} population (within CD23+ B-cells)**
Control	25.2 % ± 1.4	28 % ± 1.5
PI3K C2β–/–	48.1 % ± 1.2	82.2 ± 0.8
Difference between means	22.9 % ± 1.8	54.2 % ± 1.7
Significance	p=< 0.0001	p=< 0.0001

CD23low expressing B-cell populations at 0hr. Results are from three independent experiments, using nine control and nine PI3K C2β–/– mice. Statistical analysis was performed using an unpaired, two-tailed Student t-test. Data represent mean values ± SEM.

Table 5.6 sCD23^{low} mean forward scatter and median fluorescent intensity for CD23+ B-cells

	CD23^{low} mean forward scatter			**CD23+ median fluorescent intensity**		
	Expt1	Expt2	Expt3	Expt1	Expt2	Expt3
Control	1.3	1.5	1.2	6.8	7	6
PI3K C2β–/–	1.4	1.6	1.3	2.7	2.7	2.7
Difference between means	0.1	0.1	0.1	4.1	4.3	3.3
Significance	p= < 0.0001			p= < 0.0001		

Median fluorescent intensity and mean forward scatter over the course of three individual experiments, units used are arbitrary and are displayed to allow comparison. Statistical analysis was performed using a two-way ANOVA.

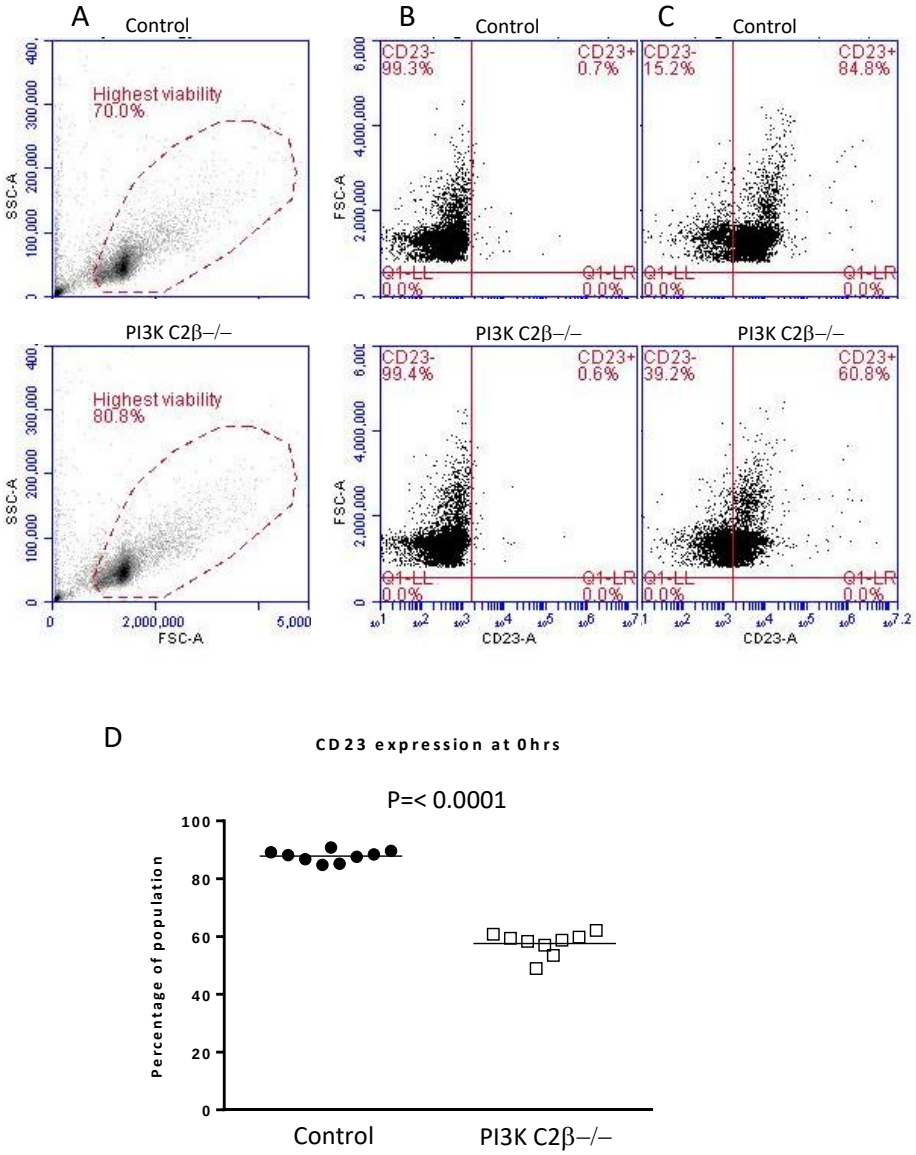

Figure 5.13 sCD23 expression at 0 hr. Following isolation, B-cells were allowed to rest for 1-2 hr before being labelled with fluorophore conjugated antibodies to CD23 or an isotype control and analysed by flow cytometry. 10,000 events were recorded per plot. **A**; representative plots showing the highest viability population that was analysed. **B**; shows the negative isotope control used for gating. **C**; characteristic positive staining for anti-CD23 (FITC). **D**; PI3K C2β−/− mice had consistently fewer CD23+ B-cells (57.6% ± 1.3) compared to the controls (87.8% ± 0.7) (p= < 0.0001). Results are from three independent experiments using nine control and nine PI3K C2β−/− mice. Statistical analysis was performed using an unpaired, two-tailed Student t-test. Data represent mean values ± SEM.

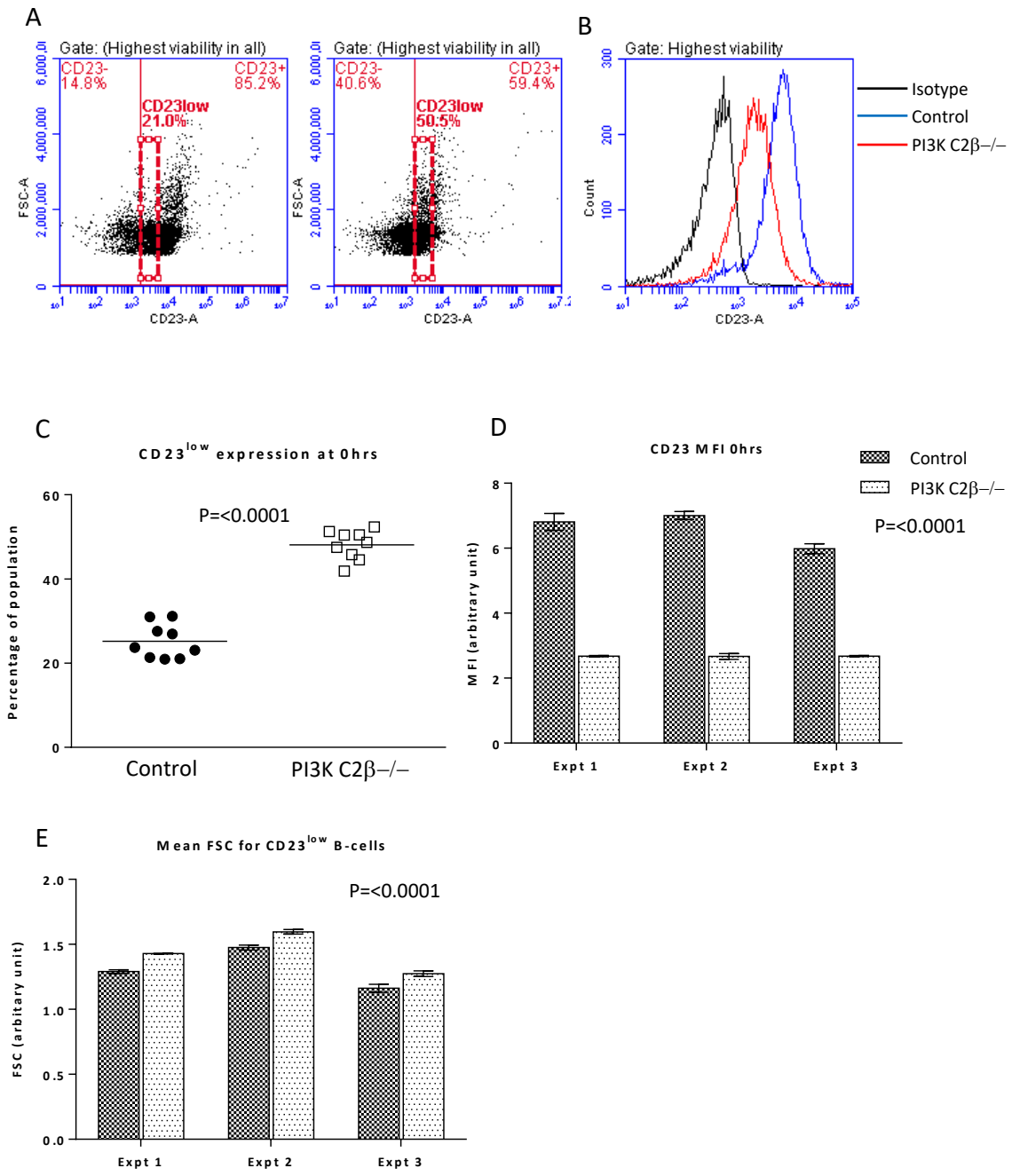

Figure 5.14 sCD23low populations at 0hr. Freshly isolated B-cells were labelled with fluorophore conjugated anti-CD23 or an isotype control and examined by flow cytometry. 10,000 events were recorded per plot (**Figure 5.13**). Median fluorescent intensity and forward scatter were analysed **A**; representative dot plots showing sCD23low populations. **B**; representative histogram showing the difference in median fluorescence between control and PI3K C2β−/− sCD23+ B-cells. **C**; analysis of results revealed PI3K C2β−/− B-cell populations had an increased population of $sCD23^{low}$ cells (82.2% ± 0.8) compared to the controls (28% ± 1.4). (P=<0.0001). **D**; The MFI of the sCD23+ PI3K C2β−/− B-cells was also consistently lower than the controls (mean reduction of 59%) (p=<0.0001), indicating that sCD23 expression was reduced. **E**; mean FSC was slightly increased in the PI3K C2β−/− samples, in each experiment (mean increase of 9%) (p=<0.0001). Results are from three independent experiments, using nine control and nine PI3K C2β−/− mice. Statistical analysis was performed using an unpaired, two-tailed Student t-test (C) and two-way ANOVA (D and E). Data represent mean values ± SEM.

5.13 PI3K C2β–/– B-cells show altered CD23/CD19 expression compared to controls

Co-staining in conjunction with flow cytometry provides a useful tool to assess cell populations. B-cell populations and subsets are often identified by way of multiple surface markers and their relative expression levels. Multiple staining involves labelling samples with each antibody and isotype control individually, as well as multi-labelling. This ensures that colour compensation can be set to avoid erroneous results due to overspill resulting in fluorophore signals being 'read' by the incorrect detector.

Analysis had shown that PI3K C2β–/– mice have approximately a 30% reduction in sCD23+ splenic B-cells (**Figure 5.13**). Reduced sCD23 expression has been linked to B-cell maturation and class switch recombination (CSR) (Rabin et al., 1992), and increased CD19 expression is associated with a reduction in B-cell "interaction thresholds" and can lead to increased survival (Nicholas et al., 2008), which has been observed in PI3K C2β–/– B-cells (**Section 5.3**). To investigate further, dual staining with anti-CD19 and anti-CD23 was performed to identify any differences between B-cell populations. Freshly isolated B-cells were used from six control mice and six PI3K C2β–/– mice, in two independent experiments and an unpaired, two-tailed Student t-test was used for statistical analysis unless otherwise stated.

Previous results had shown a reduction in the PI3K C2β–/– sCD23+ population and an upregulation in the expression of CD19 (**Figure 5.13** and

Figure 5.3). However, examining the expression profile may provide insight into the subsets present and their stage of differentiation.

5.14 CD19^{hi}/sCD23^{hi} B-cells are almost absent in PI3K C2β–/– spleens

Analysis of the co-staining results revealed a small population of CD19^{hi}/sCD23^{hi} B-cells in the controls that was almost absent in the PI3K C2β–/– B-cells (**Figure 5.15**). In control B-cells the mean CD19^{hi}/sCD23^{hi} population was 6.2% ± 0.5 of all viable B-cells analysed (7.3% of the total sCD23+/CD19+ population), whereas 1.1% ± 0.1 of the PI3K C2β–/– B-cells were CD19^{hi}/sCD23^{hi} (representing 2.3% of the total sCD23+/CD19+ population). This represents a reduction of 82.3%. Statistical significance was calculated using an unpaired two-tailed student t-test, using Welch's correction for unequal variance (p=0.0001).

5.15 CD19^{hi}/sCD23^{lo}

Enlarging the CD19/sCD23 plots revealed the presence of a CD19^{hi}/sCD23^{low} population (**Figure 5.16**) that made up 19.1% of the total PI3K C2β–/– B-cells but was significantly reduced in the control samples at 6% (p=0.0005). As sCD23 expression is downregulated following activation, the CD19^{hi}/sCD23^{low} populations were separated into low forward scatter (FSC) and high FSC gates, which showed that there was an increased percentage of PI3K C2β–/– B-cells within the high FSC gate (77.7% ± 3.5) compared to the controls (65.4% ± 2.4), the difference of 12.3% ± 4.3 was considered significant (p=0.02). In addition to having an increase in the percentage of high FSC cells, the FSC reading for CD19^{hi}/sCD23^{low} B-cells was higher in the

PI3K C2β−/− samples, compared to the controls (2.4 ± 0.05 and 2.1 ± 0.04, respectively). The unit for FSC is arbitrary and is provided to allow comparison, but the difference represents an increase of 11.8%, which was significant (p=0.002).

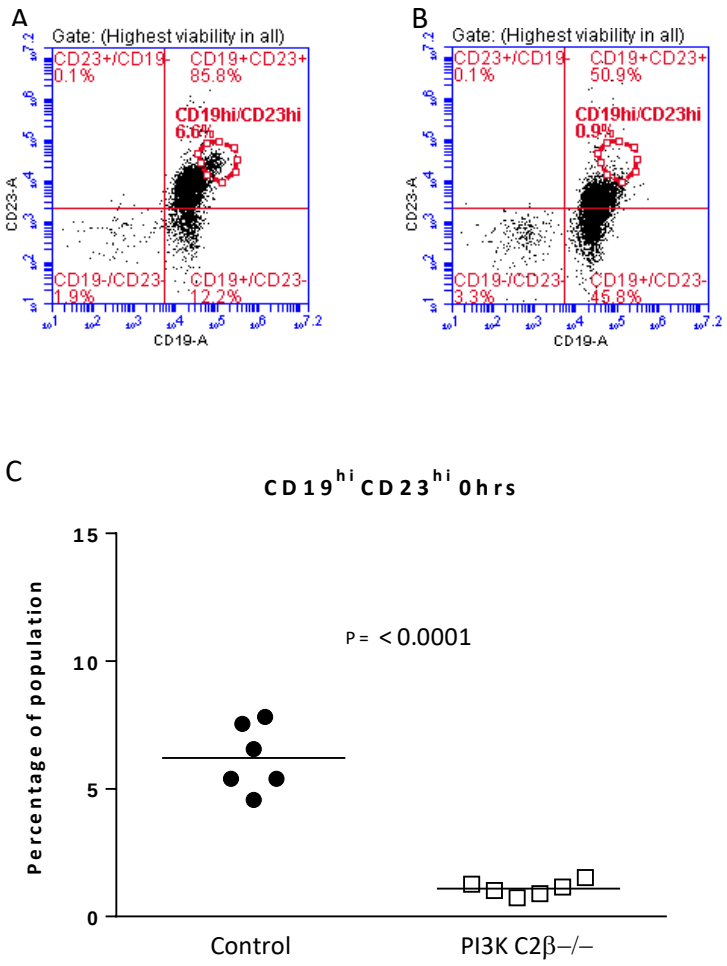

Figure 5.15 Dual staining with anti-CD23 (FITC) and anti-CD19 (Alexa Flour 647). Freshly isolated splenic B-cells were allowed to rest for 1-2 hr before being labelled with fluorophore conjugated antibodies to CD23 only, CD19 only or both CD23 and CD19, or the appropriate isotype control. Cells were then examined using flow cytometry, with 10,000 events recorded per plot. **A** and **B**; representative staining pattern showing a distinct population of control B-cells that were $CD19^{hi}/sCD23^{hi}$ (6.2% ± 0.5), which were significantly reduced in the PI3K C2β–/– populations (1.1% ± 0.1). **C**; analysis of the flow cytometry data confirmed the reduction of the $CD19^{hi}/sCD23^{hi}$ population within the PI3K C2β–/– B-cells (p=<0.0001). Results are from two independent experiments, using six control and six PI3K C2β–/– mice. Statistical analysis was performed using an unpaired, Student t-test with Welch's correction. Data represent mean values ± SEM.

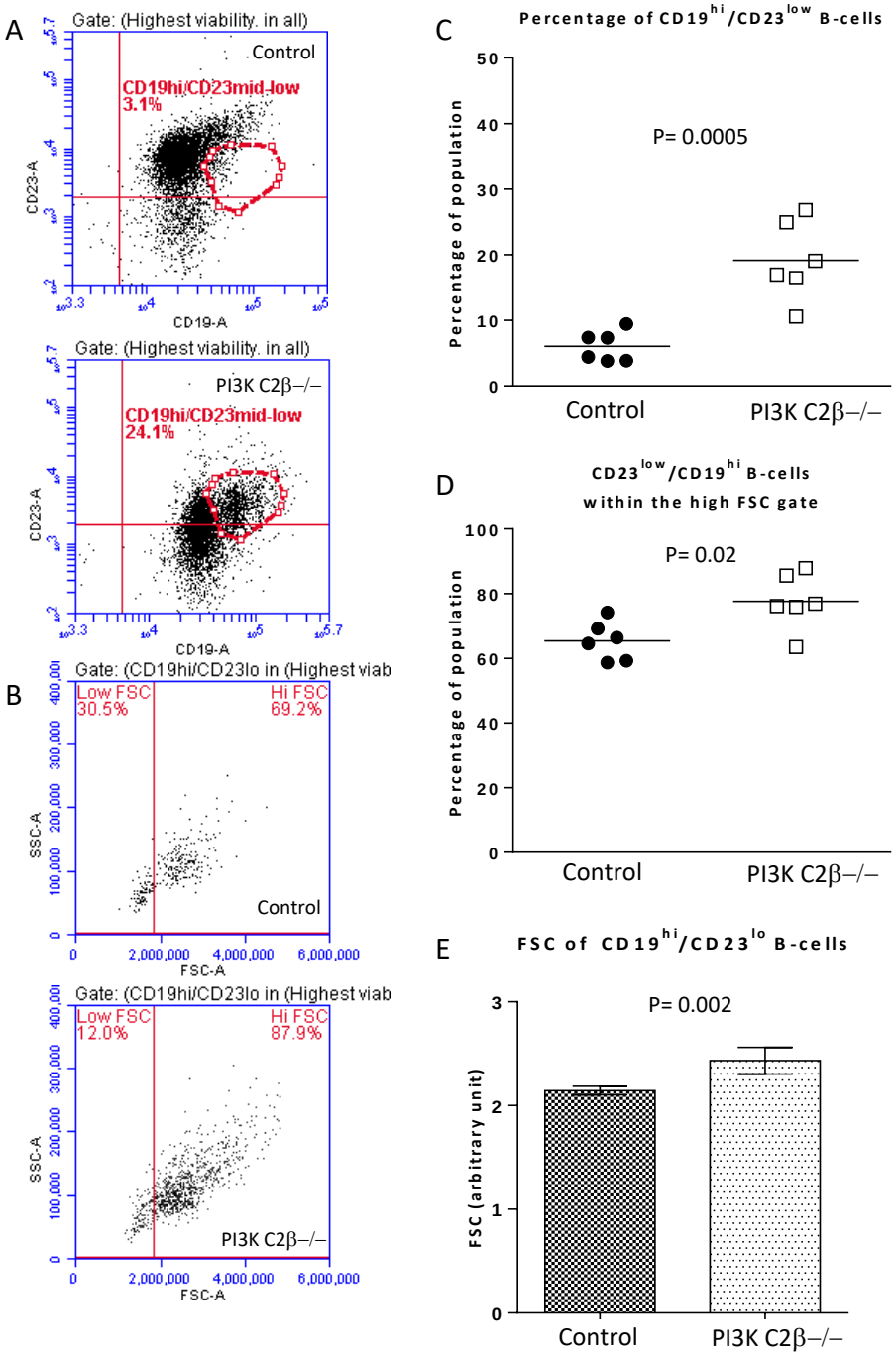

Figure 5.16 Dual staining with anti-CD19 (Alexa-fluor 647) and anti-CD23 (FITC). A; representative plots for control (top) and PI3K C2β–/– B-cells, respectively. Plots are duplicates from **Figure 5.15** that have been enlarged to show a distinct CD19^{hi}/sCD23^{low} population that is increased in the PI3K C2β–/– samples. **B**; typical plots showing the FSC/SSC of B-cells within the CD19^{hi}/sCD23^{low} gate for control (top) and PI3K C2β–/– (bottom), plots have been separated to show low FSC and high FSC populations. **C**; analysis of the results confirmed that the CD19^{hi}/sCD23^{low} population was significantly higher in the PI3K C2β–/– B-cells (19.1% ± 2.4), compared to the controls (6% ± 1) (P=0.0005). **D**; there was also an increased percentage of CD19^{hi}/sCD23^{low} PI3K C2β–/– B-cells within the high FSC gate 77.7% ± 3.5), compared to the controls (65.4% ± 2.4) (p=0.02). **E**; in addition to having a higher percentage of cells within the high FSC gate, PI3K C2β–/– B-cells that were within the CD19^{hi}/sCD23^{low} gate had a 11.8% increase in the mean FSC reading (p=0.002). Results are from two independent experiments, using six control and six PI3K C2β–/– mice. Statistical analysis was performed using an unpaired, two-tailed Student t-test. Data represent mean values ± SEM.

5.16 sCD23/sIgM

Previous assessment of sCD23+ B-cells had shown that PI3K C2β–/– samples had an increased population of sCD23^{low} B-cells, and that they had a higher FSC profile compared to the controls. Furthermore, an increased population of sIgM^{low} B-cells had also been observed in the PI3K C2β–/– samples (**Figure 5.10**). Activated, differentiating B-cells are typically sIgM^{low}/CD23^{low} (Loder et al., 1999), and an increased FSC suggests increased cell size, which is also observed in activated B-cells (Allen et al., 2012). To investigate further, a preliminary experiment was carried out. Freshly isolated B-cells were co-stained with anti-IgM (PE) and anti-CD23 (FITC) and analysed by flow cytometry. Results are from a single experiment using three control and three PI3K C2β–/– mice. Statistical analysis was performed using an unpaired, two-tailed Student's t-test and data represent mean values ± SEM. Although this form of statistical analysis is used in the literature on small sample sizes (Allen et al., 2012; Carmichael et al., 2009; Dengler et al., 2008), it may not be appropriate as the normality of the data cannot be determined. However, the power of this analysis, based on the standard deviation and difference between the means indicates that this experiment was powered at 0.9 and 0.99 respectively.

An sIgM^{low}/sCD23^{low} population was identified (**Figure 5.17**), using the gating strategy presented in **Appendix 6**, this revealed an increase within the PI3K C2β–/– samples compared to the controls (24% ± 0.7 and 15% ± 1.5, respectively). Cells with the highest FSC were also identified which showed that 17% ± 1.4 of the control sIgM+/sCD23+ population had an

increased FSC, while 32% ± 0.9 of the PI3K C2β–/– B-cells had an increased FSC.

Table 5.7 Summary of sIgM+/sCD23+ data.

	sIgM^{low}/sCD23^{low} (percentage of viable B-cells)	**Percentage of sIgM+ sCD23+ cells with increased FSC**
Control	15 ± 1.5	17 ± 1.4
PI3K C2β$^{-/-}$	24 ± 0.7	32 ± 0.9
Difference between the means	8.8 ± 1.7	15 ± 1.7

Results are from a preliminary experiment using three control and three PI3K C2β$^{-/-}$ mice. Data represent mean values ± SEM

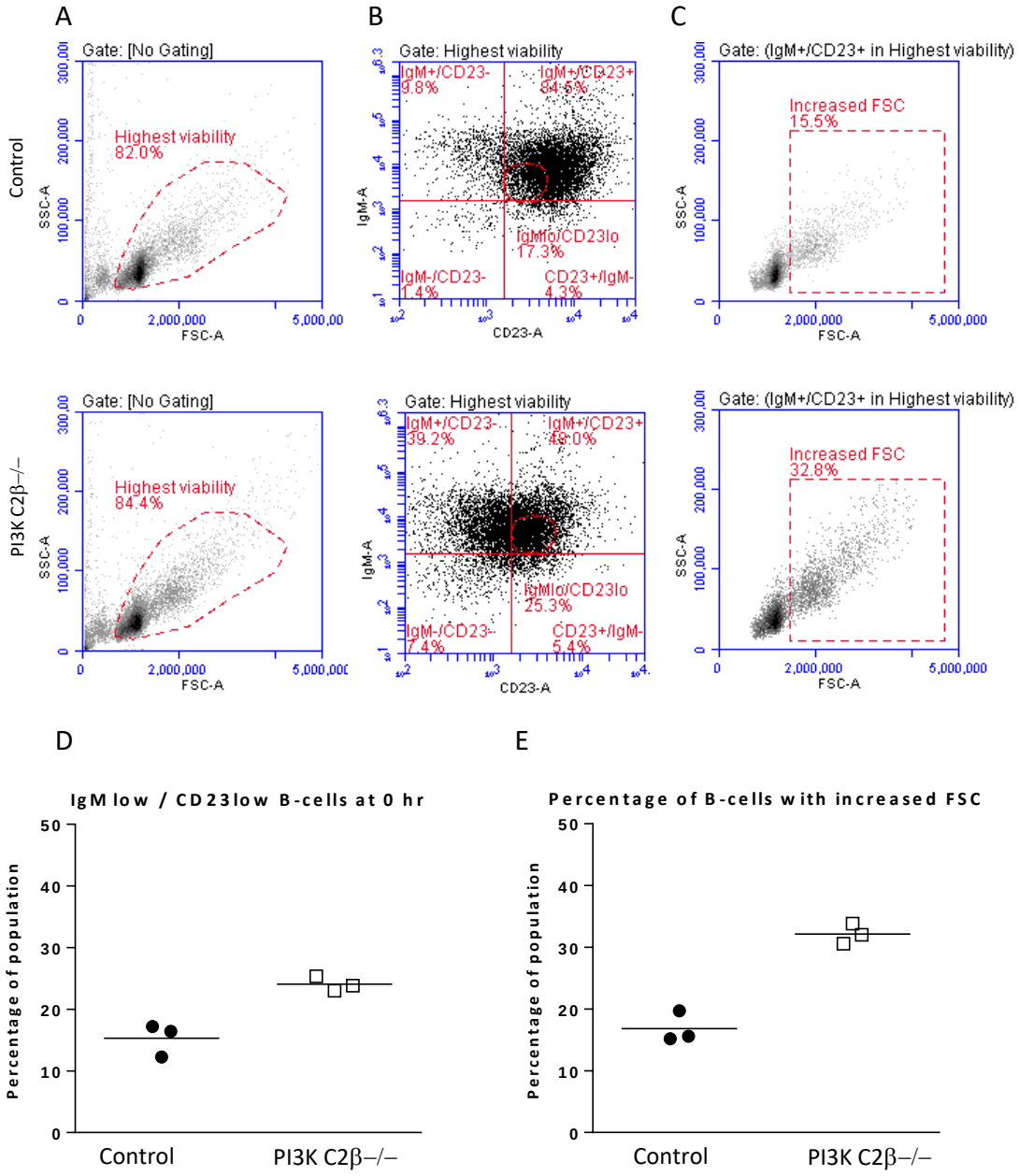

Figure 5.17 sIgM^{low}/sCD23^{low} population is increased in PI3K C2β–/– B-cells. Freshly isolated B-cells were labelled with anti-IgM (PE) and anti-CD23 (FITC) and analysed using flow cytometry, 10,000 events were recorded per plot. **A**; cells within the highest viability gate were used for analysis. **B**; representative plots showing the sIgM^{low}/sCD23^{low} populations for control (top) and PI3K C2β–/– (bottom) B-cells (see **Appendix 6** for gating strategy). **C**; plots show FSC versus SSC of the total sIgM+/sCD23+ populations (see also **Appendix 7**). **D**; the results showed an increased population of sIgM^{low}/sCD23^{low} B-cells in the PI3K C2β–/– samples (24% ± 0.7) compared to the controls (15% ± 1.5). **E**; the percentage of B-cells with an increased forward scatter, within the sIgM+/sCD23+ population, was also higher in the PI3K C2β–/– samples (32% ± 0.9), compared to the controls (17% ± 1.4). Results are from a single experiment. This experiment is powered at 0.9 (d) and 0.99 (e). Data represent mean values ± SEM

5.17 IgM^{hi}/sCD23- populations

Surface CD23 expression is absent from marginal zone (MZ) B-cells (Best et al., 1995), which in mice, are a population of mature non-circulating B-cells found within the MZ of the spleen (Loder et al., 1999). Their location places them between the red pulp and follicles, where they can react to blood borne antigens directly, in a T-cell independent (TI) manner (Tsolaki, 2011). MZ B-cells have also been shown to provide T-cell stimulation (Oliver et al., 1999). However there is also a subset of immature B-cells termed T1 (transitional stage 1), that are also sCD23-/sIgM^{hi}, these are typically small B-cells, newly arrived in the spleen from the bone marrow (Sims et al., 2005).

By gating to reveal the sIgM+/sCD23+ populations (**Appendix 6**), it was possible to also identify a distinct population of sIgM^{hi}/sCD23- B-cells within the control B-cells (**Figure 5.18**), accounting for 5.3% ± 0.4 of the total population. Within the PI3K C2β$^{-/-}$ samples there were 19% ± 0.5 sIgM^{hi}/sCD23- B-cells, a difference of 14% ± 0.6, compared to the controls. Results were powered to detect a difference, with the exception of Figure 5.2 (E), which was underpowered at 0.6.

CD19 expression was also assessed as it has been described as being upregulated in MZ B-cells (Genestier et al., 2007). Upregulation of CD19 has also been observed in MZ B-cells following activation (Palm et al., 2016a). As MZ B-cells have been shown to have an increased forward scatter (Arnon et al., 2013), this was also examined in the sIgM^{hi} / sCD23- B-cells. The gating

strategy was the same as used for the sIgM^{low}/sCD23^{low} population (**Figure 5.17**), further details are provided in **Appendix 8** and **Appendix 9**.

Analysis of the results showed that in each of the PI3K C2β–/– plots there was a population of high FSC cells that was greatly reduced in the control plots (8.3% ± 0.8 compared to 2.8% ± 0.5, respectively). Measurement of CD19 MFI revealed that there was a consistent increase in each sIgM^{hi}/sCD23- sample (mean increase: 23.3%) in the PI3K C2β–/– B-cells.

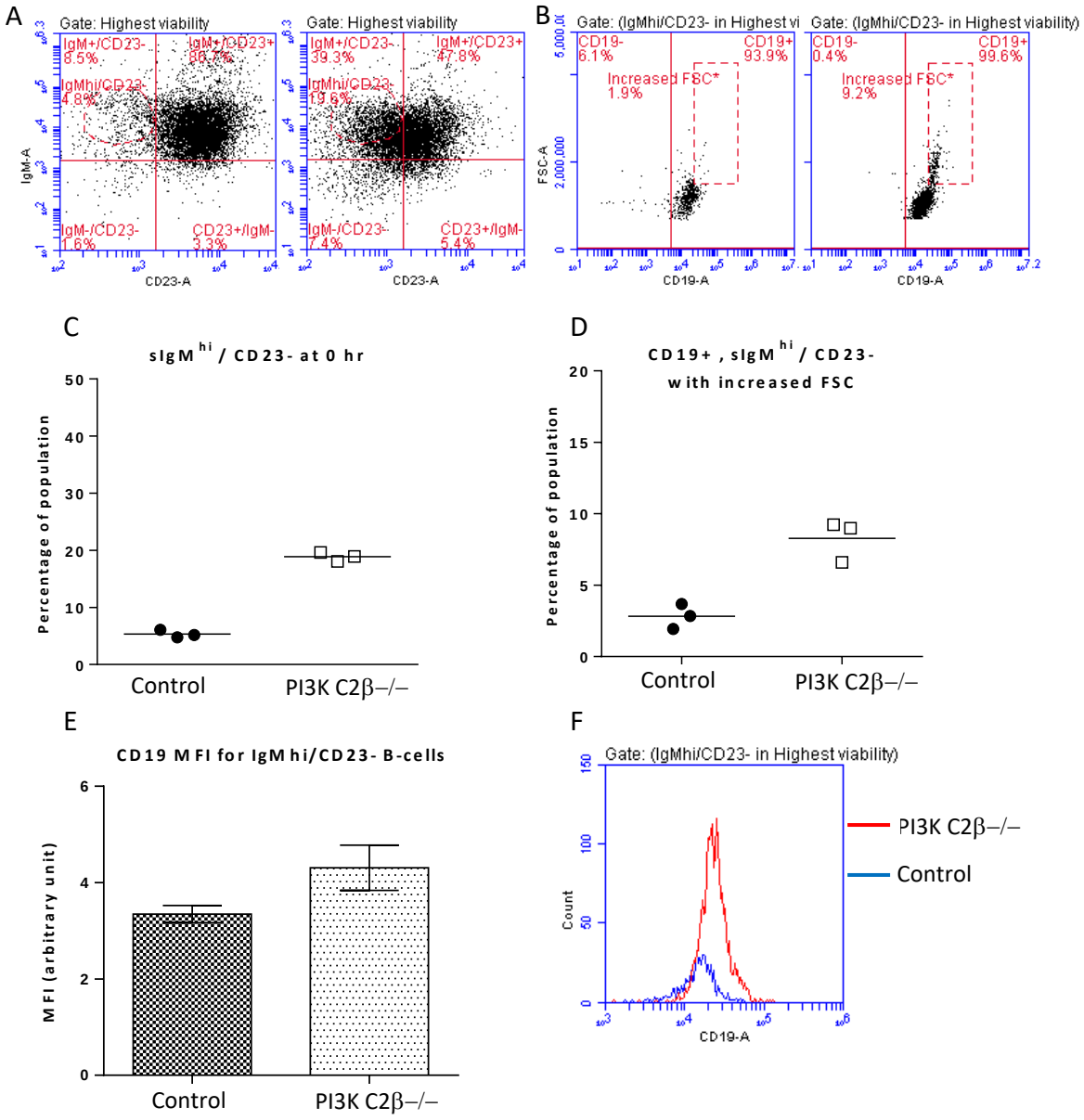

Figure 5.18 sIgM^{hi}/sCD23- B-cell populations at 0 hr. Freshly isolated B-cells were either labelled individually with anti-CD23 (FITC), IgM (PE) and CD19 (Alexa-fluor 647), the relevant isotype control, or all three antibodies and assessed by flow cytometry. A minimum of 10,000 event were recorded per plot. Cells analysed were within the highest viability gate **(Figure 5.17)** and the gating strategy used is presented in **Appendix 8** and **Appendix 9** . **A**; representative plots showing the sIgM^{hi}/sCD23- populations for control (left) and PI3K C2β–/– B-cells (right). **B**; plots showing CD19 staining of the sIgM^{hi}/sCD23- B-cells. There was a small population of B-cells with an increased FSC in PI3K C2β–/– samples (right) that was almost absent in the control samples (left). **C**; the sIgM^{hi}/sCD23- population within the PI3K C2β–/– samples was increased (19% ± 0.5) compared to the controls (5.3 ± 0.4). **D**; the percentage of CD19+, sIgM^{hi}/sCD23- within the 'increased FSC' gate (B) was increased in PI3K C2β–/– B-cells (8.3% ± 0.8) compared to the controls (2.8 ± 0.5). **E**; CD19 MFI was found to be higher in the PI3K C2β–/– B-cells (3 ± 0.1), compared to controls (2 ± 0.1). **F**; representative histogram showing the difference in fluorescent intensity. Results are from a single experiment using three control and three PI3K C2β–/– mice. These data are powered at 1 (c), 0.95 (d) and 0.57 (e).Data represent mean values ± SEM.

5.18 B-cell activation

Under normal physiological conditions, to avoid apoptosis both in vivo and in vitro, B-cells must receive 'survival' signals that are typically generated via surface receptors. For the purpose of this project lipopolysaccharide (LPS) and IL-4 were used, which are associated with isotype switching to IgG1 and IgE (György et al., 2012).

5.19 Class switching

Class switching, also referred to as isotype switching occurs in mature B-cells in response to interaction with antigen. Gene rearrangement leads to the constant region of the heavy chain (CH) being 'switched', typically from IgM or IgD to IgG, IgE or IgA. Class switching is an important step in the differentiation of mature B-cells into either memory B-cells or antibody secreting plasma cells. Identification of surface antibody expression can provide insight into effector immune pathways. B-cell activation can be achieved using various stimuli, in different combinations and concentrations. The combination of LPS and IL-4 are frequently used and optimal levels are generally considered to be 20µg/ml and 50ng/ml, respectively (Heise et al., 2014; Lin and Calame, 2004; Omori et al., 2006). Having observed CD19 upregulation and a slight increase in surface IgG1 and IgE expression on PI3K C2β–/– B-cells at 0hr in unimmunized mice, class switching under optimal conditions and also sub-optimal conditions, was examined.

5.20 Optimal conditions: LPS (20μg/ml) and IL-4 (50ng/ml)

Following activation with LPS (20μg/ml) and IL-4 (50ng/ml), B-cells were labelled with anti-IgG1 (PE) and anti-IgE (PE) and assessed by flow cytometry (**Figure 5.19**). Results are from two independent experiments using seven control and seven PI3K C2β–/– mice (IgG1) or six control and six PI3K C2β–/– mice (IgE).

The mean expression of sIgG1 at 86hr post stimulation was 19.1% ± 2.1 on control B-cells and 24% ± 2.31 on PI3K C2β–/– B-cells (p=0.2). sIgE expression was also higher on the PI3K C2β–/– B-cells (7.8% ± 1.2 and 3.7% ± 0. 6, respectively), but the difference was not significant (p=0.1). MFI was also measured (data not shown), with no difference observed in either; IgG1 (p=0.3) or IgE (p=0.7).

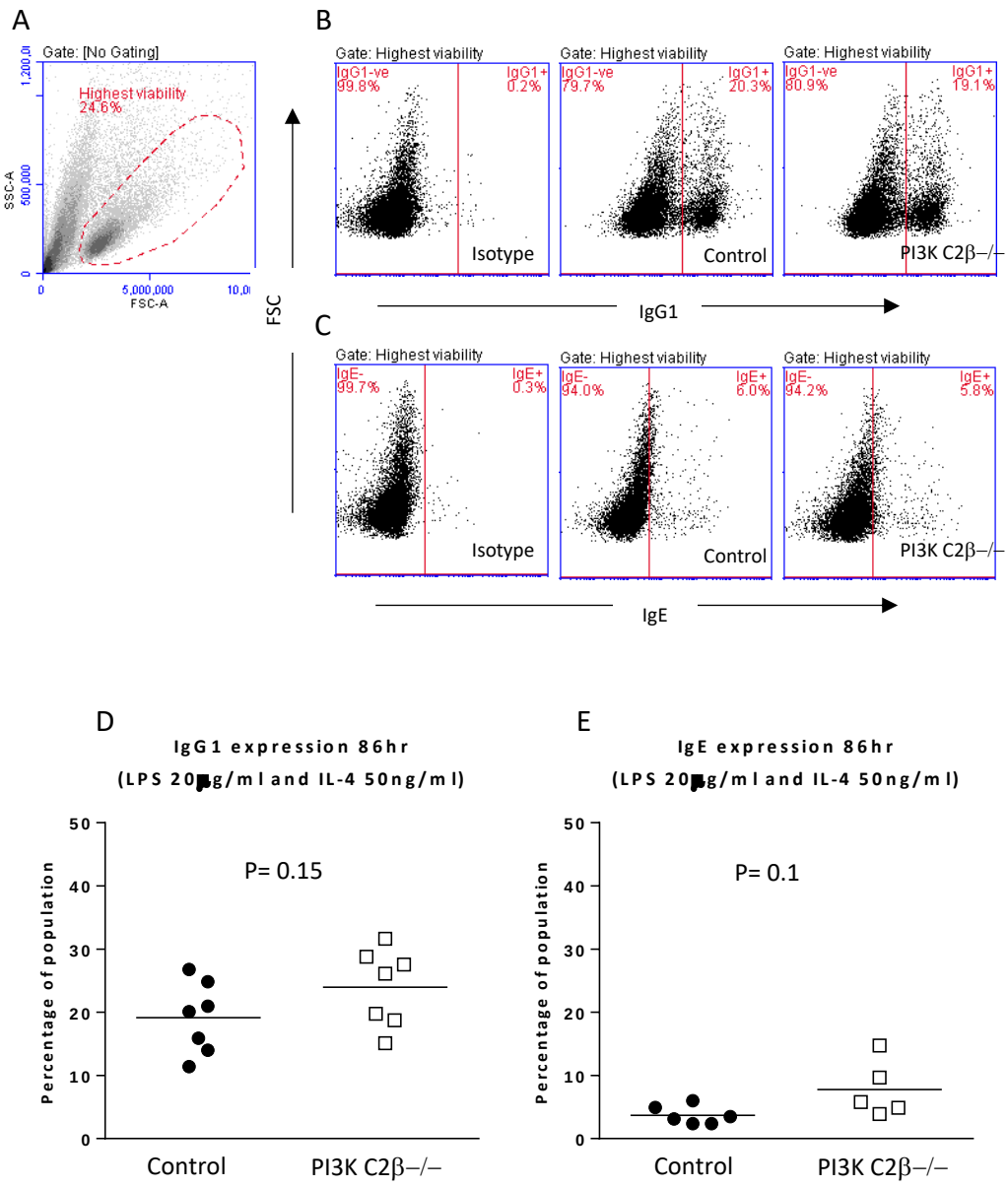

Figure 5.19 IgG1 and IgE expression 86 hr post stimulation with LPS (20µg/ml) and IL-4 (50ng/ml). B-cells were labelled with anti-IgG1 (PE) or anti IgE (PE) and assessed using flow cytometry, with 30,000 events recorded per plot. **A**; a typical plot showing FSC vs SSC at 86hr. Cells analysed fell within the highest viability gate. **B**; plots showing IgG1 labelled B-cells, isotype control (left) and representative plots from control (centre) and PI3K C2β–/– (right) B-cells. **C**; plots showing IgE labelled B-cells, isotype control (left) and representative plots from control (centre) and PI3K C2β–/– (right) B-cells. **D** and **E**; analysis of the results revealed that although PI3K C2β–/– samples had a slightly higher means, for both sIgG1+ and sIgE+ B-cells (24% ± 2.3 and 7.8% ± 2, respectively), compared to the controls (19.1% ± 2.1 and 3.7% ± 0.6) the difference was not statistically significant. Results are from two independent experiments, using seven control and seven PI3K C2β–/– mice (D) or six control and six PI3K C2β–/– mice (E). Statistical significance was calculated using an unpaired, two-tailed Student t-test (D), with Welch's correction applied (E). Data represent mean values ± SEM.

5.21 Sub-optimal conditions: LPS (2μg/ml) and IL-4 (20ng/ml)

Following activation with LPS (2μg/ml) and IL-4 (20ng/ml), B-cells were labelled with anti-IgG1 (PE) and anti-IgE (PE) and assessed by flow cytometry (**Figure 5.20** and **Figure 5.21**). Results are from three independent experiments using nine control and nine PI3K C2β−/− mice (IgG1) or four independent experiments using twelve control and twelve PI3K C2β−/− mice (IgE).

Using sub-optimal doses of LPS and IL-4 (**Appendix 2** and **Appendix 3**), sIgG1 expression was 12.4% ± 2.3 higher on PI3K C2β−/− B-cells than on the controls (25.8% ± 1.4 compared to 13.5% ± 1.8), this difference was considered significant (p=<0.0001). Additionally, the MFI for PI3K C2β−/− sIgG1 was significantly higher (p=0.001), at 3.5 (arbitrary units) compared to 2.9 (mean of three experiments), which represents a mean increase of 17.1%. sIgE expression was also significantly increased on PI3K C2β−/− B-cells (p=0.0002), with 15.5% ± 1.6 being sIgE+, compared to 7.1% ± 0.7. The difference between control and PI3K C2 C2β−/− IgE MFI was not statistically significant (p=0.07) when measured (data not shown). Data represent mean values ± SEM.

The results show that the level of class switching to IgG1 in control B-cells was higher when cultured under optimal conditions. However, this was not the case for PI3K C2β−/− B-cells, which had a slightly higher percentage of sIgG1+ cells following culture in sub-optimal conditions. The percentage of sIgE+ B-cells was significantly higher for both control and PI3K C2β−/− under

sub-optimal conditions, compared to being cultured under optimal conditions.

Surface IgM was also assessed following sub-optimal stimulation (**Figure 5.22**), showing a reduction in the PI3K C2β−/− sIgM+ population compared to the controls (69.8% ± 2.2 compared to 78.9% ± 2.5). This supports the previous data showing increased class switching to sIgE or sIgG1 in the PI3K C2β−/− populations.

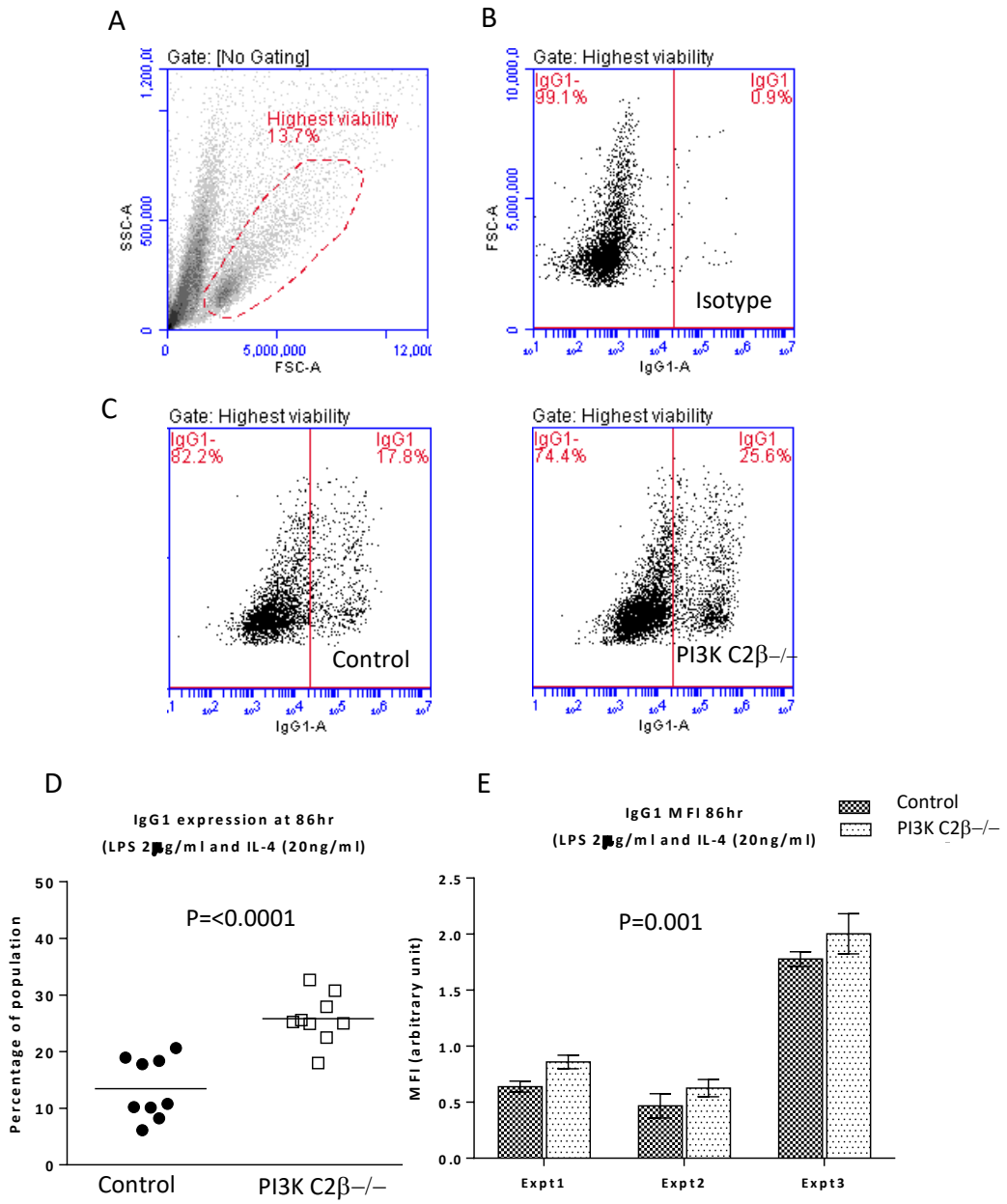

Figure 5.20 sIgG1 expression 86 hr post stimulation with LPS (2µg/ml) and IL-4 (2-ng/ml). B-cells were labelled with anti-IgG1 (PE) and assessed using flow cytometry, with 30,000 events recorded per plot. **A**; a typical plot showing FSC vs SSC at 86 hr. Cells analysed fell within the highest viability gate. **B**; typical staining pattern for the isotype control. **C**; representative plots showing sIgG1+ B-cells from control (left) and PI3K C2β–/– spleens (right). **D**; analysis of the results revealed that the percentage of sIgG1+ B-cells was significantly higher (p=<.0001) in the PI3K C2β–/– samples (25.8% ± 1.4) compared to the controls (13. 5% ± 1.8). **E**; sIgG1+ B-cells from PI3K C2β–/– spleens also had an increased MFI in each experiment, indicating that the level of expression was higher than on the control B-cells (p=0.001). Results are from three independent experiments and statistical significance was calculated using an unpaired, two-tailed student t-test Student t-test (D) and a two-way ANOVA (E). Data represent mean values ± SEM.

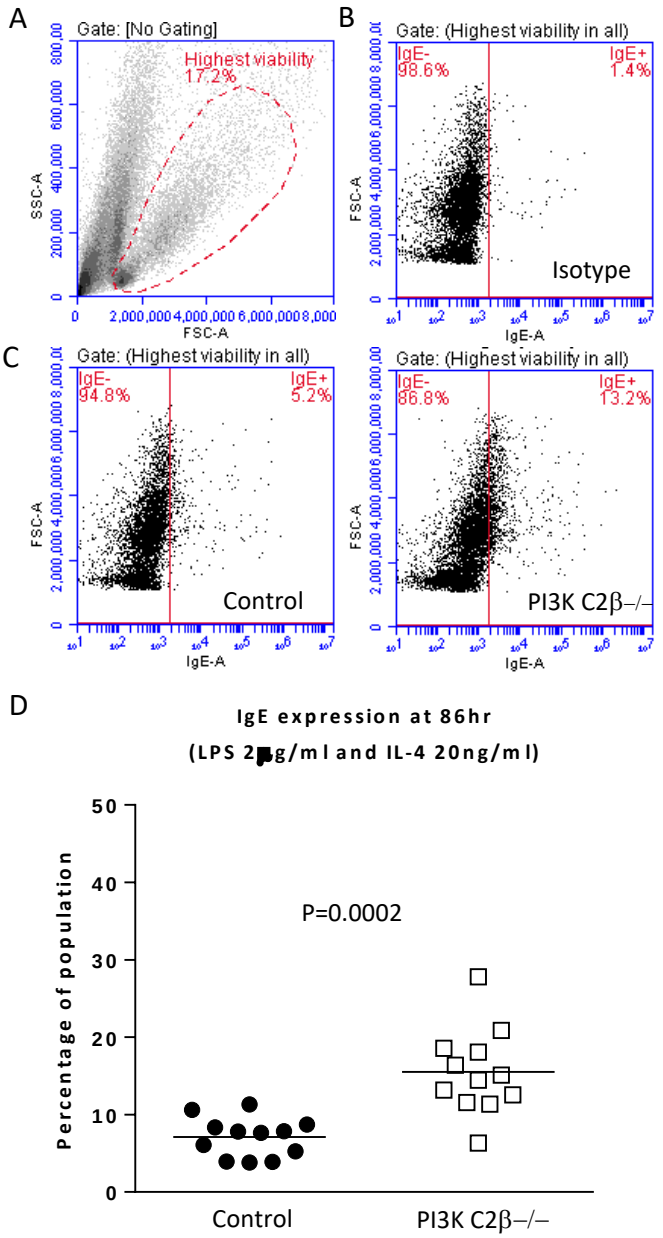

Figure 5.21 sIgE expression 86 hr post stimulation with LPS (2µg/ml) and IL-4 (20ng/ml). B-cells were labelled with anti-IgE (PE) or an isotype control, and assessed using flow cytometry. 30,000 events were recorded per plot. **A**; a typical plot showing FSC vs SSC at 86 hr. Cells analysed fell within the highest viability gate. **B**; typical staining pattern for the isotype control. **C**; representative plots showing sIgE+ B-cells from control (left) and PI3K C2β–/– spleens (right). **D**; analysis of the results revealed that the percentage of sIgE+ B-cells was significantly higher (p=0.0002) in the PI3K C2β–/– samples (15.5% ± 1.6) compared to the controls (7.1% ± 0.7). Results are from four independent experiments and statistical significance was calculated using an unpaired, two-tailed Student t-test, with Welch's correction for unequal variance. Data represent mean values ± SEM.

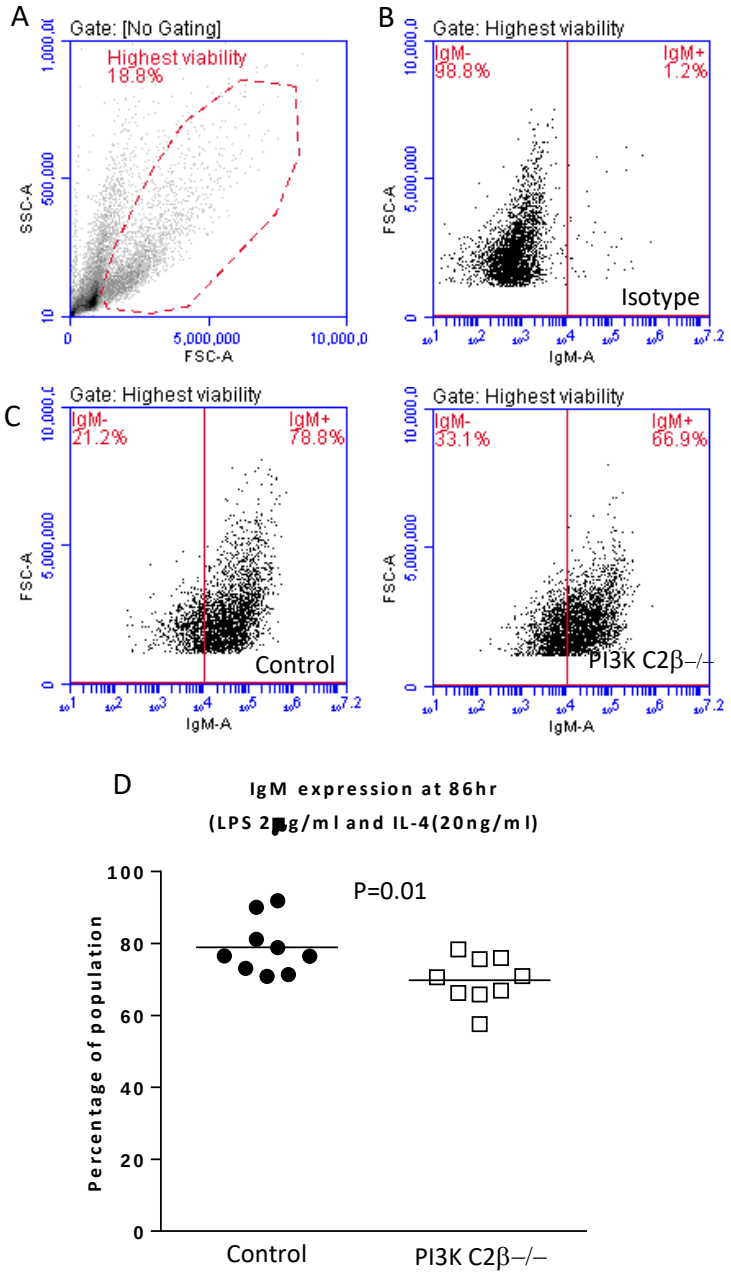

Figure 5.22 sIgM expression 86 hr post stimulation with LPS (2µg/ml) and IL-4 (2-ng/ml). B-cells were labelled with anti-IgM (PE) and assessed using flow cytometry. 30,000 events were recorded per plot. **A**; a typical plot showing FSC vs SSC at 86 hr. Cells analysed fell within the highest viability gate. **B**; shows the typical staining pattern for the isotype control. **C**; representative plots showing sIgM+ B-cells from control (left) and PI3K C2β–/– spleens (right). **D**; analysis of the results revealed that the percentage of sIgM+ B-cells was significantly lower (p=0.01) in the PI3K C2β–/– samples (69.8% ± 2.2) compared to the controls (78.9% ± 2.5). Results are from three independent experiments, using nice control and nine PI3K C2β–/– mice. Statistical significance was calculated using an unpaired, two-tailed Student t-test. Data represent mean values ± SEM.

5.22 Further downregulation of PI3K C2β–/– sCD23+ at 86hr

Having observed a difference in CD23+ populations at 0 hr, cultures were examined following sub-optimal stimulation with LPS (2μg/ml) and IL-4 (20ng/ml) for 86 hr. The reduced surface CD23+ on freshly isolated PI3K C2β–/– B-cells could indicate altered ratios of several B-cell populations, such as immature T1 and/or MZ B-cells, or activated B-cells that have undergone CSR, none of which express surface CD23 (Allman et al., 2001; Best et al., 1995; Lindsley et al., 2009; Loder et al., 1999). Stimulation with IL-4 and LPS has been shown to initially upregulate sCD23 expression on murine B-cells (Paul, 1991), before down regulation. As such, differences in the sCD23 populations following in vitro activation may shed some light on this anomaly. Control and PI3K C2β–/– B-cells were labelled with anti-CD23 and analysed as before. Results were obtained over the course of three experiments using nine control and nine PI3K C2β–/– mice. Following stimulation with sub-optimal concentrations of LPS and IL-4 for 86 hr PI3K C2β–/– B-cells had a reduced sCD23+ population of 33.3% ± 2.6 compared to the control B-cells which had a sCD23+ population of 47.6% ± 2.85, a difference of 14.25% ± 3.89 (p= 0.0014).

Table 5.8 Summary of results for sCD23+ B-cells at 0 hr and 86 hr (percentage of the B-cell population)

	0hrs	**72-86hrs**
Control B-cells	87.8 % ± 0.7	47.6% ± 2.9
PI3K C2β$^{-/-}$ B-cells	57.6 % ± 1.4	33.3% ± 2.6
Difference between means	30.2 ± 1.5	14.3 ± 3.9
Significance	p=< 0.0001	p=0.001

CD23+ B-cells following stimulation with 2μg/ml LPS and 20ng/ml IL-4.Results are from three independent experiments using nine control and nine PI3K C2β–/– mice. Statistical significance was calculated using an unpaired, two-tailed Student t-test. Data represent mean values ± SEM.

Median fluorescent intensity was also measured over the three experiments, for the sCD23+ populations. In each experiment the control B-cells had an increase in sCD23 MFI compared to the PI3K C2β−/− population (**Figure 5.23)**. The difference in MFI for sCD23+ control B-cells and sCD23+ PI3K C2β−/−B-cells was considered significant (p=0.01).

While initial activation causes an up regulation in CD23 surface expression, it is reduced during CSR and lost on plasma cells (Kehry and Yamashita, 1989; Rabin et al., 1992). It is therefore likely that any immediate increase in CD23 expression, following activation, would have been lost by 86hr.

Table 5.9 Summary of median fluorescent intensity for CD23+ B-cells at 86hr

	Experiment 1	**Experiment 2**	**Experiment 3**
MFI (arbitrary unit) Control	5.8	10.4	12.3
MFI (arbitrary unit) PI3 K C2β$^{-/-}$	4.7	5.1	7.4
Difference	1.2	5.3	7.4
Significance	p=0.01		

B-cell were stimulated with 2μg/ml LPS and 20ng/ml IL-4. Each experiment used three control and three PI3K C2β−/− mice. Statistical analysis was performed using a two-way ANOVA.

5.23 PI3K C2β−/− B-cells have increased MEK1/2 phosphorylation

Preliminary analysis of B-cells at 72hr following sub-optimal stimulation with LPS (2μg/ml) and IL-4 (20ng/ml) showed than PI3K C2β−/− B-cells had increased phosphorylation of MEK1/2. Increased MEK activation is associated with both CD19 and activation through toll-like receptors (Li and Carter, 1998; Rui et al., 2006).

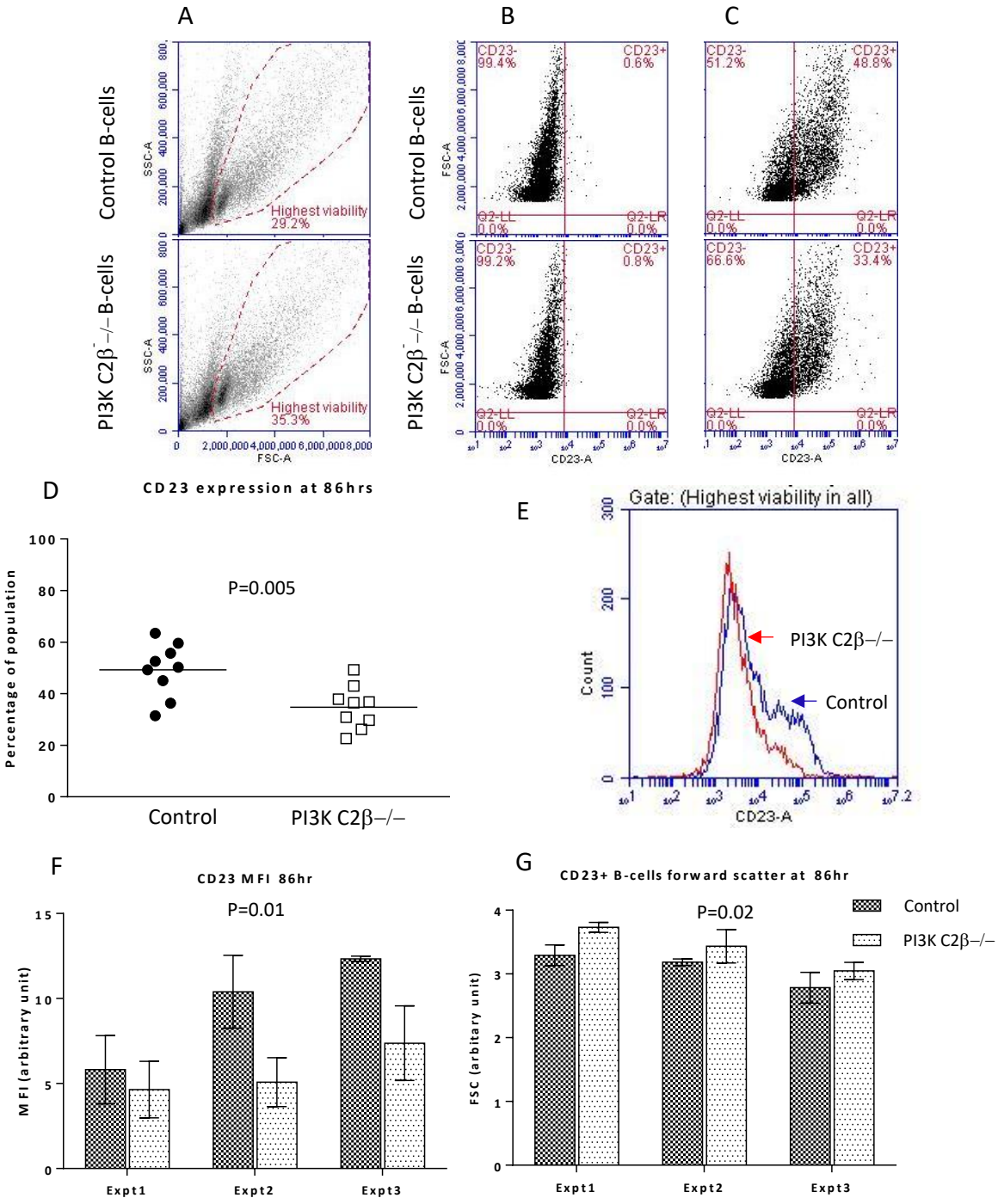

Figure 5.23 sCD23 expression at 86 hr following stimulation with LPS (2μg/ml) and IL-4 (20ng/ml). B-cells were labelled with fluorophore conjugated anti-CD23 and assessed using flow cytometry. 30,000 events were recorded per plot. **A**; representative plots showing the highest viability population that was analysed. **B**; shows the negative isotope control used for gating. **C**; plots showing characteristic positive staining for sCD23. **D**; PI3K C2β−/− mice had fewer sCD23+ B-cells (34.8% ± 2.8) compared to the controls (49.3% ± 3.5) (p=0.001) **E**; a representative histogram showing the difference in fluorescent intensity at 86hrs. **F**; Analysis of MFI showed that there was an increase in the control MFI in each of the three experiments, compared to the PI3K C2β−/− population (p=0.01). **G**; PI3K C2β−/− sCD23+ B cells were also found to have an increased forward scatter compared to the controls (p=0.02). A total of nine control and nine PI3K C2β−/− mice were used over three independent experiments. Statistical analysis was performed using an unpaired, two-tailed Student t-test (D), and two-way ANOVA (F and G). Data represent mean values ± SEM.

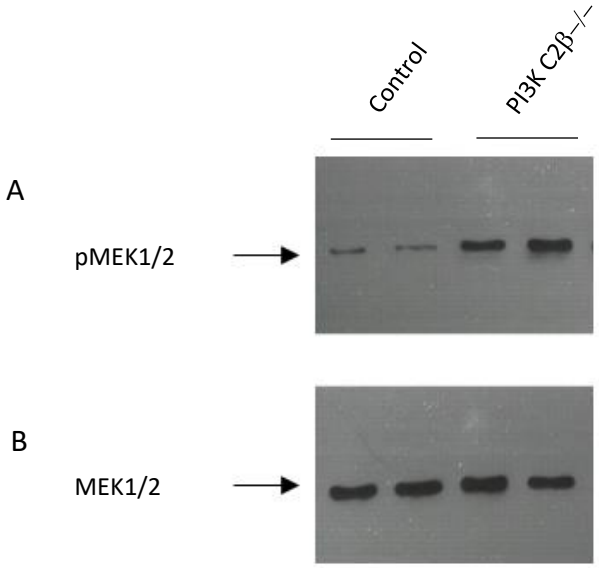

Figure 5.24 MEK1/2 is upregulated in PI3K C2β−/− B-cells. Isolated B-cells were stimulated with LPS 2μg/ml and IL-4 at 20ng/ml. At 72 hr post stimulation B-cells were lysed and following the fractionation of B-cell lysates by SDS PAGE, proteins were immunoblotted and membranes were probed with anti-pMEK1/2 followed by anti-MEK1/2 to assess loading. HRP-conjugated secondary anti-body allowed visualisation of the protein using ECL. **A**; PI3K C2β−/− B-cells had increased phosphorylated MEK1/2 compared to control B-cells at 72 hr post stimulation. **B**; anti-MEK1/2 was used to compare loading. Results are from two control mice and two PI3K C2β−/− mice.

5.24 Discussion

As described in the previous chapter, CD19 expression was increased in freshly isolated PI3K C2β−/− splenocyte cultures compared to cultures from control mice (0 hr). Following stimulation with LPS and IL-4, the CD19+ population was increased as was CD19 MFI, demonstrating its increased cell surface expression.

To investigate this further, splenic B-cells were isolated and examined. Upregulation of CD19 is associated with a reduction in B-cell activation thresholds (Carter and Fearon, 1992; Inaoki et al., 1997), isolated B-cells were stimulated with 'sub-optimal' doses of LPS and IL-4. Data showed that PI3K C2β−/− B-cells had increased viability in comparison to controls. CD19 has been shown to enhance B-cell survival via co-ligation with the BCR ensuring maximum Akt phosphorylation, which leads to the inhibition of pro-apoptotic factors (Otero et al., 2001). This has been shown to be important in propagating the tonic survival signals required for mature B-cells (Otero et al., 2003).

B-cells that lack CD19 expression show diminished activation by LPS, while over expression of CD19 leads to increased activation, even with reduced concentrations of LPS (Engel et al., 1995; Yazawa et al., 2003). LPS has been shown to stimulate B-cells through toll-like receptor 4 (TLR4) in a CD19 dependent manner (Iwata et al., 2009). This would correlate with the increased survival and metabolic activity in the PI3K C2β−/−B-cells.

Following stimulation with a sub optimal dose of LPS and IL-4, isolated PI3K C2β−/− B-cells showed a consistent reduction in propidium iodide (PI) staining compared to the controls. However, Annexin V (AnV) staining was increased suggesting increased apoptosis, but despite being in the early stages of apoptosis PI3K C2β−/− B-cells appeared healthier and had increased metabolic activity. Because AnV externalization in lymphocytes occurs at the very earliest stage of apoptosis, before DNA degradation or induction of cell lysis (Verhoven, 1995), this finding was initially interpreted as being due to a delay in which PI3K C2β−/− B-cells shift from early to late apoptosis. However, it has been shown that phosphatidylserine (PS) is externalized on viable B-cells following BCR activation, and is involved in membrane remodelling by co-capping with IgM and CD19 to ensure signalling molecules are correctly positioned (Dillon et al., 2000). A further study confirmed that PS externalization on viable splenic B-cells was dependent on their activation state, and was also associated with continuous tolerogenic signals received via the BCR (Dillon et al., 2001). These findings might indicate that PI3K C2β−/− B-cells were not in the early stages of apoptosis as initially thought, but were in a heightened activation state.

The increased CD19 expression on PI3K C2β−/− B-cells may lower the activation threshold. As such, the sub-optimal treatment with LPS/IL-4 could provide adequate stimulation, which resulted in the increased survival and metabolic activity observed. Analysis of the cell cycle correlates with these

findings, showing an increase in the G1 and a reduction in the sub-G1 populations within the PI3K C2β–/– samples over time, compared to the controls. Cells within the G1 (growth) phase of the cell cycle have been shown to have increased metabolic activity (Doughty et al., 2006), as they either prepare for the transition into S-phase thereby committing to cell division, or, carry on their effector functions as non-dividing cells. The reduced PI3K C2β–/– population within the sub G0/G1 gate suggests that there was a lower percentage of PI3K C2β–/– B-cells that were either in late apoptosis or dead, as the reduced PI signal in the sub-G0/G1 gate is likely to be as a result of fragmenting DNA. Despite the increased amount of germinal centre associated proliferation in unimmunized mice, there was no difference between the percentage of control and PI3K C2β–/– B-cells undergoing DNA synthesis or mitosis. This could be due to any increase in the G2/M phase being diluted within the total B-cell population. Mouse germinal centre B-cells have poor viability during and following isolation, with cell death often occurring within 4 hr of isolation (Cato et al., 2011), it is therefore possible that if there were any differences in G2/M they may not be observed. However, finding comparable populations of B-cells within G2/M is compatible with the lack of obvious health issues displayed by the PI3K C2β–/– mice. Disruption in the cell cycle, such as an increase in proliferation would be expected to result in a pathological phenotype (Klein and Dalla-favera, 2008; Vinuesa et al., 2009), which has not been observed in unchallenged PI3K C2β–/– mice.

In addition to identifying the stage of B-cell differentiation, the BCR isotype can help to identify potential immune dysregulation. For example, the failure of sIgM+ B-cells to switch to IgG1 following an immune challenge and elevated serum sIgM is indicative of hyper IgM syndrome, which are a group of immune deficiency disorders (Etzioni and Ochs, 2004), while elevated IgE is associated with allergy and inflammation (Galli and Tsai, 2012). There were modest differences in surface BCR isotype between PI3K C2β−/− and control B-cells at 0hr. Although the difference was significant, the differences are likely to represent a variation in the stage of B-cell differentiation following CSR. The most notable difference was the decrease in the sIgM+ population and reduced expression in the PI3K C2β−/− B-cells compared to the controls. There was also an increased sIgG1 MFI associated with the PI3K C2β−/− B-cells which might indicate that as sIgM was being downregulated, sIgG1 was being upregulated as a result of increased class switching activity. Alternatively, a $sIgM^{low}$ phenotype is a characteristic of B-cell anergy (Browne et al., 2009). Interestingly, in a study using a transgenic mouse model with functionally anergic B-cells, anergy was overcome by increased expression of CD19. Furthermore, without an additional immune challenge these B-cells did not produce autoantibodies, however treatment with complete Freund's adjuvant (CFA) led to hyper-responsiveness and eventual autoantibody production (Inaoki et al. 1997). This might suggest that upregulation of CD19 creates a predisposition for autoantibody production but is not the direct cause.

Further analysis of the sIgM+ populations revealed a distinct sIgM expression pattern in the PI3K C2β−/− population. In addition to B-cell anergy, an sIgM^{low} phenotype is observed in a subset of immature B-cells that have been developmentally arrested, they are known as transitional type 3 (T3) and represent a potentially autoreactive population (Cambier et al., 2007; Merrell et al., 2006). The T3 population is sIgM^{low} and express surface CD23 (sCD23) (Allman et al., 2001; Yarkoni et al., 2010). Anergic B-cells are typically CD19^{low} (Liubchenko et al., 2012), which does not correspond to the PI3K C2β−/− B-cells which are CD19^{hi}. This was confirmed by double staining with CD19/CD23, which showed the sCD23- population within the PI3K C2β−/− B-cells had increased CD19 expression compared to controls. An alternative explanation is that the PI3K C2β−/− sIgM^{low} B-cells could represent a population that were undergoing class switch recombination (CSR). Interestingly, a small population of CD19^{hi}/sCD23^{low} B-cells has been described that spontaneously produce IgG and IgA antibodies in unimmunized mice, which are thought to be activated by interaction with microbes that are part of the normal flora, such as intestinal bacteria. These cells also produced higher forward scatter readings than follicular B-cells, which has been attributed to an activated state (de Andres et al., 2007). Examination of BCR isotype at 0hr had shown that PI3K C2β−/− B-cells had a modest increase of sIgG1+, compared to the controls, and had shown an increased population that appeared to be in the process of upregulating sIgG1.

In order to assess CSR further, B-cells from the spleens of PI3K C2β–/– and control mice were cultured under 'optimal' conditions or 'sub-optimal' conditions. The use of a sub-optimal concentrations of LPS and IL-4 was to examine whether PI3K C2β–/– B-cells exhibited a reduction in activation threshold, that is associated with increased CD19 expression (Inaoki et al. 1997; Carter & Fearon 1992). Under optimal conditions there was a slight increase in the mean percentage of sIgG1+ B-cells in the PI3K C2β–/– populations, compared to the controls, but it was not statistically significant. A similar outcome was observed in the sIgE+ populations. However, following sub-optimal stimulation the PI3K C2β–/– cultures had a significantly higher proportion of both sIgG1+ and sIgE+ isotype switched B-cells compared to the controls after 86 hr in culture. PI3K C2β–/– B-cells appeared unaffected by the reduced LPS and IL-4 concentrations, whereas the percentage of control B-cells that had switched to sIgG1+ was reduced. Data produced at 86 hr also showed a reduction in sIgM and sCD23 populations within the PI3K C2β–/– B-cells compared to controls, which is supportive of the CSR results (Rabin et al., 1992). The finding that PI3K C2β–/– B-cells had undergone increased CSR, compared to the control B-cells when subjected to sub-optimal stimulation is in keeping with a reduction in activation threshold that is associated with CD19 upregulation. PI3K C2β–/– B-cells also had a consistent reduction in their total sCD23+ population. The two main B-cell subsets in the spleen that are sCD23 negative (sCD23-) are, marginal zone (MZ) B-cells and immature transitional stage 1 (T1) B-cells, both of which are also $sIgM^{hi}$ (Best et al., 1995; Loder et

al., 1999). Dual staining with fluorophore conjugated antibodies to CD23/IgM revealed more than a two-fold increase in the PI3K C2β–/– population of sIgM^{hi}/sCD23- B-cells. Immature T1 B-cells are new arrivals from the bone marrow and as such are associated with low forward scatter (FSC) (Sims et al., 2005), whereas MZ B-cells have a high FSC (Arnon et al., 2013). An increased FSC was seen in the PI3K C2β–/– sIgM^{hi}/CD23-B-cells which were also CD19^{hi}. As CD19 expression is higher on mature B-cells compared to immature cells, this would suggest that the increased sIgM^{hi}/sCD23- population was more likely to be MZ B-cells rather than immature T1 B-cells. However, it is not possible to confirm definitively that this population were MZ B-cells, without the use of further markers, the control population fits well with the literature which suggests MZ B-cells are approximately five to ten percent of the murine splenic B-cell population (Carsetti, 2004; Loder et al., 1999).

As a subtype, MZ B-cells have been described as potent activators of CD4 T-cells, and have been shown to shuttle back and forth between the marginal zone and the follicles to present antigen to CD4 T-cells (Arnon et al., 2013; Attanavanich and Kearney, 2004a; Cinamon et al., 2007). This would also fit well with the PI3K C2β–/– mice who had an increased CD4+ population that was observed at 0 hr and also within total splenocyte cultures, which was not observed in the isolated T-cell cultures, seen in the previous chapter. Although typically thought of as a source of 'natural' IgM, MZ B-cells have been shown to undergo CSR in response to T-cell independent (TI)

interaction with antigen (Puga et al., 2011), which occurs independently of CD40/CD40L (Cerutti, 2008; Kim et al., 2011). It has been demonstrated that autoreactive immature B-cells have reduced activated ERK compared to non-autoreactive B-cells, and that the level of basal ERK activation is proportional to the sIgM expression. Additionally, inhibition of MEK leads to a reduction in cell differentiation (Teodorovic et al., 2014).

6 Conclusion

6.1 Summary of results

Data generated during this project support previous reports that PI3K C2β–/– mice do not display an overt phenotype (Alliouachene et al., 2015; Harada et al., 2005). However, my results suggest that PI3K C2β–/– mice appear to have increased fecundity and produce offspring with a skewed sex ratio, which has not been previously reported.

The increased splenic germinal centre reactions observed under basal conditions, which were exacerbated following IgG/CFA treatment, suggest that PI3K C2β–/– mice display a more pronounced immune response compared to the control mice. Examination of lymphocyte populations in the spleen revealed that PI3K C2β–/– mice had an increased CD4+ T-cell population, which was maintained over time in splenocyte cultures. However when cultured in isolation, there was no difference in the CD4+/CD8+ ratio, compared to the controls. This finding could indicate that an alternative cell type might be maintaining the CD4+ population observed in the total splenocyte cultures.

Analysis of splenic B-cell populations revealed that, versus control B-cells, the B-cell co-receptor CD19 was consistently upregulated on PI3K C2β–/– B-cells. Cell cycle analysis indicated that while the percentage of B-cells undergoing mitosis was comparable, the PI3K C2β–/– B-cells had an increased population of live cells which were more metabolically active after

72 hr in culture. To address whether the PI3K C2β–/– B-cells had a reduced activation threshold, consistent with increased CD19 expression (Carter and Fearon, 1992; Inaoki et al., 1997), class switched populations were examined. These results showed that freshly isolated B-cells from PI3K C2β–/– mice had a slightly increased population of IgG+ and IgE+ B-cells compared to the controls. Additionally, CSR was increased in PI3K C2β–/– B-cells that were cultured with sub-optimal doses of IL-4 and LPS.

Following analysis of B-cell expression profiles, PI3K C2β–/– mice appeared to have an increased MZ population, with increased CD19 expression. This could provide a potential explanation for the increased CD4+ T-cell populations in PI3K C2β–/– spleens, as MZ B-cells are known to be efficient activators of CD4+ T-cells (Attanavanich and Kearney, 2004b). In addition, preliminary investigation of MEK1/2 activation indicated that it was increased in PI3K C2β–/– splenocytes, which is in keeping with upregulated CD19 (Li and Carter, 1998; Li and Carter, 2000).

6.2 Breeding data

The overview of PI3K C2β–/– mice showed that in matched breeding cages over the same period of time, mice lacking PI3K C2β successfully weaned 36% more offspring than the control mice. In addition, a bias towards female offspring was recorded. It should be noted that the PI3K C2β–/– mice used in this project were originally generated elsewhere and were rederived in our lab, in the original study it was reported that PI3K C2β–/– mice were born at a normal Mendelian ratio (Harada et al., 2005).

More recently a kinase dead, knockin mouse was generated, in which a point mutation resulted in a structurally intact protein that lacked kinase activity. This strategy allowed for kinase activity to be studied independently of structural interactions. This study also reported no differences in fertility and that offspring were produced at a normal Mendelian ratio (Alliouachene et al., 2015).

Housing conditions are known to affect fecundity in lab mice and the use of mating trios and carefully timed matings are strategies used to increase the number of pups born as well as producing mice that are precisely age matched (Stiles et al., 2013). As such, the breeding data reported for this project was taken from matched cages and analysed retrospectively. It is thought to be unlikely that differences in environmental factors such as the housing conditions or diet would cause differences in the number of offspring weaned or a skewed sex ratio.

It has been proposed that sex bias occurs as a form of natural selection, whereby paternal and maternal condition influence whether male or female offspring are produced. This hypothesis is based on the assumption that a male in good condition will produce more offspring than a female in good condition. However, a male in poor condition will produce fewer offspring than a female in the same condition (Trivers and Willard, 1973). It is suggested that this is because dominant males, which are typically strong and in good condition will have more opportunity to sire offspring. The condition of the female is less influential because of the competition

between dominant males to inseminate females. As such, if a healthy, strong female mates with a healthy, strong male their offspring are more likely to be in good condition. If they produce a male, he is likely to have the opportunity to produce more offspring than a female. If, on the other hand, the offspring is likely to be in poor condition, a male may not have any opportunity to produce offspring, while a female would. Therefore producing female offspring would be advantageous.

While the Trivers-Willard hypothesis is still relevant, it is often used to describe animals with small brood sizes and for those breeding in their natural habitat. It is therefore difficult to determine whether it is applicable for inbred laboratory animals which are being kept in a carefully managed environment. A study in 2003 using outbred mice found that mothers on a very high fat diet were more likely to have male offspring. This was reversed for mothers on a very low fat diet, who produced more females, suggesting that diet is a contributing factor rather than just maternal condition. While changes in diet appear to result in a sex bias, no difference in litter size or fecundity was reported (Rosenfeld et al., 2003). More recently, a study showed that anogenital distance, in addition, to maternal condition influenced gender bias in the house mouse (Mus musculus). The study found that females with a greater anogenital distance produced more male offspring. They also showed a correlation between female weight and anogenital distance in pre-pubertal mice, with a lower bodyweight being

associated with a smaller anogenital distance, although this was not observed in adult mice (Szenczi et al., 2013).

The data collected from control mice and PI3K C2β−/− mice during this project did not include anogenital distance, but female PI3K C2β−/− mice weighed slightly less than their control counterparts over time, despite being fed the same diet.

In 2008, Cameron and colleagues reported that changes in blood glucose levels resulted in skewing of the sex ratio in NMRI mice. They found that females drinking dexamethasone treated water, which reduces plasma glucose concentrations, produced more female pups in comparison to the controls (Cameron et al., 2008). This finding is of particular interest because the loss of PI3K C2β kinase activity in mice has been recently shown to increase insulin sensitivity and glucose metabolism, resulting in reduced blood glucose in comparison to controls (Alliouachene et al., 2015). Although this might be a potential mechanism to explain the skewed sex ratio, the study reported that offspring were born at the expected Mendelian ratio. However, neither of the publications provide any further information regarding the breeding data, so it is not known how many mice were assessed, how soon after birth they were sexed or how many survived weaning. My own data is unlikely to provide a complete picture either because of the way that breeding cages are typically managed. For example, it would be unusual for the cessation of breeding to occur naturally, as breeding cages are usually disbanded when mice each reach a certain age

or are deemed to be no longer optimally fertile. Therefore, although this might be of interest, particularly with regard to loss of PI3K C2β and the effect on blood glucose levels, without performing a more dedicated study it is difficult to draw any conclusions from the breeding data.

6.3 Alternative explanations and potential limitations

In keeping with previous results from our lab, PI3K C2β–/– spleens during this project consistently had an increased population of CD4+ T-cells compared to the control mice, which were maintained when cultured within a total splenocyte population. However, no difference in the size of the CD4+ population was observed in isolated T-cells, suggesting that they may not be driving the immune response. When analysed, isolated B-cells appeared to have a lower activation threshold, survived for longer and displayed a more activated phenotype compared to the control B-cells. This could provide a mechanism to explain the previously described T-cell infiltration and the increased CD4+ population (Balakrishnan, 2012). This is supported by the increased marginal zone B-cell population, which are known to effectively activate CD4+ T-cells (Attanavanich and Kearney, 2004b). However, in addition to mediating a range of effector functions, B-cells are also regulated by a range of chemokines, cytokines and cell to cell interactions within the microenvironment (Vazquez et al., 2015). A further complication is that the role of PI3K C2β–/– appears to either be cell specific or dependent on its method of activation (**Table 1.1**).

6.4 Calcium signalling

Murine lymphocytes express two K+ channels, the voltage gated Kv1.3 channel and the Ca^{2+} activated KCa3.1 channel. Their role is to regulate membrane potential, which controls the influx of Ca^{2+} required to activate signalling pathways. Expression levels are subset specific and vary depending on the activation state and stage of differentiation (Wulff et al., 2004). One of the confounding aspects of this project is the role that had been previously identified for PI3K C2β in KCa3.1 dependent calcium influx, and it was anticipated that loss of PI3K C2β may lead to lymphocyte suppression. However, PI3K C2β−/− B-cells appeared to have a more activated phenotype, which was not in keeping with the loss of PI3K C2β recorded in T-cells (Srivastava et al., 2009) .

Previous examination of K+ channel expression during B-cell differentiation indicates that class switched memory B-cells upregulate Kv1.3 expression following activation, while KCa3.1 expression remain unchanged. Additionally increased expression of Kv1.3 was observed on marginal zone B-cells (Wulff et al., 2004), suggesting that these B-cell subsets are less reliant on KCa3.1. Interestingly, KCa3.1 dysregulation has been observed in chronic lymphocytic leukaemia (CLL), which affects B-cells, and as such KCa3.1 has been identified as a potential therapeutic target (Grössinger et al., 2014). However, gene analysis has indicated that CLL cells do not express PI3K C2β (McCarthy et al., 2015), which might indicate that under certain

conditions KCa3.1 activation may not be solely dependent on PI3K C2β in B-cells.

Work performed using human CD4+ T-cells and KCa3.1 transfected Jurkat cells showed that silencing of PI3K C2β led to a reduction in KCa3.1 mediated Ca2+ influx following T-cell receptor activation (Srivastava et al., 2009). T-cells from KCa3.1−/− mice show reduced T-cell receptor mediated activation and cytokine production due to reduced Ca2+ influx. However, while Th1 and Th2 T-cells were effected, the Th17 and Treg subsets were not (Di et al., 2010). The role of KCa3.1 signalling appears to be more complex in vivo, as global knockout mice have been shown not to display an obvious phenotype. Although they are reported as having slight abnormalities in cell volume, which includes T-cells, and develop progressive splenomegaly as they age (Heike Wulff and Neil A. Castle, 2010).

6.5 Global knockout of PI3K C2β

The use of global knockout mice in this project allowed a potentially altered immune response in PI3K C2β−/− mice to be identified, which may not have been possible using a more refined targeted knockout strategy. This is due to differences between the strains being very subtle and, to date, no clear phenotypic changes have been described (Alliouachene et al., 2015; Harada et al., 2005). Therefore without a preconceived model to work from, targeting individual genes could be extremely time consuming, financially prohibitive and may not be in keeping with NC3Rs. Even considering the previous work that this project was based on, in which renal damage with

T-cell infiltration was reported (Balakrishnan, 2012), if CD4+ T-cells had been targeted for PI3K C2β knockdown, the observed renal pathology may not have developed. Such damage may have been prevented by reduced T-cell receptor associated differentiation and impaired Ca^{2+} signalling in specific T-cell subsets following the loss of PI3K C2β−/− (Cai et al., 2011; Srivastava et al., 2009). The drawback of a global knockout is that to delineate the results may not be possible, especially when studying the complex interactions within the immune system. Therefore, although this project focuses on a heightened activation state of PI3K C2β−/− splenic B-cells, it is not possible to identify if this difference originates in PI3K C2β−/− B-cells or is potentially driven by another cell type. For example, mast cells have recently be described as potent activators of B-cells, not only promoting their differentiation into $CD19^{high}$ blasts, but also into antigen presenting cells with upregulated MHCII and CD86 expression (Palm et al., 2016a). An additional drawback of a global knockout is that it is not possible to differentiate between the kinase activity mediated by PI3K C2β or a potential structural role it may have. This could be addressed by using a similar knock-in strategy as described by Alliouachene and colleagues (2015), who have generated a mouse model in which PI3K C2β is structurally intact but lacks kinase activity.

6.6 Potential role of PI3K C2β in B-cells

Data generated during this project suggest that loss of PI3K C2β results in splenic B-cells having a heightened activation state. However, a pathological

outcome only becomes apparent following an immune insult (Balakrishnan, 2012). The potential for these B-cells to mediate an inappropriate response may be due to the increased expression of the B-cell co-receptor CD19, and the observed increase in phosphorylated MEK1/2 at 72 hr is supportive of an increased activation state. Taken together this might suggest that in B-cells PI3K C2β plays a role in a negative regulatory pathway.

It has been shown that PI3K C2β binds with nucleotide free Ras, potentially mediating negative regulation of the Ras, Raf, MEK, ERK pathway (Wong et al., 2012b). Recently, targeting MEK1/2 in CLL B-cells has been shown to cause apoptosis by inhibiting ERK1/2 and AKT activity, and has been proposed as a potential therapeutic strategy for CLL (Crassini et al., 2015). As gene analysis has revealed that while PI3K C2β is moderately expressed in normal B-cells, expression is lost from B-cells of patients with chronic lymphocytic leukaemia (CLL) (McCarthy et al., 2015), this might add support to the notion PI3K C2β is involved in negatively regulating B-cell responses.

The role of PI3K C2β has typically been found to be one of positive regulation (Balzarotti et al., 2015; Cai et al., 2011; Chikh et al., 2016; Domin et al., 2005; He et al., 2015; Srivastava et al., 2009). However, it has been reported that the C2 domain within the C-terminus of PI3K C2β can negatively regulate catalytic activity by competitively binding substrate (Arcaro et al., 1998). Of particular interest, with regards to this project is the previously mentioned discovery that PI3K C2β may be involved in negatively regulating Ras (Wong et al., 2012b).

Additionally, the increased expression of CD19 is likely to play a role in the reduced activation threshold that was observed in vitro (Inaoki et al., 1997; Tedder et al., 1997). The increased CD19 expression on PI3K C2β$^{-/-}$ B-cells may be a result of defective receptor internalization. Following activation, internalization of CD19 has been shown to be clathrin dependent (Ingle et al., 2008) which could potentially be impaired by the loss of PI3K C2β. PI3K C2β has been shown to bind to clathrin and is potentially involved in clathrin coated vesicle transport (Wheeler and Domin, 2006) and loss of PI3K C2β has also been shown to result in defective receptor trafficking (Alliouachene et al., 2015). As receptor internalization in B-cells may result in the inactivation of receptor signalling (Stoddart et al., 2005), this could present a potential explanation for the increased CD19 expression and MEK1/2 phosphorylation. However, this is complicated by the recruitment of CD19 to the BCR following activation, as the BCR is not dependent on clathrin mediated endocytosis (Song et al., 2013).

PI3K C2β has been shown to associate with GRB2 (Błajecka et al., 2012; Wheeler and Domin, 2001), which is known to bind to the inhibitory signalling molecule CD22 (Jang et al., 2011) (**Section 1.6.4**). The exact function of the CD22/GRB2 interaction is not clear at present, although GRB2$^{-/-}$ B-cells have been shown to be hyper-responsive and CD22 phosphorylation in GRB2$^{-/-}$ B-cells is reduced (Ackermann et al., 2011; Jang et al., 2011). Using PathwayNet, which is an integrated strategy designed to predict functional associations, co-complexes, transcriptional regulation

and post translational regulation between human genes and protein products, PI3K C2β is predicted to form a functional association with CD22 with 0.84 confidence, and the functional association with GRB2 is predicted at 0.94 confidence (**Appendix 10**). As such, this could potentially provide a mechanism by which PI3K C2β functions in negatively regulating B-cell activation (**Figure 6.1**). This model suggests two potential roles for PI3K C2β, the first being that it negatively regulates Ras by competitively binding to it in its nucleotide free form, which prevents GTP binding and activation (Wong et al., 2012b). In this case loss of PI3K C2β could lead to increased Ras activation, which in turn would increase MEK1/2 phosphorylation. The second mechanism involves the inferred functional association between CD22, GRB2 and PI3K C2β. Loss of GRB2 has been shown to reduce CD22 phosphorylation. CD22 negatively regulates SYK which is required for activation of the effector BLNK (B-cell linker), also known as SLP65. BLNK has been shown to act as a platform for several signalling molecules that act downstream of the B-cell receptor (Baba et al., 2001). While GRB2 is associated with positive regulation in T-cells, including reduced calcium mobilization (Jang et al., 2010), it appears to play a role in negative regulation in B-cells (Ackermann et al., 2011; Jang et al., 2011). In addition the CD22 / GRB2 complex has been identified as being a negative regulator of calcium signalling in B-cells (Chen et al., 2016).

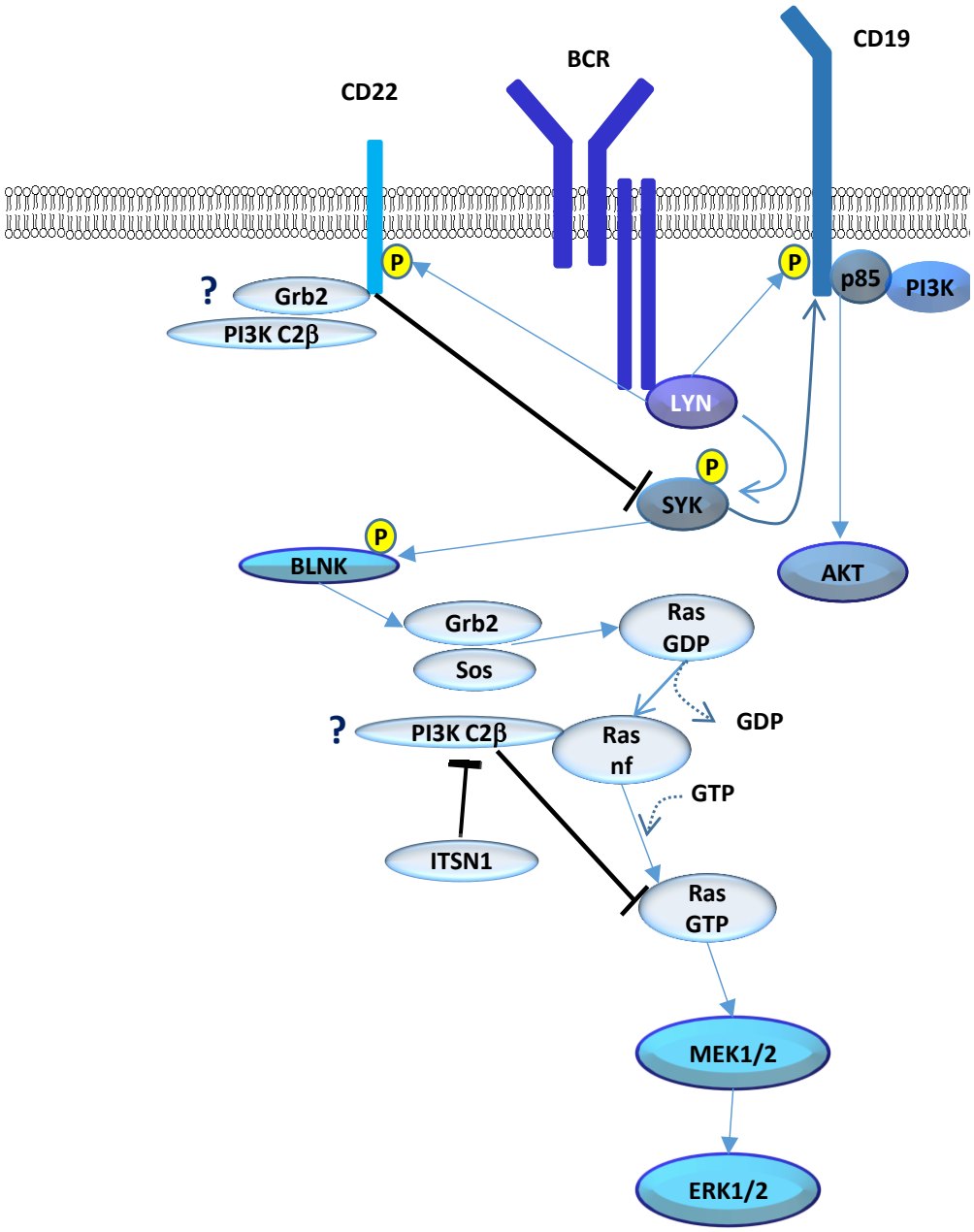

Figure 6.1. Schematic showing two mechanisms whereby PI3K C2β could play a role in inhibitory signalling in B-cells. The first mechanism involves the binding of PI3K C2β to Ras in its nucleotide free (nf) state. This prevents GTP binding, keeping Ras inactivated. The association of ITSN1 to PI3K C2β causes nucleotide free Ras to disassociate, allowing GTP to bind which causes Ras activation (Wong et al., 2012b). The second mechanism is based on software designed to predict functional associations, co-complexes, transcriptional regulation and post translational regulation between genes and protein products. PI3K C2β is predicted to form a functional association with the negative regulatory molecule CD22, and a functional association with GRB2 has already been established (Błajecka et al., 2012; Wheeler and Domin, 2001). GRB2 is known to bind to CD22 (Jang et al., 2011) and although exact function of the CD22/GRB2 interaction is not clear at present, GRB2$^{-/-}$ B-cells have been shown to be hyper-responsive and CD22 phosphorylation in GRB2$^{-/-}$ B-cells is reduced (Ackermann et al., 2011; Jang et al., 2011). If PI3K C2β were involved in optimizing the GRB2/CD22 interaction, the loss of PI3K C2β may lead to a reduction in negative regulation and increased MEK1/2 phosphorylation.

6.7 Future directions

There are several key experiments that are missing from this project that would pull together the results and provide a clearer picture regarding the role of PI3K C2β within the splenic environment. Firstly, analysis of the cytokines produced by PI3K C2β−/− splenocytes would provide more detailed information regarding the role of the different cell types within the environment. For example, stromal cells within the spleen play a role in the cytokine and chemokine production that influence immune cell behaviour (den Haan et al., 2012). Additionally, innate lymphoid cells within the spleen are important mediators of T-cell independent marginal zone B-cell activation (Magri et al., 2014) and mast cells have been shown to promote B-cell differentiation (Palm et al., 2016b). Cytokine arrays are available as a membrane based sandwich assay or a 96 well multiplex ELISA and are designed to detect and quantify a range of cytokines and chemokines. Further activation assays would confirm the preliminary finding that phosphorylated MEK1/2 may be upregulated in PI3K C2β−/− B-cells. Downstream expression of phosphorylated AKT should also be examined, as if PI3K C2β plays an inhibitory role in MEK1/2 signalling, pAKT may be affected (Crassini et al., 2015; Otipoby et al., 2008).

Immunoprecipitation assays may provide missing information regarding the possible functional interactions or co-complexes formed by PI3K C2β in control B-cells. In particular GRB2 and CD22 may be of particular interest

due to the inferred functional association (**Figure 6.1**) and the potential role in negative regulation.

It may also be beneficial to perform a more comprehensive multi-parameter flow cytometric analysis, which may identify whether specific B-cell subsets are affected by the loss of PI3K C2β. This might have an ongoing relevance with regard to the loss of PI3K C2β in CLL cells (McCarthy et al., 2015). This could be undertaken using combinations of the markers listed in **Tables 6.1** and **6.2** below.

Table 6.1 B-cell subset markers

B1a	B1b	MZ	Fo	Breg
CD5+	CD5-	CD5-	CD5-	CD5+
$CD19^{hi}$	$CD19^{hi}$	$CD19^{mid}$	$CD19^{mid}$	$CD19^{hi}$
CD1d	$CD1d^{mid}$	$CD1d^{hi}$	$CD1d^{mid}$	$CD1d^{hi}$
CD23-	CD23-	CD23-	CD23+	CD23+/-
CD43+	CD43+	CD43-	CD43-	CD43-
IgM^{hi}	IgM^{hi}	IgM^{hi}	IgM^{low}	IgM^{hi}
IgD^{low}	IgD^{low}	IgD^{low}	IgD^{hi}	IgD^{mid}

MZ; marginal zone, Fo; follicular (Baumgarth, 2011)

Table 6.2 B-cell differentiation markers

Mature Activated	Plasma blast	Plasma cell	Memory	CS Memory
CD21+	$CD27^{hi}$	$CD27^{hi}$	CD27+	CD27+
CD19+	CD19+	CD19-	CD19+	CD19+
IgM+	IgM-	Ig+	IgM+	IgM-
IgD+	CD20-	CD20+	IgD^{low}	IgD-
CD38+	$CD38^{hi}$	$CD38^{hi}$	CD38-	CD38-
	$CD28^{hi}$			

CS; class switched. (Edwards and Cambridge, 2006; Park et al., 2008)

6.8 Concluding comments

Despite ongoing investigation, the biological role of the PI3K C2β isoform remains poorly understood. The data presented in this thesis indicate that PI3K C2β may play an inhibitory role in the murine immune system, and this may be mediated by B-cells. Given the complexity of immune system regulation, which involves a variety of cell types and a spectrum of cytokines and chemokines, a robust interpretation of my data is difficult. Therefore, although the context in which these experiments were conducted offer the potential for future therapeutic intervention using PI3K C2β as a drug target, many questions remain unanswered.

Bibliography

Acharya, M., Borland, G., Edkins, A. L., Maclellan, L. M., Matheson, J., Ozanne, B. W. and Cushley, W. (2010). CD23/FcεRII: molecular multi-tasking. *Clin. Exp. Immunol.* **162**, 12–23.

Ackermann, J. A., Radtke, D., Maurberger, A., Winkler, T. H. and Nitschke, L. (2011). Grb2 regulates B-cell maturation, B-cell memory responses and inhibits B-cell Ca2+ signalling. *EMBO J.* **30**, 1621–33.

Adachi, Y., Onodera, T., Yamada, Y., Daio, R., Tsuiji, M., Inoue, T., Kobayashi, K., Kurosaki, T., Ato, M. and Takahashi, Y. (2015). Distinct germinal center selection at local sites shapes memory B cell response to viral escape. *J. Exp. Med.* **212**, 1709–1723.

Allen, C. D. C., Ansel, K. M., Low, C., Lesley, R., Tamamura, H., Fujii, N. and Cyster, J. G. (2004). Germinal center dark and light zone organization is mediated by CXCR4 and CXCR5. *Nat. Immunol.* **5**, 943–952.

Allen, C. D. C., Okada, T. and Cyster, J. G. (2007). Germinal-center organization and cellular dynamics. *Immunity* **27**, 190–202.

Allen, J. L., Fore, M. S., Wooten, J., Roehrs, P. A., Bhuiya, N. S., Hoffert, T., Sharf, A., Deal, A. M., Armistead, P., Coghill, J., et al. (2012). B cells from patients with chronic GVHD are activated and primed for survival via BAFF-mediated pathways. *Blood* **120**, 2529–36.

Alliouachene, S., Bilanges, B., Chicanne, G., Anderson, K. E., Pearce, W., Ali, K., Valet, C., Posor, Y., Low, P. C., Chaussade, C., et al. (2015). Inactivation of the Class II PI3K-C2B Potentiates Insulin Signaling and Sensitivity. *Cell Rep.* 1881–1894.

Allman, D. and Pillai, S. (2008). Peripheral B cell subsets. *Curr. Opin. Immunol.* **20**, 149–57.

Allman, D., Lindsley, R. C., DeMuth, W., Rudd, K., Shinton, S. A. and Hardy, R. R. (2001). Resolution of Three Nonproliferative Immature Splenic B Cell Subsets Reveals Multiple Selection Points During Peripheral B Cell Maturation. *J. Immunol.* **167**, 6834–6840.

Arcaro, A., Volinia, S., Zvelebil, M. J., Stein, R., Watton, S. J., Layton, M. J., Gout, I., Ahmadi, K., Downward, J. and Waterfield, M. D. (1998). Human Phosphoinositide 3-Kinase C2beta , the Role of Calcium and the

C2 Domain in Enzyme Activity. *J. Biol. Chem.* **273**, 33082–33090.

Arcaro, A., Khanzada, U. K., Vanhaesebroeck, B., Tetley, T. D., Waterfield, M. D. and Seckl, M. J. (2002). Two distinct phosphoinositide 3-kinases mediate polypeptide growth factor-stimulated PKB activation. *EMBO J.* **21**, 5097–5108.

Arnon, T. I., Horton, R. M., Grigorova, I. L. and Cyster, J. G. (2013). Visualization of splenic marginal zone B cell shuttling and follicular B cell egress. *Nature* **493**, 684–688.

Attanavanich, K. and Kearney, J. F. (2004a). Marginal Zone, but Not Follicular B Cells, Are Potent Activators of Naive CD4 T Cells. *J. Immunol.* **172**, 803–811.

Attanavanich, K. and Kearney, J. F. (2004b). Marginal zone, but not follicular B cells, are potent activators of naive CD4 T cells. *J. Immunol.* **172**, 803–811.

Baba, Y., Hashimoto, S., Matsushita, M., Watanabe, D., Kishimoto, T., Kurosaki, T. and Tsukada, S. (2001). BLNK mediates Syk-dependent Btk activation. *Proc. Natl. Acad. Sci.* **98**, 2582–2586.

Balakrishnan, S. (2012). Establishing a Biological Role for Class II Phosphoinositide 3-Kinase (PI3K) Enzyme PI3K-C2β.

Ballesteros-Tato, A. and Randall, T. D. (2014). Priming of T follicular helper cells by dendritic cells. *Immunol. Cell Biol.* **92**, 22–27.

Balzarotti, G., Tibolla, G., Bonacina, F., D'Alonzo, C., Dhyani, A., Falasca, M., Norata, G. D. and Catapano, A. (2015). PI3K-C2B plays a key role in the activation and the proliferation of t lymphocytes: Impact on vascular diseases. *Atherosclerosis* **241**, e35.

Baumgarth, N. (2011). The double life of a B-1 cell: self-reactivity selects for protective effector functions. *Nat. Rev. Immunol.* **11**, 34–46.

Baumjohann, D., Preite, S., Reboldi, A., Ronchi, F., Ansel, K. M., Lanzavecchia, A. and Sallusto, F. (2013). Persistent antigen and germinal center B cells sustain T follicular helper cell responses and phenotype. *Immunity* **38**, 596–605.

Berry, R., Chen, Z., McCluskey, J. and Rossjohn, J. (2011). Insight into the

basis of autonomous immunoreceptor activation. *Trends Immunol.* **32**, 165–70.

Best, C. G., Kemp, J. D. and Waldschmidt, T. J. (1995). Murine B-Cell Subsets Defined by CD23. *Methods* **8**, 3–10.

Blaho, V. A. and Hla, T. (2014). An update on the biology of sphingosine 1-phosphate receptors. *J. Lipid Res.* **55**, 1596–1608.

Błajecka, K., Marinov, M., Leitner, L., Uth, K., Posern, G. and Arcaro, A. (2012). Phosphoinositide 3-kinase C2β regulates RhoA and the actin cytoskeleton through an interaction with Dbl. *PLoS One* **7**, e44945.

Blunt, M. D. and Ward, S. G. (2012). Targeting PI3K isoforms and SHIP in the immune system: new therapeutics for inflammation and leukemia. *Curr. Opin. Pharmacol.* **12**, 444–51.

Bowles, S. L., Jaeger, C., Ferrara, C., Fingeroth, J., Van De Venter, M. and Oosthuizen, V. (2011). Comparative binding of soluble fragments (derCD23, sCD23, and exCD23) of recombinant human CD23 to CD21 (SCR 1-2) and native IgE, and their effect on IgE regulation. *Cell. Immunol.* **271**, 371–8.

Braccini, L., Ciraolo, E., Campa, C. C., Perino, A., Longo, D. L., Tibolla, G., Pregnolato, M., Cao, Y., Tassone, B., Damilano, F., et al. (2015). PI3K-C2γ is a Rab5 effector selectively controlling endosomal Akt2 activation downstream of insulin signalling. *Nat. Commun.* **6**, 7400.

Broere, F., Apasov, S. G., Sitkovsky, M. V and Eden, W. Van (2011). A2 T cell subsets and T cell-mediated immunity. In *Principles of Immunopharmacology* (ed. Nijkamp, F. P. and Parnham, M. J.), pp. 15–28. Basel: Birkhäuser Basel.

Browne, C. D., Del Nagro, C. J., Cato, M. H., Dengler, H. S. and Rickert, R. C. (2009). Suppression of phosphatidylinositol 3,4,5-trisphosphate production is a key determinant of B cell anergy. *Immunity* **31**, 749–60.

Cai, X., Srivastava, S., Sun, Y., Li, Z., Wu, H., Zuvela-Jelaska, L., Li, J., Salamon, R. S., Backer, J. M. and Skolnik, E. Y. (2011). Tripartite motif containing protein 27 negatively regulates CD4 T cells by ubiquitinating and inhibiting the class II PI3K-C2β. *Proc. Natl. Acad. Sci. U. S. A.* **108**, 20072–7.

Cambier, J. C., Gauld, S. B., Merrell, K. T. and Vilen, B. J. (2007). B-cell anergy: from transgenic models to naturally occurring anergic B cells? *Nat. Rev. Immunol.* **7**, 633–43.

Cameron, E. Z., Lemons, P. R., Bateman, P. W., Bennett, N. C., Battilana, P., Seematter, G., Schneiter, P., Jequier, E., Tappy, L., Brown, G. R., et al. (2008). Experimental alteration of litter sex ratios in a mammal. *Proc. Biol. Sci.* **275**, 323–7.

Carlsson, F., Hjelm, F., Conrad, D. H. and Heyman, B. (2007). IgE enhances specific antibody and T-cell responses in mice overexpressing CD23. *Scand. J. Immunol.* **66**, 261–70.

Carmichael, C. L., Majewski, I. J., Alexander, W. S., Metcalf, D., Hilton, D. J., Hewitt, C. A. and Scott, H. S. (2009). Hematopoietic defects in the Ts1Cje mouse model of Down syndrome. *Blood* **113**, 1929–1937.

Carsetti, R. (2004). Characterization of B-Cell Maturation in the Peripheral Immune System. *Methods Mol. Biol.* **271**, 25–35.

Carsetti, R., Köhler, G. and Lamers, M. C. (1995). Transitional B cells are the target of negative selection in the B cell compartment. *J. Exp. Med.* **181**, 2129–40.

Carter, R. and Fearon, D. (1992). CD19: lowering the threshold for antigen receptor stimulation of B lymphocytes. *Science (80-.).* **256**, 105–107.

Castigli, E., Wilson, S. A., Scott, S., Dedeoglu, F., Xu, S., Lam, K.-P., Bram, R. J., Jabara, H. and Geha, R. S. (2005). TACI and BAFF-R mediate isotype switching in B cells. *J. Exp. Med.* **201**, 35–9.

Cato, M. H., Yau, I. W. and Rickert, R. C. (2011). Magnetic-based purification of untouched mouse germinal center B cells for ex vivo manipulation and biochemical analysis. *Nat. Protoc.* **6**, 953–60.

Cattoretti, G., Mandelbaum, J., Lee, N., Chaves, A. H., Mahler, A. M., Chadburn, A., Dalla-Favera, R., Pasqualucci, L. and MacLennan, A. J. (2009). Targeted disruption of the S1P2 sphingosine 1-phosphate receptor gene leads to diffuse large B-cell lymphoma formation. *Cancer Res.* **69**, 8686–92.

Cerutti, A. (2008). The regulation of IgA class switching. *Nat. Rev. Immunol.* **8**, 421–34.

Cerutti, A., Cols, M. and Puga, I. (2013). Marginal zone B cells: virtues of innate-like antibody-producing lymphocytes. *Nat. Rev. Immunol.* **13**, 118–32.

Cesta, M. F. (2006). Normal structure, function, and histology of the spleen. *Toxicol. Pathol.* **34**, 455–65.

Chan, J. K. C., Ng, C. S. and Hui, P. K. (1988). A simple guide to the terminology and application of leucocyte monoclonal antibodies. *Histopathology* **12**, 461–480.

Chappell, C. P., Draves, K. E., Giltiay, N. V. and Clark, E. A. (2012). Extrafollicular B cell activation by marginal zone dendritic cells drives T cell-dependent antibody responses. *J. Exp. Med.* **209**, 1825–1840.

Charles A Janeway, J., Travers, P., Walport, M. and Shlomchik, M. J. (2001a). The Development and Survival of Lymphocytes.

Charles A Janeway, J., Travers, P., Walport, M. and Shlomchik, M. J. (2001b). The distribution and functions of immunoglobulin isotypes.

Chaudhuri, J. and Alt, F. W. (2004). Class-switch recombination: interplay of transcription, DNA deamination and DNA repair. *Nat. Rev. Immunol.* **4**, 541–552.

Chen, W. (2004). The late stage of T cell development within mouse thymus. *Cell. Mol. Immunol.* **1**, 3–11.

Chen, J., Wang, H., Xu, W.-P., Wei, S.-S., Li, H. J., Mei, Y.-Q., Li, Y.-G. and Wang, Y.-P. (2016). Besides an ITIM/SHP-1-dependent pathway, CD22 collaborates with Grb2 and plasma membrane calcium-ATPase in an ITIM/SHP-1-independent pathway of attenuation of Ca2+i signal in B cells. *Oncotarget* **7**, 56129–56146.

Cherukuri, A., Cheng, P. C., Sohn, H. W. and Pierce, S. K. (2001). The CD19/CD21 Complex Functions to Prolong B Cell Antigen Receptor Signaling from Lipid Rafts. *Immunity* **14**, 169–179.

Chikh, A., Ferro, R., Abbott, J. J., Piñeiro, R., Buus, R., Iezzi, M., Ricci, F., Bergamaschi, D., Ostano, P., Chiorino, G., et al. (2016). Class II phosphoinositide 3-kinase C2β regulates a novel signaling pathway involved in breast cancer progression. *Oncotarget* **7**, 18325–18345.

Chung, J. B., Silverman, M. and Monroe, J. G. (2003). Transitional B cells: step by step towards immune competence. *Trends Immunol.* **24**, 342–348.

Chung, E. Y., Psathas, J. N., Yu, D., Li, Y., Weiss, M. J. and Thomas-tikhonenko, A. (2012). CD19 is a major B cell receptor – independent activator of MYC-driven B-lymphomagenesis. *J. Clin. Invest.* **122**, 30–33.

Cinamon, G., Matloubian, M., Lesneski, M. J., Xu, Y., Low, C., Lu, T., Proia, R. L. and Cyster, J. G. (2004). Sphingosine 1-phosphate receptor 1 promotes B cell localization in the splenic marginal zone. *Nat. Immunol.* **5**, 713–720.

Cinamon, G., Zachariah, M. A., Lam, O. M., Foss, F. W. and Cyster, J. G. (2007). Follicular shuttling of marginal zone B cells facilitates antigen transport. *Nat. Immunol.* **9**, 54–62.

Ciraolo, E., Gulluni, F. and Hirsch, E. (2014). Methods to Measure the Enzymatic Activity of PI3Ks. In *Cell-wide Metabolic Alterations Associated With Malignancy* (ed. Galluzzi, L.) and Kroemer, G.), pp. 115–140. Academic Press.

Cockcroft, S. (2000). PI3K and membrane trafficking. In *Biology of Phosphoinositides* (ed. Cockcroft, S.), pp. 239–260. Oxford University Press.

Crassini, K., Stevenson, W. S., Mulligan, S. P. and Best, O. G. (2015). The MEK1/2 inhibitor, MEKi-1, induces cell death in chronic lymphocytic leukemia cells under conditions that mimic the tumor microenvironment and is synergistic with fludarabine. *Leuk. Lymphoma* **56**, 3407–17.

Darzynkiewicz, Z., Bruno, S., Del Bino, G., Gorczyca, W., Hotz, M. A., Lassota, P. and Traganos, F. (1992). Features of apoptotic cells measured by flow cytometry. *Cytometry* **13**, 795–808.

Das, M., Scappini, E., Martin, N. P., Wong, K. A., Dunn, S., Chen, Y.-J., Miller, S. L. H., Domin, J. and O'Bryan, J. P. (2007). Regulation of neuron survival through an intersectin-phosphoinositide 3'-kinase C2beta-AKT pathway. *Mol. Cell. Biol.* **27**, 7906–17.

de Andres, B., Cortegano, I., Serrano, N., del Rio, B., Martin, P., Gonzalo,

P., Marcos, M. a. R. and Gaspar, M. L. (2007). A Population of CD19highCD45R-/lowCD21low B Lymphocytes Poised for Spontaneous Secretion of IgG and IgA Antibodies. *J. Immunol.* **179**, 5326–5334.

De Silva, N. S. and Klein, U. (2015). Dynamics of B cells in germinal centres. *Nat. Rev. Immunol.* **15**, 137–48.

Deenick, E. K., Hasbold, J. and Hodgkin, P. D. (2005). Decision criteria for resolving isotype switching conflicts by B cells. *Eur. J. Immunol.* **35**, 2949–55.

Demishtein, A., Porat, Z., Elazar, Z. and Shvets, E. (2015). Applications of flow cytometry for measurement of autophagy. *Methods* **75**, 87–95.

den Haan, J. M. M. and Kraal, G. (2012). Innate Immune Functions of Macrophage Subpopulations in the Spleen. *J. Innate Immun.* **4**, 437–445.

den Haan, J. M., Mebius, R. E. and Kraal, G. (2012). Stromal cells of the mouse spleen. *Front. Immunol.* **3**, 201.

Dengler, H. S., Baracho, G. V, Omori, S. A., Bruckner, S., Arden, K. C., Castrillon, D. H., DePinho, R. A. and Rickert, R. C. (2008). Distinct functions for the transcription factor Foxo1 at various stages of B cell differentiation. *Nat. Immunol.* **9**, 1388–98.

Depoil, D., Fleire, S., Treanor, B. L., Weber, M., Harwood, N. E., Marchbank, K. L., Tybulewicz, V. L. J. and Batista, F. D. (2008). CD19 is essential for B cell activation by promoting B cell receptor-antigen microcluster formation in response to membrane-bound ligand. *Nat. Immunol.* **9**, 63–72.

Devereaux, K., Armi, C. D., Alcazar-roman, A., Ogasawara, Y., Zhou, X., Yamamoto, A., Camilli, P. De and Paolo, G. Di (2013). Regulation of Mammalian Autophagy by Class II and III PI 3-Kinases through PI3P Synthesis. *PLoS One* **8**, 10–12.

Di, L., Srivastava, S., Zhdanova, O., Ding, Y., Li, Z., Wulff, H. and Lafaille, M. (2010). Inhibition of the K + channel KCa3 . 1 ameliorates T cell – mediated colitis. *Proc. Natl. Acad. Sci.* **107**, 1541–1546.

Dillon, S. R., Mancini, M., Rosen, A. and Schlissel, M. S. (2000). Annexin V Binds to Viable B Cells and Colocalizes with a Marker of Lipid Rafts upon

B Cell Receptor Activation. *J. Immunol.* **164**, 1322–1332.

Dillon, S. R., Constantinescu, A. and Schlissel, M. S. (2001). Annexin V Binds to Positively Selected B Cells. *J. Immunol.* **166**, 58–71.

Ding, Y., Li, J., Wu, Q., Yang, P., Luo, B., Xie, S., Druey, K. M., Zajac, A. J., Hsu, H.-C. and Mountz, J. D. (2013). IL-17RA is essential for optimal localization of follicular Th cells in the germinal center light zone to promote autoantibody-producing B cells. *J. Immunol.* **191**, 1614–24.

Domin, J. (2006). Phosphoinositide 3-Kinase Signalling Pathways. In *Phosphoinositide 3-Kinase Signalling Pathways The key to cell proliferation and death* (ed. Eric W-F lam), pp. 49–158. Imperial College Press.

Domin, J. and Waterfield, M. D. (1997). Using structure to define the function of phosphoinositide 3-kinase family members. *FEBS Lett.* **410**, 91–95.

Domin, J., Pages, F., Volinia, S., Rittenhouse, S. E., Zvelebil, M. J., Stein, R. C. and Waterfield, M. D. (1997). Cloning of human phosphoinositide 3-kinase with a C2 domain that displays reduced sensitivity to the inhibitor wortmannin. *Biochem. J.* **147**, 139–147.

Domin, J., Harper, L., Aubyn, D., Wheeler, M., Florey, O., Haskard, D., Yuan, M. and Zicha, D. (2005). The class II phosphoinositide 3-kinase PI3K-C2beta regulates cell migration by a PtdIns3P dependent mechanism. *J. Cell. Physiol.* **205**, 452–62.

Doughty, C. A., Bleiman, B. F., Wagner, D. J., Dufort, F. J., Mataraza, J. M., Roberts, M. F. and Chiles, T. C. (2006). Antigen receptor-mediated changes in glucose metabolism in B lymphocytes: role of phosphatidylinositol 3-kinase signaling in the glycolytic control of growth. *Blood* **107**, 4458–65.

Drutman, S. B., Kendall, J. C. and Trombetta, E. S. (2012). Inflammatory spleen monocytes can upregulate CD11c expression without converting into dendritic cells. *J. Immunol.* **188**, 3603–10.

Durandy, A., Kracker, S. and Fischer, A. (2013). Primary antibody deficiencies. *Nat. Rev. Immunol.* **13**, 519–33.

Edry, E. and Melamed, D. (2004). Receptor Editing in Positive and Negative

Selection of B Lymphopoiesis. *J. Immunol.* **173**, 4265–4271.

Edwards, J. C. W. and Cambridge, G. (2006). B-cell targeting in rheumatoid arthritis and other autoimmune diseases. *Nat. Rev. Immunol.* **6**, 394–403.

El Sheikh, S. S., Domin, J., Tomtitchong, P., Abel, P., Stamp, G. and Lalani, E.-N. (2003). Topographical expression of class IA and class II phosphoinositide 3-kinase enzymes in normal human tissues is consistent with a role in differentiation. *BMC Clin. Pathol.* **3**, 4.

Elis, W., Triantafellow, E., Wolters, N. M., Sian, K. R., Caponigro, G., Borawski, J., Gaither, L. A., Murphy, L. O., Finan, P. M. and Mackeigan, J. P. (2008). Down-regulation of class II phosphoinositide 3-kinase alpha expression below a critical threshold induces apoptotic cell death. *Mol. Cancer Res.* **6**, 614–23.

Engel, P., Zhou, L. J., Ord, D. C., Sato, S., Koller, B. and Tedder, T. F. (1995). Abnormal B lymphocyte development, activation, and differentiation in mice that lack or overexpress the CD19 signal transduction molecule. *Immunity* **3**, 39–50.

Eto, D., Lao, C., DiToro, D., Barnett, B., Escobar, T. C., Kageyama, R., Yusuf, I. and Crotty, S. (2011). IL-21 and IL-6 are critical for different aspects of B cell immunity and redundantly induce optimal follicular helper CD4 T cell (Tfh) differentiation. *PLoS One* **6**, e17739.

Etzioni, A. and Ochs, H. D. (2004). The hyper IgM syndrome--an evolving story. *Pediatr. Res.* **56**, 519–25.

Falasca, M. and Maffucci, T. (2007). Role of class II phosphoinositide 3-kinase in cell signalling. *Biochem. Soc. Trans.* **35**, 211–4.

Fillatreau, S., Gray, D. and Anderton, S. M. (2008). Not always the bad guys: B cells as regulators of autoimmune pathology. *Nat. Rev. Immunol.* **8**, 391–7.

Foster, J. G., Blunt, M. D., Carter, E. and Ward, S. G. (2012). Inhibition of PI3K signaling spurs new therapeutic opportunities in inflammatory/autoimmune diseases and hematological malignancies. *Pharmacol. Rev.* **64**, 1027–54.

Fujimoto, M. and Sato, S. (2007). B cell signaling and autoimmune diseases:

CD19/CD22 loop as a B cell signaling device to regulate the balance of autoimmunity. *J. Dermatol. Sci.* **46**, 1–9.

Fujimoto, M., Poe, J. C., Jansen, P. J., Sato, S. and Tedder, T. F. (1999). CD19 amplifies B lymphocyte signal transduction by regulating Src-family protein tyrosine kinase activation. *J. Immunol.* **162**, 7088–94.

Fujimoto, M., Fujimoto, Y., Poe, J. C., Jansen, P. J., Lowell, C. A., DeFranco, A. L. and Tedder, T. F. (2000). CD19 Regulates Src Family Protein Tyrosine Kinase Activation in B Lymphocytes through Processive Amplification. *Immunity* **13**, 47–57.

Gatto, D. and Brink, R. (2010). The germinal center reaction. *J. Allergy Clin. Immunol.* **126**, 898–907.

Gauld, S. B. and Cambier, J. C. (2004). Src-family kinases in B-cell development and signaling. *Oncogene* **23**, 8001–8006.

Genestier, L., Taillardet, M., Mondiere, P., Gheit, H., Bella, C. and Defrance, T. (2007). TLR agonists selectively promote terminal plasma cell differentiation of B cell subsets specialized in thymus-independent responses. *J. Immunol.* **178**, 7779–7786.

Gitlin, A. D., Shulman, Z. and Nussenzweig, M. C. (2014). Clonal selection in the germinal centre by regulated proliferation and hypermutation. *Nature* **509**, 637–40.

Givan, A. L. (2001). *Flow Cytometry First Principles Second Edition*. 2nd ed. New York: Wiley-Liss.

Goenka, R., Matthews, A. H., Zhang, B., O'Neill, P. J., Scholz, J. L., Migone, T.-S., Leonard, W. J., Stohl, W., Hershberg, U. and Cancro, M. P. (2014). Local BLyS production by T follicular cells mediates retention of high affinity B cells during affinity maturation. *J. Exp. Med.* **211**, 45–56.

González-Navajas, J. M., Fine, S., Law, J., Datta, S. K., Nguyen, K. P., Yu, M., Corr, M., Katakura, K., Eckman, L., Lee, J., et al. (2010). TLR4 signaling in effector CD4+ T cells regulates TCR activation and experimental colitis in mice. *J. Clin. Invest.* **120**, 570–81.

Gould, H. J. and Sutton, B. J. (2008). IgE in allergy and asthma today. *Nat. Rev. Immunol.* **8**, 205–17.

Green, J. A., Suzuki, K., Cho, B., Willison, L. D., Palmer, D., Allen, C. D. C., Schmidt, T. H., Xu, Y., Proia, R. L., Coughlin, S. R., et al. (2011). The sphingosine 1-phosphate receptor S1P2 maintains the homeostasis of germinal center B cells and promotes niche confinement. *Nat. Immunol.* **12**, 672–80.

Grössinger, E. M., Weiss, L., Zierler, S., Rebhandl, S., Krenn, P. W., Hinterseer, E., Schmölzer, J., Asslaber, D., Hainzl, S., Neureiter, D., et al. (2014). Targeting proliferation of chronic lymphocytic leukemia (CLL) cells through KCa3.1 blockade. *Leukemia* **28**, 954–958.

Gupta, N. and DeFranco, A. L. (2007). Lipid rafts and B cell signaling. *Semin. Cell Dev. Biol.* **18**, 616–26.

Hall, T. (1999). BioEdit: a user-friendly biological sequence alignment editor and analysis program for Windows 95/98/NT. *Nucleic Acids Symp. Ser.* **41**, 95–98.

Hampel, F., Ehrenberg, S., Hojer, C., Draeseke, A., Marschall-Schröter, G., Kühn, R., Mack, B., Gires, O., Vahl, C. J., Schmidt-Supprian, M., et al. (2011). CD19-independent instruction of murine marginal zone B-cell development by constitutive Notch2 signaling. *Blood* **118**, 6321–31.

Hancock, R. E. W., Nijnik, A. and Philpott, D. J. (2012). Modulating immunity as a therapy for bacterial infections. *Nat. Rev. Microbiol.* **10**, 243–254.

Harada, K., Truong, A. B., Cai, T. and Khavari, P. A. (2005). The class II phosphoinositide 3-kinase C2beta is not essential for epidermal differentiation. *Mol. Cell. Biol.* **25**, 11122–30.

Hardy, R. R. and Hayakawa, K. (2001). B CELL DEVELOPMENT PATHWAYS. *Annu. Rev. Immunol.* **19**, 595–621.

Hasegawa, M., Fujimoto, M., Poe, J. C., Steeber, D. A., Lowell, C. A. and Tedder, T. F. (2001a). A CD19-Dependent Signaling Pathway Regulates Autoimmunity in Lyn-Deficient Mice. *J. Immunol.* **167**, 2469–2478.

Hasegawa, M., Fujimoto, M., Poe, J. C., Steeber, D. A. and Tedder, T. F. (2001b). CD19 Can Regulate B Lymphocyte Signal Transduction Independent of Complement Activation. *J. Immunol.* **167**, 3190–3200.

Hawkins, P. T. and Stephens, L. R. (2015). PI3K signalling in inflammation. *Biochim. Biophys. Acta* **1851**, 882–897.

He, Q., Johnston, J., Zeitlinger, J., City, K. and City, K. (2015). Phosphatidylinositol 3-kinase, Class 2 beta (PI3KC2β) isoform contributes to neuroblastoma tumorigenesis. *Cancer Lett.* **33**, 395–401.

Heike Wulff and Neil A. Castle (2010). Therapeutic potential of KCa3.1 blockers: an overview of recent advances, and promising trends. *Expert Rev. Clin. Pharmacol.* **3**, 385–396.

Heise, N., De Silva, N. S., Silva, K., Carette, A., Simonetti, G., Pasparakis, M. and Klein, U. (2014). Germinal center B cell maintenance and differentiation are controlled by distinct NF-κB transcription factor subunits. *J. Exp. Med.* **211**, 2103–18.

Henningsson, F., Ding, Z., Dahlin, J. S., Linkevicius, M., Carlsson, F., Grönvik, K.-O., Hallgren, J. and Heyman, B. (2011). IgE-mediated enhancement of CD4+ T cell responses in mice requires antigen presentation by CD11c+ cells and not by B cells. *PLoS One* **6**, e21760.

Hibbert, R. G., Teriete, P., Grundy, G. J., Beavil, R. L., Reljic, R., Holers, V. M., Hannan, J. P., Sutton, B. J., Gould, H. J. and McDonnell, J. M. (2005). The structure of human CD23 and its interactions with IgE and CD21. *J. Exp. Med.* **202**, 751–60.

Hsu, H.-C., Yang, P., Wang, J., Wu, Q., Myers, R., Chen, J., Yi, J., Guentert, T., Tousson, A., Stanus, A. L., et al. (2008). Interleukin 17-producing T helper cells and interleukin 17 orchestrate autoreactive germinal center development in autoimmune BXD2 mice. *Nat. Immunol.* **9**, 166–75.

Inaoki, M., Sato, S., Weintraub, B. C., Goodnow, C. C. and Tedder, T. F. (1997). CD19-Regulated Signaling Thresholds Control Peripheral Tolerance and Autoantibody Production in B Lymphocytes. *J. Exp. Med.* **186**, 1923–1931.

Ingle, G. S., Chan, P., Elliott, J. M., Chang, W. S., Koeppen, H., Stephan, J.-P. and Scales, S. J. (2008). High CD21 expression inhibits internalization of anti-CD19 antibodies and cytotoxicity of an anti-CD19-drug conjugate. *Br. J. Haematol.* **140**, 46–58.

Ireland, S. J., Blazek, M., Harp, C. T., Greenberg, B., Frohman, E. M., Davis, L. S. and Monson, N. L. (2012). Antibody-independent B cell effector

functions in relapsing remitting multiple sclerosis: clues to increased inflammatory and reduced regulatory B cell capacity. *Autoimmunity* **45**, 400–14.

Ishiura, N., Nakashima, H., Watanabe, R., Kuwano, Y., Adachi, T., Takahashi, Y., Tsubata, T., Okochi, H., Tamaki, K., Tedder, T. F., et al. (2010). Differential phosphorylation of functional tyrosines in CD19 modulates B-lymphocyte activation. *Eur. J. Immunol.* **40**, 1192–204.

Iwasaki, A. and Medzhitov, R. (2015). Control of adaptive immunity by the innate immune system. *Nat. Immunol.* **16**, 343–353.

Iwata, Y., Yoshizaki, A., Komura, K., Shimizu, K., Ogawa, F., Hara, T., Muroi, E., Bae, S., Takenaka, M., Yukami, T., et al. (2009). CD19, a response regulator of B lymphocytes, regulates wound healing through hyaluronan-induced TLR4 signaling. *Am. J. Pathol.* **175**, 649–60.

Janeway, C. A. and Medzhitov, R. (2002). Innate immune recognition. *Annu. Rev. Immunol.* **20**, 197–216.

Janeway Jr, C. (2001). *The Development and Survival of Lymphocytes*. 7th ed. (ed. Murphy, K., Travers, P., and Walport, M). Garland Science.

Jang, I. K., Zhang, J., Chiang, Y. J., Kole, H. K., Cronshaw, D. G., Zou, Y. and Gu, H. (2010). Grb2 functions at the top of the T-cell antigen receptor-induced tyrosine kinase cascade to control thymic selection. *Proc. Natl. Acad. Sci. U. S. A.* **107**, 10620–5.

Jang, I. K., Cronshaw, D. G., Xie, L., Fang, G., Zhang, J., Oh, H., Fu, Y.-X., Gu, H. and Zou, Y. (2011). Growth-factor receptor-bound protein-2 (Grb2) signaling in B cells controls lymphoid follicle organization and germinal center reaction. *Proc. Natl. Acad. Sci. U. S. A.* **108**, 7926–31.

Jelinek, D. F., Tschumper, R. C., Stolovitzky, G. A., Iturria, S. J., Tu, Y., Lepre, J., Shah, N. and Kay, N. E. (2003). Identification of a global gene expression signature of B-chronic lymphocytic leukemia. *Mol. Cancer Res.* **1**, 346–61.

Jolly, C. A., Muthukumar, A., Avula, C. P., Troyer, D. and Fernandes, G. (2001). Life span is prolonged in food-restricted autoimmune-prone (NZB x NZW)F(1) mice fed a diet enriched with (n-3) fatty acids. *J. Nutr.* **131**, 2753–60.

Jung, S., Siebenkotten, G. and Radbruch, A. (1994). Frequency of immunoglobulin E class switching is autonomously determined and independent of prior switching to other classes. *J. Exp. Med.* **179**, 2023–6.

Kawai, T. and Akira, S. (2010). The role of pattern-recognition receptors in innate immunity: update on Toll-like receptors. *Nat. Immunol.* **11**, 373–84.

Kim, H.-A., Seo, G.-Y. and Kim, P.-H. (2011). Macrophage-derived BAFF induces AID expression through the p38MAPK/CREB and JNK/AP-1 pathways. *J. Leukoc. Biol.* **89**, 393–8.

Kitatani, K., Usui, T., Sriraman, S. K., Toyoshima, M., Ishibashi, M., Shigeta, S., Nagase, S., Sakamoto, M., Ogiso, H., Okazaki, T., et al. (2015). Ceramide limits phosphatidylinositol-3-kinase C2β-controlled cell motility in ovarian cancer: potential of ceramide as a metastasis-suppressor lipid. *Oncogene* 1–12.

Klein, U. and Dalla-favera, R. (2008). Germinal centres : role in B- cell physiology and malignancy. *Nat. Rev. Immunol.* **8**, 22–33.

Kono, H. and Rock, K. L. (2008). How dying cells alert the immune system to danger. *Nat. Rev. Immunol.* **8**, 279–89.

Kono, M., Mi, Y., Liu, Y., Sasaki, T., Allende, M. L., Wu, Y.-P., Yamashita, T. and Proia, R. L. (2004). The Sphingosine-1-phosphate Receptors S1P1, S1P2, and S1P3 Function Coordinately during Embryonic Angiogenesis. *J. Biol. Chem.* **279**, 29367–29373.

Koopman, G., Reutelingsperger, C. P., Kuijten, G. A., Keehnen, R. M., Pals, S. T. and van Oers, M. H. (1994). Annexin V for flow cytometric detection of phosphatidylserine expression on B cells undergoing apoptosis. *Blood* **84**, 1415–20.

Koshy, S., Wu, D., Hu, X., Tajhya, R. B., Huq, R., Khan, F. S., Pennington, M. W., Wulff, H., Yotnda, P. and Beeton, C. (2013). Blocking KCa3.1 channels increases tumor cell killing by a subpopulation of human natural killer lymphocytes. *PLoS One* **8**, e76740.

Lai, L., Alaverdi, N., Maltais, L. and Morse, H. C. (1998). Mouse Cell Surface Antigens: Nomenclature and Immunophenotyping. *J. Immunol.* **160**, 3861–3868.

Le Gros, G., Ben-Sasson, S. Z., Seder, R., Finkelman, F. D. and Paul, W. E. (1990). Generation of interleukin 4 (IL-4)-producing cells in vivo and in vitro: IL-2 and IL-4 are required for in vitro generation of IL-4-producing cells. *J. Exp. Med.* **172**, 921–9.

Lemieux, G. A., Blumenkron, F., Yeung, N., Zhou, P., Williams, J., Grammer, A. C., Petrovich, R., Lipsky, P. E., Moss, M. L. and Werb, Z. (2007). The low affinity IgE receptor (CD23) is cleaved by the metalloproteinase ADAM10. *J. Biol. Chem.* **282**, 14836–44.

Li, X. and Carter, R. H. (1998). Convergence of CD19 and B cell antigen receptor signals at MEK1 in the ERK2 activation cascade. *J. Immunol.* **161**, 5901–8.

Li, X. and Carter, R. H. (2000). CD19 signal transduction in normal human B cells: Linkage to downstream pathways requires phosphatidylinositol 3-kinase, protein kinase C and Ca2+. *Eur. J. Immunol.* **30**, 1576–1586.

Lin, K.-I. and Calame, K. (2004). *Springer Protocols: B Cell Protocols*. Volume 271. (ed. Gu, H.) and Rajewsky, K.) Totowa, NJ: Humana Press.

Liu, Z., Sun, C., Zhang, Y., Ji, Z. and Yang, G. (2011). Phosphatidylinositol 3-Kinase-C2b Inhibits Cisplatin-Mediated Apoptosis via the Akt Pathway in Oesophageal Squamous Cell Carcinoma. *J. Int. Med. Res.* **39**, 1319–1332.

Liubchenko, G. A., Appleberry, H. C., Holers, V. M., Banda, N. K., Willis, V. C. and Lyubchenko, T. (2012). Potentially autoreactive naturally occurring transitional T3 B lymphocytes exhibit a unique signaling profile. *J. Autoimmun.* **38**, 293–303.

Loder, F., Mutschler, B., Ray, R. J., Paige, C. J., Sideras, P., Torres, R., Lamers, M. C. and Carsetti, R. (1999). B cell development in the spleen takes place in discrete steps and is determined by the quality of B cell receptor-derived signals. *J. Exp. Med.* **190**, 75–89.

Lund, F. E. (2008). Cytokine-producing B lymphocytes-key regulators of immunity. *Curr. Opin. Immunol.* **20**, 332–8.

Luning Prak, E. T., Monestier, M. and Eisenberg, R. A. (2011). B cell receptor editing in tolerance and autoimmunity. *Ann. N. Y. Acad. Sci.* **1217**, 96–121.

Luzina, I. G., Atamas, S. P., Storrer, C. E., daSilva, L. C., Kelsoe, G., Papadimitriou, J. C. and Handwerger, B. S. (2001). Spontaneous formation of germinal centers in autoimmune mice. *J. Leukoc. Biol.* **70**, 578–584.

Maceyka, M., Harikumar, K. B., Milstien, S. and Spiegel, S. (2012). Sphingosine-1-phosphate signaling and its role in disease. *Trends Cell Biol.* **22**, 50–60.

M Graeler and E J Goetzl (2002). Activation-regulated expression and chemotactic function of sphingosine 1-phosphate receptors in mouse splenic T cells. *FASEB J.* **16**, 1874–1878.

Magri, G., Miyajima, M., Bascones, S., Mortha, A., Puga, I., Cassis, L., Barra, C. M., Comerma, L., Chudnovskiy, A., Gentile, M., et al. (2014). Innate lymphoid cells integrate stromal and immunological signals to enhance antibody production by splenic marginal zone B cells. *Nat. Immunol.* **15**, 354–64.

Majerus, P. W. and York, J. D. (2009). Phosphoinositide phosphatases and disease. *J. Lipid Res.* **50 Suppl**, S249-54.

Matsushita, T., Horikawa, M., Iwata, Y. and Tedder, T. F. (2010). Regulatory B cells (B10 cells) and regulatory T cells have independent roles in controlling experimental autoimmune encephalomyelitis initiation and late-phase immunopathogenesis. *J. Immunol.* **185**, 2240–52.

Mattern, T., Flad, H. D., Brade, L., Rietschel, E. T. and Ulmer, A. J. (1998). Stimulation of human T lymphocytes by LPS is MHC unrestricted, but strongly dependent on B7 interactions. *J. Immunol.* **160**, 3412–8.

Mauri, C. and Bosma, A. (2012). Immune regulatory function of B cells. *Annu. Rev. Immunol.* **30**, 221–41.

Mavrommati, I., Cisse, O., Falasca, M. and Maffucci, T. (2016). Novel roles for class II Phosphoinositide 3-Kinase C2β in signalling pathways involved in prostate cancer cell invasion. *Sci. Rep.* **6**,.

McAleer, J. P. and Vella, A. T. (2008). Understanding how lipopolysaccharide impacts CD4 T-cell immunity. *Crit. Rev. Immunol.* **28**, 281–99.

McCarthy, B. A., Yancopoulos, S., Tipping, M., Yan, X., Wang, X. P.,

Bennett, F., Li, W., Lesser, M., Paul, S., Boyle, E., et al. (2015). A seven-gene expression panel distinguishing clonal expansions of pre-leukemic and chronic lymphocytic leukemia B cells from normal B lymphocytes. *Immunol. Res.*

Mebius, R. E. and Kraal, G. (2005). Structure and function of the spleen. *Nat. Rev. Immunol.* **5**, 606–16.

Medema, J. P., Planelles-Carazo, L., Hardenberg, G. and Hahne, M. (2003). The uncertain glory of APRIL. *Cell Death Differ.* **10**, 1121–5.

Merrell, K. T., Benschop, R. J., Gauld, S. B., Aviszus, K., Decote-Ricardo, D., Wysocki, L. J. and Cambier, J. C. (2006). Identification of anergic B cells within a wild-type repertoire. *Immunity* **25**, 953–62.

Meyer-Hermann, M., Mohr, E., Pelletier, N., Zhang, Y., Victora, G. D. and Toellner, K.-M. (2012). A theory of germinal center B cell selection, division, and exit. *Cell Rep.* **2**, 162–74.

Montes, C. L., Acosta-Rodríguez, E. V, Merino, M. C., Bermejo, D. A. and Gruppi, A. (2007). Polyclonal B cell activation in infections: infectious agents' devilry or defense mechanism of the host? *J. Leukoc. Biol.* **82**, 1027–32.

Mountz, J. D., Wang, J. H., Xie, S. and Hsu, H.-C. (2011). Cytokine regulation of B-cell migratory behavior favors formation of germinal centers in autoimmune disease. *Discov. Med.* **11**, 76–85.

Nicot, A.-S. and Laporte, J. (2008). Endosomal phosphoinositides and human diseases. *Traffic* **9**, 1240–9.

Nitschke, L. (2014). CD22 and Siglec-G regulate inhibition of B-cell signaling by sialic acid ligand binding and control B-cell tolerance. *Glycobiology* **24**, 807–17.

Noack, M. and Miossec, P. (2014). Th17 and regulatory T cell balance in autoimmune and inflammatory diseases. *Autoimmun. Rev.* **13**, 668–77.

Nunès, J. A. and Guittard, G. (2013). An Emerging Role for PI5P in T Cell Biology. *Front. Immunol.* **4**,.

O'Neill, S. K., Getahun, A., Gauld, S. B., Merrell, K. T., Tamir, I., Smith, M. J., Dal Porto, J. M., Li, Q.-Z. and Cambier, J. C. (2011).

Monophosphorylation of CD79a and CD79b ITAM motifs initiates a SHIP-1 phosphatase-mediated inhibitory signaling cascade required for B cell anergy. *Immunity* **35**, 746–56.

Ohya, S. and Imaizumi, Y. (2014). Intermediate-conductance Ca2+-activated K+ channel KCa3.1 and its related molecules in T-lymphocytes. *Inflamm. Cell Signal.* **1**, 10–14800/ics.327.

Okkenhaug, K., Turner, M. and Gold, M. R. (2014). PI3K Signaling in B Cell and T Cell Biology. *Front. Immunol.* **5**,.

Omori, S. A., Cato, M. H., Anzelon-mills, A., Puri, K. D., Shapiro-shelef, M., Calame, K. and Rickert, R. C. (2006). Regulation of Class-Switch Recombination and Plasma Cell Differentiation by Phosphatidylinositol 3-Kinase Signaling. 545–557.

Ono, F., Nakagawa, T., Saito, S., Owada, Y., Sakagami, H., Goto, K., Suzuki, M., Matsuno, S. and Kondo, H. (1998). A novel class II phosphoinositide 3-kinase predominantly expressed in the liver and its enhanced expression during liver regeneration. *J. Biol. Chem.* **273**, 7731–6.

Oropallo, M. A. and Cerutti, A. (2014). Germinal center reaction: antigen affinity and presentation explain it all. *Trends Immunol.* **35**, 287–9.

Otero, D. C., Omori, S. a and Rickert, R. C. (2001). Cd19-dependent activation of Akt kinase in B-lymphocytes. *J. Biol. Chem.* **276**, 1474–8.

Otero, D. C., Anzelon, A. N. and Rickert, R. C. (2003). CD19 Function in Early and Late B Cell Development: I. Maintenance of Follicular and Marginal Zone B Cells Requires CD19-Dependent Survival Signals. *J. Immunol.* **170**, 73–83.

Otipoby, K. L., Sasaki, Y., Schmidt-Supprian, M., Patke, A., Gareus, R., Pasparakis, M., Tarakhovsky, A. and Rajewsky, K. (2008). BAFF activates Akt and Erk through BAFF-R in an IKK1-dependent manner in primary mouse B cells. *Proc. Natl. Acad. Sci.* **105**, 12435–12438.

Palm, A.-K. E., Garcia-Faroldi, G., Lundberg, M., Pejler, G., Kleinau, S., Barral, P., Bergtold, A., Desai, D. D., Gavhane, A., Clynes, R., et al. (2016a). Activated mast cells promote differentiation of B cells into effector cellsActivated mast cells promote differentiation of B cells into effector cells. *Sci. Rep.* **6**, 20531.

Palm, A.-K. E. K., Garcia-Faroldi, G., Lundberg, M., Pejler, G., Kleinau, S., Barral, P., Bergtold, A., Desai, D. D., Gavhane, A., Clynes, R., et al. (2016b). Activated mast cells promote differentiation of B cells into effector cells. *Sci. Rep.* **6**, 20531.

Parham, P. (2014). *The Immune System, Fourth Edition*. Garland Science.

Park, M. A., Li, J. T., Hagan, J. B., Maddox, D. E. and Abraham, R. S. (2008). Common variable immunodefi ciency : a new look at an old disease. *Lancet* **372**, 489–502.

Pelanda, R. and Torres, R. M. (2012). Central B-cell tolerance: where selection begins. *Cold Spring Harb. Perspect. Biol.* **4**, a007146.

Poe, J. C., Fujimoto, M., Jansen, P. J., Miller, A. S. and Tedder, T. F. (2000). CD22 forms a quaternary complex with SHIP, Grb2, and Shc. A pathway for regulation of B lymphocyte antigen receptor-induced calcium flux. *J. Biol. Chem.* **275**, 17420–7.

Poe, J. C., Tedder, T. F. and Jonathan C. Poe and Thomas F.Tedder (2012). CD22 and Siglec-G in B cell function and tolerance. *Trends Immunol.* **33**, 413–420.

Pone, E. J., Zan, H., Zhang, J., Al-Qahtani, A., Xu, Z. and Casali, P. (2010). Toll-like receptors and B-cell receptors synergize to induce immunoglobulin class-switch DNA recombination: relevance to microbial antibody responses. *Crit. Rev. Immunol.* **30**, 1–29.

Ponnusamy, S., Meyers-Needham, M., Senkal, C. E., Saddoughi, S. A., Sentelle, D., Selvam, S. P., Salas, A. and Ogretmen, B. (2010). Sphingolipids and cancer: ceramide and sphingosine-1-phosphate in the regulation of cell death and drug resistance. *Future Oncol.* **6**, 1603–24.

Puga, I., Cols, M., Barra, C. M., He, B., Cassis, L., Gentile, M., Comerma, L., Chorny, A., Shan, M., Xu, W., et al. (2011). B cell–helper neutrophils stimulate the diversification and production of immunoglobulin in the marginal zone of the spleen. *Nat. Immunol.* **13**, 170–180.

Rabin, E., Cong, Y. Z. and Wortis, H. H. (1992). Loss of CD23 is a consequence of B-cell activation. Implications for the analysis of B-cell lineages. *Ann. N. Y. Acad. Sci.* **651**, 130–42.

Raphael, I., Nalawade, S., Eagar, T. N. and Forsthuber, T. G. (2014). T cell subsets and their signature cytokines in autoimmune and inflammatory diseases. *Cytokine* **74**, 1043–4666.

Rosenfeld, C. S., Grimm, K. M., Livingston, K. A., Brokman, A. M., Lamberson, W. E. and Roberts, R. M. (2003). Striking variation in the sex ratio of pups born to mice according to whether maternal diet is high in fat or carbohydrate. *Proc. Natl. Acad. Sci. U. S. A.* **100**, 4628–32.

Rui, L., Healy, J. I., Blasioli, J. and Goodnow, C. C. (2006). ERK Signaling Is a Molecular Switch Integrating Opposing Inputs from B Cell Receptor and T Cell Cytokines to Control TLR4-Driven Plasma Cell Differentiation. *J. Immunol.* **177**, 5337–5346.

Sandel, P. C. and Monroe, J. G. (1999). Negative Selection of Immature B Cells by Receptor Editing or Deletion Is Determined by Site of Antigen Encounter. *Immunity* **10**, 289–299.

Sato, S., Ono, N., Steeber, D. A., Pisetsky, D. S. and Tedder, T. F. (1996). CD19 regulates B lymphocyte signaling thresholds critical for the development of B-1 lineage cells and autoimmunity. *J. Immunol.* **157**, 4371–8.

Sellers, R. S., Morton, D., Michael, B., Roome, N., Johnson, J. K., Yano, B. L., Perry, R. and Schafer, K. (2007). Society of Toxicologic Pathology Position Paper: Organ Weight Recommendations for Toxicology Studies. *Toxicol. Pathol.* **35**, 751–755.

Shen, P. and Fillatreau, S. (2015). Antibody-independent functions of B cells: a focus on cytokines. *Nat. Rev. Immunol.* **15**, 441–451.

Shrivastava, P., Katagiri, T., Ogimoto, M., Mizuno, K. and Yakura, H. (2004). Dynamic regulation of Src-family kinases by CD45 in B cells. *Blood* **103**, 1425–32.

Sic, H., Kraus, H., Madl, J., Flittner, K.-A., von Münchow, A. L., Pieper, K., Rizzi, M., Kienzler, A.-K., Ayata, K., Rauer, S., et al. (2014). Sphingosine-1-phosphate receptors control B-cell migration through signaling components associated with primary immunodeficiencies, chronic lymphocytic leukemia, and multiple sclerosis. *J. Allergy Clin. Immunol.* **134**, 420–8.

Sims, G. P., Ettinger, R., Shirota, Y., Yarboro, C. H., Illei, G. G. and Lipsky, P.

E. (2005). Identification and characterization of circulating human transitional B cells. *Blood* **105**, 4390–4398.

Singh, N., Chandler, P. R., Seki, Y., Baban, B., Takezaki, M., Kahler, D. J., Munn, D. H., Larsen, C. P., Mellor, A. L. and Iwashima, M. (2007). Role of CD28 in fatal autoimmune disorder in scurfy mice. *Blood* **110**, 1199–1206.

Singh, R. P., Hasan, S., Sharma, S., Nagra, S., Yamaguchi, D. T., Wong, D., Bh, H. and Hossain, A. (2014). Th17 cells in inflammation and autoimmunity. *Autoimmun. Rev.* **13**, 1174–1181.

Song, W., Liu, C., Seeley-Fallen, M. K., Miller, H., Ketchum, C. and Upadhyaya, A. (2013). Actin-mediated feedback loops in B-cell receptor signaling. *Immunol. Rev.* **256**, 177–89.

Spellberg, B. and Edwards, J. E. (2001). Type 1/Type 2 immunity in infectious diseases. *Clin. Infect. Dis.* **32**, 76–102.

Srinivasan, A. and McSorley, S. J. (2007). Pivotal advance: exposure to LPS suppresses CD4+ T cell cytokine production in Salmonella-infected mice and exacerbates murine typhoid. *J. Leukoc. Biol.* **81**, 403–11.

Srivastava, S., Di, L., Zhdanova, O., Li, Z., Vardhana, S., Wan, Q., Yan, Y., Varma, R., Backer, J., Wulff, H., et al. (2009). The class II phosphatidylinositol 3 kinase C2beta is required for the activation of the K+ channel KCa3.1 and CD4 T-cells. *Mol. Biol. Cell* **20**, 3783–91.

Srivastava, S., Cai, X., Li, Z., Sun, Y. and Skolnik, E. Y. (2012). Phosphatidylinositol-3-kinase C2β and TRIM27 function to positively and negatively regulate IgE receptor activation of mast cells. *Mol. Cell. Biol.* **32**, 3132–9.

Stavnezer, J., Guikema, J. E. J. and Schrader, C. E. (2008). Mechanism and regulation of class switch recombination. *Annu. Rev. Immunol.* **26**, 261–92.

Stein, J. V and Nombela-Arrieta, C. (2005). Chemokine control of lymphocyte trafficking: a general overview. *Immunology* **116**, 1–12.

Steiniger, B. (2005). Spleen. *Encycl. LIFE Sci.* 1–9.

Steiniger, B. S. (2015). Human spleen microanatomy: why mice do not

suffice. *Immunology* **145**, 334–46.

Steiniger, B. and Barth, P. (1999). *Microanatomy and Function of the Spleen*. Springer Science & Business Media.

Steiniger, B., Timphus, E. M., Jacob, R. and Barth, P. J. (2005). CD27+ B cells in human lymphatic organs: Re-evaluating the splenic marginal zone. *Immunology* **116**, 429–442.

Stiles, R. J., Schrum, A. G. and Gil, D. (2013). A co-housing strategy to improve fecundity of mice in timed matings. *Lab Anim. (NY).* **42**, 62–5.

Stoddart, A., Jackson, A. P. and Brodsky, F. M. (2005). Plasticity of B Cell Receptor Internalization upon Conditional Depletion of Clathrin □. *Mol. Biol. Cell* **16**, 2339–2348.

Strauss-Ayali, D., Conrad, S. M. and Mosser, D. M. (2007). Monocyte subpopulations and their differentiation patterns during infection. *J. Leukoc. Biol.* **82**, 244–52.

Sukumar, S., Conrad, D. H., Szakal, A. K. and Tew, J. G. (2006). Differential T Cell-Mediated Regulation of CD23 (Fc RII) in B Cells and Follicular Dendritic Cells. *J. Immunol.* **176**, 4811–4817.

Suttie, A. W. (2006). Histopathology of the spleen. *Toxicol. Pathol.* **34**, 466–503.

Swain, S. L., Weinberg, A. D., English, M. and Huston, G. (1990). IL-4 directs the development of Th2-like helper effectors. *J. Immunol.* **145**, 3796–806.

Swirski, F. K., Nahrendorf, M., Etzrodt, M., Wildgruber, M., Cortez-Retamozo, V., Panizzi, P., Figueiredo, J.-L., Kohler, R. H., Chudnovskiy, A., Waterman, P., et al. (2009). Identification of splenic reservoir monocytes and their deployment to inflammatory sites. *Science* **325**, 612–6.

Szenczi, P., Bánszegi, O., Groó, Z., Altbäcker, V., Trivers, R., Willard, D., Rosenfeld, C., Roberts, R., Williams, G., Cameron, E., et al. (2013). Anogenital Distance and Condition as Predictors of Litter Sex Ratio in Two Mouse Species: A Study of the House Mouse (Mus musculus) and Mound-Building Mouse (Mus spicilegus). *PLoS One* **8**, e74066.

Teague, B. N., Pan, Y., Mudd, P. A., Nakken, B., Zhang, Q., Szodoray, P., Kim-Howard, X., Wilson, P. C. and Farris, A. D. (2007). Cutting Edge: Transitional T3 B Cells Do Not Give Rise to Mature B Cells, Have Undergone Selection, and Are Reduced in Murine Lupus. *J. Immunol.* **178**, 7511–7515.

Tedder, T. F., Zhou, L.-J. and Engel, P. (1994). The CD19/CD21 signal transduction complex of B lymphocytes. *Immunol. Today* **15**, 437–442.

Tedder, T. F., Inaoki, M. and Sato, S. (1997). The CD19–CD21 Complex Regulates Signal Transduction Thresholds Governing Humoral Immunity and Autoimmunity. *Immunity* **6**, 107–118.

Teodorovic, L. S., Babolin, C., Rowland, S. L., Greaves, S. A., Baldwin, D. P., Torres, R. M. and Pelanda, R. (2014). Activation of Ras overcomes B-cell tolerance to promote differentiation of autoreactive B cells and production of autoantibodies. *Proc. Natl. Acad. Sci. U. S. A.* **111**, E2797-806.

Tibolla, G., Piñeiro, R., Chiozzotto, D., Mavrommati, I., Wheeler, A. P., Norata, G. D., Catapano, A. L., Maffucci, T. and Falasca, M. (2013). Class II phosphoinositide 3-kinases contribute to endothelial cells morphogenesis. *PLoS One* **8**, e53808.

Trivers, R. L. and Willard, D. E. (1973). Natural selection of parental ability to vary the sex ratio of offspring. *Science* **179**, 90–2.

Tsolaki, A. G. (2011). Marginal zone B-cells , a gatekeeper of innate immunity. *Front. Immunol.* **2**, 1–10.

Tsubata, T. (2012). Role of inhibitory BCR co-receptors in immunity. *Infect. Disord. Drug Targets* **12**, 181–90.

Tussiwand, R., Rauch, M., Flück, L. A. and Rolink, A. G. (2012). BAFF-R expression correlates with positive selection of immature B cells. *Eur. J. Immunol.* **42**, 206–16.

Vanhaesebroeck, B. and Waterfield, M. D. (1999). Signaling by Distinct Classes of Phosphoinositide 3-Kinases. *Exp. Cell Res.* **253**, 239–254.

Vazquez, M. I., Catalan-Dibene, J. and Zlotnik, A. (2015). B cells responses and cytokine production are regulated by their immune microenvironment. *Cytokine* **72**, 318–326.

Verhoven, B. (1995). Mechanisms of phosphatidylserine exposure, a phagocyte recognition signal, on apoptotic T lymphocytes. *J. Exp. Med.* **182**, 1597–1601.

Victora, G. D., Schwickert, T. A., Fooksman, D. R., Kamphorst, A. O., Meyer-Hermann, M., Dustin, M. L. and Nussenzweig, M. C. (2010). Germinal center dynamics revealed by multiphoton microscopy with a photoactivatable fluorescent reporter. *Cell* **143**, 592–605.

Vincent, F. B., Saulep-Easton, D., Figgett, W. A., Fairfax, K. A. and Mackay, F. (2013). The BAFF/APRIL system: emerging functions beyond B cell biology and autoimmunity. *Cytokine Growth Factor Rev.* **24**, 203–15.

Vinuesa, C. G., Sanz, I. and Cook, M. C. (2009). Dysregulation of germinal centres in autoimmune disease. *Nat. Rev. Immunol.* **9**, 845–857.

Vossenkämper, A., Lutalo, P. M. K. and Spencer, J. (2012). Translational Mini-Review Series on B cell subsets in disease. Transitional B cells in systemic lupus erythematosus and Sjögren's syndrome: clinical implications and effects of B cell-targeted therapies. *Clin. Exp. Immunol.* **167**, 7–14.

Walker, J. A. and Smith, K. G. C. (2008). CD22: an inhibitory enigma. *Immunology* **123**, 314–25.

Wang, Y., Brooks, S. R., Li, X., Anzelon, A. N., Rickert, R. C. and Carter, R. H. (2002). The Physiologic Role of CD19 Cytoplasmic Tyrosines. *Immunity* **17**, 501–514.

Wang, H., Feng, J., Qi, C.-F., Li, Z., Morse, H. C. and Clarke, S. H. (2007). Transitional B cells lose their ability to receptor edit but retain their potential for positive and negative selection. *J. Immunol.* **179**, 7544–52.

Wang, K., Wei, G. and Liu, D. (2012). CD19: a biomarker for B cell development, lymphoma diagnosis and therapy. *Exp. Hematol. Oncol.* **1**, 36.

Weinreich, M. A. and Hogquist, K. A. (2008). Thymic Emigration: When and How T Cells Leave Home. *J. Immunol.* **181**, 2265–2270.

Werner, M., Hobeika, E. and Jumaa, H. (2010). Role of PI3K in the generation andsurvival of B cells. *Immunol. Rev.* 55–71.

Westin, J. R. (2014). Status of PI3K/Akt/mTOR pathway inhibitors in lymphoma. *Clin. Lymphoma. Myeloma Leuk.* **14**, 335–42.

Wheeler, M. and Domin, J. A. N. (2001). Recruitment of the class II phosphoinositide 3-kinase C2beta to the epidermal growth factor receptor: role of Grb2. *Mol. Cell. Biol.* **21**, 6660–7.

Wheeler, M. and Domin, J. (2006). The N-terminus of phosphoinositide 3-kinase-C2beta regulates lipid kinase activity and binding to clathrin. *J. Cell. Physiol.* **206**, 586–93.

Wollenberg, I., Agua-Doce, A., Hernández, A., Almeida, C., Oliveira, V. G., Faro, J. and Graca, L. (2011). Regulation of the germinal center reaction by Foxp3+ follicular regulatory T cells. *J. Immunol.* **187**, 4553–60.

Wong, K. A., Wilson, J., Russo, A., Wang, L., Okur, M. N., Wang, X., Martin, N. P., Scappini, E., Carnegie, G. K. and Bryan, J. P. O. (2012a). Intersectin (ITSN) Family of Scaffolds Function as Molecular Hubs in Protein Interaction Networks. *PLoS One* **7**, 1–9.

Wong, K. A., Russo, A., Wang, X., Chen, Y.-J., Lavie, A. and O'Bryan, J. P. (2012b). A New Dimension to Ras Function: A Novel Role for Nucleotide-Free Ras in Class II Phosphatidylinositol 3-Kinase Beta (PI3KC2β) Regulation. *PLoS One* **7**, e45360.

Wulff, H., Knaus, H.-G. H.-G., Pennington, M. and Chandy, K. G. (2004). K+ Channel Expression during B Cell Differentiation: Implications for Immunomodulation and Autoimmunity. *J. Immunol.* **173**, 776–786.

Xiong, H., Dolpady, J., Wabl, M., Lafaille, M. A. C. De and Lafaille, J. J. (2012). Sequential class switching is required for the generation of high affinity IgE antibodies. *J. Exp. Med.* **209**, 353–364.

Xu, H., Liew, L. N., Chun, I., Huang, C. H., Goh, L. and Yan, K. (2008). The modulatory effects of lipopolysaccharide-stimulated B cells on differential T-cell polarization. *Immunology* **125**, 218–228.

Yan, J., Wolff, M. J., Unternaehrer, J., Mellman, I. and Mamula, M. J. (2005). Targeting antigen to CD19 on B cells efficiently activates T cells. *Int. Immunol.* **17**, 869–77.

Yarkoni, Y., Getahun, A. and Cambier, J. C. (2010). Molecular underpinning of B-cell anergy. *Immunol. Rev.* **237**, 249–63.

Yazawa, N., Fujimoto, M., Sato, S., Miyake, K., Asano, N., Nagai, Y., Takeuchi, O., Takeda, K., Okochi, H., Akira, S., et al. (2003). CD19 regulates innate immunity by the toll-like receptor RP105 signaling in B lymphocytes. *Blood* **102**, 1374–80.

Yoshioka, K., Yoshida, K., Cui, H., Wakayama, T., Takuwa, N., Okamoto, Y., Du, W., Qi, X., Asanuma, K., Sugihara, K., et al. (2012). Endothelial PI3K-C2α, a class II PI3K, has an essential role in angiogenesis and vascular barrier function. *Nat. Med.* **18**, 1560–9.

Young, F. M., Phungtamdet, W. and Sanderson, B. J. S. (2005). Modification of MTT assay conditions to examine the cytotoxic effects of amitraz on the human lymphoblastoid cell line, WIL2NS. *Toxicol. In Vitro* **19**, 1051–9.

Yu, D. and Vinuesa, C. G. (2010). The elusive identity of T follicular helper cells. *Trends Immunol.* **31**, 377–383.

Zhu, J. and Paul, W. E. (2015). CD4 T cells : fates , functions , and faults. *Blood* **112**, 1557–1570.

Zikherman, J., Doan, K., Parameswaran, R., Raschke, W. and Weiss, A. (2012). Quantitative differences in CD45 expression unmask functions for CD45 in B-cell development, tolerance, and survival. *Proc. Natl. Acad. Sci. U. S. A.* **109**, E3-12.

Appendix

A

Controls

M DOB	F DOB	F DOB	Litters	Av.litter size	Period (months)
16/10/2012	27/10/2012		6	7	8
16/10/2012	27/10/2012		7	7	9
16/07/2013	15/07/2013	28/08/2013	9	5	6
28/08/2013	01/09/2013		9	6	5
		Total/Average	***31***	***6***	***7***

PI3K C2β–/–

M DOB	F DOB	F DOB	Litters	Av.litter size	Period (months)
22/10/2012	22/10/2012		9	4	7
13/08/2012	30/09/2012		12	5	9
26/07/2013	26/07/2013	16/08/2013	11	6	6
16/08/2013	01/08/2013		9	5	6
		Total/Average	***41***	***5***	***7***

B

Controls

	Number of offspring per litter			
	7	10 FD	7	FD
	6 FD	7	5	FD
	9	10	4	7
	9	FD	5	FD
	8	7	4	5
	4	4	4	8
	3		FD	6
			FD	4 FD
			1 runt	5
Total	40	28	29	31
Av. Litter	7	7	5	6

101 mice survived past weaning

Males	Females
48	53

PI3K C2β–/–

	Number of offspring per litter			
	2	3	6	8
	3	3	5	8
	3	5	FD	5
	5	10	FD	6
	5	8	FD	3
	8	6	10	2
	6	5	9	2
	3	1FD	7	5
	4	2	3	1FD
		2	FD	
		eaten	5	
		eaten		
Total	39	44	45	39
Av. Litter	4	5	6	5

158 mice survived past weaning

Males	Females
66	92

Appendix 1. Breakdown of breeding data (see also Figure 3.2). Data were collected over the same time period from cages set up at the same time, using mice that were aged matched as closely as possible. **A**; shows the date of birth (DOB) of the female (F) and male (M) mice, the number of litters produced, the average litter size and the period of time that the mice were actively breeding. **B**; provides details about the litters including those that were found dead (FD) or eaten. 101 control mice were successfully weaned (48M and 51F) compared to 158 PI3K C2β–/– mice (66M and 92F). Data were obtained from stockfiles provided by the animal technicians at CSB, Imperial College London, Hammersmith Campus.

A

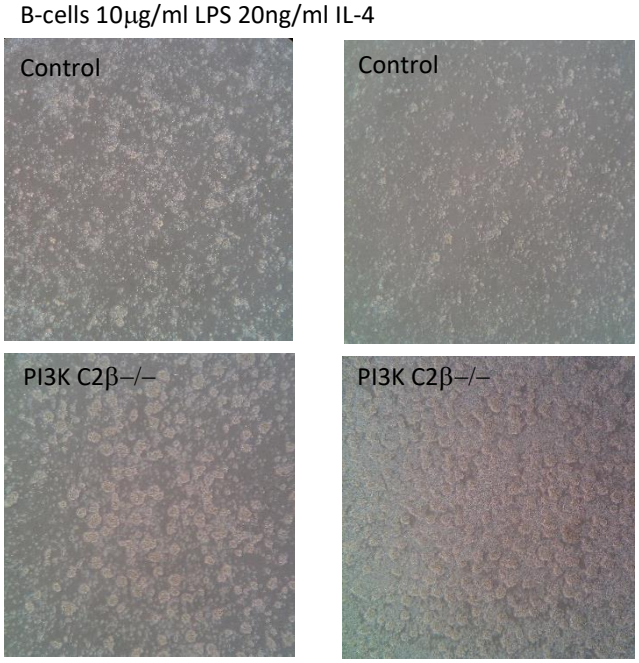

B

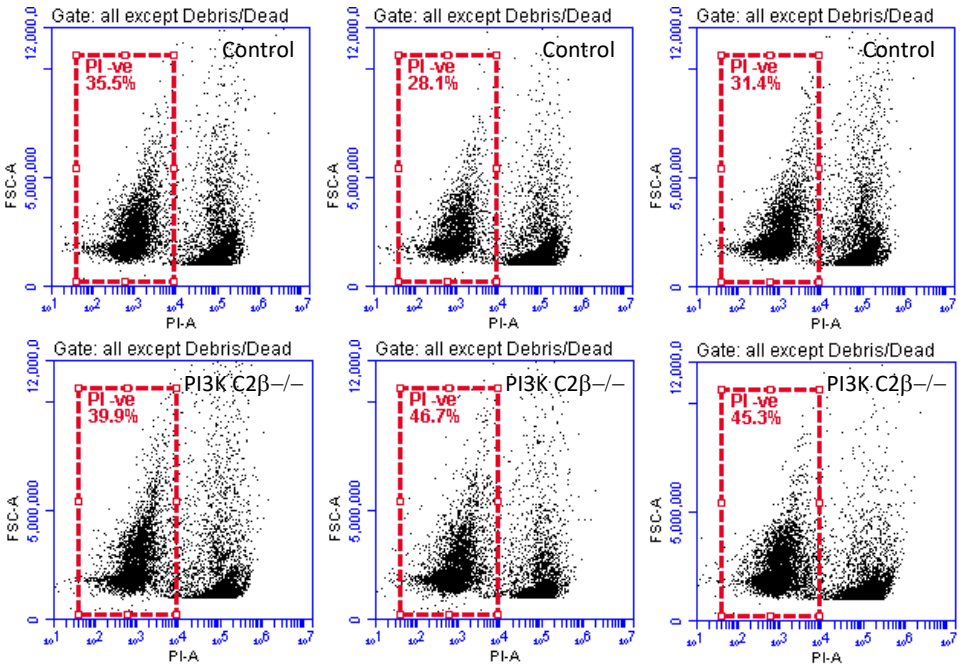

Appendix 2. Reducing the concentration of LPS and IL-4. Initially B-cells were stimulated with 20μg/ml LPS and 50ng/ml IL-4, which are concentrations that have previously been used in our lab. Examination of CD19 expression had shown that levels were increased on PI3K C2β–/– B-cells. This was of interest because increased CD19 has been shown to lower the activation threshold in B-cells. To examine the theory that PI3K C2β–/– B-cells may have a reduced activation threshold compared to control B-cells the concentration of LPS and IL-4 were reduced. **A**; At 10μg/ml LPS and 20ng/ml IL-4 both the control and PI3K C2β–/– cultures had formed foci at 48 hr, which is associated with proliferation. B-cells were plated at 1 x 10^6 per ml and kept at 37°C in a humidified 5% CO_2 incubator. **B**; Dot plots showing that PI3K C2β–/– B-cells had an increased population of PI negative cells following 72 hr stimulation with 5μg/ml LPS and 20ng/ml IL-4. Cells were gated to exclude debris and dead cells, 10,000 events were recorded for each plot.

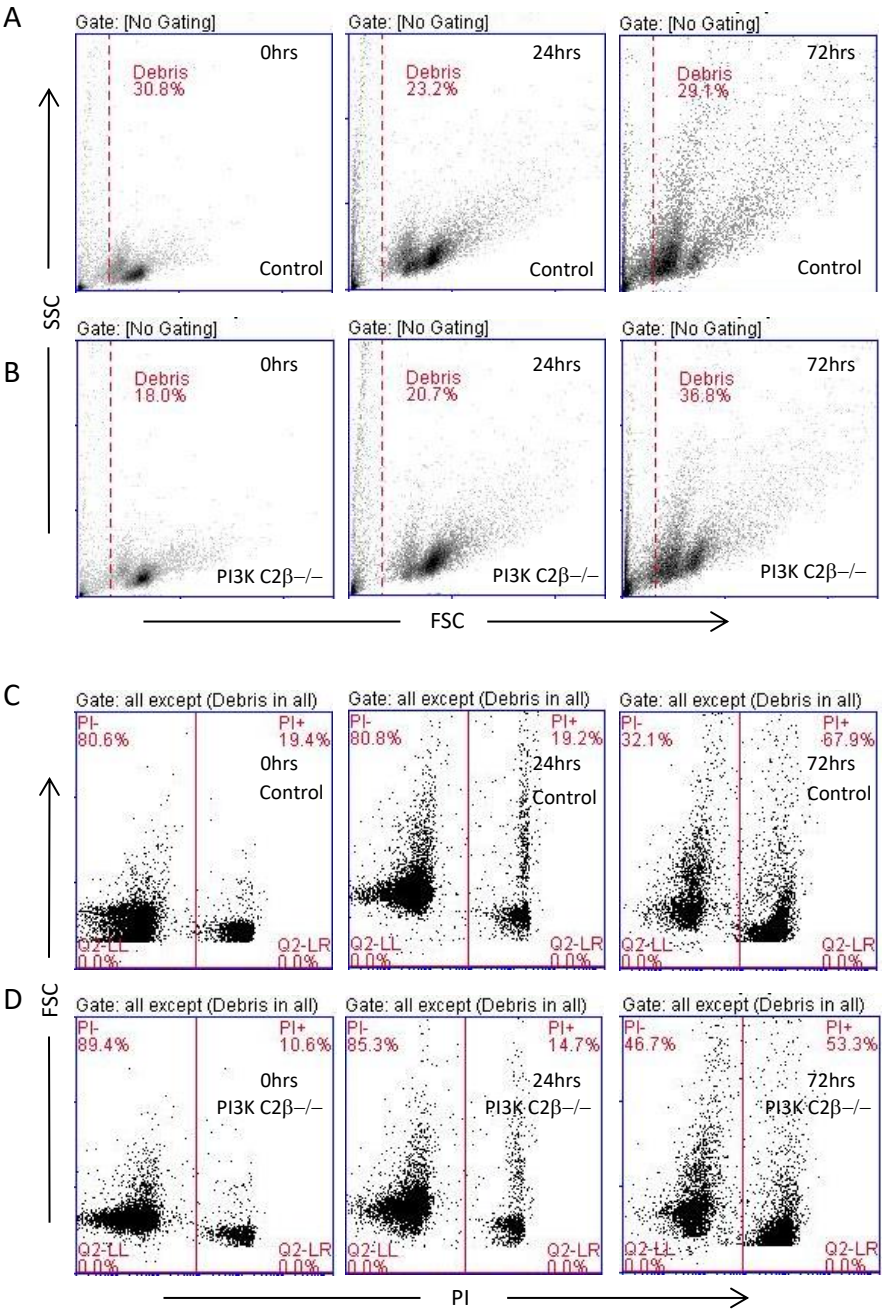

Appendix 3. Initial assessment of B-cell viability following stimulation with 2μg/ml LPS and 20ng/ml IL-4. Propidium iodide staining of PI3K C2β–/– and control B-Cells at 0, 24 and 72 hr, analysed using flow cytometry. A minimum of 10,000 events were recorded per plot. **A** and **B**; representative plots showing forward scatter and side scatter of control and PI3K C2β–/– B-cells and at 0, 24 and 72 hr respectively. **C** and **D**; representative dot plots of PI stained control and PI3K C2β–/– B-cells at 0, 24 and 72 hr respectively, gated to exclude debris, which may result in false PI negative results.

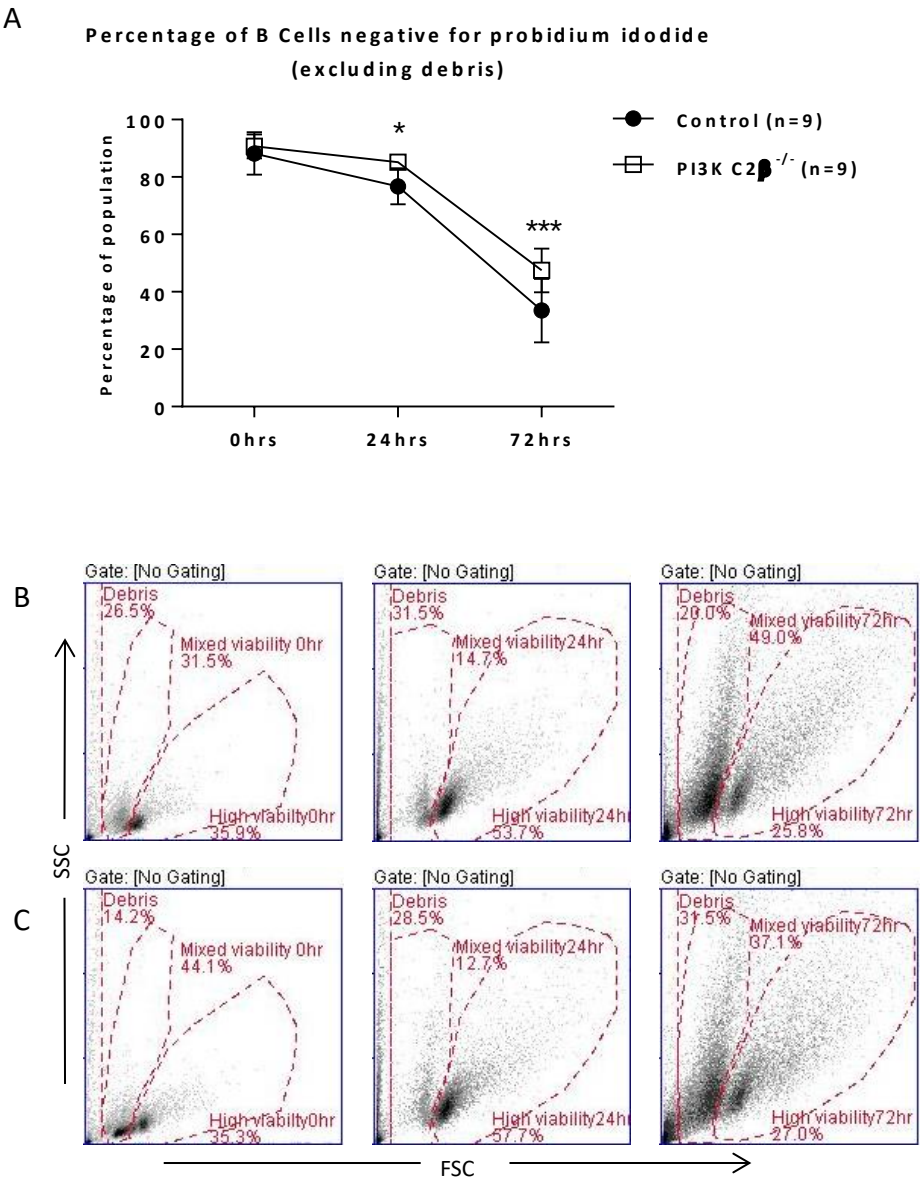

Appendix 4. Propidium iodide staining of control and PI3K C2β−/− B-cells over 72 hr. **A**; analysis of results (**Appendix 3**) showed that following stimulation with 2μg/ml LPS and 20ng/ml IL-4 there was an increased percentage of live cells (PI-ve) in the PI3K C2β−/− population compared to the controls at both 24 hr and at 72 hr. The results of three separate experiments were analysed by two-way ANOVA (P=0.0002). **B** and **C**; representative plots (FSC vs SSC) at 0, 24 and 72 hr for control and PI3K C2β−/−B-cells respectively. Two distinct populations were observed, which were identified as highest viability and mixed viability according to the percentage of cells that were PI positive or negative. 10,000 events were recorded per plot.

Total population (excluding debris/ doublets)

0 hr	**Control**	**PI3K C2β–/–**	**Difference**	**p value**
Sub G0/G1	8.01% ± 0.66	6.61% ± 0.56	1.4± 0.86	p=0.136
G0/G1	88.27% ± 0.63	89.78% ± 0.60	1.51 ± 0.87	p=0.114
Synthesis	1.10% ± 0.1	1.08% ± 0.16	0.022 ± 0.19	p=0.912
G2/M	2.08% ± 0.2	2.24% ± 0.15	0.16 ± 0.25	p=0.545
24hr				
Sub G0/G1	20.18% ± 2.7	14.37% ± 2.01	5.81 ± 3.37	p=0.116
G0/G1	75.28% ± 2.79	79.62% ± 2.79	4.34 ± 3.95	p=0.297
Synthesis	6.24% ± 0.94	7.37% ± 0.51	1.13 ± 1.07	p=0.316
G2/M	1.23% ± 0.09	2.11% ± 0.42	0.88 ± 0.43	p=0.068
72 hr				
Sub G0/G1	67.76% ± 3.44	58.58% ± 1.4	9.18 ± 3.71	p= 0.033
G0/G1	23.54% ± 3.07	33.66% ± 1.81	10.12 ± 3.56	p= 0.017
Synthesis	4.81% ± 0.43	3.91% ± 0.32	0.9 ± 0.54	p=0.128
G2/M	0.46% ± 0.1	0.48% ± 0.05	0.02 ± 0.11	p=0.858
Highest viability population				
0 hr	**Control**	**PI3K C2β–/–**	**Difference**	**p value**
Sub G0/G1	2.74% ± 0.50	2.7% ± 0.29	0.042 ± 0.58	p=0.989
G0/G1	94.39% ± 0.46	94.30% ± 0.40	0.10 ± 0.61	p=0.973
Synthesis	2.52% ± 0.73	1.57% ± 0.39	0.94 ± 0.83	p=0.727
G2/M	2.41% ± 0.23	2.45% ± 0.17	0.4 ± 0.29	p=0.990
24 hr				
Sub G0/G1	15.90% ± 3.23	8.19% ± 1.75	7.70 ± 3.68	p=0.005
G0/G1	84.42% ± 2.45	88.62% ± 2.3	4.26 ± 3.36	p=0.117
Synthesis	2.45% ± 0.28	2.66% ± 0.54	0.21 ± 0.61	p=0.937
G2/M	1.41% ± 0.088	2.51% ± 0.56	1.10 ± 0.57	p=0.684
72 hr				
Sub G0/G1	43.51% ± 5.3	31.36% ± 2	12.15 ± 5.65	p=<0.001
G0/G1	42.95% ± 4.64	57.81% ± 2.46	14.86 ± 5.25	p=<0.001
Synthesis	7.76% ± 0.99	6.05 ± 0.50	1.70 ± 1.11	P=0.530
G2/M	0.79% ± 0.19	0.80% ± 0.09	0.015 ± 0.22	p=0.996

Appendix 5. Summary of cell cycle data for each time point. Statistical significance was calculated using multiple t-tests, corrected for multiple comparisons using the Sidak-Bonferroni method. Data represent mean values ± SEM.

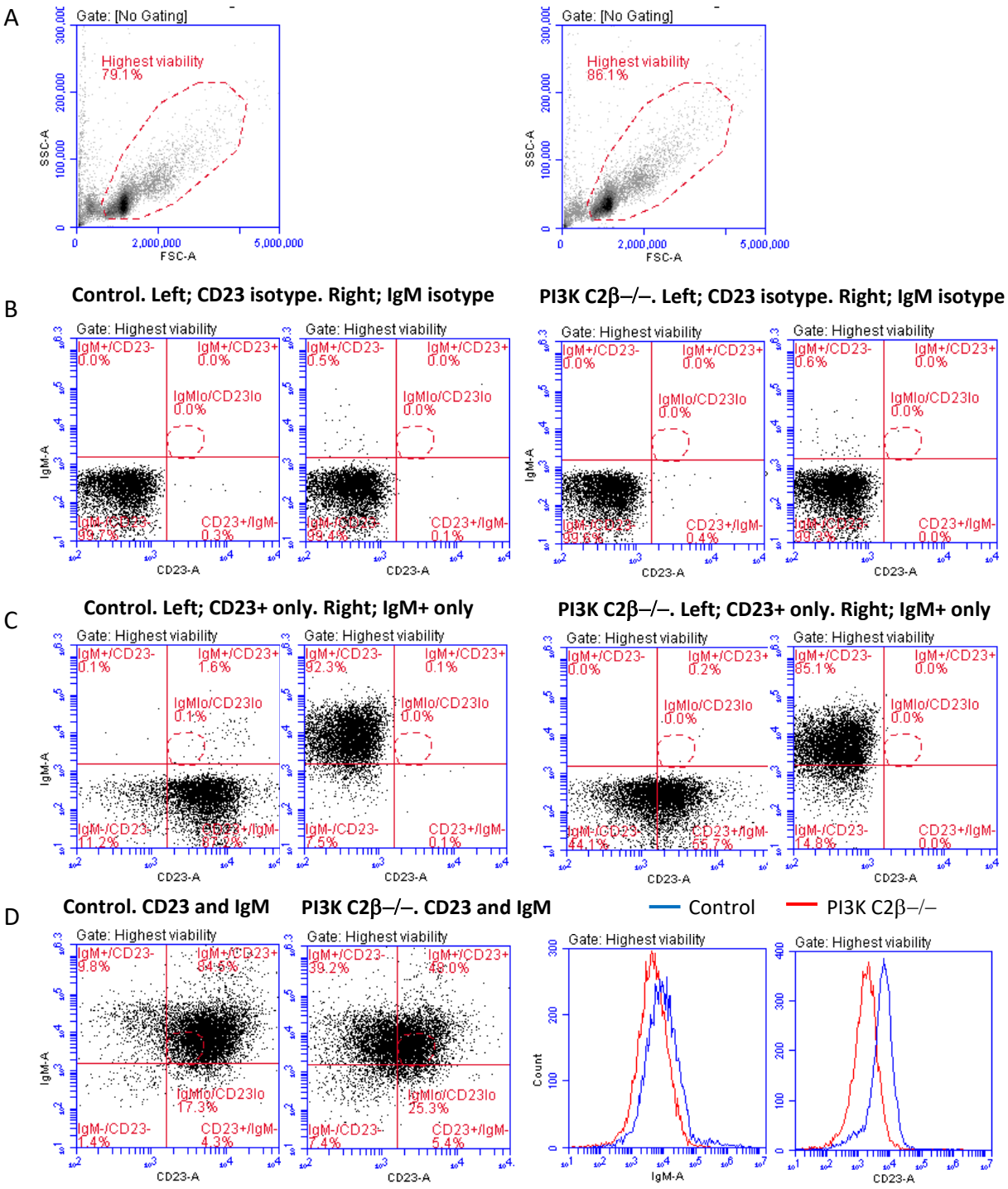

Appendix 6. Supporting information to explain the gating strategy used in Figure 5.17. A; The top dot plots show the highest viability gates, on which further analysis was based. **B;** The dot plots in the second row show the staining pattern for the CD23 and IgM isotype controls. **C;** shows the results from single staining with CD23 or IgM. **D;** the dot plots on the left show dual staining with CD23 and IgM for control (left) and PI3K C2β–/– (right) B-cells. The IgM^{low} / CD23^{low} gate was determined using results from the control B-cells (left). The histograms on the right reveal that a higher proportion of PI3K C2β–/– B-cell are both IgM^{low} and CD23^{low}. This correlates with the increased percentage of PI3K C2β–/– B-cells falling within the IgM^{low} / CD23^{low} gate. These data are representative of a single experiment using three control and three PI3K C2β–/– mice.

A

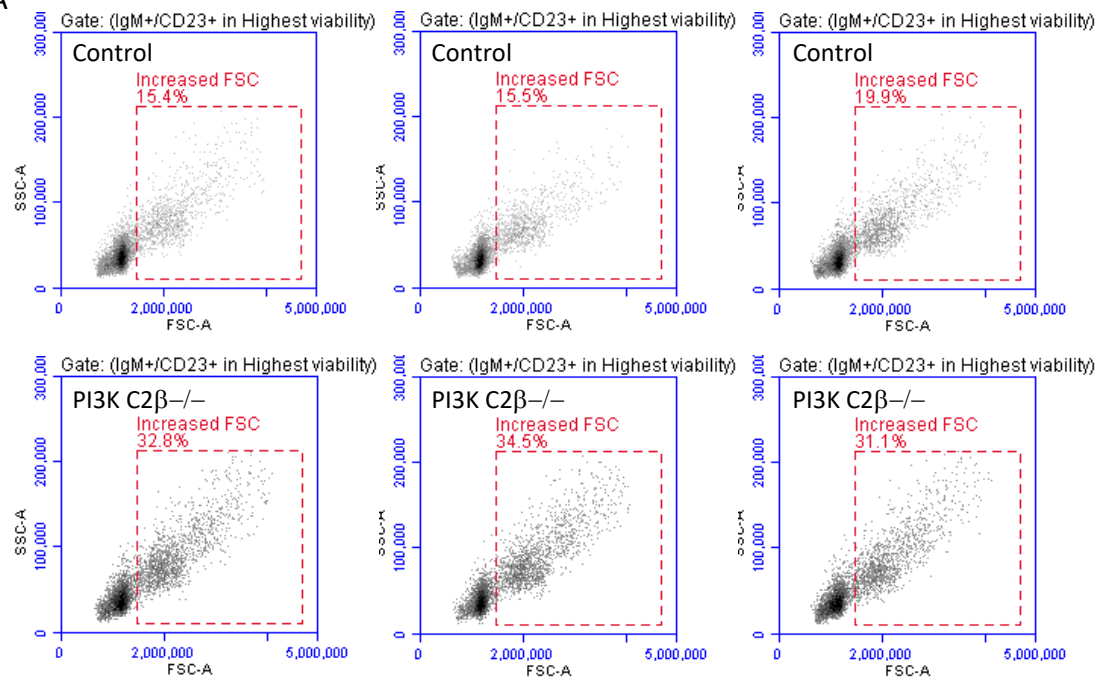

Appendix 7. Plots showing forward scatter (FSC) versus side scatter (SSC) for B-cells labelled with fluorophore conjugated antibodies to IgM and CD23 at 0 hr. Using the gating strategy presented in **Appendix 6**, the FSC was analysed in control and PI3K C2β–/– B-cells. **A**; CD23+ / IgM+ PI3K C2β–/– B-cells were shown to have a consistently higher FSC than CD23+ / IgM+ control B-cells. This is in keeping with the previous data that showed both IgM and CD23 appear to be down regulated in PI3K C2β–/– B-cells. Activated, differentiating B-cells have a larger FSC than naïve B-cells and are typically IgM^{low} / $CD23^{low}$. These data are from a single experiment using three control and three PI3K C2β–/– mice.

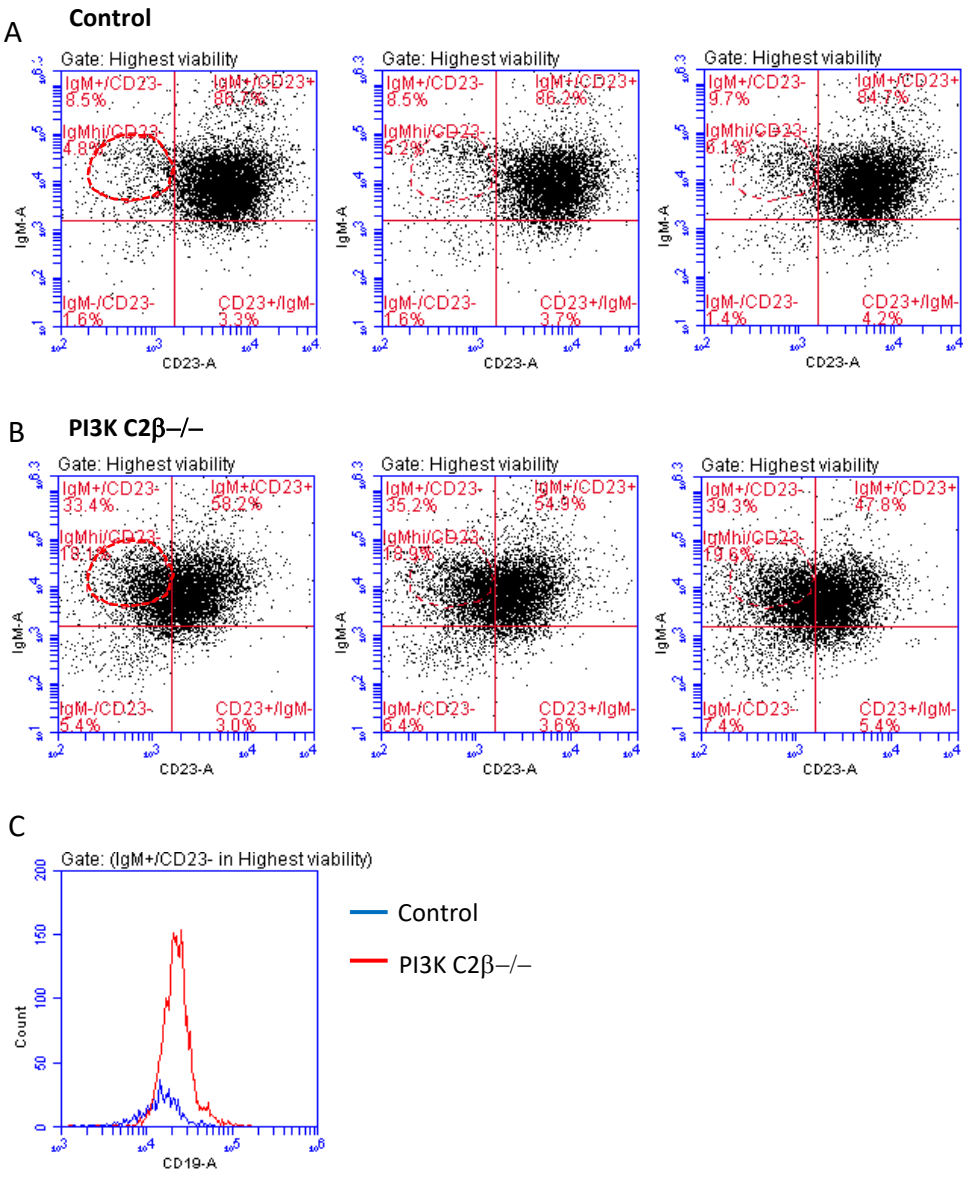

Appendix 8. The same gating strategy was used as described in Appendix 6. Freshly isolated B-cells were labelled with fluorophore conjugated antibodies to CD23, IgM, CD19, relevant isotype controls or all three antibodies. The dot plots show dual staining with CD23 and IgM for control (**A**) and PI3K C2β–/– (**B**) B-cells. The IgM^{low} / $CD23^{low}$ gate was determined using results from the control B-cells. C; Representative histogram showing CD19 expression within the IgM+/ CD23- quadrants. These data are from a single experiment using three control and three PI3K C2β–/– mice.

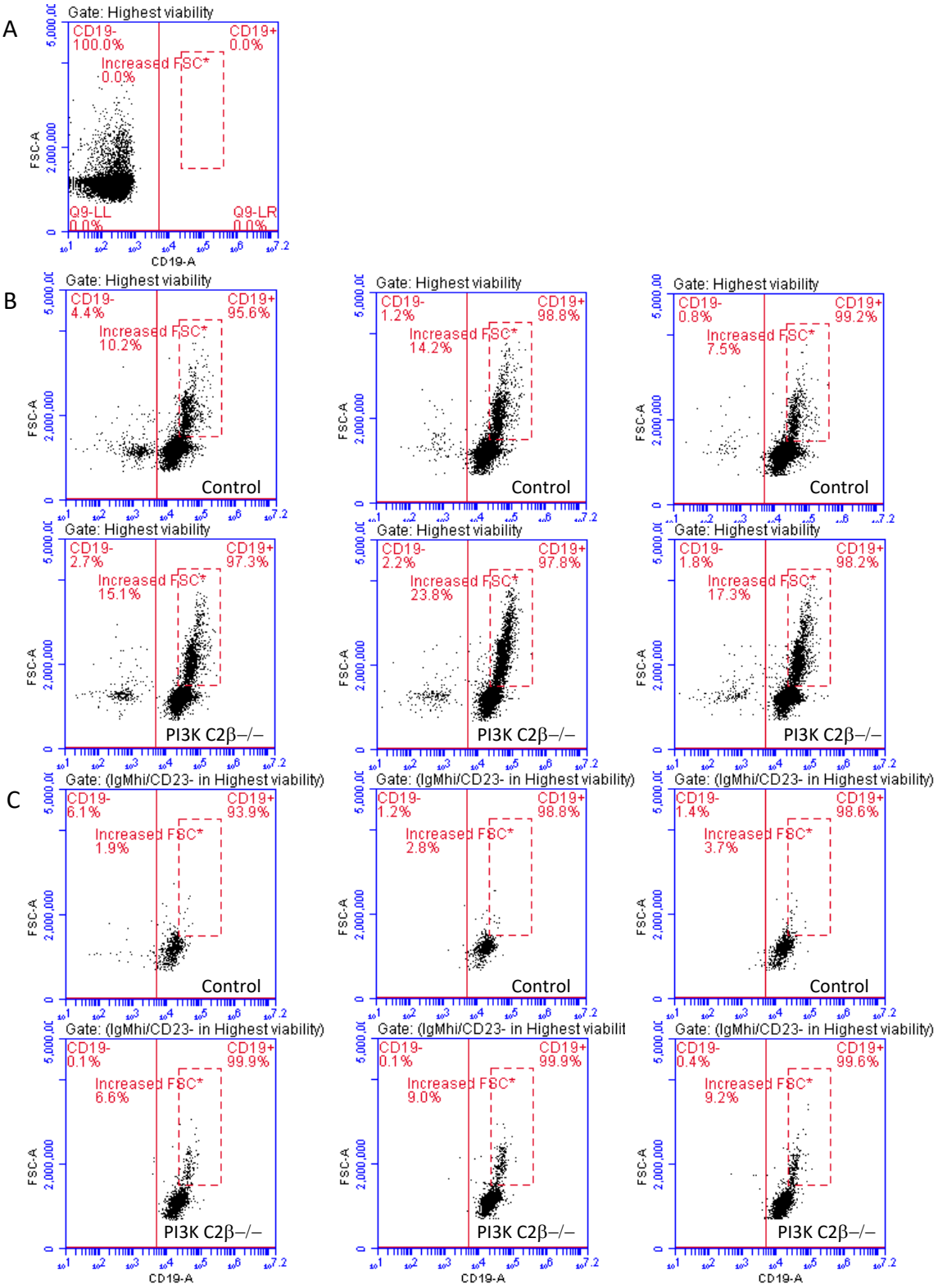

Appendix 9. Gating strategy to determine FSC of CD19+, sIgM^{hi}/sCD23^{low} B-cells. A; A representative dot plot showing the staining pattern for the CD19 isotype control. B; Initially cells were gated using the single stained CD19+ B-cells. This allowed identification of a CD19+ population with increased forward scatter. C; Using the same plot, the triple stained B-cells CD19 was analysed within the sIgM^{hi}/sCD23- population (**Appendix 8**).

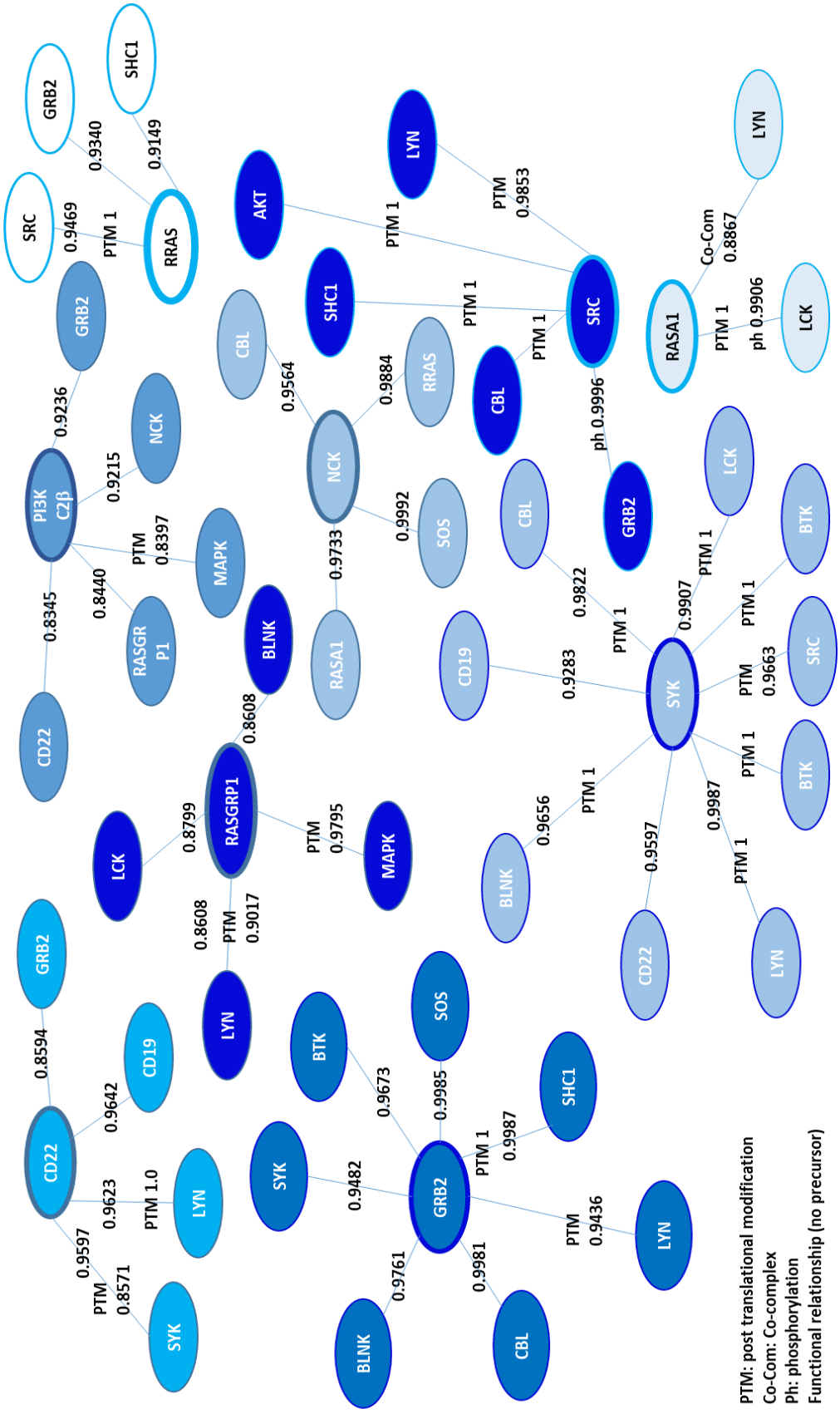

Appendix 10. Predicted protein interactions generated using PathwayNet (http://pathwaynet.princeton.edu/predictions/gene/?network=human-posttranslational-regulation&gene=5694).